

# Corrugated elliptical horn antennas for the generation of radiation patterns with elliptical cross-section

**Citation for published version (APA):**

Worm, S. C. J. (1985). *Corrugated elliptical horn antennas for the generation of radiation patterns with elliptical cross-section*. [Phd Thesis 1 (Research TU/e / Graduation TU/e), Mathematics and Computer Science]. Technische Hogeschool Eindhoven. <https://doi.org/10.6100/IR173905>

**DOI:**

[10.6100/IR173905](https://doi.org/10.6100/IR173905)

**Document status and date:**

Published: 01/01/1985

**Document Version:**

Publisher's PDF, also known as Version of Record (includes final page, issue and volume numbers)

**Please check the document version of this publication:**

- A submitted manuscript is the version of the article upon submission and before peer-review. There can be important differences between the submitted version and the official published version of record. People interested in the research are advised to contact the author for the final version of the publication, or visit the DOI to the publisher's website.
- The final author version and the galley proof are versions of the publication after peer review.
- The final published version features the final layout of the paper including the volume, issue and page numbers.

[Link to publication](#)

**General rights**

Copyright and moral rights for the publications made accessible in the public portal are retained by the authors and/or other copyright owners and it is a condition of accessing publications that users recognise and abide by the legal requirements associated with these rights.

- Users may download and print one copy of any publication from the public portal for the purpose of private study or research.
- You may not further distribute the material or use it for any profit-making activity or commercial gain
- You may freely distribute the URL identifying the publication in the public portal.

If the publication is distributed under the terms of Article 25fa of the Dutch Copyright Act, indicated by the "Taverne" license above, please follow below link for the End User Agreement:

[www.tue.nl/taverne](http://www.tue.nl/taverne)

**Take down policy**

If you believe that this document breaches copyright please contact us at:

[openaccess@tue.nl](mailto:openaccess@tue.nl)

providing details and we will investigate your claim.

**CORRUGATED ELLIPTICAL HORN ANTENNAS  
FOR THE GENERATION OF  
RADIATION PATTERNS WITH ELLIPTICAL CROSS-SECTION**

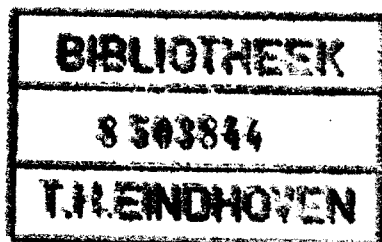
**S.C.J. Worm**

CORRUGATED ELLIPTICAL HORN ANTENNAS

FOR THE GENERATION OF

RADIATION PATTERNS WITH ELLIPTICAL CROSS-SECTION

CORRUGATED ELLIPTICAL HORN ANTENNAS  
FOR THE GENERATION OF  
RADIATION PATTERNS WITH ELLIPTICAL CROSS-SECTION



PROEFSCHRIFT

ter verkrijging van de graad van doctor in de  
technische wetenschappen aan de Technische  
Hogeschool Eindhoven, op gezag van de rector  
magnificus, prof.dr. S.T.M. Ackermans, voor  
een commissie aangewezen door het college van  
dekanen in het openbaar te verdedigen op  
dinsdag 14 mei 1985 te 16.00 uur

door

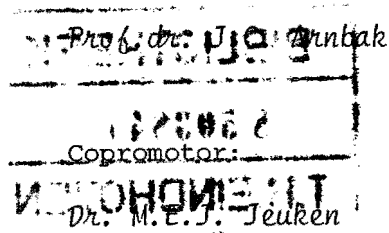
Simon Cornelis Joseph Worm

geboren te Bladel

Dit proefschrift is goedgekeurd  
door de promotoren:

Prof.dr. J. Boersma

en



CIP-GEGEVENS KONINKLIJKE BIBLIOTHEEK, DEN HAAG

Worm, Simon Cornelis Joseph

Corrugated elliptical horn antennas for the generation of  
radiation patterns with elliptical cross-section / Simon  
Cornelis Joseph Worm. - [S.l. : s.n.]. - Fig.

Proefschrift Technische Hogeschool Eindhoven. - Met lit.  
opg., reg.

ISBN 90-9000918-3

SISO 669.2 UDC 621.396.677 UGI 650

Trefw.: elektromagnetische golfvoortplanting / antennes.



This study was performed as part of the research program of the professional group Electromagnetism and Circuit Theory, Department of Electrical Engineering, Eindhoven University of Technology, P.O. Box 513, 5600 MB Eindhoven, The Netherlands.

CONTENTS

ABSTRACT

1. GENERAL INTRODUCTION	1
1.1. Introduction	1
1.2. Aspects of broadcasting by satellite	5
1.3. Designs for broadcasting-satellite transmitting antennas	14
1.4. Survey of the contents	18
1.5. References	21
2. SPHERO-CONAL COORDINATES AND LAMÉ FUNCTIONS	23
2.1. Introduction	23
2.2. The trigonometric representation of sphero-conal coordinates	24
2.3. Differential operators and integral theorems	35
2.4. The scalar Helmholtz equation	37
2.5. The Lamé functions	42
2.5.1. Lamé functions regular inside the elliptical cone	42
2.5.2. Lamé functions regular on the unit sphere	51
2.6. References	65
3. WAVE PROPAGATION IN ELLIPTICAL CONES	67
3.1. Introduction	67
3.2. The perfectly conducting elliptical cone	70
3.3. The elliptical cone with anisotropic boundary	81
3.4. Appendix	99
3.5. References	100
4. RADIATION CHARACTERISTICS OF ELLIPTICAL HORNS WITH ANISOTROPIC BOUNDARY	101
4.1. Introduction	101
4.2. General properties of radiation fields from elliptical horns with anisotropic boundary	102
4.3. Sphero-conal wave-expansion method for radiation computation	106
4.4. Aperture-field integration method for radiation computation	116
4.4.1. The spherical cap aperture	117
4.4.2. The planar aperture	124

4.5. Numerical and experimental results	128
4.6. Appendices	143
4.6.1. Evaluation of the numerators of (4.39) and (4.40)	143
4.6.2. Expressions for $h_i(x,y)$ , $i = 1,2,\dots,24$	144
4.6.3. Properties of $\Phi(\alpha,\beta)$	145
4.6.4. Expressions for $g_i(x,y)$ , $i = 1,2,\dots,14$	146
4.7. References	147
5. ELECTRICAL PERFORMANCE OF AN OFFSET REFLECTOR ANTENNA SYSTEM FED BY A CORRUGATED ELLIPTICAL HORN RADIATOR	149
5.1. Introduction	149
5.2. Evaluation of the radiation field of the antenna system	150
5.3. Numerical and experimental results	157
5.4. Appendix	163
5.5. References	165
6. SUMMARY AND CONCLUSIONS	167
ACKNOWLEDGEMENTS	171
SAMENVATTING	173
CURRICULUM VITAE	175

ABSTRACT

This thesis deals with the evaluation of the electrical performance of the antenna system that consists of a single offset parabolic reflector fed by a corrugated elliptical horn radiator. Such an antenna system can be designed to have a radiation pattern characterized by a main lobe with an elliptical cross-section, by low sidelobes, and by a low level of cross-polarized radiation, in the case of circular polarization. Then the antenna system is suitable for application as the transmitting antenna of a broadcasting satellite.

The investigation of the antenna-system performance proceeds in two steps. The first contribution of this study concerns the development of a theory that explains the wave propagation and radiation characteristics of a corrugated elliptical horn with arbitrary geometrical parameters. The problem of wave propagation is solved on the basis of the anisotropic surface-impedance model for the corrugated boundary of the horn. The analysis of the horn radiation is based on the Kirchhoff-Huygens approximation in which it is assumed that the radiation field is completely determined by the field distribution at the horn aperture only. Two methods are employed for the calculation of the horn radiation, namely, the aperture-field integration method and the wave-expansion method. Numerical results obtained by both methods and experimental results are presented.

The second contribution of this thesis pertains to a computational procedure developed to numerically determine the radiation field of the antenna system. This (secondary) radiation field is considered as arising from the surface current that is induced in the parabolic reflector by the (primary) radiation field from the horn. The computational procedure contains the horn and reflector geometries as input parameters, and by varying these parameters one may search for an antenna system design that is optimal in some sense with respect to electrical performance. In this manner the computational procedure provides a design through computation versus the alternative of a design based on experimentation. Various numerical and experimental results for the electrical performance of the antenna system are presented.



## 1. GENERAL INTRODUCTION

### 1.1. Introduction

Man-made satellites are nowadays used for many purposes, e.g., for radiocommunications, meteorological observations, navigation, resources exploration and space research. The first communication satellites were placed in low-altitude orbits. Such satellites are not permanently visible from a fixed point on the earth; their positions are not stationary, hence, earth-station antennas with complicated tracking facilities are needed. At present, however, most communication satellites are positioned in the geostationary orbit, which is nominally the circle in the equatorial plane with radius 42164.04 km, centred at the centre of gravity of the earth.

As early as 1945, Arthur C. Clarke suggested the idea to use geostationary satellites for communication purposes [3]. Some 20 years later radiocommunication systems using geostationary satellites indeed became operational. Presently, another important step forward in the application of satellites is due to be made with the introduction of geostationary satellites for the broadcasting-satellite service.

Up till now, broadcast programmes have been transmitted by terrestrial systems. Under normal propagation conditions the reach of a television signal is then confined to the relatively small area of optical coverage around the transmitter. To make possible nation-wide reception of broadcast programmes several terrestrial transmitters are required, thus leading to the use of a lot of frequency assignments. For coverage of sparsely populated, mountainous or remote areas, a terrestrial transmit system is not very attractive from an economic point of view. Also, interference-free reception of additional programmes may not be guaranteed because of the limited frequency spectrum available for terrestrial services.

Economic coverage of large geographical areas, as well as relief from the frequency shortage, can be achieved by use of broadcasting satellites in the geostationary orbit that operate in other (higher) frequency bands. According to the Radio Regulations [10], the broadcasting-satellite service is "a radiocommunication service in which signals transmitted or retransmitted by space stations are intended for direct reception by the general public. In the broadcasting-satellite service, the term 'direct reception'

shall encompass both individual reception and community reception". The planning of the broadcasting-satellite service has been based on the following desiderata:

- individual reception;
- nation-wide coverage;
- efficient use of the radio-frequency spectrum and of the geostationary orbit.

At the World Administrative Radio Conference for the planning of the broadcasting-satellite service held in Geneva in January 1977, regulations have been drawn up for the efficient and orderly use of the frequency spectrum and the geostationary orbit by countries in Region 1 (Europe, USSR, Africa), and in Region 3 (Asia, Australia) [6]. At the Regional Administrative Conference held in Geneva in June - July 1983, regulations have been adopted for the broadcasting-satellite service for the countries in Region 2 (North and South America) [7]. At these conferences various provisions have been agreed on with regard to:

- the reference patterns for the copolarized radiation and the cross-polarized radiation of both the satellite transmitting antenna and the earth-station receiving antenna;
  - the power flux-density from the satellite antenna;
  - the required signal quality at reception;
  - the frequency channels for each country (in the frequency band 11.7 - 12.2 GHz for countries in Regions 2 and 3; in the frequency band 11.7 - 12.5 GHz for countries in Region 1);
  - the use of circularly polarized radiation;
  - the satellite orbital positions;
- and other performance requirements.

The regulations adopted give rise to particularly stringent requirements to be imposed on the electrical performance of the satellite transmitting antenna, namely [6], [7]:

- the radiation must be circularly polarized in the service area;
- in Regions 1 and 3 the main lobe of the radiation pattern should have an elliptical cross-section, and in Region 2 the cross-section may be either elliptically or irregularly shaped;
- the radiation patterns may not exceed certain reference patterns for copolarized and cross-polarized radiation.

If the agreed specifications are not met, a signal with unacceptable level may be received outside the intended coverage area, thus leading to potential interference with signals present in a neighbouring coverage area. In Figure 1.1 coverage areas for some European countries, assuming radiation patterns with an elliptical cross-section, are shown. The various aspects of satellite-broadcasting are discussed in more detail in section 1.2, where we shall also explain the basic concepts and terminology employed.

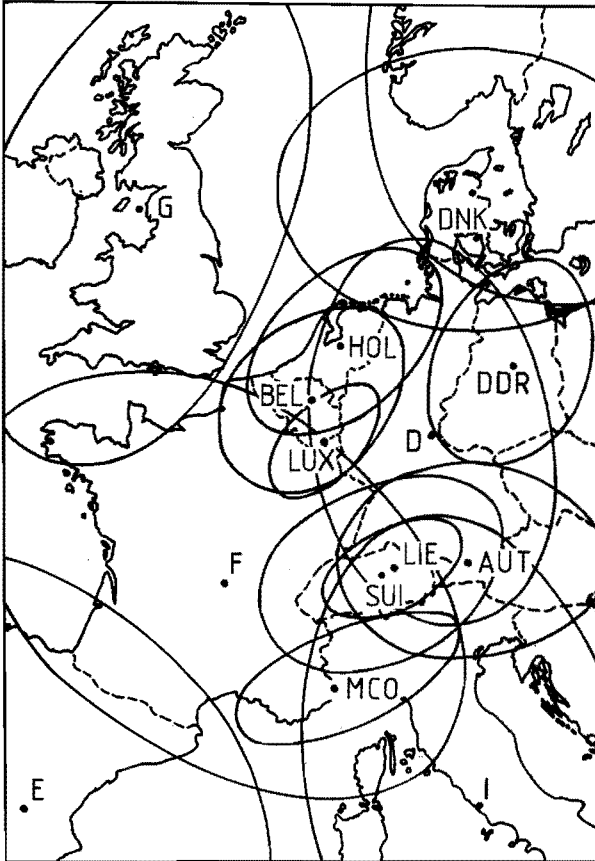


Fig. 1.1. Coverage areas for some European countries, assuming radiation patterns with an elliptical cross-section. The country symbols are taken from Table 1 of the Preface to the International Frequency List [9].

Antennas are key elements in radiocommunication systems. The antenna-system performance depends critically on the feed or the primary radiator. Designs for a broadcasting-satellite transmitting antenna which meets the requirements listed above, are discussed in section 1.3. One of these designs concerns the transmitting antenna of TV-SAT, the broadcasting satellite of the Federal Republic of Germany. The antenna configuration consists of a corrugated elliptical horn radiator and an offset parabolic reflector (see Figure 1.2), and its radiation pattern has a main lobe with an elliptical cross-section. From experiments it was found [5] that the transmitting antenna of TV-SAT has most favourable properties with respect to electrical performance, weight and reflector dimensions. In particular, the electrical performance of the antenna is claimed to meet the stringent requirements that apply in Region 1 [6].

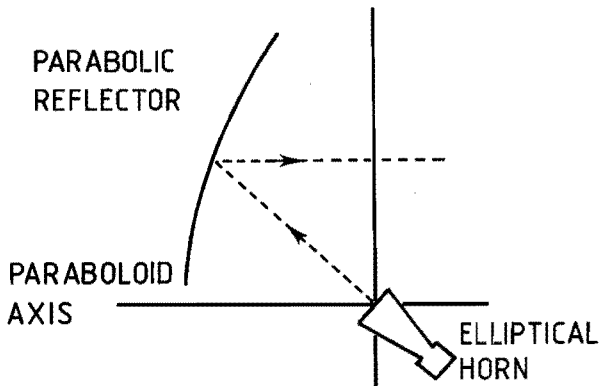


Fig. 1.2. Design for the transmitting antenna for satellite-broadcasting.

In the present thesis we are concerned with a theoretical study of the antenna configuration of Figure 1.2, consisting of an offset parabolic reflector fed by a corrugated elliptical horn radiator. The electrical performance of the antenna configuration is investigated by analytical and numerical methods, and the results obtained are compared with those of experiments. Our investigation proceeds in two steps. In chapters 3 and 4 we present a detailed analysis of the wave propagation and the radiation associated with a corrugated elliptical horn. In chapter 5 a numerical procedure is developed for the calculation of the radiation field of the antenna system, due to the combined action of the corrugated elliptical horn (primary radiator) and the parabolic reflector (secondary

radiator). For a more detailed survey of the contents of this thesis we refer to section 1.4.

In conclusion, we feel that the present study makes two contributions. The main contribution which is also of independent interest, concerns the development of a theory that explains the wave propagation and radiation characteristics of a corrugated elliptical horn with arbitrary geometrical parameters. Our second contribution pertains to the computational procedure developed to numerically determine the radiation field of the antenna system, with the horn and reflector geometries as input parameters. This procedure can be used to predict the electrical performance of an antenna system with given horn and reflector parameters. Next, by varying these parameters one may search for an antenna design that is optimal in some sense with respect to electrical performance. In this manner the computational procedure is a most useful tool in the actual designing of the antenna system. The procedure provides a design through computation versus the alternative of a design based on costly experimentation.

## 1.2. Aspects of broadcasting by satellite

The main feature of a geostationary satellite is its fixed position relative to the earth (except for small but manageable perturbations). Such a satellite is permanently visible from a certain fixed part of the surface of the earth. Hence, the electromagnetic field transmitted by a directional satellite antenna can be received in a specific area on the earth. Another important consequence of the fixed satellite position is that a small earth-station antenna need not be equipped with costly tracking facilities, due to the wide main lobe of its radiation pattern. A disadvantage of operating from the geostationary orbit is the large basic signal attenuation associated with radio-wave propagation over long distances, i.e. the free-space attenuation. Modern satellites, however, can provide sufficient power flux-density for adequate signal reception by means of a small, inexpensive earth-station antenna, thus making possible direct reception by the general public. The required power flux-density at the surface of the earth should be the larger, the smaller the dimensions of the receiving antenna are. Furthermore, the total power transmitted by a satellite antenna is proportional to the size of the area to be covered.

From the Radio Regulations [10] we quote:

"In the broadcasting-satellite service the term 'direct reception by the general public' shall encompass both individual reception (see [10, No. 123]): the reception of emissions from a space station in the broadcasting-satellite service by simple domestic installations and in particular those possessing small antennae; and community reception (see [10, No. 124]): the reception of emissions from a space station in the broadcasting-satellite service by receiving equipment, which in some cases may be complex and have antennae larger than those used for individual reception, and intended for use:

- by a group of the general public at one location; or
- through a distribution system covering a limited area".

In general, an inexpensive receiving antenna of small dimensions has a radiation pattern with rather high sidelobes and a wide main lobe. Consequently, such an antenna has a poor ability to discriminate between different signal sources that transmit electromagnetic fields with similar characteristics such as frequency and polarization. As a result, coordination of services is necessary to keep signal interference at acceptable levels.

Furthermore, the poor ability to discriminate between signal sources limits the spacing of geostationary satellites, and limits the number of times that a frequency can be re-assigned. Receiving earth-station antennas that have a radiation pattern with a narrower main lobe and lower sidelobes towards the geostationary orbit, would make possible a smaller spacing of geostationary satellites and, consequently, a more efficient use of the geostationary orbit, at the expense of earth-station cost. From the Radio Regulations [10] we now quote the definitions of "service area", "coverage area", and "beam area", and the accompanying notes; see Annex 8 to Appendix 30 of [10]. The additional remarks, not between quotation-marks, are ours.

"The service area is the area on the surface of the Earth in which the administration responsible for the service has the right to demand that the agreed protection conditions be provided.

Note: In the definition of service area, it is made clear that within the service area the agreed protection conditions can be demanded. This is the area where there should be at least the wanted power flux-density and protection against interference based on the agreed protection ratio for the agreed percentage of time".

"The coverage area is the area on the surface of the Earth delineated by a contour of a constant given value of power flux-density which would permit the wanted quality of reception in the absence of interference.

Note 1: In accordance with the provisions of No. 2674 of the Radio Regulations, the coverage area must be the smallest area which encompasses the service area.

Note 2: The coverage area, which will normally encompass the entire service area, will result from the intersection of the antenna beam (elliptical or circular) with the surface of the Earth, and will be defined by a given value of power flux-density. For example, in the case of a Region 1 or 3 country with a service planned for individual reception, it would be the area delineated by the contour corresponding to a level of  $-103 \text{ dB(W/m}^2\text{)}$  for 99% of the worst month. There will usually be an area outside the service area but within the coverage area in which the power flux-density will be at least equivalent to the minimum specified value; however, protection against interference will not be provided in this area".

Remark 1: In the case of a Region 2 country, the level should be  $-107 \text{ dB (W/m}^2\text{)}$  [7].

Remark 2: In Region 2, the main lobe of the radiation pattern of a satellite transmitting antenna may have either an elliptically or an irregularly shaped cross-section [7]. The latter cross-section should match with a coverage area bounded by an irregular contour.

"The beam area is the area delineated by the intersection of the half-power beam of the satellite transmitting antenna with the surface of the Earth.

Note: The beam area is simply that area on the Earth's surface corresponding to the  $-3 \text{ dB}$  points on the satellite antenna radiation pattern. In many cases the beam area would almost coincide with the coverage area, the discrepancy being accounted for by the permanent difference in path lengths from the satellite throughout the beam area, and also by the permanent variations, if any, in propagation factors across the area. However, for a service area where the maximum dimension as seen from the satellite position is less than  $0.6^\circ$  (the agreed minimum practicable satellite half-power beamwidth), there could be a significant difference between the beam area and the coverage area".

Remark: The minimum value of  $0.6^\circ$  for the half-power beamwidth applies for countries in Regions 1 and 3 [6]. For Region 2 countries a minimum value of  $0.8^\circ$  has been adopted [7].

For a Region 2 country the coverage area may be irregularly shaped. In that case the satellite transmitting antenna is required to have a radiation pattern with its main lobe having a cross-section that matches the irregular shape. Such a radiation pattern can be realized by means of multiple narrow beams transmitted by multiple primary radiators, which are suitably combined to form the required shape of the main lobe. A specially shaped beam has a number of advantages over a simple elliptical beam, viz.

- the power flux-density throughout the coverage area can be made nearly uniform;
- the transmitted power can be concentrated in the service area;
- the total power transmitted by the satellite antenna is therefore smaller;
- the undesirable spillover of radiation into neighbouring areas is reduced, while coverage of the intended area is maintained. As a result, the number of times that a frequency can be re-assigned, is larger.

However, also some disadvantages should be mentioned, viz.

- an antenna with a radiation pattern of a specially shaped cross-section has larger reflector dimensions;
- the feed system is complex, voluminous and heavy.

In section 1.1 we listed several requirements to be imposed on the electrical performance of a satellite transmitting antenna. In these requirements the polarization of the radiation plays a prominent role. For convenience of the reader we now explain in some detail the concepts of polarization, orthogonal polarization, copolarization and cross polarization.

According to the usual convention the polarization of an electromagnetic field at an observation point P refers to the physical electric field vector  $\vec{E}(\vec{r}, t)$ , where  $\vec{r}$  is the position vector of P and t stands for time. We assume that P is sufficiently far from the sources of the field. Then the field vector at P lies in a plane V, normal to the direction of wave propagation at P. In the case of a harmonic time dependence  $\exp(j\omega t)$  with  $\omega$  denoting the angular frequency, the physical electric field vector  $\vec{E}(\vec{r}, t)$  is given by

$$\vec{E}(\vec{r}, t) = \text{Re}\{\vec{E}(\vec{r}) \exp(j\omega t)\} , \quad (1.1)$$

where Re means taking the real part and  $\vec{E}(\vec{r})$  is the complex electric field vector at P. The latter vector is expressed as

$$\bar{E}(\bar{r}) = \bar{E}_1(\bar{r}) + j\bar{E}_2(\bar{r}), \quad (1.2)$$

where  $\bar{E}_1(\bar{r})$  is the real part and  $\bar{E}_2(\bar{r})$  is the imaginary part of  $\bar{E}(\bar{r})$ ; see Figure 1.3. Then it follows that

$$\bar{E}(\bar{r}, t) = \bar{E}_1(\bar{r})\cos\omega t - \bar{E}_2(\bar{r})\sin\omega t. \quad (1.3)$$

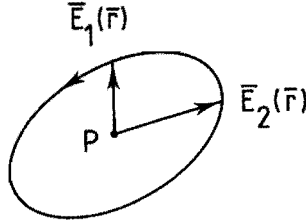


Fig. 1.3. Electric field vectors at the observation point P and polarization ellipse.

It can easily be shown that the extremity of the vector  $\bar{E}(\bar{r}, t)$  at P traverses an ellipse in the plane V, with centre at P. This ellipse is called the polarization ellipse (see Figure 1.3), and the field at P is said to be elliptically polarized. Furthermore, the polarization is called right-handed (left-handed) if the polarization ellipse is traversed in a clockwise (anti-clockwise) direction for an observer looking in the direction of wave propagation at P.

Two special cases are of interest. The extremity of the vector  $\bar{E}(\bar{r}, t)$  at P describes a line segment if the vectors  $\bar{E}_1(\bar{r})$  and  $\bar{E}_2(\bar{r})$  are linearly dependent, or equivalently if

$$\bar{E}(\bar{r}) \times \bar{E}^*(\bar{r}) = 0, \quad \bar{E}(\bar{r}) \neq 0, \quad (1.4)$$

where the asterisk means complex conjugation. In that case the field at P is said to be linearly polarized, and the axial ratio of the polarization ellipse (minor axis divided by major axis) is equal to 0. The polarization ellipse degenerates into a circle if the vectors  $\bar{E}_1(\bar{r})$  and  $\bar{E}_2(\bar{r})$  are perpendicular and have equal length, or equivalently if

$$\bar{E}(\bar{r}) \cdot \bar{E}(\bar{r}) = 0, \quad \bar{E}(\bar{r}) \neq 0. \quad (1.5)$$

Then the field at P is said to be circularly polarized, and the axial ratio of the polarization ellipse is equal to 1.

From (1.2) it is clear that an elliptically polarized field can be represented by the sum of two linearly polarized fields with a phase difference  $\pi/2$ . Generally, any elliptically polarized field can be decomposed into two linearly polarized fields with field vectors pointing in perpendicular directions, but not necessarily with a phase difference  $\pi/2$ . The same result holds for a circularly polarized field but now the linearly polarized constituents do have a phase difference  $\pi/2$ . Furthermore, any elliptically polarized field can also be decomposed into two circularly polarized fields, one with a right-handed polarization and the other with a left-handed polarization. To show this we introduce unit vectors  $\hat{e}_p$  and  $\hat{e}_q$  at P in the plane V, such that  $\hat{e}_p \perp \hat{e}_q$  and  $\hat{e}_p \times \hat{e}_q = \hat{e}_r$  where  $\hat{e}_r$  is the unit vector in the direction of wave propagation at P. Next the electric field  $\bar{E}(\vec{r})$  is expressed as

$$\bar{E}(\vec{r}) = \bar{E}_R(\vec{r}) + \bar{E}_L(\vec{r}), \quad (1.6)$$

in which the complex field vectors  $\bar{E}_R(\vec{r})$  and  $\bar{E}_L(\vec{r})$  are given by

$$\bar{E}_R(\vec{r}) = \frac{1}{2} \{ \bar{E}(\vec{r}) \cdot \hat{e}_p + j \bar{E}(\vec{r}) \cdot \hat{e}_q \} (\hat{e}_p - j \hat{e}_q), \quad (1.7)$$

$$\bar{E}_L(\vec{r}) = \frac{1}{2} \{ \bar{E}(\vec{r}) \cdot \hat{e}_p - j \bar{E}(\vec{r}) \cdot \hat{e}_q \} (\hat{e}_p + j \hat{e}_q). \quad (1.8)$$

Since  $\bar{E}_R(\vec{r}) \cdot \bar{E}_R(\vec{r}) = \bar{E}_L(\vec{r}) \cdot \bar{E}_L(\vec{r}) = 0$ , the fields  $\bar{E}_R(\vec{r})$  and  $\bar{E}_L(\vec{r})$  are circularly polarized, and it can easily be verified that the polarization is right-handed for  $\bar{E}_R(\vec{r})$  and left-handed for  $\bar{E}_L(\vec{r})$ . As a special case of the present result we have: any linearly polarized field can be represented by the sum of a right-handed and a left-handed circularly polarized field with the same strength.

We now come to the definition of the concept of orthogonal polarization. Two elliptically polarized fields are said to be orthogonally polarized if their polarization ellipses

- have the same axial ratio;
- have perpendicular major axes (not applicable for circular polarizations);
- are traversed in opposite senses (not applicable for linear polarizations).

By means of this concept the previous decomposition results can be reformulated as follows. Any elliptically polarized field can be decomposed into an orthogonally polarized pair of linearly polarized fields, and

into an orthogonally polarized pair of circularly polarized fields.

Finally, the polarization type of an antenna radiation field is conveniently described in terms of "copolarization" and "cross polarization". The copolarization is a reference polarization which is usually taken to be a linear polarization with a given direction or a circular polarization with a given sense of rotation. The term cross polarization refers to the polarization orthogonal to the copolarization.

For convenience we also assign a polarization type to antennas, and we shortly speak of elliptically, linearly and circularly polarized antennas. For a transmitting antenna the polarization type is identical to that of the field radiated by the antenna. The polarization type of a receiving antenna is identical to the polarization type of the incident field that gives rise to maximum signal reception. For maximum signal transfer between a transmitting antenna and a receiving antenna, it is necessary that the polarization ellipses associated with the antennas

- have the same axial ratio;
- have parallel major axes (not applicable for circular polarizations);
- are traversed in the same directions (not applicable for linear polarizations);

in that case the antennas are said to be copolarized [11]. A circularly polarized receiving antenna, located in the coverage area of a circularly polarized transmitting antenna, should be simply pointed at the latter antenna, without further alignment being necessary for maximum signal reception. In this respect circularly polarized radiation is preferable to radiation of another polarization type, and this explains the requirement that the radiation must be circularly polarized in the service area [6], [7]. The absence of the need to align the receiving antenna makes circularly polarized radiation particularly attractive for satellite-broadcasting in the 12 GHz frequency band, where a very large number of receiving antennas (whether for individual or community reception) is a condition for economic viability of the service.

Signal transfer will be suppressed if the transmitting antenna and the receiving antenna are orthogonally polarized. Hence, by use of orthogonally polarized fields, emissions in the same frequency band from neighbouring satellites can be discriminated from each other. Frequency re-use by polarization discrimination therefore contributes to the efficient use

of the frequency spectrum and of the geostationary orbit. In practice, the suppression of orthogonally polarized signals is not complete, due to imperfect polarization characteristics of both the satellite transmitting antenna and the earth-station receiving antenna, i.e., the copolarized wave as well as the cross-polarized wave are radiated and received. In addition, a transmitted wave will be depolarized on its path through the atmosphere, due to various atmospheric effects, for instance rain [8]. Depolarization means that an initially copolarized radiation is converted into radiation that also contains a cross-polarized component, which may lead to interference. Because of the depolarization effects induced by the atmosphere it is necessary to further tighten the requirements on the antenna polarization characteristics.

We end this section by specifying the reference patterns for the copolarized radiation and the cross-polarized radiation of a broadcasting-satellite transmitting antenna. The reference patterns in Figure 1.4 apply to the circularly polarized radiation of a transmitting antenna for countries in Regions 1 and 3 [6]. The abscissa in Figure 1.4 is the angle  $\Phi$  normalized to  $\Phi_0$ , that is the angle corresponding to the -3 dB beam-width of the reference pattern for the copolarized radiation. In practice, it may be difficult to meet the specification for the copolarized radiation at angles  $\Phi/\Phi_0 \approx 1.5$  which requires the sidelobe radiation level to be below -30 dB, and the specification for the cross-polarized radiation which must not exceed a level of -33 dB. The reference patterns in Figure 1.5 apply to the circularly polarized radiation of a transmitting antenna for countries in Region 2 [7]. Also some other reference patterns, showing a faster roll-off of the main lobe of the copolarized radiation beyond the angle  $\Phi/\Phi_0 = 0.5$  (leading to reduced interference), have been adopted [7]. From Figure 1.5 we observe that the sidelobe radiation level of the copolarized radiation is required to be below -25 dB, whereas the cross-polarized radiation must not exceed a level of -30 dB. These specifications are less severe than the specifications shown in Figure 1.4.

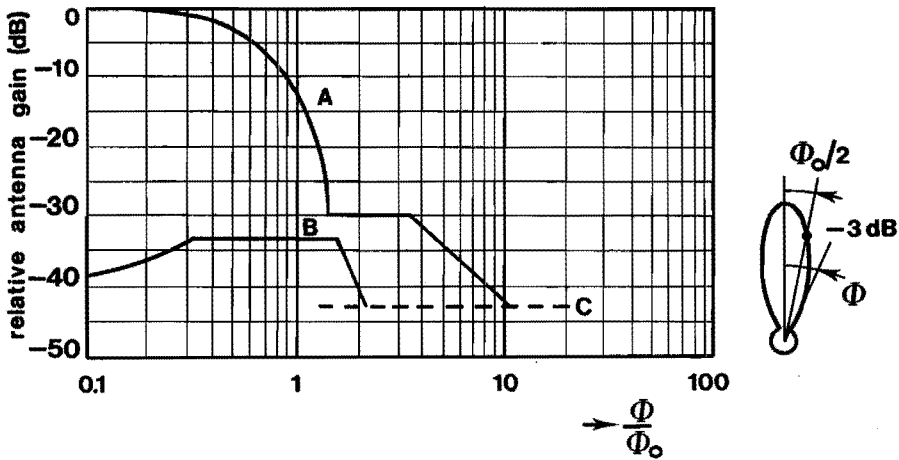


Fig. 1.4. Reference patterns for copolarized radiation (A) and cross-polarized radiation (B) from a broadcasting-satellite transmitting antenna for countries in Regions 1 and 3. Curve C represents the minus on-axis gain. Curves A and B continue as curve C after their intersections with curve C [6].

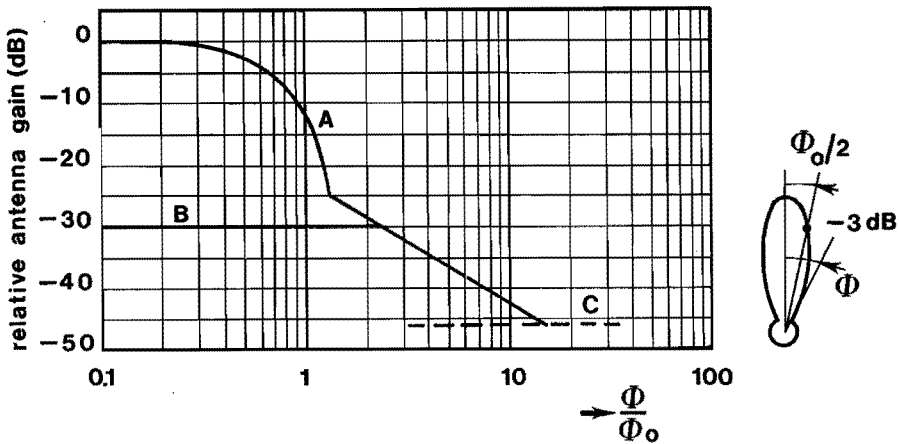


Fig. 1.5. Reference patterns for copolarized radiation (A) and cross-polarized radiation (B) from a broadcasting-satellite transmitting antenna for countries in Region 2. Curve C represents the minus on-axis gain. Curve A continues as curve C after its intersection with curve C. Curve B continues as curve A after its intersection with curve A [7].

### 1.3. Designs for broadcasting-satellite transmitting antennas

As pointed out in the previous sections, the electrical performance of a satellite transmitting antenna should meet stringent requirements, in particular with regard to the sidelobe radiation level of the copolarized radiation and to the level of the cross-polarized radiation. These requirements cannot possibly be met by a transmitting antenna system in which blockage of radiation occurs, i.e. where the wave reflected by the main reflector is partly blocked and scattered by the feed system and its supporting struts [4]. Therefore, an axisymmetric single reflector antenna such as the front-fed parabolic antenna, and axisymmetric dual reflector antennas such as the Cassegrain antenna and the Gregorian antenna (both with a parabolic main reflector), deserve no further consideration. Blockage can be avoided by tilting the feed system so as to use another portion of the reflecting parabolic surface as the main reflector. The resulting designs are known as the single offset parabolic reflector antenna, the offset Cassegrain antenna and the offset Gregorian antenna, respectively. The latter two are known as double offset antennas.

An additional advantage of an offset transmitting antenna is the absence of direct reflection of radiation power back into the feed system. This results in a low voltage standing-wave ratio and, in case of multiple feed elements, in a low electromagnetic coupling between the elements via the reflector. Offset Cassegrain and offset Gregorian antennas are not as compact as the single offset reflector antenna. Therefore, the use of a double offset antenna as a satellite antenna is restricted by the volumetric constraints imposed by the dimensions of present-day launch vehicles [5]. Also, in a double offset antenna the requirement on the sidelobe radiation level may not easily be met owing to the spillover of primary radiation beyond the subreflector into directions close to the main beam direction, and owing to diffraction effects arising at the rim of the subreflector [5]. Obviously, these effects do not occur in a single offset reflector antenna.

In view of the stringent requirements imposed on the dimensions and on the electrical performance of a broadcasting-satellite transmitting antenna, the single offset reflector antenna is the most likely candidate to be used in an antenna-system design. Therefore, the discussion is now further restricted to antenna systems with a single offset parabolic reflector that is fed by a primary radiator.

According to the provisions agreed on in [6], [7] (see section 1.1), circularly polarized radiation is to be used for satellite broadcasting in the 12 GHz frequency band. Now a circularly polarized field when reflected by a parabolic reflector, remains circularly polarized but with opposite sense of rotation [2]. Therefore, the requirement on the polarization of the secondary radiation translates into the requirement that the primary radiation incident on the parabolic reflector must be circularly polarized. A single offset parabolic reflector antenna transmitting circularly polarized radiation, is known to exhibit a slightly displaced (squinted) radiation pattern. The squint occurs in the plane perpendicular to the plane of offset, and its direction depends on whether the circular polarization is right-handed or left-handed [2]. The squint effect can be compensated for by antenna pointing.

Turning to the requirement that the main lobe of the secondary radiation pattern should have either an elliptically or an irregularly shaped cross-section, we shall discuss two current types of antenna systems.

The first type employs a single offset parabolic reflector with an elliptical aperture, and a feed system that consists of an array of primary radiators fed by a power distribution network. The required secondary radiation pattern is realized by a proper combination of the radiation patterns caused by each of the primary radiators. For each array element one needs a polarizer, a transition from the feeding waveguide to the radiator, an attenuator and a phase shifter. Such an array-type feed tends to become complex, bulky and heavy. Apart from the power loss in the feeding network, an array-type feed exhibits some further drawbacks such as

- degradation of the polarization purity of the radiation of the array, due to the electromagnetic coupling between the array elements;
- high spillover loss of radiation beyond the main reflector, due to high sidelobes in the radiation pattern of the feed system.

Two examples of such an antenna system with multiple feed elements are now briefly reviewed. The first example concerns the transmitting antenna of the broadcasting satellite of Japan [12]. In this case the array-type feed consists of three conical horns, the focal length of the reflector is 0.85 m, and the elliptical aperture of the reflector has a major and a minor axis of 1.59 m and 1.03 m, respectively. According to the regulations in [6], the angles of -3 dB beamwidth in the principal planes of the secondary radiation pattern are allowed to be  $3.50^\circ$  and  $3.30^\circ$ . The

radiation patterns due to the three primary radiators have been properly combined such that the resultant secondary radiation pattern has a main lobe with an irregularly shaped cross-section that effectively covers the service area of Japan. From measured results published in [12] it is concluded that the levels of both the copolarized sidelobe radiation and the cross-polarized radiation meet the requirements which are in force [6].

Our second example of an antenna system with multiple feed elements concerns the satellite transmitting antenna proposed for the coverage of Great Britain [1]. Here, the angles of  $-3$  dB beamwidth in the principal planes of the secondary radiation pattern should be  $1.84^\circ$  and  $0.72^\circ$  [6]. The array-type feed consists of ten cylindrical waveguides, the focal length of the parabolic reflector is 1.64 m, and the elliptical aperture of the reflector has a major and a minor axis of 2.72 m and 1.05 m, respectively. The radiation patterns due to the primary radiators are combined to yield a resultant radiation pattern, the main lobe of which has the required elliptical cross-section at the  $-3$  dB power level. From the measured results reported in [1], it is concluded that both the requirement on the elliptical cross-section of the main lobe and the requirement on the copolarized sidelobe radiation (level below  $-30$  dB), can be met. However, the requirement on the cross-polarized radiation (level below  $-33$  dB) will not be satisfied, due to the degraded polarization purity of the radiation of the array-type feed.

We now come to our second type of antenna system, which employs a single offset parabolic reflector and a feed system that consists of one single primary radiator, viz., either a corrugated rectangular horn or a corrugated elliptical horn. For both types of horns the copolarized radiation has a pattern with an elliptical cross-section. Therefore, such a primary radiator can be used for the efficient illumination of a reflector with a (nearly) elliptical boundary. Whether a rectangular or an elliptical horn is considered for application in a broadcasting-satellite transmitting antenna, depends on the polarization purity of the circularly polarized radiation obtainable with such a horn.

As an example of an antenna system with a single primary radiator, we refer to the transmitting antenna of the broadcasting satellite TV-SAT of the Federal Republic of Germany [5]. According to the provisions in [6], the angles of  $-3$  dB beamwidth in the principal planes of the secondary radiation pattern should be  $1.62^\circ$  and  $0.72^\circ$ . The primary radiator of the

antenna system is a corrugated elliptical horn. From theoretical and experimental analyses it has been found that an elliptical horn is preferable to a corrugated rectangular horn, because for an elliptical horn the required polarization purity of the radiation is obtainable over a broader frequency band [5]. Well-designed corrugated elliptical horns are indeed capable of generating circularly polarized radiation with a radiation pattern that has an elliptical cross-section, in a frequency band that is sufficiently large for the application under consideration [13]. It has also been found for the transmitting antenna of TV-SAT, that a feed system consisting of a corrugated elliptical horn is preferable to an array-type feed [5]. Advantages reported concern the directive gain which is 0.3 dB higher, a lower level of the sidelobe radiation, and a lower weight. The focal length of the parabolic reflector of TV-SAT is 1.5 m. The offset reflector coincides with that part of the parabolic surface that matches the radiation pattern with elliptical cross-section, caused by the tilted horn [5]. As a result, a nearly elliptical reflector aperture is obtained, see Figure 1.6. The aperture dimensions in the offset plane and in the plane perpendicular to that, are 1.4 m and 2.7 m, respectively. From the measured results published in [5], it is concluded that the electrical performance of the transmitting antenna of TV-SAT meets both the requirements on the copolarized radiation (sidelobe radiation level below -30 dB, and elliptical cross-section of the main lobe of the secondary radiation pattern), and the cross-polarized radiation (level below -33 dB).

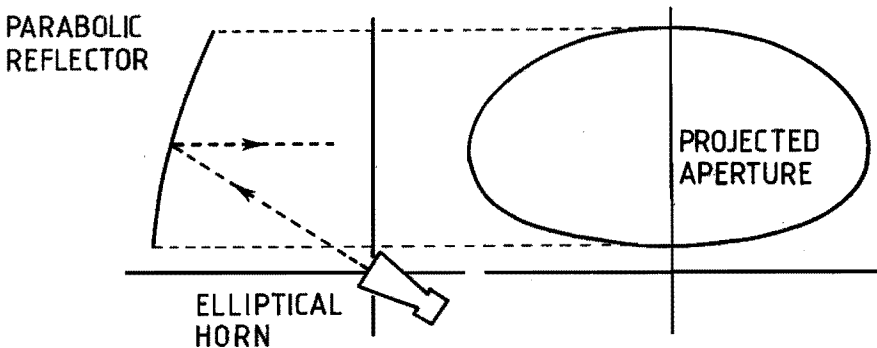


Fig. 1.6. Offset parabolic reflector antenna and its projected aperture.

Finally we summarize the main results of this section:

1. The stringent requirements on the dimensions and on the electrical performance of a broadcasting-satellite transmitting antenna can be met by an antenna system in which a single offset reflector antenna is used.
2. The main lobe of the secondary radiation pattern of a multiple-feed antenna system can be composed to have an irregularly shaped cross-section by use of a properly excited array-type feed.
3. In order to realize that the main lobe has an elliptically shaped cross-section, either a multiple-element or a single-element feed system can be employed. Suitable feed systems with a single element are the corrugated rectangular and elliptical horns.
4. Disadvantages of a multiple-element feed system versus a single-element feed system, refer to a greater complexity, larger dimensions and weight, and potentially, a degraded electrical performance. Advantages include operational flexibility (use for different countries) and, potentially, more efficient coverage of the service area.

#### 1.4. Survey of the contents

The ultimate goal of this thesis is to determine the radiation field of an antenna system that consists of an offset parabolic reflector fed by a corrugated elliptical horn radiator. The approach to achieve this goal is most conveniently described in backward order. The final radiation field of the antenna system is considered to be due to the surface current  $\bar{J}_s$  induced in the parabolic reflector surface. Then the radiation field can be determined from a well-known integral representation for the electromagnetic field in terms of the current  $\bar{J}_s$ . The surface current is induced by the primary radiation of the corrugated elliptical horn, which acts as an incident wave on the reflector surface. The exact value of the current  $\bar{J}_s$  cannot be determined analytically. Therefore we employ the standard physical-optics approximation in which the surface current is approximated by  $\bar{J}_s = 2\hat{n} \times \bar{H}^i$ . Here,  $\bar{H}^i$  is the magnetic field of the incident primary radiation at the reflector surface, and  $\hat{n}$  is the unit vector normal to the reflector surface at the point of incidence pointing towards the illuminated side of the reflector.

The next step deals with the evaluation of the magnetic field  $\bar{H}^i$  at the reflector surface. As a first option the field  $\bar{H}^i$  can be found from

measured data [5]. However, such a specification of the field at the reflector surface requires a large number of measurements to be performed on an already manufactured horn. Secondly, the magnetic field  $\vec{H}^{-i}$  can be determined from an integral representation for the primary radiation field in terms of the field distribution in the aperture of the elliptical horn, based on the Kirchhoff-Huygens approximation. Of course, the latter analytical approach is feasible only if the aperture field is known. The second approach has been followed by Vokurka [13] in the case of an elliptical horn with a small flare angle. Thereby the field in the aperture of the corrugated horn is taken to be equal to the modal field of an infinitely long corrugated elliptical waveguide. More accurate results are obtained if the modal field is multiplied by a proper phase distribution function that accounts for the spherical-wave nature of the aperture field. Clearly, Vokurka's analysis [13] is only valid for elliptical horns with small flare angle.

In the present thesis the magnetic field  $\vec{H}^{-i}$  at the reflector surface is analytically determined by means of the Kirchhoff-Huygens integral representation involving the field distribution in the aperture of the corrugated elliptical horn. The aperture field is now taken to be equal to the modal field of an infinitely long corrugated elliptical cone. In order to determine this modal field we develop a new theory of electromagnetic wave propagation in a corrugated elliptical cone with an arbitrary flare angle. In this manner the previous restriction to elliptical horns with small flare angle [13] is removed. The modal field components are found to be represented by series of Lamé functions. The latter special functions come up in the solution of the Helmholtz equation by separation of variables in sphero-conal coordinates. These coordinates are most convenient for the present purpose because they fit the geometry of the elliptical cone.

In conclusion, to evaluate the secondary radiation pattern of a single offset parabolic reflector antenna fed by a corrugated elliptical horn, we need to know:

1. the induced current distribution on the reflector surface;
2. the electromagnetic field at the reflector, due to the primary radiation of the horn;
3. the field in the aperture of the corrugated elliptical horn;
4. the modal field in the corrugated elliptical cone.

The topics in this list determine, in reversed order, the subject-matter of the subsequent chapters of the present thesis.

Chapter 2 deals with a number of mathematical preliminaries. The geometry of the elliptical-conical horn is described in terms of spherical coordinates. In these coordinates the Helmholtz equation can be solved by separation of variables, and the mathematical functions involved, viz. Lamé functions, are treated in detail.

In chapter 3 the problem of wave propagation in a corrugated elliptical cone is solved on the basis of the anisotropic surface-impedance model for the corrugated wall of the cone. As a result, the modal fields in a corrugated elliptical cone are determined.

In chapter 4 the radiation properties of corrugated elliptical horns are investigated. Two analytical methods are developed for the evaluation of the radiation patterns, namely, the wave-expansion method and the aperture-field integration method. General properties of radiation fields from corrugated elliptical horns are derived, and numerical and experimental results are presented for the radiation fields of a number of horns.

Chapter 5 deals with the radiation characteristics of the antenna system that consists of a single offset parabolic reflector illuminated by a corrugated elliptical horn. Numerical results for the final radiation field are compared with experimental results.

In chapter 6 the main results of this thesis are summarized.

1.5. References

- [1] Christie, M.G., D.A. Hawthorne, A.G. Martin, and P.C. Wilcockson, A cluster primary feed for an elliptical pattern antenna requiring R.F. sensing. Proc. Europ. Microw. Conf., Helsinki, 1982, 649-654.
- [2] Chu, T.S., and R.H. Turrin, Depolarization properties of offset reflector antennas. IEEE Trans. Antennas and Propagat. AP-21 (1973), 339-345.
- [3] Clarke, A.C., Extra-terrestrial relays. Can rocket stations give world-wide radio coverage? Wireless World 51 (1945), 305-308.
- [4] Clarricoats, P.J.B., Some recent advances in microwave reflector antennas. Proc. IEE 126 (1979), 9-25.
- [5] Fasold, D., and M. Lieke, A circularly polarized offset reflector antenna for direct broadcasting satellites. Proc. Europ. Microw. Conf., Nürnberg, 1983, 896-901.
- [6] Final Acts of the World Administrative Radio Conference for the Planning of the Broadcasting-Satellite Service in Frequency Bands 11.7 - 12.2 GHz (in Regions 2 and 3) and 11.7 - 12.5 GHz (in Region 1). International Telecommunication Union, Geneva, 1977.
- [7] Final Acts of the Regional Administrative Conference for the Planning of the Broadcasting-Satellite Service in Region 2 (SAT-83). International Telecommunication Union, Geneva, 1984.
- [8] Ippolito, L.J., Radio propagation for space communications systems. Proc. IEEE 69 (1981), 697-727.
- [9] Preface to the International Frequency List. International Telecommunication Union, Geneva, 1979.
- [10] Radio Regulations. International Telecommunication Union, Geneva, 1982.
- [11] Rumsey, V.H., G.A. Deschamps, M.L. Kales, and J.L. Bohnert, Techniques for handling elliptically polarized waves with special reference to antennas. Proc. IRE 39 (1951), 533-552.
- [12] Sonoda, S., M. Kajikawa, T. Ohtake, and M. Ueno, BS-2 spacecraft design, with emphasis on shaped beam antenna. Proc. 1st Canadian Domestic and Int. Satellite Communications Conf., Ottawa, June 1983. Ed. by K Feher, North-Holland Publishing Co., Amsterdam, 1983, 22.5.1 - 22.5.4.
- [13] Vokurka, V.J., Elliptical corrugated horn for broadcasting-satellite antennas. Electronics Letters 15 (1979), 652-654.



## 2. SPHERO-CONAL COORDINATES AND LAMÉ FUNCTIONS

### 2.1. Introduction

In this chapter we give, in sufficient detail, the tools needed in the investigation of wave propagation and radiation problems for elliptical conical horns, which will be dealt with in subsequent chapters. Our first concern is to introduce suitable coordinates to describe the geometry of the horn. Furthermore, the mathematical functions which are the solutions of the separated Helmholtz equation will be discussed. A familiar method for solving the scalar Helmholtz equation is separation of variables. For that purpose we need an orthogonal system of coordinates that fits the elliptical-conical geometry of the horn. In addition, separation into ordinary differential equations, having easy-to-find solutions, must be possible. The coordinate system that meets these requirements is the sphero-conal system in trigonometric form [5], [7]. As we will see, its coordinate surfaces have a simple geometrical interpretation and their computation only involves sines and cosines. Furthermore, the transition to the well-known spherical coordinate system can be easily established. Thus the solutions to field problems for circular-conical devices are contained in the elliptical-conical solutions.

Separating the Helmholtz equation we arrive at three ordinary differential equations:

- (a) the differential equation of "spherical" Bessel functions;
- (b) the Lamé differential equation with nonperiodic boundary conditions;
- (c) the Lamé differential equation with periodic boundary conditions.

The solutions of the first and third equations have been well documented for quite a long time. For "spherical" Bessel functions we can refer to [1, Chapter 10], and for the periodic Lamé functions to [3], [4]. It is, however, only recently that the solutions of the nonperiodic Lamé equation have been shown to be connected with those of the periodic Lamé equation. This contribution to the theory of Lamé functions is due to Jansen and can be found in his Ph.D. thesis [5] and in a slightly revised version [6]. This knowledge of the nonperiodic Lamé functions will facilitate the investigation of wave propagation and radiation problems for elliptical horns.

2.2. The trigonometric representation of sphero-conal coordinates

The sphero-conal coordinates, denoted by  $(r, \theta, \phi)$ , are related to Cartesian coordinates  $(x, y, z)$  by

$$x = r \sin \theta \cos \phi, \tag{2.1}$$

$$y = r(1 - k^2 \cos^2 \theta)^{\frac{1}{2}} \sin \phi, \tag{2.2}$$

$$z = r \cos \theta (1 - k'^2 \sin^2 \phi)^{\frac{1}{2}}, \tag{2.3}$$

where

$$k^2 + k'^2 = 1, \quad 0 \leq k \leq 1, \quad 0 \leq k' \leq 1, \tag{2.4}$$

$$r \geq 0, \quad 0 \leq \theta \leq \pi, \quad 0 \leq \phi \leq 2\pi.$$

The representation by equations (2.1)-(2.3) is chosen to let the sphero-conal system coincide with the spherical coordinate system, in its commonly used form, when  $k' = 0$ .

The surfaces  $r = r_0$ ,  $\theta = \theta_0$  and  $\phi = \phi_0$ , where  $r_0$ ,  $\theta_0$  and  $\phi_0$  are constants, are called coordinate surfaces (see Figure 2.1a). Before

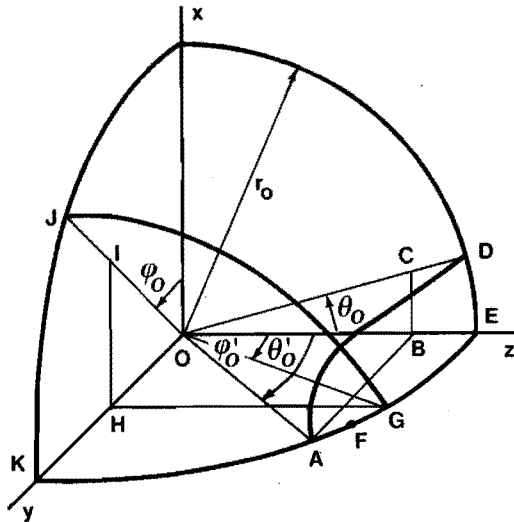


Fig. 2.1a. The sphero-conal coordinate system.

investigating the geometry of the coordinate surfaces, we will briefly discuss coordinate curves, unit vectors and scale factors of the spherical coordinate system.

Each pair of coordinate surfaces intersects in a coordinate curve, designated by the variable coordinate. A  $\phi$ -curve, for instance, is given by  $r = r_0$ ,  $\theta = \theta_0$  and  $0 \leq \phi < 2\pi$ . The various coordinate curves on the surface  $r = r_0$  in Figures 2.1a and 2.1b are described in terms of the angular coordinates  $\theta, \phi$  as follows (at point F,  $\theta = 0$  and  $\phi = \pi/2$ ),

- DA:  $\theta = \theta_0$ ,  $0 \leq \phi \leq \pi/2$ ;
- ED:  $0 \leq \theta \leq \theta_0$ ,  $\phi = 0$ ;
- EF:  $\theta = 0$ ,  $0 \leq \phi \leq \pi/2$  or  $\pi \geq \phi \geq \pi/2$ ;
- FA:  $0 \leq \theta \leq \theta_0$ ,  $\phi = \pi/2$ ;
- GJ:  $0 \leq \theta \leq \pi/2$ ,  $\phi = \phi_0$ ;
- JK:  $\theta = \pi/2$ ,  $\phi_0 \leq \phi \leq \pi/2$ .

We note that GJ is part of a  $\theta$ -curve, along which only the coordinate  $\theta$  varies, while DA is part of a  $\phi$ -curve, along which only the coordinate  $\phi$  varies. Furthermore, we observe that each point of EF is described by two coordinate triples, viz.  $(r_0, 0, \phi)$  and  $(r_0, 0, \pi - \phi)$ . The coordinate system is called orthogonal if the coordinate surfaces intersect at right angles. For such a system, the set of unit vectors tangent to the coordinate curves, and in the direction of increasing coordinate values, is at each point identical with a set of unit vectors normal to the coordinate surfaces. Denote the unit vectors of the Cartesian coordinate system by  $\hat{e}_x, \hat{e}_y, \hat{e}_z$  and let  $\bar{r} = x \hat{e}_x + y \hat{e}_y + z \hat{e}_z$  be the position vector of a point P. Then the vectors tangent to the  $r$ -,  $\theta$ - and  $\phi$ -curves at P are given by, respectively

$$\frac{\partial}{\partial r}(\bar{r}) = \begin{bmatrix} \sin\theta \cos\phi \\ (1 - k^2 \cos^2\theta)^{1/2} \sin\phi \\ \cos\theta(1 - k^2 \sin^2\phi)^{1/2} \end{bmatrix} \quad (2.5)$$

$$\frac{\partial}{\partial \theta} (\bar{r}) = r \begin{bmatrix} \cos \theta \cos \phi \\ \frac{k^2 \cos \theta \sin \theta}{(1 - k^2 \cos^2 \theta)^{\frac{1}{2}}} \sin \phi \\ -\sin \theta (1 - k'^2 \sin^2 \phi)^{\frac{1}{2}} \end{bmatrix} , \quad (2.6)$$

$$\frac{\partial}{\partial \phi} (\bar{r}) = r \begin{bmatrix} -\sin \theta \sin \phi \\ (1 - k^2 \cos^2 \theta)^{\frac{1}{2}} \cos \phi \\ -k'^2 \cos \theta \frac{\sin \phi \cos \phi}{(1 - k'^2 \sin^2 \phi)^{\frac{1}{2}}} \end{bmatrix} . \quad (2.7)$$

These vectors are not necessarily of unit length. Their lengths are called the scale factors of the coordinate system. Denoting these factors by  $h_r$ ,  $h_\theta$  and  $h_\phi$ , we find from equations (2.5)-(2.7) that

$$h_r = \left| \frac{\partial}{\partial r} (\bar{r}) \right| = 1 , \quad (2.8)$$

$$h_\theta = \left| \frac{\partial}{\partial \theta} (\bar{r}) \right| = r \frac{(k^2 \sin^2 \theta + k'^2 \cos^2 \phi)^{\frac{1}{2}}}{1 - k^2 \cos^2 \theta} , \quad (2.9)$$

$$h_\phi = \left| \frac{\partial}{\partial \phi} (\bar{r}) \right| = r \frac{(k^2 \sin^2 \theta + k'^2 \cos^2 \phi)^{\frac{1}{2}}}{1 - k'^2 \sin^2 \phi} . \quad (2.10)$$

The unit vectors  $\hat{e}_r$ ,  $\hat{e}_\theta$ ,  $\hat{e}_\phi$ , respectively in the direction of increasing  $r$ ,  $\theta$  and  $\phi$ , are given by

$$\hat{e}_r = h_r^{-1} \frac{\partial}{\partial r} (\bar{r}) , \quad (2.11)$$

$$\hat{e}_\theta = h_\theta^{-1} \frac{\partial}{\partial \theta} (\bar{r}) , \quad (2.12)$$

$$\hat{e}_\phi = h_\phi^{-1} \frac{\partial}{\partial \phi} (\bar{r}) . \quad (2.13)$$

We note that the vector product  $\hat{e}_r \times \hat{e}_\theta$  equals  $\hat{e}_\phi$ . Hence  $r, \theta, \phi$  form in this order a right-handed system of coordinates. In Figure 2.1b it is

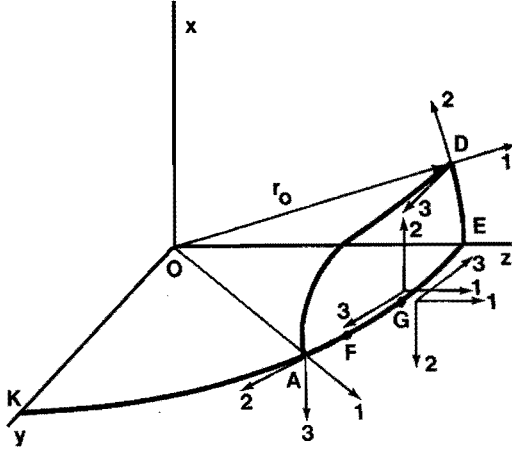


Fig. 2.1b. Unit vectors at various points.

1:  $\hat{e}_r$ ; 2:  $\hat{e}_\theta$ ; 3:  $\hat{e}_\phi$ .

shown how the sphero-conal unit vectors change direction from point to point. Special attention must be paid to the unit vectors  $\hat{e}_\theta$ ,  $\hat{e}_\phi$ , tangent to the surface  $r = r_0$ , at points in the  $yz$ -plane. Expressions for the latter unit vectors in terms of the Cartesian unit vectors  $\hat{e}_x$ ,  $\hat{e}_y$ ,  $\hat{e}_z$  follow from equations (2.11)-(2.13) and are given below. We will distinguish three cases:

1. Curve EF:  $\theta = 0$ ,  $0 \leq \phi \leq \pi/2$ . Then we find

$$\hat{e}_\theta = \hat{e}_x, \hat{e}_\phi = (1 - k'^2 \sin^2 \phi)^{1/2} \hat{e}_y - k' \sin \phi \hat{e}_z.$$

2. Curve FE:  $\theta = 0$ ,  $\pi/2 \leq \phi \leq \pi$ . In this case we get

$$\hat{e}_\theta = -\hat{e}_x, \hat{e}_\phi = -(1 - k'^2 \sin^2 \phi)^{1/2} \hat{e}_y + k' \sin \phi \hat{e}_z.$$

3. Curve FK:  $0 \leq \theta \leq \pi/2$ ,  $\phi = \pi/2$ . Now we have

$$\hat{e}_\theta = k \cos \theta \hat{e}_y - (1 - k^2 \cos^2 \theta)^{1/2} \hat{e}_z, \hat{e}_\phi = -\hat{e}_x.$$

Note that, for points with  $r = r_0$  and  $\theta = 0$ , we must specify the  $\phi$ -interval in order to obtain an unambiguous relation between sphero-conal and Cartesian unit vectors.

The arc-length element  $ds$  along a coordinate curve at  $P$  is

$$ds = dr \quad , \quad (r\text{-curve}), \quad (2.14)$$

$$ds = h_\theta d\theta \quad , \quad (\theta\text{-curve}), \quad (2.15)$$

$$ds = h_\phi d\phi \quad , \quad (\phi\text{-curve}). \quad (2.16)$$

Now we will discuss the geometry of the coordinate surfaces in more detail. The following equations for the coordinate surfaces can be obtained from (2.1)-(2.3) by eliminating the sphero-conal coordinates which are variable for the surface under consideration:

$$r = r_0 : x^2 + y^2 + z^2 = r_0^2 ; \quad (2.17)$$

$$\theta = \theta_0 : \frac{x^2}{\sin^2 \theta_0} + \frac{k^2 y^2}{1 - k^2 \cos^2 \theta_0} = \frac{z^2}{\cos^2 \theta_0} ; \quad (2.18)$$

$$\phi = \phi_0 : \frac{x^2}{\cos^2 \phi_0} + \frac{k'^2 z^2}{1 - k'^2 \sin^2 \phi_0} = \frac{y^2}{\sin^2 \phi_0} . \quad (2.19)$$

Equation (2.17) represents a sphere of radius  $r_0$  with centre at the origin (see Figure 2.1a). Equation (2.18) describes an elliptical cone along the  $z$ -axis with vertex at the origin. The intersection of this cone  $\theta = \theta_0$  and the plane  $z = z_1 = r_0 k \cos \theta_0$  ( $= OB$ ) is an ellipse, described by

$$\frac{x^2}{z_1^2 \tan^2 \theta_0} + \frac{y^2}{z_1^2 (k^{-2} \sec^2 \theta_0 - 1)} = 1 ; \quad (2.19a)$$

see Figure 2.1a. We note that  $\tan^2 \theta_0 \leq k^{-2} \sec^2 \theta_0 - 1$ , hence the minor axis lies in the  $xz$ -plane and the major axis in the  $yz$ -plane. The semi-minor axis  $b_\theta$  is

$$b_\theta = BC = |z_1 \tan \theta_0| , \quad (2.20)$$

and the semi-major axis  $a_\theta$  is

$$a_{\theta} = AB = \left| \frac{z_1 (1 - k^2 \cos^2 \theta_o)^{1/2}}{k \cos \theta_o} \right| = |z_1 \tan \theta'_o|, \quad (2.21)$$

where  $\theta'_o$  is the angle between OA and the z-axis; see Figure 2.1a. From equation (2.20) it can be seen that the cone has a semi-opening angle  $\theta_o$  in the xz-plane, measured from the positive z-axis. The aspect ratio of the ellipse (minor axis divided by major axis) is

$$a_{r\theta}(k, \theta_o) = \tan \theta_o / \tan \theta'_o. \quad (2.22)$$

In Figures 2.2 and 2.3,  $\theta'_o$  is plotted against  $\theta_o$  and  $a_{r\theta}$ , respectively.

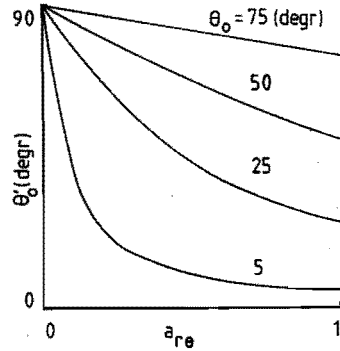
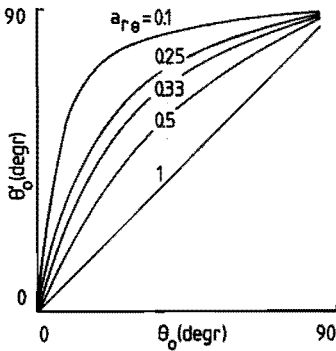


Fig. 2.2.  $\theta'_o$  as a function of  $\theta_o$ ; parameter  $a_{r\theta}$ .

Fig. 2.3.  $\theta'_o$  as a function of  $a_{r\theta}$ ; parameter  $\theta_o$ .

The semi-interfocal distance or linear eccentricity  $e_{\theta}$ , defined by  $e_{\theta}^2 = a_{\theta}^2 - b_{\theta}^2$ , is measured along AB and equals

$$e_{\theta} = \frac{k' z_1}{k \cos \theta_o} = r_o k'. \quad (2.23)$$

Inversely, when the aspect ratio  $a_{r\theta}$  of the elliptical cone  $\theta = \theta_o$  is given, we can determine the parameter k from

$$k^2 = \frac{a_{r\theta}^2}{1 - (1 - a_{r\theta}^2) \cos^2 \theta_0} \quad (2.24)$$

and  $k'$  from equation (2.4). In Figure 2.4,  $k'^2$  is plotted as a function of  $\theta_0$ , with  $a_{r\theta}$  as a parameter.

The coordinate surface  $\theta = \theta_0$ , described by equation (2.18), can serve as the surface of a z-oriented horn with elliptical cross-section.

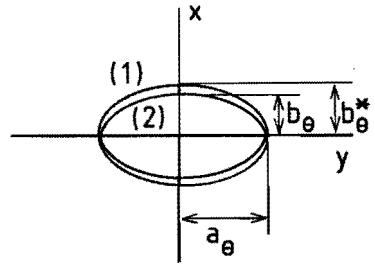
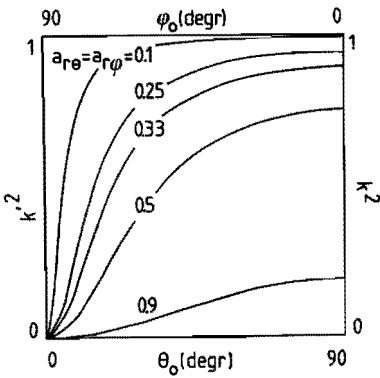


Fig.2.4.  $k'^2$  as a function of  $\theta_0$ ; Fig. 2.5. (1) Projection onto the  $xy$ -plane of the  $\phi$ -curve parameter  $a_{r\theta}$ .  
 $k^2$  as a function of  $\phi_0$ ; parameter  $a_{r\phi}$ .  
 (2) Cross-section of the cone  $\theta = \theta_0$  and the plane  $z = z_1$ .

Next we consider the  $\phi$ -curve, described by  $r = r_0$ ,  $\theta = \theta_0$ ,  $0 \leq \phi < 2\pi$ . Its projection onto the  $xy$ -plane is an ellipse (see Figure 2.5) given by

$$\frac{x^2}{r_0^2 \sin^2 \theta_0} + \frac{y^2}{r_0^2 (1 - k^2 \cos^2 \theta_0)} = 1 \quad (2.24a)$$

This ellipse has a semi-minor axis  $b_\theta^*$  and a semi-major axis  $a_\theta^*$  given by

$$b_{\theta}^* = r_{\circ} \sin \theta_{\circ} = \frac{b_{\theta}}{k}, \quad a_{\theta}^* = r_{\circ} (1 - k^2 \cos^2 \theta_{\circ})^{\frac{1}{2}} = a_{\theta}, \quad (2.25)$$

where  $b_{\theta}$ ,  $a_{\theta}$  are given by (2.20), (2.21); see Figure 2.5. The aspect ratio  $a_{r\theta}^*$  of the ellipse (2.24a) is

$$a_{r\theta}^* = \frac{a_{r\theta}}{k} = (1 - (1 - a_{r\theta}^2) \cos^2 \theta_{\circ})^{\frac{1}{2}}. \quad (2.26)$$

The relationship between  $a_{r\theta}$  and  $a_{r\theta}^*$  is graphically shown in Figure 2.6. Because  $0 < a_{r\theta} \leq 1$ , we find that  $a_{r\theta}^*$  assumes values between  $\sin \theta_{\circ}$  and 1.

Equation (2.19) represents an elliptical cone along the  $y$ -axis with vertex at the origin. Although this cone will not be used in the present study, we will discuss some of its properties here for the sake of completeness. The coordinate surface  $\phi = \phi_{\circ}$  is a cone in the half-space  $y > 0$  if  $0 \leq \phi_{\circ} < \pi$ , and in the half-space  $y \leq 0$  if  $\pi \leq \phi_{\circ} < 2\pi$ . The intersection of the cone (2.19) and the plane  $y = y_1 = r_{\circ} k' \sin \phi_{\circ}$  (=OH) is an ellipse (see Figure 2.1a), given by

$$\frac{x^2}{y_1^2 \cot^2 \phi_{\circ}} + \frac{z^2}{y_1^2 (k'^{-2} \csc^2 \phi_{\circ} - 1)} = 1. \quad (2.26a)$$

We note that  $\cot^2 \phi_{\circ} \leq k'^{-2} \csc^2 \phi_{\circ} - 1$ , hence the minor axis lies in the  $xy$ -plane and the major axis in the  $yz$ -plane. The semi-minor axis  $b_{\phi}$  is

$$b_{\phi} = IH = |y_1 \cot \phi_{\circ}|, \quad (2.27)$$

and the semi-major axis  $a_{\phi}$  is

$$a_{\phi} = GH = \left| \frac{y_1 (1 - k'^2 \sin^2 \phi_{\circ})^{\frac{1}{2}}}{k' \sin \phi_{\circ}} \right| = |y_1 \cot \phi_{\circ}'|, \quad (2.28)$$

where  $\phi_{\circ}'$  is the angle between OG and the  $z$ -axis (see Figure 2.1a). From equation (2.27) it is seen that the cone  $\phi = \phi_{\circ}$  has a semi-opening angle  $\pi/2 - \phi_{\circ}$  in the  $xy$ -plane, measured from the positive  $y$ -axis. The aspect ratio of the ellipse is

$$a_{r\phi}(k', \phi_0) = \tan\phi'_0 / \tan\phi_0 \quad (2.29)$$

The semi-interfocal distance  $e_\phi$ , defined by  $e_\phi^2 = a_\phi^2 - b_\phi^2$ , is measured along GH and equals

$$e_\phi = \frac{ky_1}{k' \sin\phi_0} = r_0 k \quad (2.30)$$

Inversely, when the aspect ratio  $a_{r\phi}$  of the elliptical cone  $\phi = \phi_0$  is given, we can determine the parameter  $k'$  from

$$k'^2 = \frac{a_{r\phi}^2}{1 - (1 - a_{r\phi}^2) \sin^2\phi_0} \quad (2.31)$$

and  $k$  from equation (2.4). In Figure 2.4,  $k^2$  is plotted as a function of  $\phi_0$ , with  $a_{r\phi}$  as a parameter.

The projection of the  $\theta$ -curve, described by  $r = r_0$ ,  $0 \leq \theta \leq \pi$ ,  $\phi = \phi_0$  or  $\phi = \pi - \phi_0$ , onto the  $xz$ -plane is an ellipse given by

$$\frac{x^2}{r_0^2 \cos^2\phi_0} + \frac{z^2}{r_0^2 (1 - k'^2 \sin^2\phi_0)} = 1 \quad (2.31a)$$

This ellipse has a semi-minor axis  $b_\phi^*$  and a semi-major axis  $a_\phi^*$  given by

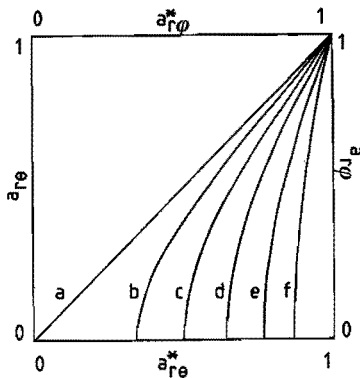
$$b_\phi^* = r_0 \cos\phi_0 = \frac{b_\phi}{k'} \quad , \quad a_\phi^* = r_0 (1 - k'^2 \sin^2\phi_0)^{1/2} = a_\phi \quad , \quad (2.32)$$

where  $b_\phi$ ,  $a_\phi$  are given by (2.27), (2.28). The aspect ratio  $a_{r\phi}^*$  of the ellipse is

$$a_{r\phi}^* = \frac{a_\phi}{b_\phi} = (1 - (1 - a_{r\phi}^2) \sin^2\phi_0)^{1/2} \quad (2.33)$$

Figure 2.6 depicts the relationship between  $a_{r\phi}^*$  and  $a_{r\phi}$ . We find that  $a_{r\phi}^*$  assumes values between  $|\cos\phi_0|$  and 1.

Degenerate surfaces of the coordinate system are also of practical interest [8], [9]. These surfaces are angular sectors of the  $yz$ -plane.



curve	$\theta_0$ (degr)	$\phi_0$ (degr)
a	0	90
b	20	70
c	30	60
d	40	50
e	50	40
f	60	30

Fig. 2.6. Relationship between  $a_{r\theta}^*$  and  $a_{r\phi}^*$ ; parameter  $\theta_0$ .  
Relationship between  $a_{r\theta}^*$  and  $a_{r\phi}^*$ ; parameter  $\phi_0$ .

If  $\theta_0 = 0$  (or  $\theta_0 = \pi$ ), equation (2.18) describes a sector symmetric with respect to the  $z$ -axis and having a semi-angle equal to  $\arctan(k'/k)$ . When crossing the sector  $\theta_0 = 0$  (or  $\theta_0 = \pi$ ), the unit vectors  $\hat{e}_\theta, \hat{e}_\phi$  change direction (see Figure 2.1b). It is at these sectors that additional conditions must be imposed upon the Lamé functions as we will see in sections 2.4 and 2.5. If  $\phi_0 = \pi/2$  (or  $\phi_0 = 3\pi/2$ ) equation (2.19) describes a sector symmetric with respect to the  $y$ -axis and having a semi-angle equal to  $\arctan(k/k')$ . Together, these four sectors cover the complete  $yz$ -plane.

In some of the computations in the sections 4.4.1 and 4.4.2 we use a rectangular grid of points imposed upon an elliptical area like the projection in Figure 2.5. At the grid points we need to know  $r, \theta$  and  $\phi$  as functions of  $x, y$  and  $z$ . The relationship between the two sets of coordinates is best obtained in two steps: first, determine the spherical coordinates  $r, \theta'$  and  $\phi'$  as functions of  $x, y$  and  $z$ ; second, determine the sphero-conal coordinates  $\theta$  and  $\phi$  as functions of  $r, \theta'$  and  $\phi'$ . The results of the two steps are given below. The coordinate  $r$  is determined by  $r = (x^2 + y^2 + z^2)^{1/2}$ . The spherical coordinates  $(r, \theta', \phi')$  are related to Cartesian coordinates by

$$x = r \sin\theta' \cos\phi' \quad , \quad (2.34)$$

$$y = r \sin\theta' \sin\phi' \quad , \quad (2.35)$$

$$z = r \cos\theta' \quad . \quad (2.36)$$

From these equations we find

$$\cos\theta' = z/r \quad , \quad \sin\theta' = \left(1 - \frac{z^2}{r^2}\right)^{\frac{1}{2}} \quad , \quad (2.37)$$

$$\cos\phi' = x(r^2 - z^2)^{-\frac{1}{2}} \quad , \quad \sin\phi' = y(r^2 - z^2)^{-\frac{1}{2}} \quad . \quad (2.38)$$

The sphero-conal coordinates are then obtained from

$$\sin\theta' \cos\phi' = \sin\theta \cos\phi \quad , \quad (2.39)$$

$$\sin\theta' \sin\phi' = (1 - k^2 \cos^2\theta)^{\frac{1}{2}} \sin\phi \quad , \quad (2.40)$$

$$\cos\theta' = \cos\theta (1 - k'^2 \sin^2\phi)^{\frac{1}{2}} \quad . \quad (2.41)$$

From equations (2.39) and (2.40) we have

$$\cos\phi = \sin\theta' \cos\phi' / \sin\theta \quad ,$$

$$\sin\phi = \sin\theta' \sin\phi' (1 - k^2 \cos^2\theta)^{-\frac{1}{2}} \quad . \quad (2.42)$$

By adding the squares of the two equations (2.42) we are led to a quadratic equation in  $\cos^2\theta$ , viz.

$$k^2 \cos^4\theta - (1 + k^2 \cos^2\theta' - k'^2 \sin^2\theta' \sin^2\phi') \cos^2\theta + \cos^2\theta' = 0 \quad . \quad (2.43)$$

The latter equation can easily be solved for  $\cos^2\theta$  and we find

$$\begin{aligned} \cos^2\theta = & \frac{1}{2k^2} [1 + k^2 \cos^2\theta' - k'^2 \sin^2\theta' \sin^2\phi' + \\ & \pm \{(1+k^2 \cos^2\theta' - k'^2 \sin^2\theta' \sin^2\phi')^2 - 4k^2 \cos^2\theta'\}^{\frac{1}{2}}] \quad . \quad (2.44) \end{aligned}$$

Since  $\theta = \theta'$  if  $\phi' = 0$ , it is readily seen that in equation (2.44) the minus sign must be used. From equation (2.44) we know  $\cos\theta$ , except for the sign, hence we find  $\theta$  or  $\pi - \theta$ . Knowing  $\cos^2\theta$  we can determine  $\phi$  from the equations (2.42). The computations of  $\theta$  and  $\phi$  simplify for special values of  $\phi'$ . If  $\phi' = 0$  we find  $\phi = 0$  and  $\theta = \theta'$ . If  $\phi' = \pi/2$ , which corresponds to the half-plane

$$x = 0, \quad y \geq 0, \quad -\infty < z < \infty, \quad (2.45)$$

we get, using equation (2.39),  $\phi = \pi/2$  or  $\theta = 0$  or  $\theta = \pi$ . If  $\phi = \pi/2$  we derive from equation (2.41)

$$\theta = \arccos(k^{-1} \cos\theta'), \text{ if } |\cos\theta'| \leq k. \quad (2.46)$$

If  $\theta = 0$  we find from equation (2.40)

$$\phi = \arcsin(k'^{-1} \sin\theta') \text{ or } \phi = \pi - \arcsin(k'^{-1} \sin\theta'), \text{ if } \cos\theta' \geq k. \quad (2.47)$$

If  $\theta = \pi$  we derive from equation (2.40)

$$\phi = \arcsin(k'^{-1} \sin\theta') \text{ or } \phi = \pi - \arcsin(k'^{-1} \sin\theta'), \text{ if } \cos\theta' \leq -k. \quad (2.48)$$

### 2.3. Differential operators and integral theorems

In this section we present expressions for the differential operators gradient, divergence, curl and Laplacian in the system of sphero-conal coordinates. These operators can be shortly written in terms of the vector differential operator  $\nabla$  (del or nabla). The latter operator is split into a radial operator  $\nabla_r$ , and a transversal operator  $\nabla_t$ , i.e. transversal with respect to  $r$ . Let  $\psi$  define a differentiable scalar function and let  $\bar{F} = F_r \hat{e}_r + F_\theta \hat{e}_\theta + F_\phi \hat{e}_\phi$  be a differentiable vector function of position. Then we have for the gradient, divergence, curl and Laplacian in sphero-conal coordinates:

$$\nabla\psi = \text{grad } \psi = \nabla_r \psi + \frac{1}{r} \nabla_t \psi, \quad (2.49a)$$

$$\nabla_r \psi = \frac{\partial\psi}{\partial r} \hat{e}_r, \quad (2.49b)$$

$$\nabla_t \psi = \frac{1}{h_\theta^*} \frac{\partial\psi}{\partial\theta} \hat{e}_\theta + \frac{1}{h_\phi^*} \frac{\partial\psi}{\partial\phi} \hat{e}_\phi, \quad (2.49c)$$

where  $h_\theta^* = \frac{h_\theta}{r}$ ,  $h_\phi^* = \frac{h_\phi}{r}$ , and  $h_\theta$ ,  $h_\phi$  are given by (2.9), (2.10);

$$\nabla \cdot \bar{F} = \text{div } \bar{F} = \nabla_r \cdot \bar{F} + \frac{1}{r} \nabla_t \cdot \bar{F}, \quad (2.50a)$$

$$\nabla_r \cdot \bar{F} = \frac{1}{r^2} \frac{\partial}{\partial r} (r^2 F_r), \quad (2.50b)$$

$$\nabla_{\mathbf{t}} \cdot \bar{\mathbf{F}} = (h_{\theta}^* h_{\phi}^*)^{-1} \left\{ \frac{\partial}{\partial \theta} (h_{\phi}^* F_{\theta}) + \frac{\partial}{\partial \phi} (h_{\theta}^* F_{\phi}) \right\} ; \quad (2.50c)$$

$$\nabla_{\mathbf{x}} \bar{\mathbf{F}} = \text{curl } \bar{\mathbf{F}} = \nabla_{\mathbf{r}} \times \bar{\mathbf{F}} + \frac{1}{r} \nabla_{\mathbf{t}} \times \bar{\mathbf{F}} , \quad (2.51a)$$

$$\nabla_{\mathbf{t}} \times \bar{\mathbf{F}} = (h_{\theta}^* h_{\phi}^*)^{-1} \left\{ \frac{\partial}{\partial \theta} (h_{\phi}^* F_{\phi}) - \frac{\partial}{\partial \phi} (h_{\theta}^* F_{\theta}) \right\} \mathbf{e}_{\mathbf{r}} , \quad (2.51b)$$

$$\nabla_{\mathbf{r}} \times \bar{\mathbf{F}} = \frac{1}{h_{\phi}} \left\{ \frac{\partial}{\partial \phi} (F_{\mathbf{r}}) - \frac{\partial}{\partial r} (h_{\phi} F_{\phi}) \right\} \mathbf{e}_{\theta} + \frac{1}{h_{\theta}} \left\{ \frac{\partial}{\partial r} (h_{\theta} F_{\theta}) - \frac{\partial}{\partial \theta} (F_{\mathbf{r}}) \right\} \mathbf{e}_{\phi} ; \quad (2.51c)$$

$$\nabla^2 \psi = \Delta \psi = \nabla_{\mathbf{r}}^2 \psi + \frac{1}{r^2} \nabla_{\mathbf{t}}^2 \psi , \quad (2.52a)$$

$$\nabla_{\mathbf{r}}^2 \psi = \frac{1}{r^2} \frac{\partial}{\partial r} \left( r^2 \frac{\partial \psi}{\partial r} \right) , \quad (2.52b)$$

$$\nabla_{\mathbf{t}}^2 \psi = (h_{\theta}^* h_{\phi}^*)^{-1} \left\{ \frac{\partial}{\partial \theta} \left( \frac{h_{\phi}^*}{h_{\theta}^*} \frac{\partial \psi}{\partial \theta} \right) + \frac{\partial}{\partial \phi} \left( \frac{h_{\theta}^*}{h_{\phi}^*} \frac{\partial \psi}{\partial \phi} \right) \right\} . \quad (2.52c)$$

The following formulas from vector analysis are useful for further work and can easily be proved:

$$\nabla_{\mathbf{t}} \times \nabla_{\mathbf{t}} \psi = 0 ; \quad (2.53)$$

$$\nabla_{\mathbf{t}} \cdot \nabla_{\mathbf{t}} \times (\psi \bar{\mathbf{F}}) = 0 ; \quad (2.54)$$

$$\nabla_{\mathbf{t}} \cdot (\mathbf{e}_{\mathbf{r}} \times \nabla_{\mathbf{t}} \psi) = 0 ; \quad (2.55)$$

$$\mathbf{e}_{\mathbf{r}} \cdot \nabla_{\mathbf{t}} \times (\mathbf{e}_{\mathbf{r}} \times \nabla_{\mathbf{t}} \psi) = \nabla_{\mathbf{t}}^2 \psi . \quad (2.56)$$

For later use we present some integral theorems which relate surface integrals over a spherical cap to line integrals along its boundary [2]. Let  $\Omega$  be a spherical cap of the unit sphere, described by  $r = 1$ ,  $0 \leq \theta \leq \theta_0$ ,  $0 \leq \phi < 2\pi$ . The boundary  $c$  of  $\Omega$  is a  $\phi$ -curve, given by  $r = 1$ ,  $\theta = \theta_0$ ,  $0 \leq \phi < 2\pi$ . Let  $\bar{\mathbf{F}}_{\mathbf{t}}$  be the transverse component of the vector  $\bar{\mathbf{F}}$ . Then the surface divergence theorem reads

$$\iint_{\Omega} \nabla_{\mathbf{t}} \cdot \bar{\mathbf{F}}_{\mathbf{t}} \, d\Omega = \int_c \bar{\mathbf{F}}_{\mathbf{t}} \cdot \mathbf{e}_{\theta} \, dc , \quad (2.57)$$

where  $d\Omega = h_\theta^* h_\phi^* d\theta d\phi$  is the surface area element and  $dc = h_\phi^* d\phi$  is the arc-length element. If  $\Omega$  denotes the complete unit sphere, we have

$$\iint_{\Omega} \nabla_t \cdot \bar{F}_t \, d\Omega = 0 . \quad (2.57a)$$

By substituting  $\bar{F}_t = \psi_1 \nabla_t \psi_2$  into equation (2.57) we find

$$\iint_{\Omega} (\nabla_t \psi_1 \cdot \nabla_t \psi_2 + \psi_1 \nabla_t^2 \psi_2) d\Omega = \int_c \psi_1 \nabla_t \psi_2 \cdot \hat{e}_\theta \, dc , \quad (2.58)$$

which is Green's first identity for a surface. Interchanging the subscripts 1 and 2 and subtracting the result from equation (2.58), we obtain Green's second identity for a surface:

$$\iint_{\Omega} (\psi_1 \nabla_t^2 \psi_2 - \psi_2 \nabla_t^2 \psi_1) d\Omega = \int_c (\psi_1 \nabla_t \psi_2 - \psi_2 \nabla_t \psi_1) \cdot \hat{e}_\theta \, dc . \quad (2.59)$$

Replacing  $\bar{F}_t$  in equation (2.57) by  $\hat{e}_r \times \psi \bar{F}$ , we find

$$\iint_{\Omega} \psi \nabla_t \times \bar{F} \cdot \hat{e}_r \, d\Omega + \iint_{\Omega} \nabla_t \psi \times \bar{F} \cdot \hat{e}_r \, d\Omega = \int_c \psi \bar{F} \cdot \hat{e}_\phi \, dc . \quad (2.60)$$

If  $\psi = \text{constant}$ , equation (2.60) becomes

$$\iint_{\Omega} \nabla_t \times \bar{F} \cdot \hat{e}_r \, d\Omega = \int_c \bar{F} \cdot \hat{e}_\phi \, dc , \quad (2.61)$$

which is Stokes' theorem.

By substituting  $\bar{F}_t = \hat{e}_r \times \psi_1 \nabla_t \psi_2$  into the divergence theorem (2.57) we obtain

$$\iint_{\Omega} \nabla_t \psi_1 \times \nabla_t \psi_2 \cdot \hat{e}_r \, d\Omega = \int_c \psi_1 \nabla_t \psi_2 \cdot \hat{e}_\phi \, dc = - \int_c \psi_2 \nabla_t \psi_1 \cdot \hat{e}_\phi \, dc . \quad (2.62)$$

In subsequent sections these integral theorems will be used, for instance, in proving orthogonality properties of the solutions for the scalar Helmholtz equation in a region bounded by an elliptical cone.

#### 2.4. The scalar Helmholtz equation

In the next chapter we will study the electromagnetic fields inside a cone of elliptical cross-section. As a preliminary we now investigate

the solutions of the scalar Helmholtz equation in sphero-conal coordinates. We employ separation of variables to solve the homogeneous scalar Helmholtz equation

$$\nabla^2 \psi + k^{*2} \psi = 0 , \quad (2.63)$$

where  $k^* = 2\pi/\lambda_0$  is the free-space wave number and  $\lambda_0$  the free-space wavelength. In addition the wave function  $\psi$  must satisfy some homogeneous boundary condition and the resulting boundary value problem will be shown to have a discrete set of eigensolutions or modes. The simplest boundary value problems that we will encounter involve the coordinate surface  $S$ , given by  $\theta = \theta_0$ , on which the wave function  $\psi$  satisfies either of the following boundary conditions

$$\psi \Big|_{\theta_0} = 0 , \quad (2.64)$$

$$\frac{\partial \psi}{\partial \theta} \Big|_{\theta_0} = 0 , \quad (2.65)$$

the Dirichlet and Neumann conditions, or short-circuit and open-circuit conditions, respectively. The Helmholtz equation (2.63) is to be solved in the region  $r > 0$ ,  $0 \leq \theta < \theta_0$ ,  $0 \leq \phi < 2\pi$ , i.e. inside the elliptical cone  $S$ . We shall look for solutions of the form

$$\psi = R(r) v(\theta, \phi) , \quad (2.66)$$

in which the radial and transverse dependence of  $\psi$  have been separated. By substitution of (2.66) into (2.63) the Helmholtz equation becomes

$$v(\theta, \phi) \nabla_r^2 R(r) + R(r) \frac{1}{r^2} \nabla_t^2 v(\theta, \phi) + k^{*2} R(r) v(\theta, \phi) = 0 . \quad (2.67)$$

Then by the standard separation argument we arrive at the following equations for  $R(r)$  and  $v(\theta, \phi)$ ,

$$r^2 \nabla_r^2 R(r) + \{k^{*2} r^2 - v(v+1)\} R(r) = 0 , \quad (2.68)$$

$$\nabla_t^2 v(\theta, \phi) + v(v+1) v(\theta, \phi) = 0 , \quad (2.69)$$

where  $v(v+1) = \mu^*$  is the separation constant. The boundary conditions

(2.64) and (2.65) reduce to

$$v(\theta, \phi) \Big|_{\theta_0} = 0, \quad (2.70)$$

$$\frac{\partial v(\theta, \phi)}{\partial \theta} \Big|_{\theta_0} = 0. \quad (2.71)$$

The differential equation (2.69) together with the boundary condition (2.70) or (2.71) constitute an eigenvalue problem. For specific values of  $\mu^*$ , called eigenvalues, the problem has a non-trivial solution  $v \neq 0$ , which is called the corresponding eigenfunction. Jansen [6, p. 24] has shown that there exists a denumerable set of eigenvalues and corresponding eigenfunctions in both cases of the Dirichlet condition (2.70) and the Neumann condition (2.71). It is readily seen that all eigenvalues are non-negative. Indeed, let  $(\mu^*, v)$  be a solution of the eigenvalue problem and let  $v^*$  be the complex conjugate of  $v$ . Then by substituting  $\psi_1 = v^*$ ,  $\psi_2 = v$  into Green's first identity (2.58) and using the boundary condition (2.70) or (2.71) we obtain

$$\mu^* = \frac{\iint_{\Omega} |\nabla_{\mathbf{t}} v|^2 d\Omega}{\iint_{\Omega} |v|^2 d\Omega} \geq 0. \quad (2.72)$$

Here  $\Omega$  is the spherical cap, described by  $r = 1$ ,  $0 \leq \theta \leq \theta_0$ ,  $0 \leq \phi < 2\pi$ . Consider next a pair of solutions  $(\mu_1^*, v_1)$  and  $(\mu_2^*, v_2)$  of the eigenvalue problem. Then by substituting  $\psi_1 = v_1$ ,  $\psi_2 = v_2$  into Green's identities (2.58), (2.59), we arrive at the following results:

if  $\mu_1^* \neq \mu_2^*$ ,

$$\iint_{\Omega} v_1 v_2 d\Omega = 0, \quad (2.73)$$

$$\iint_{\Omega} \nabla_{\mathbf{t}} v_1 \cdot \nabla_{\mathbf{t}} v_2 d\Omega = 0; \quad (2.74)$$

if  $\mu_1^* = \mu_2^* = \mu^*$  and  $v_1 = v_2 = v$ ,

$$\iint_{\Omega} |\nabla_{\mathbf{t}} v|^2 d\Omega = \mu^* \iint_{\Omega} v^2 d\Omega. \quad (2.75)$$

Hence, the two eigenfunctions  $v_1$  and  $v_2$  as well as their gradients are orthogonal if  $\mu_1^* \neq \mu_2^*$ .

We now come to a more detailed study of the differential equations for the radial and transversal parts of  $\psi$ . Written out in full equation (2.68) yields

$$\frac{d}{dr} \left( r^2 \frac{dR(r)}{dr} \right) + \{k^*{}^2 r^2 - \nu(\nu+1)\} R(r) = 0, \quad (2.76)$$

which is the differential equation of the "spherical" Bessel functions [1, Chapter 10]. Solutions are the "spherical" Bessel functions of the first kind

$$j_\nu(k^*r) = \left( \frac{\pi}{2k^*r} \right)^{\frac{1}{2}} J_{\nu+\frac{1}{2}}(k^*r), \quad (2.77)$$

the "spherical" Bessel functions of the second kind

$$y_\nu(k^*r) = \left( \frac{\pi}{2k^*r} \right)^{\frac{1}{2}} Y_{\nu+\frac{1}{2}}(k^*r), \quad (2.78)$$

and the "spherical" Bessel functions of the third kind, the "spherical" Hankel functions,

$$h_\nu^{(1)}(k^*r) = j_\nu(k^*r) + jy_\nu(k^*r), \quad (2.79)$$

$$h_\nu^{(2)}(k^*r) = j_\nu(k^*r) - jy_\nu(k^*r). \quad (2.80)$$

Here,  $J_{\nu+\frac{1}{2}}$  and  $Y_{\nu+\frac{1}{2}}$  are the Bessel functions of the first and second kind, respectively, and  $j$  is the imaginary unit. The kind of solution to be employed depends on the particular problem under consideration. In forthcoming chapters use will be made of the asymptotic expansions of the "spherical" Bessel functions for large argument  $k^*r$ . For convenience they are listed below:

$$j_\nu(k^*r) \approx (k^*r)^{-1} \cos\left(k^*r - \frac{\nu+1}{2}\pi\right), \quad (2.81)$$

$$y_\nu(k^*r) \approx (k^*r)^{-1} \sin\left(k^*r - \frac{\nu+1}{2}\pi\right), \quad (2.82)$$

$$h_{\nu}^{(1)}(k^*r) \approx (k^*r)^{-1} \exp\{+j(k^*r - \frac{\nu+1}{2}\pi)\} , \quad (2.83)$$

$$h_{\nu}^{(2)}(k^*r) \approx (k^*r)^{-1} \exp\{-j(k^*r - \frac{\nu+1}{2}\pi)\} . \quad (2.84)$$

A useful relation in power-flow calculations is

$$\text{Im}[h_{\nu}^{(1)}(k^*r) \frac{d}{dr}\{rh_{\nu}^{(1)}(k^*r)\}^*] = - (k^*r)^{-1} , \quad (2.85)$$

where the asterisk, except for that in  $k^*$ , means complex conjugation. In the derivation of equation (2.85) we have made use of the Wronskian for the "spherical" Bessel functions [1, form. 10.1.6]. If  $h_{\nu}^{(1)}$  is replaced by  $h_{\nu}^{(2)}$ , the right-hand side of (2.85) changes sign.

The partial differential equation (2.69) for the transverse dependence written out in full yields

$$\frac{1}{h_{\theta}^* h_{\phi}^*} \left\{ \frac{\partial}{\partial \theta} \left( \frac{h_{\phi}^*}{h_{\theta}^*} \frac{\partial v(\theta, \phi)}{\partial \theta} \right) + \frac{\partial}{\partial \phi} \left( \frac{h_{\theta}^*}{h_{\phi}^*} \frac{\partial v(\theta, \phi)}{\partial \phi} \right) \right\} + \mu^* v(\theta, \phi) = 0 . \quad (2.86)$$

To avoid singularities we have to explicitly require that the wave function  $\psi$  is a single-valued continuously differentiable function in the region inside the cone S. Thus, in addition to the boundary conditions (2.70) and (2.71), the following conditions must be satisfied:

$$v(\theta, 0) = v(\theta, 2\pi) , \quad \frac{\partial v(\theta, 0)}{\partial \phi} = \frac{\partial v(\theta, 2\pi)}{\partial \phi} , \quad (2.87)$$

$$v(0, \phi) = v(0, \pi - \phi) , \quad \frac{\partial v(0, \phi)}{\partial \theta} = - \frac{\partial v(0, \pi - \phi)}{\partial \theta} . \quad (2.88)$$

These conditions imply "periodicity" of  $\psi$  with respect to the coordinate  $\phi$ , and continuity of  $\psi$  and its gradient across the sector  $\theta = 0$ . Separating  $v(\theta, \phi)$  as

$$v(\theta, \phi) = \Theta(\theta)\Phi(\phi) , \quad (2.89)$$

and introducing the separation constant  $\lambda^*$ , we find that equation (2.86) separates into the following two Lamé equations:

$$(1 - k^2 \cos^2 \theta)^{\frac{1}{2}} \frac{d}{d\theta} \left\{ (1 - k^2 \cos^2 \theta)^{\frac{1}{2}} \frac{d\Theta(\theta)}{d\theta} \right\} + (\mu^* k^2 \sin^2 \theta - \lambda^*) \Theta(\theta) = 0 , \quad (2.90)$$

$$(1-k'^2 \sin^2 \phi)^{\frac{1}{2}} \frac{d}{d\phi} \left\{ (1-k'^2 \sin^2 \phi)^{\frac{1}{2}} \frac{d\Phi(\phi)}{d\phi} \right\} + (\mu^* k'^2 \cos^2 \phi + \lambda^*) \Phi(\phi) = 0 . \quad (2.91)$$

Let

$$\lambda = \lambda^* + k'^2 \mu^* , \quad (2.92)$$

then equations (2.90) and (2.91) become

$$(1-k^2 \cos^2 \theta)^{\frac{1}{2}} \frac{d}{d\theta} \left\{ (1-k^2 \cos^2 \theta)^{\frac{1}{2}} \frac{d\Theta(\theta)}{d\theta} \right\} + \{ \mu^* (1-k^2 \cos^2 \theta) - \lambda \} \Theta(\theta) = 0 , \quad (2.93)$$

$$(1-k'^2 \sin^2 \phi)^{\frac{1}{2}} \frac{d}{d\phi} \left\{ (1-k'^2 \sin^2 \phi)^{\frac{1}{2}} \frac{d\Phi(\phi)}{d\phi} \right\} + \{ \mu^* (1-k'^2 \sin^2 \phi) - (\mu^* - \lambda) \} \Phi(\phi) = 0 . \quad (2.94)$$

Solutions of the  $\theta$  Lamé equation are the odd and even nonperiodic Lamé functions. Solutions of the  $\phi$  Lamé equation are the odd and even simple-periodic Lamé functions with period  $\pi$  or  $2\pi$ . A function  $\Phi(\phi)$  is called even symmetric if  $\Phi(\pi-\phi)=\Phi(\phi)$ , and odd symmetric if  $\Phi(\pi-\phi)=-\Phi(\phi)$ , corresponding to symmetries with respect to  $\phi = \pi/2$  and  $\phi = 3\pi/2$ .

As a consequence of these symmetry relations we find from equation (2.88),

$$\frac{d\Theta(0)}{d\theta} = 0, \text{ if } \Phi \text{ is even symmetric ,} \quad (2.94a)$$

and

$$\Theta(0) = 0, \text{ if } \Phi \text{ is odd symmetric .} \quad (2.94b)$$

So far we have separated the scalar Helmholtz equation into three ordinary differential equations and we have indicated some properties of the solutions of these equations. In the next section we will deal in more detail with the nonperiodic and the simple-periodic Lamé functions.

## 2.5. The Lamé functions

### 2.5.1 Lamé functions regular inside the elliptical cone

We first consider the simple-periodic Lamé functions which are solutions of the  $\phi$  Lamé equation (2.94). The symmetry (odd or even), and the periodicity (period  $\pi$  or  $2\pi$ ) of the simple-periodic Lamé functions are reflected in the Fourier-series representations of these

functions. Based on these symmetry and periodicity properties, we distinguish four classes of Lamé functions. The notation is taken from Jansen [6, p. 48]. We note again that the symmetry holds with respect to  $\phi = \pi/2$  and  $\phi = 3\pi/2$ .

Class I. The functions are even symmetric with period  $\pi$ , and have the property  $\Phi(\phi) = \Phi(\pi+\phi) = \Phi(\pi-\phi)$ . The functions are denoted by  $L_{cv}^{(2n)}(\phi)$  and their series representation is

$$L_{cv}^{(2n)}(\phi) = \sum_{r=0}^{\infty} A_{2r}^{(2n)} \cos 2r\phi, \quad n = 0, 1, 2, \dots \quad (2.95)$$

Class II. The functions are odd symmetric with period  $2\pi$ , and have the property  $\Phi(\phi) = -\Phi(\pi+\phi) = -\Phi(\pi-\phi)$ . The functions are denoted by  $L_{cv}^{(2n+1)}(\phi)$  and their series representation is

$$L_{cv}^{(2n+1)}(\phi) = \sum_{r=0}^{\infty} A_{2r+1}^{(2n+1)} \cos(2r+1)\phi, \quad n = 0, 1, 2, \dots \quad (2.96)$$

Class III. The functions are odd symmetric with period  $\pi$ , and have the property  $\Phi(\phi) = \Phi(\pi+\phi) = -\Phi(\pi-\phi)$ . The functions are denoted by  $L_{sv}^{(2n)}(\phi)$  and their series representation is

$$L_{sv}^{(2n)}(\phi) = \sum_{r=1}^{\infty} B_{2r}^{(2n)} \sin 2r\phi, \quad n = 1, 2, 3, \dots \quad (2.97)$$

Class IV. The functions are even symmetric with period  $2\pi$ , and have the property  $\Phi(\phi) = -\Phi(\pi+\phi) = \Phi(\pi-\phi)$ . The functions are denoted by  $L_{sv}^{(2n+1)}(\phi)$  and their series representation is

$$L_{sv}^{(2n+1)}(\phi) = \sum_{r=0}^{\infty} B_{2r+1}^{(2n+1)} \sin(2r+1)\phi, \quad n = 0, 1, 2, \dots \quad (2.98)$$

For each type of periodic solution the coefficients  $A_r$  or  $B_r$  must satisfy a three-term recurrence relation, which is obtained by substitution of the series representation into the  $\phi$  Lamé equation (2.94). The recurrence relations can be rewritten in matrix notation thus leading to an eigenvalue problem for infinite tridiagonal matrices.

For a given  $\nu$  and  $k'$ , the eigenvalues and the corresponding eigenvectors can be computed. The eigenvalues determine the admissible values of the parameter  $\lambda$  in equation (2.94); whereas the eigenvectors are proportional to the sequences of  $A_r$  or  $B_r$ . According to [6, Lemma 2.6, p. 31] only the eigenvalues  $\lambda$  satisfying  $0 < \lambda < \mu^*$  need to be considered. In the proof of this lemma use has been made of the conditions at  $\theta = 0$  and the boundary conditions at  $\theta = \theta_0$  for the nonperiodic Lamé functions. Having determined the coefficients  $A_r$  and  $B_r$ , the various Lamé functions can be numerically evaluated by means of their series representations. Details regarding the calculation of the eigenvalues and eigenvectors of the infinite tridiagonal matrices are to be found in [6, Chapter 4]. According to [6, Theorem 3.1, p. 50] the Fourier series (2.95)-(2.98) and their derivatives converge uniformly in  $[0, 2\pi]$ .

For later use in chapters 3 and 4 we establish some integral relations for periodic Lamé functions. Let  $(\lambda_m^*, L_{cv_1}^{(m)}(\phi))$  and  $(\lambda_n^*, L_{cv_2}^{(n)}(\phi))$  be solutions of the  $\phi$  Lamé equation (2.91) with  $\mu^* = \mu_1^* = \nu_1(\nu_1+1)$  and  $\mu^* = \mu_2^* = \nu_2(\nu_2+1)$ , respectively. In equation (2.91) we replace  $\mu^*$ ,  $\lambda^*$ ,  $\Phi(\phi)$  by  $\mu_1^*$ ,  $\lambda_m^*$ ,  $L_{cv_1}^{(m)}(\phi)$ , and the result is multiplied by  $L_{cv_2}^{(n)}(\phi)$ . Then, by integrating over  $\phi$  from 0 to  $2\pi$  and using the periodicity of  $\Phi$ , we obtain

$$\begin{aligned} & \mu_1^* \int_0^{2\pi} k'^2 \cos^2 \phi (1-k'^2 \sin^2 \phi)^{-\frac{1}{2}} L_{cv_1}^{(m)}(\phi) L_{cv_2}^{(n)}(\phi) d\phi + \\ & + \lambda_m^* \int_0^{2\pi} (1-k'^2 \sin^2 \phi)^{-\frac{1}{2}} L_{cv_1}^{(m)}(\phi) L_{cv_2}^{(n)}(\phi) d\phi = \\ & = \int_0^{2\pi} (1-k'^2 \sin^2 \phi)^{\frac{1}{2}} \frac{d}{d\phi} \{L_{cv_1}^{(m)}(\phi)\} \frac{d}{d\phi} \{L_{cv_2}^{(n)}(\phi)\} d\phi . \end{aligned} \tag{2.99}$$

By interchanging the two solutions we are led to the relation (2.99) with  $\mu_1^*$  and  $\lambda_m^*$  replaced by  $\mu_2^*$  and  $\lambda_n^*$ , respectively. By subtracting the latter relation from equation (2.99) we find

$$\begin{aligned}
 & (\mu_1^* - \mu_2^*) \int_0^{2\pi} k'^2 \cos^2 \phi (1 - k'^2 \sin^2 \phi)^{-\frac{1}{2}} L_{cv_1}^{(m)}(\phi) L_{cv_2}^{(n)}(\phi) d\phi = \\
 & = -(\lambda_m^* - \lambda_n^*) \int_0^{2\pi} (1 - k'^2 \sin^2 \phi)^{-\frac{1}{2}} L_{cv_1}^{(m)}(\phi) L_{cv_2}^{(n)}(\phi) d\phi . \quad (2.100)
 \end{aligned}$$

From equations (2.99) and (2.100) we furthermore derive

$$\begin{aligned}
 & \int_0^{2\pi} (1 - k'^2 \sin^2 \phi)^{\frac{1}{2}} \frac{d}{d\phi} \{L_{cv_1}^{(m)}(\phi)\} \frac{d}{d\phi} \{L_{cv_2}^{(n)}(\phi)\} d\phi = \\
 & = (\mu_1^* \lambda_n^* - \mu_2^* \lambda_m^*) (\mu_1^* - \mu_2^*)^{-1} \int_0^{2\pi} (1 - k'^2 \sin^2 \phi)^{-\frac{1}{2}} L_{cv_1}^{(m)}(\phi) L_{cv_2}^{(n)}(\phi) d\phi . \quad (2.101)
 \end{aligned}$$

If  $\mu_1^* = \mu_2^* = \mu^* = \nu(\nu+1)$  and  $\lambda_m^* \neq \lambda_n^*$ , we have from equations (2.99) and (2.100),

$$\int_0^{2\pi} (1 - k'^2 \sin^2 \phi)^{-\frac{1}{2}} L_{cv}^{(m)}(\phi) L_{cv}^{(n)}(\phi) d\phi = 0, \quad (2.102)$$

$$\begin{aligned}
 & \int_0^{2\pi} (1 - k'^2 \sin^2 \phi)^{\frac{1}{2}} \frac{d}{d\phi} \{L_{cv}^{(m)}(\phi)\} \frac{d}{d\phi} \{L_{cv}^{(n)}(\phi)\} d\phi = \\
 & = \mu^* \int_0^{2\pi} k'^2 \cos^2 \phi (1 - k'^2 \sin^2 \phi)^{-\frac{1}{2}} L_{cv}^{(m)}(\phi) L_{cv}^{(n)}(\phi) d\phi . \quad (2.103)
 \end{aligned}$$

If  $\mu_1^* = \mu_2^* = \mu^* = \nu(\nu+1)$  and  $m = n$ , we have from equation (2.99),

$$\begin{aligned}
 & \int_0^{2\pi} (1 - k'^2 \sin^2 \phi)^{\frac{1}{2}} \left\{ \frac{d}{d\phi} L_{cv}^{(m)}(\phi) \right\}^2 d\phi = \\
 & = \mu^* \int_0^{2\pi} k'^2 \cos^2 \phi (1 - k'^2 \sin^2 \phi)^{-\frac{1}{2}} \{L_{cv}^{(m)}(\phi)\}^2 d\phi + \lambda_m^* \int_0^{2\pi} (1 - k'^2 \sin^2 \phi)^{-\frac{1}{2}} \{L_{cv}^{(m)}(\phi)\}^2 d\phi . \quad (2.104)
 \end{aligned}$$

Similar integral relations can be derived for periodic Lamé functions of other classes. Equation (2.102) is a special case of the general orthogonality relation for two solutions  $(\lambda_m^*, \phi_m)$  and  $(\lambda_n^*, \phi_n)$  of the  $\phi$  Lamé equation (2.91),

$$\int_0^{2\pi} (1-k'^2 \sin^2 \phi)^{-\frac{1}{2}} \Phi_m(\phi) \Phi_n(\phi) d\phi = 0, \quad (2.105)$$

valid if  $\lambda_m^* \neq \lambda_n^*$ ; compare with [6, p. 35].

Next we consider the  $\theta$  Lamé equation (2.93), in which  $\mu^* = \nu(\nu+1)$  and the parameter  $\lambda$  has been determined as part of the solution of the  $\phi$  Lamé equation (2.94). Corresponding to the four classes of simple-periodic  $\phi$  Lamé functions, Jansen [6, section 3.2] introduced four classes of nonperiodic  $\theta$  Lamé functions. The latter functions must satisfy the  $\theta$  Lamé equation (2.93) and the boundary condition

$$\frac{d\theta(0)}{d\theta} = 0, \text{ for classes I and IV,} \quad (2.106)$$

$$\theta(0) = 0, \text{ for classes II and III;} \quad (2.107)$$

see (2.94a) and (2.94b). If  $k' = 0$ , one has  $\lambda = m^2$ ,  $m = 0, 1, 2, \dots$ , in the Lamé differential equations (2.94) and (2.93). Then the  $\theta$  Lamé equation (2.93) reduces to the Legendre differential equation

$$\sin\theta \frac{d}{d\theta} \left\{ \sin\theta \frac{d\theta(\theta)}{d\theta} \right\} + \{ \nu(\nu+1) \sin^2\theta - m^2 \} \theta(\theta) = 0, \quad (2.108)$$

of which the fundamental solutions are the associated Legendre functions of the first and second kind,  $P_\nu^m(\cos\theta)$  and  $Q_\nu^m(\cos\theta)$ . Guided by this result, Jansen [6, section 3.2] then constructed solutions of equation (2.93), that are represented by series of Legendre functions  $P_\nu^m(\cos\theta)$ . For the solutions of classes I and II he started from the series representation

$$\theta(\theta) = \sum_{m=0}^{\infty} c_m P_\nu^m(\cos\theta), \quad (2.109)$$

whereas the solutions of classes III and IV are represented by

$$\theta(\theta) = \frac{(1-k^2 \cos^2 \theta)^{\frac{1}{2}}}{\sin\theta} \sum_{m=0}^{\infty} d_m P_\nu^m(\cos\theta). \quad (2.110)$$

By substitution of these series representations into the  $\theta$  Lamé equation (2.93) and by application of the known recurrence relations

for Legendre functions, one is led to three-term recurrence relations for the coefficients  $c_m$  and  $d_m$ . Jansen [6, p. 55-58] has shown that these recurrence relations can be transformed into the recurrence relations for the coefficients  $A_m$  and  $B_m$  occurring in the Fourier-series representations of the periodic Lamé functions. More specific, Jansen found that

$$c_m = T(m) A_m, \tag{2.111}$$

$$d_m = m T(m) B_m, \tag{2.112}$$

where  $T(m)$  satisfies the recurrence relation

$$T(m) = -(\nu-m)(\nu+m+1) T(m+2), \quad m = 0, 1, 2, \dots, \tag{2.113}$$

and can be taken as, for instance,

$$T(m) = \frac{2^{-m} \Gamma(\frac{\nu+1}{2}) \Gamma(-\frac{\nu}{2})}{\Gamma(\frac{\nu+m+1}{2}) \Gamma(\frac{m-\nu}{2})}. \tag{2.114}$$

We now introduce four classes of nonperiodic Lamé functions represented by series of Legendre functions  $P_\nu^m(\cos\theta)$ . The notation is taken from Jansen [6, p. 58].

Class I. The functions satisfy the boundary condition  $d\theta(0)/d\theta=0$  and are denoted by  $L_{cp\nu}^{(2n)}(\theta)$ ; their series representation is

$$L_{cp\nu}^{(2n)}(\theta) = \sum_{m=0}^{\infty} T(2m) A_{2m}^{(2n)} P_\nu^{2m}(\cos\theta), \quad n = 0, 1, 2, \dots. \tag{2.115}$$

Class II. The functions satisfy the boundary condition  $\theta(0) = 0$  and are denoted by  $L_{cp\nu}^{(2n+1)}(\theta)$ ; their series representation is

$$L_{cp\nu}^{(2n+1)}(\theta) = \sum_{m=0}^{\infty} T(2m+1) A_{2m+1}^{(2n+1)} P_\nu^{2m+1}(\cos\theta), \quad n = 0, 1, 2, \dots. \tag{2.116}$$

Class III. The functions satisfy the boundary condition  $\theta(0) = 0$  and are denoted by  $L_{sp\nu}^{(2n)}(\theta)$ ; their series representation is

$$L_{spv}^{(2n)}(\theta) = \frac{(1-k^2 \cos^2 \theta)^{\frac{1}{2}}}{\sin \theta} \sum_{m=1}^{\infty} 2m T(2m) B_{2m}^{(2n)} P_v^{2m}(\cos \theta), \quad n = 1, 2, 3, \dots \quad (2.117)$$

Class IV. The functions satisfy the boundary condition  $d\theta(0)/d\theta=0$  and are denoted by  $L_{spv}^{(2n+1)}(\theta)$ ; their series representation is

$$L_{spv}^{(2n+1)}(\theta) = \frac{(1-k^2 \cos^2 \theta)^{\frac{1}{2}}}{\sin \theta} \sum_{m=0}^{\infty} (2m+1) T(2m+1) B_{2m+1}^{(2n+1)} P_v^{2m+1}(\cos \theta),$$

$n = 0, 1, 2, \dots$  . . . . . (2.118)

According to [6, Theorem 3.3, p. 59] these series converge uniformly on any closed subinterval of the interval  $0 \leq \theta < 2 \arctan\{(1+k)/(1-k)\}^{\frac{1}{2}}$ . In [6, Chapter 7] other series representations have been derived which converge uniformly on any closed subinterval of  $[0, \pi)$ . However, in the present study the series represented by (2.115)-(2.118), suffice.

The recurrence relations for the functions  $P_v^m(\cos \theta)$ ,  $m = 0, 1, 2, \dots$ ,  $v > 0$ , also hold for the functions  $Q_v^m(\cos \theta)$ . Consequently, there are another four classes of nonperiodic Lamé functions. They are given by the series representations (2.115)-(2.118), with  $P_v^m(\cos \theta)$  replaced by  $Q_v^m(\cos \theta)$ ; they are denoted by  $L_{cqv}^{(2n)}(\theta)$ ,  $L_{cqv}^{(2n+1)}(\theta)$ ,  $L_{sqv}^{(2n)}(\theta)$  and  $L_{sqv}^{(2n+1)}(\theta)$ , [6, p. 59]. These solutions are not bounded at  $\theta = 0$ .

Finally, from (2.89) the solutions for  $v(\theta, \phi)$  are found to be products of a simple-periodic Lamé function of class I, II, III or IV, given by (2.95)-(2.98), and the corresponding nonperiodic Lamé function of the same class, given by (2.115)-(2.118). The function  $v(\theta, \phi)$  is required to satisfy the Dirichlet condition (2.70) or the Neumann condition (2.71) on the coordinate surface  $S$ , given by  $\theta = \theta_0$ . On imposing these conditions we are led to the equation

$$L_{cpv}^{(2n)}(\theta_0) = 0, \text{ or } d L_{cpv}^{(2n)}(\theta_0)/d\theta = 0 \quad , \quad (2.119)$$

and similar equations for the other classes of Lamé functions. Equation (2.119), which is to be considered as a transcendental equation in the variable  $v$ , has a denumerable set of non-negative roots  $v$ . The corresponding values of  $\mu^* = v(v+1)$  are the eigenvalues of the problem (2.69)-(2.71), and the functions  $v(\theta, \phi)$  determined

above are the corresponding eigenfunctions. Thus we have completely solved now the eigenvalue problem (2.69)-(2.71), in terms of Lamé functions.

For later use in chapters 3 and 4 we establish some integral relations for nonperiodic Lamé functions. To keep the presentation general, we shall not require that the Dirichlet condition (2.70) or the Neumann condition (2.71) applies on the coordinate surface  $S$ , given by  $\theta = \theta_0$ . Let  $(\lambda_m^*, L_{cpv_1}^{(m)}(\theta))$  and  $(\lambda_n^*, L_{cpv_2}^{(n)}(\theta))$  be solutions of the  $\theta$  Lamé equation (2.90) with  $\mu_1^* = \nu_1(\nu_1+1)$  and  $\mu_2^* = \nu_2(\nu_2+1)$ , respectively. In equation (2.90) we replace  $\mu^*$ ,  $\lambda^*$ ,  $\theta(\theta)$  by  $\mu_1^*$ ,  $\lambda_m^*$ ,  $L_{cpv_1}^{(m)}(\theta)$ , and the result is multiplied by  $L_{cpv_2}^{(n)}(\theta)$ . Then by integrating over  $\theta$  from 0 to  $\theta_0$  and using the boundary conditions (2.106), (2.107), we obtain

$$\begin{aligned} & \mu_1^* \int_0^{\theta_0} (1-k^2 \cos^2 \theta)^{-\frac{1}{2}} k^2 \sin^2 \theta L_{cpv_1}^{(m)}(\theta) L_{cpv_2}^{(n)}(\theta) d\theta + \\ & + (1-k^2 \cos^2 \theta_0)^{\frac{1}{2}} L_{cpv_2}^{(n)}(\theta_0) \frac{d}{d\theta} \{L_{cpv_1}^{(m)}(\theta_0)\} = \\ & = \lambda_m^* \int_0^{\theta_0} (1-k^2 \cos^2 \theta)^{-\frac{1}{2}} L_{cpv_1}^{(m)}(\theta) L_{cpv_2}^{(n)}(\theta) d\theta + \\ & + \int_0^{\theta_0} (1-k^2 \cos^2 \theta)^{\frac{1}{2}} \frac{d}{d\theta} \{L_{cpv_1}^{(m)}(\theta)\} \frac{d}{d\theta} \{L_{cpv_2}^{(n)}(\theta)\} d\theta . \end{aligned} \quad (2.120)$$

By interchanging the two solutions we are led to the relation (2.120) with  $\mu_1^*$  and  $\lambda_m^*$  replaced by  $\mu_2^*$  and  $\lambda_n^*$ , respectively. By subtracting the latter relation from equation (2.120) we find

$$\begin{aligned} & (\mu_1^* - \mu_2^*) \int_0^{\theta_0} (1-k^2 \cos^2 \theta)^{-\frac{1}{2}} k^2 \sin^2 \theta L_{cpv_1}^{(m)}(\theta) L_{cpv_2}^{(n)}(\theta) d\theta = \\ & = (\lambda_m^* - \lambda_n^*) \int_0^{\theta_0} (1-k^2 \cos^2 \theta)^{-\frac{1}{2}} L_{cpv_1}^{(m)}(\theta) L_{cpv_2}^{(n)}(\theta) d\theta + \\ & - (1-k^2 \cos^2 \theta_0)^{\frac{1}{2}} L_{cpv_2}^{(n)}(\theta_0) \frac{d}{d\theta} \{L_{cpv_1}^{(m)}(\theta_0)\} + (1-k^2 \cos^2 \theta_0)^{\frac{1}{2}} L_{cpv_1}^{(m)}(\theta_0) \frac{d}{d\theta} \{L_{cpv_2}^{(n)}(\theta_0)\} . \end{aligned} \quad (2.121)$$

From equations (2.120) and (2.121) we furthermore derive

$$\begin{aligned}
 & (\mu_1^* - \mu_2^*) \int_0^{\theta_0} (1 - k^2 \cos^2 \theta)^{\frac{1}{2}} \frac{d}{d\theta} \{L_{cpv_1}^{(m)}(\theta)\} \frac{d}{d\theta} \{L_{cpv_2}^{(n)}(\theta)\} d\theta = \\
 & = (\lambda_m^* \mu_2^* - \lambda_n^* \mu_1^*) \int_0^{\theta_0} (1 - k^2 \cos^2 \theta)^{-\frac{1}{2}} L_{cpv_1}^{(m)}(\theta) L_{cpv_2}^{(n)}(\theta) d\theta - \\
 & - (1 - k^2 \cos^2 \theta_0)^{\frac{1}{2}} \mu_2^* L_{cpv_2}^{(n)}(\theta_0) \frac{d}{d\theta} \{L_{cpv_1}^{(m)}(\theta_0)\} + \\
 & + (1 - k^2 \cos^2 \theta_0)^{\frac{1}{2}} \mu_1^* L_{cpv_1}^{(m)}(\theta_0) \frac{d}{d\theta} \{L_{cpv_2}^{(n)}(\theta_0)\}. \tag{2.122}
 \end{aligned}$$

If  $\mu_1^* = \mu_2^* = \mu^* = \nu(\nu+1)$  and  $\lambda_m^* \neq \lambda_n^*$ , we have from equations (2.121) and (2.120),

$$\begin{aligned}
 & \int_0^{\theta_0} (1 - k^2 \cos^2 \theta)^{-\frac{1}{2}} L_{cpv}^{(m)}(\theta) L_{cpv}^{(n)}(\theta) d\theta = \\
 & = (1 - k^2 \cos^2 \theta_0)^{\frac{1}{2}} [L_{cpv}^{(n)}(\theta_0) \frac{d}{d\theta} \{L_{cpv}^{(m)}(\theta_0)\} - L_{cpv}^{(m)}(\theta_0) \frac{d}{d\theta} \{L_{cpv}^{(n)}(\theta_0)\}] / (\lambda_m^* - \lambda_n^*), \tag{2.123}
 \end{aligned}$$

$$\begin{aligned}
 & \int_0^{\theta_0} (1 - k^2 \cos^2 \theta)^{\frac{1}{2}} \frac{d}{d\theta} \{L_{cpv}^{(m)}(\theta)\} \frac{d}{d\theta} \{L_{cpv}^{(n)}(\theta)\} d\theta = \\
 & = \mu^* \int_0^{\theta_0} (1 - k^2 \cos^2 \theta)^{-\frac{1}{2}} k^2 \sin^2 \theta L_{cpv}^{(m)}(\theta) L_{cpv}^{(n)}(\theta) d\theta + \\
 & + (1 - k^2 \cos^2 \theta_0)^{\frac{1}{2}} \lambda_m^* L_{cpv}^{(m)}(\theta_0) \frac{d}{d\theta} \{L_{cpv}^{(n)}(\theta_0)\} / (\lambda_m^* - \lambda_n^*) - \\
 & - (1 - k^2 \cos^2 \theta_0)^{\frac{1}{2}} \lambda_n^* L_{cpv}^{(n)}(\theta_0) \frac{d}{d\theta} \{L_{cpv}^{(m)}(\theta_0)\} / (\lambda_m^* - \lambda_n^*). \tag{2.124}
 \end{aligned}$$

If  $\mu_1^* = \mu_2^* = \mu^* = \nu(\nu+1)$  and  $m = n$ , we have from equation (2.120),

$$\begin{aligned} & \mu^* \int_0^{\theta_0} (1-k^2 \cos^2 \theta)^{-\frac{1}{2}} k^2 \sin^2 \theta \{L_{cpv}^{(m)}(\theta)\}^2 d\theta + (1-k^2 \cos^2 \theta_0)^{\frac{1}{2}} L_{cpv}^{(m)}(\theta_0) \frac{d}{d\theta} \{L_{cpv}^{(m)}(\theta_0)\} = \\ & = \int_0^{\theta_0} (1-k^2 \cos^2 \theta)^{\frac{1}{2}} \left[ \frac{d}{d\theta} \{L_{cpv}^{(m)}(\theta)\} \right]^2 d\theta + \lambda_m^* \int_0^{\theta_0} (1-k^2 \cos^2 \theta)^{-\frac{1}{2}} \{L_{cpv}^{(m)}(\theta)\}^2 d\theta . \end{aligned} \tag{2.125}$$

Similar integral relations can be derived for the nonperiodic Lamé functions of other classes.

If  $\mu_1^* = \mu_2^* = \mu^* = \nu(\nu+1)$  and  $\lambda_m^* \neq \lambda_n^*$ , and if the Dirichlet or Neumann condition applies, we have from equation (2.123),

$$\int_0^{\theta_0} (1-k^2 \cos^2 \theta)^{-\frac{1}{2}} L_{cpv}^{(m)}(\theta) L_{cpv}^{(n)}(\theta) d\theta = 0 . \tag{2.125a}$$

Using equation (2.105) and equations of the type (2.125a), we can easily show that equations (2.73) and (2.74) also hold if  $\mu_1^* = \mu_2^*$  and  $\lambda_m^* \neq \lambda_n^*$ .

### 2.5.2. Lamé functions regular on the unit sphere

So far we have investigated the solutions of the scalar Helmholtz equation

$$\nabla^2 \psi + k^*{}^2 \psi = 0 ,$$

which are regular in the region  $r > 0$ ,  $0 \leq \theta < \theta_0$ ,  $0 \leq \phi < 2\pi$ , i.e. inside the elliptical cone  $S$ , and which satisfy some homogeneous boundary condition at the surface  $\theta = \theta_0$ . In this section we study the solutions which are regular in the region  $r > r_0$ ,  $0 \leq \theta \leq \pi$ ,  $0 \leq \phi < 2\pi$ , outside a sphere of radius  $r_0$ . Such solutions are needed in chapter 4, in the analysis of the radiation of an elliptical horn. As in (2.66) we look for solutions of the form

$$\psi = R(r) v(\theta, \phi) ,$$

in which the radial and transverse dependence have been separated. By substitution of  $\psi$  into the Helmholtz equation and using the standard separation argument, we arrive at the following equations for  $R(r)$  and

$v(\theta, \phi),$

$$r^2 \nabla_r^2 R(r) + (k^2 r^2 - \mu^*) R(r) = 0, \quad r > r_0, \quad (2.126)$$

$$\nabla_t^2 v(\theta, \phi) + \mu^* v(\theta, \phi) = 0, \quad 0 \leq \theta \leq \pi, \quad 0 \leq \phi < 2\pi, \quad (2.127)$$

where  $\mu^*$  is the separation constant. The solutions of equation (2.126) have been presented in (2.77)-(2.80). Equation (2.127) constitutes again an eigenvalue problem: for specific values of  $\mu^*$ , called eigenvalues, equation (2.127) has a non-trivial solution  $v \neq 0$ , which is called the corresponding eigenfunction. Notice that in the present case there is no additional boundary condition, but instead the eigenfunction  $v$  is required to be regular for  $0 \leq \theta \leq \pi$ ,  $0 \leq \phi < 2\pi$ , i.e. on the unit sphere. Different from the previous treatment of the eigenvalue problem in a conical region, the eigenvalues  $\mu^*$  can now be determined a priori. To that end we express the operator  $\nabla_t^2$  in (2.127) in terms of spherical coordinates  $\theta', \phi'$ , as defined in (2.34)-(2.36). Then it is well known [2a] that the eigenvalues and eigenfunctions are given by

$$\mu^* = v(v+1), \quad v = 0, 1, 2, \dots; \quad v = P_v^m(\cos\theta') \frac{\cos}{\sin}(m\phi'), \quad m = 0, 1, \dots, v. \quad (2.128)$$

To each eigenvalue  $\mu^* = v(v+1)$  correspond  $2v+1$  linearly independent eigenfunctions which are spherical harmonics of order  $v$ . Furthermore, the eigenfunctions (2.128) form a complete orthogonal system on the unit sphere. We now set  $\mu^* = v(v+1)$  in (2.127), where it is understood throughout that  $v$  stands for a non-negative integer, i.e.  $v = 0, 1, 2, \dots$ . Then it remains to determine the eigenfunctions  $v(\theta, \phi)$  in terms of the sphero-conal coordinates  $\theta, \phi$ . It will be shown that  $v(\theta, \phi)$  can be represented by a product of  $\theta$  and  $\phi$  Lamé functions which are regular for  $0 \leq \theta \leq \pi$ ,  $0 \leq \phi < 2\pi$ , i.e. on the entire unit sphere. Proceeding as in (2.89)-(2.94), we substitute  $v(\theta, \phi) = \Theta(\theta)\Phi(\phi)$ , then equation (2.127) separates into the two Lamé equations

$$(1-k^2 \cos^2 \theta)^{\frac{1}{2}} \frac{d}{d\theta} \left\{ (1-k^2 \cos^2 \theta)^{\frac{1}{2}} \frac{d\Theta(\theta)}{d\theta} \right\} + \{v(v+1)k^2 \sin^2 \theta - \lambda^*\} \Theta(\theta) = 0,$$

$$0 \leq \theta \leq \pi, \quad (2.129)$$

$$(1-k'^2 \sin^2 \phi)^{\frac{1}{2}} \frac{d}{d\phi} \left\{ (1-k'^2 \sin^2 \phi)^{\frac{1}{2}} \frac{d\Phi(\phi)}{d\phi} \right\} + \{v(v+1)k'^2 \cos^2 \phi + \lambda^*\} \Phi(\phi) = 0,$$

$$0 \leq \phi < 2\pi, \quad (2.130)$$

where  $\lambda^*$  is the separation constant. Next, by setting  $\lambda = \lambda^* + v(v+1)k'^2$ , the Lamé equations transform into

$$(1-k^2 \cos^2 \theta)^{\frac{1}{2}} \frac{d}{d\theta} \left\{ (1-k^2 \cos^2 \theta)^{\frac{1}{2}} \frac{d\Theta(\theta)}{d\theta} \right\} + \{v(v+1)(1-k^2 \cos^2 \theta) - \lambda\} \Theta(\theta) = 0,$$

$$0 \leq \theta \leq \pi, \quad (2.131)$$

$$(1-k'^2 \sin^2 \phi)^{\frac{1}{2}} \frac{d}{d\phi} \left\{ (1-k'^2 \sin^2 \phi)^{\frac{1}{2}} \frac{d\Phi(\phi)}{d\phi} \right\} + \{\lambda - v(v+1)k'^2 \sin^2 \phi\} \Phi(\phi) = 0,$$

$$0 \leq \phi < 2\pi. \quad (2.132)$$

The solutions of the  $\phi$  Lamé equation (2.132) are again the odd and even simple-periodic Lamé functions with period  $\pi$  or  $2\pi$ . Four classes of  $\phi$  Lamé functions are distinguished, which are represented by the Fourier series (2.95)-(2.98). The  $\theta$  Lamé equation (2.131) is accompanied by the boundary conditions

$$\frac{d\Theta(0)}{d\theta} = \frac{d\Theta(\pi)}{d\theta} = 0, \text{ if } \Phi \text{ is even symmetric (classes I and IV),} \quad (2.133)$$

$$\Theta(0) = \Theta(\pi) = 0, \text{ if } \Phi \text{ is odd symmetric (classes II and III);} \quad (2.134)$$

compare (2.94a), (2.94b). These conditions reflect the requirement that  $\Theta(\theta)$  should be regular over the entire range  $0 \leq \theta \leq \pi$ , in particular at  $\theta = 0$  and  $\theta = \pi$ . Similar to [6, Lemma 2.6, p. 31], one can easily show now that for given  $k'$  and  $v$ , the separation constant  $\lambda$  must satisfy

$$0 \leq \lambda \leq v(v+1). \quad (2.135)$$

The solutions of the  $\theta$  Lamé equation (2.131) are the nonperiodic Lamé functions. The four classes of  $\theta$  Lamé functions can be represented by series of Legendre functions  $P_v^m(\cos\theta)$  as in (2.115)-(2.118). These series involve the coefficient  $T(m)$  given by (2.114). Note that  $T(m)$  contains  $\Gamma$ -functions of arguments  $-v/2$  and  $(m-v)/2$ . Since  $\Gamma(z)$  has simple poles at  $z = 0, -1, -2, \dots$  [1, Chapter 6], the choice of  $T(m)$  is inadequate in the present case where  $v$  and  $m$  are integers. Therefore



(i)  $v = 2\ell+1, \ell = 0,1,2,\dots,$  (2.140)

(ii)  $v = 2\ell+2, \ell = 0,1,2,\dots.$  (2.141)

Case (i). For odd integer  $v = 2\ell+1$ , it is found that the element  $b_{2\ell+1} = 0$  in (2.139). Hence, the matrix  $M$  can be partitioned as

$$M = \left[ \begin{array}{c|c} M_1 & O \\ \hline O & M_2 \end{array} \right] , \quad (2.142)$$

$c_{2\ell+1}$

where  $M_1$  is an  $(\ell+1) \times (\ell+1)$  tridiagonal matrix and  $M_2$  is an infinite tridiagonal matrix. The matrix  $M_1$  has  $\ell+1$  eigenvalues denoted by  $\Lambda_{2n+1}, n = 0,1,\dots,\ell$ , with corresponding eigenvectors  $[A_1^{(2n+1)}, A_3^{(2n+1)}, \dots, A_{2\ell+1}^{(2n+1)}]^T$ . Each of these eigenvectors is supplemented by zero-elements  $A_{2\ell+3}^{(2n+1)} = A_{2\ell+5}^{(2n+1)} = \dots = 0$ .

Then the resulting vectors are eigenvectors of the infinite matrix  $M$ , corresponding to the eigenvalues  $\Lambda_{2n+1}$ . In this manner we have found  $\ell+1$  eigenvalues and eigenvectors of the matrix  $M$ . The simple-periodic Lamé functions corresponding to these eigenvectors, are consequently represented by finite series (trigonometric polynomials)

$$L_{cv}^{(2n+1)}(\phi) = \sum_{r=0}^{\ell} A_{2r+1}^{(2n+1)} \cos(2r+1)\phi, \quad n = 0,1,\dots,\ell, \quad v = 2\ell+1. \quad (2.143)$$

It can be shown that only the  $\ell+1$  eigenvalues  $\Lambda_{2n+1}$  of  $M_1$  and  $M$  give rise to values of  $\lambda$  that satisfy the criterion (2.135). Hence, the remaining eigenvalues and eigenvectors of  $M$  may be discarded. The  $\theta$  Lamé functions of class II are also represented by finite series, viz.

$$L_{cpv}^{(2n+1)}(\theta) = \sum_{m=0}^{\ell} T^*(2m+1) A_{2m+1}^{(2n+1)} P_v^{2m+1}(\cos\theta), \quad n = 0,1,2,\dots,\ell, \quad (2.144)$$

$v = 2\ell+1.$

Here, the truncation is due to the fact that  $A_{2m+1}^{(2n+1)} = 0$  if  $m > \ell$ , whereas  $T^*(2m+1) P_v^{2m+1}(\cos\theta)$  is finite if  $m > \ell$ . For given  $k'$  and

$\nu = 2\ell+1$ , we have found  $\ell+1$   $\phi$  Lamé functions and  $\ell+1$  corresponding  $\theta$  Lamé functions of class II. The  $\theta$  Lamé functions (2.144) are in fact polynomials in  $\cos\theta$  and  $\sin\theta$ , hence they are regular for  $0 \leq \theta \leq \pi$ .

Case (ii). For even integer  $\nu = 2\ell+2$ , it is found that the element  $c_{2\ell+1} = 0$  in (2.139). The matrix  $M$  is therefore partitioned as

$$M = \left[ \begin{array}{c|c} M_1 & O \\ \hline O & M_2 \end{array} \right], \quad (2.145)$$

in which  $M_1$  is again an  $(\ell+1) \times (\ell+1)$  tridiagonal matrix. The matrix  $M_1$  has  $\ell+1$  eigenvalues denoted by  $\Lambda_{2n+1}$ ,  $n = 0, 1, \dots, \ell$ , with corresponding eigenvectors  $[A_1^{(2n+1)}, A_3^{(2n+1)}, \dots, A_{2\ell+1}^{(2n+1)}]^T$ . Each of these eigenvectors is supplemented by elements  $A_{2\ell+3}^{(2n+1)}, A_{2\ell+5}^{(2n+1)}, \dots$ , that are determined by the remaining equations of the infinite eigenvalue problem, viz.

$$b_{2r-1} A_{2r-1}^{(2n+1)} + a_{2r+1} A_{2r+1}^{(2n+1)} + c_{2r+1} A_{2r+3}^{(2n+1)} = \Lambda_{2n+1} A_{2r+1}^{(2n+1)},$$

$$r = \ell+1, \ell+2, \ell+3, \dots \quad (2.146)$$

These elements are not all zero and the resulting extended vectors are eigenvectors of the infinite matrix  $M$ , corresponding to the eigenvalues  $\Lambda_{2n+1}$ . Thus we have found  $\ell+1$  eigenvalues and eigenvectors of the matrix  $M$ . The remaining eigenvalues of  $M$  are identical to the eigenvalues of the infinite matrix  $M_2$ , and the eigenvectors of  $M$  are equal to those of  $M_2$  supplemented by the zero-elements  $A_1^{(2n+1)} = A_3^{(2n+1)} = \dots = A_{2\ell+1}^{(2n+1)} = 0$ . However, these eigenvalues and eigenvectors may be discarded because they give rise to values of  $\lambda$  that violate the criterion (2.135). The  $\phi$  Lamé functions of class II, corresponding to the first  $\ell+1$  eigenvectors, are now represented by infinite series

$$L_{\nu}^{(2n+1)}(\phi) = \sum_{r=0}^{\infty} A_{2r+1}^{(2n+1)} \cos(2r+1)\phi, \quad n = 0, 1, \dots, \ell, \quad \nu = 2\ell+2 \quad (2.147)$$

The corresponding  $\theta$  Lamé functions of class II, however, are given by finite series

$$L_{cpv}^{(2n+1)}(\theta) = \sum_{m=0}^{\ell} T^*(2m+1) A_{2m+1}^{(2n+1)} P_{\nu}^{2m+1}(\cos\theta), \quad n = 0, 1, 2, \dots, \ell, \\ \nu = 2\ell + 2, \quad (2.148)$$

because  $P_{\nu}^{2m+1}(\cos\theta) = 0$  and  $T^*(2m+1)$  is finite by (2.136), if  $m > \ell$ . For given  $k'$  and  $\nu = 2\ell + 2$ , we have found  $\ell + 1$   $\phi$  Lamé functions and  $\ell + 1$  corresponding  $\theta$  Lamé functions of class II. As for the Lamé functions  $L_{cv}^{(2n+1)}(\phi)$  the Fourier series (2.147) and its derivative converge uniformly in  $[0, 2\pi]$  by [6, Theorem 3.1, p. 50]. The  $\theta$  Lamé functions (2.148) are in fact polynomials in  $\cos\theta$  and  $\sin\theta$ , hence they are regular for  $0 \leq \theta \leq \pi$ .

The previous analysis for functions of class II, immediately carries over to Lamé functions of classes I, III, IV. In the case of functions of class IV, the underlying matrix  $M$  can be partitioned in exactly the same manner as in (2.142) and (2.145), for odd and even integer  $\nu$ , respectively. Both for  $\nu = 2\ell + 1$  and  $\nu = 2\ell + 2$ ,  $\ell = 0, 1, 2, \dots$ , we find that only the first  $\ell + 1$  eigenvalues of  $M$  give rise to values of  $\lambda$  that satisfy the criterion (2.135). The corresponding simple-periodic Lamé functions of class IV are represented by

$$L_{sv}^{(2n+1)}(\phi) = \sum_{r=0}^{\ell} B_{2r+1}^{(2n+1)} \sin(2r+1)\phi, \quad n = 0, 1, 2, \dots, \ell, \quad \text{if } \nu = 2\ell + 1, \quad (2.149)$$

$$L_{sv}^{(2n+1)}(\phi) = \sum_{r=0}^{\infty} B_{2r+1}^{(2n+1)} \sin(2r+1)\phi, \quad n = 0, 1, 2, \dots, \ell, \quad \text{if } \nu = 2\ell + 2. \quad (2.150)$$

The corresponding  $\theta$  Lamé functions of class IV are represented by

$$L_{spv}^{(2n+1)}(\theta) = \frac{(1-k^2 \cos^2 \theta)^{\frac{1}{2}}}{\sin \theta} \sum_{m=0}^{\ell} (2m+1) T^*(2m+1) B_{2m+1}^{(2n+1)} P_{\nu}^{2m+1}(\cos\theta), \\ n = 0, 1, 2, \dots, \ell, \quad (2.151)$$

both for  $\nu = 2\ell + 1$  and  $\nu = 2\ell + 2$ . For given  $k'$  and  $\nu = 2\ell + 1$  or  $\nu = 2\ell + 2$ , we find  $\ell + 1$   $\phi$  Lamé functions and  $\ell + 1$  corresponding  $\theta$  Lamé functions of

class IV, which are regular for  $0 \leq \phi < 2\pi$  and  $0 \leq \theta \leq \pi$ , respectively.

In the cases of Lamé functions of classes I and III the underlying matrices  $M$  can be partitioned as in (2.142) if  $\nu = 2\ell+2$ , and as in (2.145) if  $\nu = 2\ell+1$ . Thus, compared to the previous analysis of classes II and IV, the roles of odd and even integers  $\nu$  have interchanged. As before we only take into account the eigenvalues of  $M$  which give rise to values of  $\lambda$  that satisfy the criterion (2.135). Then the simple-periodic Lamé functions of class I are represented by

$$L_{c\nu}^{(2n)}(\phi) = \sum_{r=0}^{\infty} A_{2r}^{(2n)} \cos 2r\phi, \quad n = 0, 1, 2, \dots, \ell, \quad \text{if } \nu = 2\ell+1, \quad (2.152)$$

$$L_{c\nu}^{(2n)}(\phi) = \sum_{r=0}^{\ell+1} A_{2r}^{(2n)} \cos 2r\phi, \quad n = 0, 1, 2, \dots, \ell+1, \quad \text{if } \nu = 2\ell+2. \quad (2.153)$$

The corresponding  $\theta$  Lamé functions of class I are given by

$$L_{cp\nu}^{(2n)}(\theta) = \sum_{m=0}^{[\nu/2]} T^*(2m) A_{2m}^{(2n)} P_{\nu}^{2m}(\cos\theta), \quad n = 0, 1, 2, \dots, [\nu/2], \quad (2.154)$$

both for  $\nu = 2\ell+1$  and  $\nu = 2\ell+2$ ; here,  $[\nu/2]$  denotes the largest integer  $\leq \nu/2$ .

The simple-periodic Lamé functions of class III are represented by

$$L_{s\nu}^{(2n)}(\phi) = \sum_{r=1}^{\infty} B_{2r}^{(2n)} \sin 2r\phi, \quad n = 1, 2, 3, \dots, \ell, \quad \text{if } \nu = 2\ell+1, \quad (2.155)$$

$$L_{s\nu}^{(2n)}(\phi) = \sum_{r=1}^{\ell+1} B_{2r}^{(2n)} \sin 2r\phi, \quad n = 1, 2, 3, \dots, \ell+1, \quad \text{if } \nu = 2\ell+2. \quad (2.156)$$

The corresponding  $\theta$  Lamé functions of class III are

$$L_{sp\nu}^{(2n)}(\theta) = \frac{(1-k^2 \cos^2 \theta)^{\frac{1}{2}}}{\sin \theta} \sum_{m=1}^{[\nu/2]} 2m T^*(2m) B_{2m}^{(2n)} P_{\nu}^{2m}(\cos \theta),$$

$$n = 1, 2, \dots, [\nu/2], \quad (2.157)$$

both for  $\nu = 2\ell+1$  and  $\nu = 2\ell+2$ . For given  $k'$  and integer  $\nu$ , we have

thus found  $[\nu/2]+1$  Lamé functions of class I and  $[\nu/2]$  Lamé functions of class III. The  $\phi$  and  $\theta$  Lamé functions of classes I and III are regular for  $0 \leq \phi < 2\pi$  and  $0 \leq \theta \leq \pi$ , respectively. For completeness' sake we also consider the case  $\nu = 0$ . Then it is found from the criterion (2.135) that  $\lambda = 0$ . Correspondingly we have one  $\phi$  Lamé function and one  $\theta$  Lamé function, both of class I and given by  $L_{co}^{(0)}(\phi) = 1$ ,  $L_{cpo}^{(0)}(\theta) = 1$ , in accordance with (2.128).

Summarizing, for given  $k'$  and integer  $\nu = 0, 1, 2, \dots$ , we have found  $[\nu/2]+1$  Lamé functions of class I,  $[(\nu+1)/2]$  Lamé functions of class II,  $[\nu/2]$  Lamé functions of class III, and  $[(\nu+1)/2]$  Lamé functions of class IV. Thus the total number of Lamé functions is  $2\nu+1$ , which is equal to the number of eigenfunctions in (2.128) corresponding to the eigenvalue  $\mu^* = \nu(\nu+1)$ . The eigenfunctions  $v(\theta, \phi)$  can now be represented by products of  $\theta$  and  $\phi$  Lamé functions according to the following list:

$$I. \quad v_{cv}^{(2n)}(\theta, \phi) = L_{cpv}^{(2n)}(\theta) L_{cv}^{(2n)}(\phi), \quad \nu = 0, 1, 2, \dots, \quad n = 0, 1, \dots, [\nu/2], \quad (2.158a)$$

$$II. \quad v_{cv}^{(2n+1)}(\theta, \phi) = L_{cpv}^{(2n+1)}(\theta) L_{cv}^{(2n+1)}(\phi), \quad \nu = 1, 2, 3, \dots, \\ n = 0, 1, \dots, [(\nu-1)/2], \quad (2.158b)$$

$$III. \quad v_{sv}^{(2n)}(\theta, \phi) = L_{spv}^{(2n)}(\theta) L_{sv}^{(2n)}(\phi), \quad \nu = 2, 3, \dots, \quad n = 1, 2, \dots, [\nu/2], \quad (2.158c)$$

$$IV. \quad v_{sv}^{(2n+1)}(\theta, \phi) = L_{spv}^{(2n+1)}(\theta) L_{sv}^{(2n+1)}(\phi), \quad \nu = 1, 2, 3, \dots, \\ n = 0, 1, \dots, [(\nu-1)/2]. \quad (2.158d)$$

The eigenfunctions are regular for  $0 \leq \theta \leq \pi$ ,  $0 \leq \phi < 2\pi$ , i.e. on the unit sphere.

For later use we present some integral theorems, similar to those given in (2.57)-(2.62). Let  $\Omega$  be the unit sphere, described by  $r = 1$ ,  $0 \leq \theta \leq \pi$ ,  $0 \leq \phi < 2\pi$ , and let  $\bar{F}_t$  be the transverse component of the vector  $\bar{F}$ . Then the surface divergence theorem reads

$$\iint_{\Omega} \nabla_{\mathbf{t}} \cdot \bar{\mathbf{F}}_{\mathbf{t}} \, d\Omega = 0, \quad (2.159)$$

where  $d\Omega = h_{\theta}^* h_{\phi}^* d\theta d\phi$  is the surface area element. By substituting  $\bar{\mathbf{F}}_{\mathbf{t}} = v_1 \nabla_{\mathbf{t}} v_2$  into equation (2.159) we find

$$\iint_{\Omega} (\nabla_{\mathbf{t}} v_1 \cdot \nabla_{\mathbf{t}} v_2 + v_1 \nabla_{\mathbf{t}}^2 v_2) \, d\Omega = 0, \quad (2.160)$$

which is Green's first identity for the surface  $\Omega$ . Interchanging the subscripts 1 and 2 and subtracting the result from equation (2.160), we obtain Green's second identity for the surface  $\Omega$ :

$$\iint_{\Omega} (v_1 \nabla_{\mathbf{t}}^2 v_2 - v_2 \nabla_{\mathbf{t}}^2 v_1) \, d\Omega = 0. \quad (2.161)$$

Replacing  $\bar{\mathbf{F}}_{\mathbf{t}}$  in equation (2.159) by  $\hat{\mathbf{e}}_{\mathbf{r}} \times v \bar{\mathbf{F}}$ , we find

$$\iint_{\Omega} v \nabla_{\mathbf{t}} \times \bar{\mathbf{F}} \cdot \hat{\mathbf{e}}_{\mathbf{r}} \, d\Omega + \iint_{\Omega} \nabla_{\mathbf{t}} v \times \bar{\mathbf{F}} \cdot \hat{\mathbf{e}}_{\mathbf{r}} \, d\Omega = 0. \quad (2.162)$$

If  $v = \text{constant}$ , equation (2.162) becomes

$$\iint_{\Omega} \nabla_{\mathbf{t}} \times \bar{\mathbf{F}} \cdot \hat{\mathbf{e}}_{\mathbf{r}} \, d\Omega = 0,$$

which is Stokes' theorem.

By substituting  $\bar{\mathbf{F}}_{\mathbf{t}} = \hat{\mathbf{e}}_{\mathbf{r}} \times v_1 \nabla_{\mathbf{t}} v_2$  into the divergence theorem (2.159) we obtain

$$\iint_{\Omega} \nabla_{\mathbf{t}} v_1 \times \nabla_{\mathbf{t}} v_2 \cdot \hat{\mathbf{e}}_{\mathbf{r}} \, d\Omega = 0. \quad (2.163)$$

The integral theorems presented above are now used to establish integral relations and orthogonality properties for the  $\theta$  and  $\phi$  Lamé functions which are regular on the unit sphere. Let  $(\mu_1^*, v_1)$  and  $(\mu_2^*, v_2)$  be solutions of the eigenvalue problem (2.127) with  $\mu_1^* = v_1(v_1+1)$ ,  $\mu_2^* = v_2(v_2+1)$ , where  $v_1, v_2$  are non-negative integers. Then by substituting these solutions into Green's identities (2.160), (2.161), we

obtain the following results.

If  $\mu_1^* \neq \mu_2^*$ ,

$$\iint_{\Omega} v_1 v_2 d\Omega = 0, \tag{2.164}$$

$$\iint_{\Omega} \nabla_t v_1 \cdot \nabla_t v_2 d\Omega = 0; \tag{2.165}$$

if  $\mu_1^* = \mu_2^* = \mu^*$  and  $v_1 = v_2 = v$ ,

$$\iint_{\Omega} |\nabla_t v|^2 d\Omega = \mu^* \iint_{\Omega} v^2 d\Omega. \tag{2.166}$$

Thus the two eigenfunctions  $v_1$  and  $v_2$  as well as their transverse gradients are orthogonal if  $\mu_1^* \neq \mu_2^*$ .

It is easily verified that the integral relations (2.99)-(2.105) for periodic Lamé functions remain valid for the  $\phi$  Lamé functions corresponding to integer values of  $\nu$ , as derived in this section. Next we establish integral relations for the  $\theta$  Lamé functions corresponding to integer values of  $\nu$ ; compare (2.120)-(2.125a). Let  $(\lambda_m^*, L_{cp\nu_1}^{(m)}(\theta))$  and  $(\lambda_n^*, L_{cp\nu_2}^{(n)}(\theta))$  be solutions of the  $\theta$  Lamé equation (2.129) with  $\nu = \nu_1$  and  $\nu = \nu_2$ , respectively, where  $\nu_1, \nu_2$  are non-negative integers. In equation (2.129) we replace  $\nu, \lambda^*, \Theta(\theta)$  by  $\nu_1, \lambda_m^*, L_{cp\nu_1}^{(m)}(\theta)$ , and the result is multiplied by  $L_{cp\nu_2}^{(n)}(\theta)$ . Then by integrating over  $\theta$  from 0 to  $\pi$  and using the boundary conditions (2.133) or (2.134), we obtain

$$\begin{aligned} & \nu_1(\nu_1+1) \int_0^\pi (1-k^2 \cos^2 \theta)^{-\frac{1}{2}} k^2 \sin^2 \theta L_{cp\nu_1}^{(m)}(\theta) L_{cp\nu_2}^{(n)}(\theta) d\theta = \\ & = \lambda_m^* \int_0^\pi (1-k^2 \cos^2 \theta)^{-\frac{1}{2}} L_{cp\nu_1}^{(m)}(\theta) L_{cp\nu_2}^{(n)}(\theta) d\theta + \\ & + \int_0^\pi (1-k^2 \cos^2 \theta)^{\frac{1}{2}} \frac{d}{d\theta} \{L_{cp\nu_1}^{(m)}(\theta)\} \frac{d}{d\theta} \{L_{cp\nu_2}^{(n)}(\theta)\} d\theta. \end{aligned} \tag{2.167}$$

By interchanging the two solutions we find the relation (2.167) with  $v_1$  and  $\lambda_m^*$  replaced by  $v_2$  and  $\lambda_n^*$ , respectively. By subtracting the latter result from equation (2.167), we obtain

$$\begin{aligned} & \{v_1(v_1+1)-v_2(v_2+1)\} \int_0^\pi (1-k^2 \cos^2 \theta)^{-\frac{1}{2}} k^2 \sin^2 \theta L_{cpv_1}^{(m)}(\theta) L_{cpv_2}^{(n)}(\theta) d\theta = \\ & = (\lambda_m^* - \lambda_n^*) \int_0^\pi (1-k^2 \cos^2 \theta)^{-\frac{1}{2}} L_{cpv_1}^{(m)}(\theta) L_{cpv_2}^{(n)}(\theta) d\theta. \end{aligned} \quad (2.168)$$

From equations (2.168) and (2.167) we derive

$$\begin{aligned} & \{\lambda_m^* v_2(v_2+1) - \lambda_n^* v_1(v_1+1)\} \int_0^\pi (1-k^2 \cos^2 \theta)^{-\frac{1}{2}} L_{cpv_1}^{(m)}(\theta) L_{cpv_2}^{(n)}(\theta) d\theta = \\ & = \{v_1(v_1+1) - v_2(v_2+1)\} \int_0^\pi (1-k^2 \cos^2 \theta)^{\frac{1}{2}} \frac{d}{d\theta} \{L_{cpv_1}^{(m)}(\theta)\} \frac{d}{d\theta} \{L_{cpv_2}^{(n)}(\theta)\} d\theta. \end{aligned} \quad (2.169)$$

If  $v_1 = v_2 = v$  and  $\lambda_m^* \neq \lambda_n^*$ , we have from equations (2.168) and (2.167),

$$\int_0^\pi (1-k^2 \cos^2 \theta)^{-\frac{1}{2}} L_{cpv}^{(m)}(\theta) L_{cpv}^{(n)}(\theta) d\theta = 0, \quad (2.170)$$

$$\begin{aligned} & v(v+1) \int_0^\pi (1-k^2 \cos^2 \theta)^{-\frac{1}{2}} k^2 \sin^2 \theta L_{cpv}^{(m)}(\theta) L_{cpv}^{(n)}(\theta) d\theta = \\ & = \int_0^\pi (1-k^2 \cos^2 \theta)^{\frac{1}{2}} \frac{d}{d\theta} \{L_{cpv}^{(m)}(\theta)\} \frac{d}{d\theta} \{L_{cpv}^{(n)}(\theta)\} d\theta. \end{aligned} \quad (2.171)$$

If  $v_1 = v_2 = v$  and  $m = n$ , we find from equation (2.167),

$$\begin{aligned} & v(v+1) \int_0^\pi (1-k^2 \cos^2 \theta)^{-\frac{1}{2}} k^2 \sin^2 \theta \{L_{cpv}^{(m)}(\theta)\}^2 d\theta = \\ & = \lambda_m^* \int_0^\pi (1-k^2 \cos^2 \theta)^{-\frac{1}{2}} \{L_{cpv}^{(m)}(\theta)\}^2 d\theta + \int_0^\pi (1-k^2 \cos^2 \theta)^{\frac{1}{2}} \left[ \frac{d}{d\theta} \{L_{cpv}^{(m)}(\theta)\} \right]^2 d\theta. \end{aligned} \quad (2.172)$$

Similar integral relations can be easily derived for the  $\theta$  Lamé functions of other classes, corresponding to integer values of  $\nu$ .

The eigenfunctions  $v(\theta, \phi)$ , regular on the unit sphere, have been listed in (2.158), represented by products of  $\theta$  and  $\phi$  Lamé functions. According to (2.164), any two eigenfunctions corresponding to different eigenvalues are orthogonal, hence, for example,

$$\iint_{\Omega} v_{cv_1}^{(m)}(\theta, \phi) v_{cv_2}^{(n)}(\theta, \phi) d\Omega = 0, \text{ if } \nu_1 \neq \nu_2. \quad (2.173)$$

It follows immediately from (2.102) and (2.170) that the relation (2.173) also holds if  $\nu_1 = \nu_2$ ,  $m \neq n$ , i.e. for two different eigenfunctions corresponding to the same eigenvalue. Thus we conclude that the eigenfunctions  $v_{cv}^{(n)}(\theta, \phi)$ ,  $v_{sv}^{(n)}(\theta, \phi)$ , given by (2.158), form an orthogonal system on the unit sphere  $\Omega$ , with the orthogonality relations

$$\iint_{\Omega} v_{cv_1}^{(m)}(\theta, \phi) v_{cv_2}^{(n)}(\theta, \phi) d\Omega = 0 \text{ if } \nu_1 \neq \nu_2, \text{ and if } \nu_1 = \nu_2, m \neq n; \quad (2.174a)$$

$$\iint_{\Omega} v_{cv_1}^{(m)}(\theta, \phi) v_{sv_2}^{(n)}(\theta, \phi) d\Omega = 0; \quad (2.174b)$$

$$\iint_{\Omega} v_{sv_1}^{(m)}(\theta, \phi) v_{sv_2}^{(n)}(\theta, \phi) d\Omega = 0 \text{ if } \nu_1 \neq \nu_2, \text{ and if } \nu_1 = \nu_2, m \neq n. \quad (2.174c)$$

According to (2.165), the transverse gradients of any two eigenfunctions (2.158), corresponding to different eigenvalues are orthogonal, hence, for instance,

$$\iint_{\Omega} \nabla_t v_{cv_1}^{(m)}(\theta, \phi) \cdot \nabla_t v_{cv_2}^{(n)}(\theta, \phi) d\Omega = 0 \text{ if } \nu_1 \neq \nu_2. \quad (2.175)$$

By using (2.49c), (2.102) and (2.170), we can easily show that (2.175) also holds if  $\nu_1 = \nu_2$ ,  $m \neq n$ , i.e. for the transverse gradients of two different eigenfunctions corresponding to the same eigenvalue. Hence, the transverse gradients of the eigenfunctions (2.158) form an orthogonal system on the unit sphere  $\Omega$ , with the orthogonality relations

$$\oint_{\Omega} \nabla_t v_{cv_1}^{(m)}(\theta, \phi) \cdot \nabla_t v_{cv_2}^{(n)}(\theta, \phi) d\Omega = 0 \text{ if } v_1 \neq v_2, \text{ and if } v_1 = v_2, m \neq n; \quad (2.176a)$$

$$\oint_{\Omega} \nabla_t v_{cv_1}^{(m)}(\theta, \phi) \cdot \nabla_t v_{sv_2}^{(n)}(\theta, \phi) d\Omega = 0; \quad (2.176b)$$

$$\oint_{\Omega} \nabla_t v_{sv_1}^{(m)}(\theta, \phi) \cdot \nabla_t v_{sv_2}^{(n)}(\theta, \phi) d\Omega = 0 \text{ if } v_1 \neq v_2, \text{ and if } v_1 = v_2, m \neq n. \quad (2.176c)$$

Finally, we summarize the main results of this section.

1. For integer values of  $\nu$  the  $\theta$  Lamé functions can be represented by finite series of Legendre functions  $P_{\nu}^m(\cos\theta)$ , and are regular for  $0 \leq \theta \leq \pi$ .
2. For odd integer values of  $\nu$  the  $\phi$  Lamé functions of classes II and IV can be represented by finite Fourier series, and those of classes I and III by infinite Fourier series.  
For even integer values of  $\nu$  the  $\phi$  Lamé functions of classes I and III can be represented by finite Fourier series, and those of classes II and IV by infinite Fourier series.
3. The eigenfunctions  $v_{cv}^{(n)}(\theta, \phi)$ ,  $v_{sv}^{(n)}(\theta, \phi)$ , represented in (2.158) by products of  $\theta$  and  $\phi$  Lamé functions, form a complete orthogonal system on the unit sphere  $\Omega$ :  $0 \leq \theta \leq \pi$ ,  $0 \leq \phi < 2\pi$ . Let  $f(\theta, \phi)$  be an arbitrary scalar function defined on the unit sphere, which together with its first and second derivatives is continuous. Then  $f(\theta, \phi)$  can be represented by the series-expansion

$$f(\theta, \phi) = \sum_{\nu=0}^{\infty} \sum_{n=0}^{\nu} a_{\nu n} v_{cv}^{(n)}(\theta, \phi) + \sum_{\nu=1}^{\infty} \sum_{n=1}^{\nu} b_{\nu n} v_{sv}^{(n)}(\theta, \phi), \quad (2.177)$$

in which the expansion coefficients  $a_{\nu n}$  and  $b_{\nu n}$  are determined by

$$a_{\nu n} = \frac{\oint_{\Omega} f(\theta, \phi) v_{cv}^{(n)}(\theta, \phi) d\Omega}{\oint_{\Omega} \{v_{cv}^{(n)}(\theta, \phi)\}^2 d\Omega}, \quad (2.178)$$

$$b_{\nu n} = \frac{\oint_{\Omega} f(\theta, \phi) v_{sv}^{(n)}(\theta, \phi) d\Omega}{\oint_{\Omega} \{v_{sv}^{(n)}(\theta, \phi)\}^2 d\Omega}. \quad (2.179)$$

## 2.6. References

- [1] Abramowitz, M., and I.A. Stegun (Editors), Handbook of Mathematical Functions, with Formulas, Graphs and Mathematical Tables. National Bureau of Standards, Washington, 1964. (Applied Mathematics Series, no. 55).
- [2] Bladel, J. van, Electromagnetic Fields. McGraw-Hill, New York, 1964, p. 499-505.
- [2a] Courant, R., and D. Hilbert, Methods of Mathematical Physics, Vol. I. Interscience, New York, 1953, Chapter VII, § 5.
- [3] Ince, E.L., The periodic Lamé functions. Proc. Roy. Soc. Edinburgh Sect. A 60 (1940), 47-63.
- [4] Ince, E.L., Further investigations into the periodic Lamé functions. Proc. Roy. Soc. Edinburgh Sect. A 60 (1940), 83-99.
- [5] Jansen, J.K.M., Simple-periodic and Non-periodic Lamé Functions and their Application in the Theory of Conical Waveguides. Ph.D. Thesis, Eindhoven University of Technology, Eindhoven, 1976.
- [6] Jansen, J.K.M., Simple-periodic and Non-periodic Lamé Functions. Mathematical Centre Tracts 72, Math. Centrum, Amsterdam, 1977.
- [7] Kong, A.C., The Propagation and Radiation Properties of Waveguides and Horns of Elliptical Cross-section. Ph.D. Thesis, University of Surrey, Guildford, 1971.
- [8] Sahalos, J.N., and G.A. Thiele, The eigenfunction solution to scattered fields and surface currents of a vertex. IEEE Trans. Antennas and Propagat. AP-31 (1983), 206-210.
- [9] Satterwhite, R., Diffraction by a quarter plane, the exact solution, and some numerical results. IEEE Trans. Antennas and Propagat. AP-22 (1974), 500-503.



### 3. WAVE PROPAGATION IN ELLIPTICAL CONES

#### 3.1. Introduction

We start this chapter with a survey of previous researches relevant to our present study.

In 1971 Kong [8] reported about his investigation of wave propagation and radiation problems for elliptical-cylindrical waveguides and elliptical-conical horns with smooth walls of perfectly conducting material. The modes in the waveguide have been classified into four classes, reflecting that the fields of the modes are odd or even symmetric, and transverse electric or transverse magnetic. The field components of the modes have been expressed in terms of Mathieu functions. The beamwidths of the radiation patterns of the guide, when excited by one of the lowest modes, the  ${}_{e}TE_{11}$  or  ${}_{o}TE_{11}$  cylindrical mode, are controlled by varying the aspect ratio of the elliptical guide. The two modes mentioned give rise to radiation patterns that differ from each other. Consequently, the guide cannot radiate circularly polarized waves in all directions in space. Furthermore, it has been found that for both modes of operation the beamwidths are frequency-dependent: they decrease monotonically with increasing frequency for all aspect ratios.

Kong has also studied the propagation of waves in elliptical-conical horns of infinite length. As in the case of the elliptical guide the modes have been classified into four classes. The field components of the conical modes have been expressed in terms of spherical Bessel functions, simple-periodic Lamé functions and nonperiodic Lamé functions. The latter functions have been computed by numerical integration methods. The radiation patterns due to the two principal modes, the  ${}_{e}TE_{11}$  and  ${}_{o}TE_{11}$  conical modes, have been determined by a Kirchhoff-Huygens integration of the modal fields at the aperture of a truncated cone. The radiation patterns associated with these modes are not identical, which implies that the horn cannot radiate circularly polarized waves in all directions in space. The variation of beamwidth with frequency has been studied. It has been found that radiation patterns with beamwidths that are frequency-independent, can be achieved.

In 1973 Jansen and Jeuken [6] published the results of their research of wave propagation and radiation problems for elliptical-cylindrical waveguides with anisotropic impedance boundary. Their objective has been to study whether such devices can radiate circularly polarized waves in all directions in space, whereas the radiation patterns have elliptical cross-sections. Some interesting properties have been derived for electromagnetic fields for which  $\vec{E} = + jZ_0 \vec{H}$ . Here,  $Z_0$  is the free-space wave impedance which equals  $(\mu_0/\epsilon_0)^{1/2}$ , where  $\mu_0$  is the permeability and  $\epsilon_0$  the permittivity of free space. It has been shown that, if  $\vec{E} = + jZ_0 \vec{H}$  on a closed surface  $S$  enclosing the field sources, then the same relation holds for the electric and magnetic fields at any observation point  $P$  outside  $S$ . If  $P$  is in the far-field region of the sources, then the fields at  $P$  are circularly polarized.

It has been found in [6] that the impedance boundary conditions are only satisfied by hybrid modes which involve both transverse electric and transverse magnetic fields. The modes have been classified into odd and even symmetric modes, that have pairwise identical cut-off frequencies, identical propagation constants and identical radiation patterns of elliptical cross-section. These modes, when added with a phase difference of  $90^\circ$ , give rise to fields for which  $\vec{E} = + jZ_0 \vec{H}$ . Hence, the waveguide has, in theory, the required radiation properties. Several corrugated antennas have been constructed and tested to check the validity of the theory. In the analysis of these antennas the influence of the corrugations has been accounted for by the anisotropic impedance boundary conditions. Reasonable agreement between theoretical and measured results has been found provided the dimensions of the aperture of the antenna are not small in terms of wavelength.

In 1976 Jansen [7] investigated the electromagnetic fields in elliptical cones with smooth walls of perfectly conducting material. He has expressed the fields in terms of spherical Bessel functions, simple-periodic Lamé functions and nonperiodic Lamé functions, as it was done before by Kong [8]. In Jansen's study emphasis has been on theoretical and computational aspects of the Lamé functions. The main results from [7] have already been recalled in chapter 2 of the present thesis.

In 1979 and 1980, Vokurka [9], [10] published results of measurements

and computations for corrugated elliptical horn radiators with small flare angles. Special attention has been paid to the mode excitation. The coupling section between the exciting waveguide and the horn is important for single-mode excitation. Excellent polarization purity and equality of radiation patterns have been found for odd and even hybrid modes. The theoretical results for the copolarized radiation are in good agreement with experimental results. The computed results have been obtained by approximating the aperture field of the elliptical horn by the waveguide modal field multiplied by a quadratic phase distribution. Vokurka has concluded that the corrugated elliptical horn radiators with small flare angles are eminently suitable for applications where radiation patterns with elliptical cross-sections and high polarization purity are required, such as for the broadcasting-satellite service.

In 1982 Fasold et al. [3] reported on the design of an antenna system intended for use on board of TV-SAT for the coverage of Western Germany by a circularly polarized elliptical beam. They have used an antenna system consisting of an offset parabolic reflector fed by a corrugated elliptical horn. The measured radiation patterns of an experimental model of the antenna system show that it is possible to meet the WARC-77 regulations [4]. Measured radiation patterns of the horn radiator have been used in the computation of the secondary radiation patterns.

The main point of this survey is that corrugated elliptical horn radiators have radiation patterns with elliptical cross-sections and high polarization purity. These properties can be utilized in, for instance, reflector antennas of broadcasting satellites. For the computation of the radiation pattern of a reflector antenna we need to know the performance of its feeding element. In this and the following chapters we will develop methods for determining the wave propagation and radiation behaviour for anisotropic elliptical horns with arbitrary flare angles and aspect ratios. The investigation of wave propagation in elliptical cones starts with the introduction of transverse electric (TE) and transverse magnetic (TM) field solutions for Maxwell's equations in the sphero-conal coordinate system. These solutions constitute a complete set of waves (modes), in terms of

which an arbitrary field can be expanded. In perfectly conducting cones TE and TM solutions can exist independently. In anisotropic cones, however, the field solutions are of a hybrid nature. They are represented by TE- and TM-fields that are coupled. The analysis for the elliptical cone with a corrugated boundary will be based on the anisotropic surface-impedance model which does not take into account the actual electromagnetic fields inside the corrugations.

### 3.2. The perfectly conducting elliptical cone

This section deals with the solution of Maxwell's equations inside a perfectly conducting elliptical cone. The solutions are expressed in terms of the sphero-conal coordinates  $r, \theta, \phi$ , as introduced in (2.1)-(2.3). The semi-infinite elliptical cone is described by  $\theta = \theta_0$  (see Figure 2.1a), and its aspect ratio is  $a_{r\theta}$ . The medium inside the cone is free space with permittivity  $\epsilon_0$  and permeability  $\mu_0$ . Inside the cone, that is, for  $r > 0$ ,  $0 \leq \theta < \theta_0$ ,  $0 \leq \phi < 2\pi$ , the solutions of Maxwell's equations separate into two sets as has been proved by Jansen [7, Theorem 5.3, p. 86]. For one set the electric field has a zero radial component: these solutions are of transverse electric (TE) type. The TE-field components are derivable from a magnetic vector potential that has a single component in the radial direction. For the second set the magnetic field has a zero radial component: these solutions are of transverse magnetic (TM) type. The TM-field components are derivable from an electric vector potential that has a single component in the radial direction.

Assuming a time dependence  $\exp(j\omega t)$ , Maxwell's equations read

$$\nabla \times \bar{E} = -j\omega \mu_0 \bar{H}, \quad (3.1)$$

$$\nabla \times \bar{H} = j\omega \epsilon_0 \bar{E}. \quad (3.2)$$

The decomposition of the electromagnetic field inside an elliptical cone into TE- and TM-fields follows from [7, Theorem 5.3, p. 86]. This theorem states that any electromagnetic field in a simply connected, source-free space domain can be written as

$$\bar{E} = -j\omega\mu_0 \nabla x(r\psi_h \hat{e}_r) + \nabla x \nabla x(r\psi_e \hat{e}_r), \quad (3.3)$$

$$\bar{H} = \nabla x \nabla x(r\psi_h \hat{e}_r) + j\omega\epsilon_0 \nabla x(r\psi_e \hat{e}_r), \quad (3.4)$$

where the potentials  $\psi_h$  and  $\psi_e$  satisfy the Helmholtz equation

$$\nabla^2 \psi_{h,e} + k^{*2} \psi_{h,e} = 0, \quad (3.4a)$$

in which  $k^* = \omega(\epsilon_0 \mu_0)^{1/2} = 2\pi/\lambda_0$  is the free-space wave number and  $\lambda_0$  is the free-space wavelength. From equations (3.3) and (3.4) we find that the TE-field is given by

$$\bar{E} = -j\omega\mu_0 \nabla x(r\psi_h \hat{e}_r), \quad (3.5)$$

$$\bar{H} = \nabla x \nabla x(r\psi_h \hat{e}_r), \quad (3.6)$$

and the TM-field by

$$\bar{E} = \nabla x \nabla x(r\psi_e \hat{e}_r), \quad (3.7)$$

$$\bar{H} = j\omega\epsilon_0 \nabla x(r\psi_e \hat{e}_r). \quad (3.8)$$

Hence, in terms of the sphero-conal coordinates  $r, \theta, \phi$ , the components of the TE-field are

$$E_r = 0, \quad H_r = \frac{-1}{rh_\theta^* h_\phi^*} \left\{ \frac{\partial}{\partial \theta} \left( \frac{h_\phi^*}{h_\theta^*} \frac{\partial \psi_h}{\partial \theta} \right) + \frac{\partial}{\partial \phi} \left( \frac{h_\theta^*}{h_\phi^*} \frac{\partial \psi_h}{\partial \phi} \right) \right\},$$

$$E_\theta = \frac{-j\omega\mu_0}{h_\phi^*} \frac{\partial \psi_h}{\partial \phi}, \quad H_\theta = \frac{1}{rh_\theta^*} \frac{\partial^2 (r\psi_h)}{\partial r \partial \theta}, \quad (3.9)$$

$$E_\phi = \frac{j\omega\mu_0}{h_\theta^*} \frac{\partial \psi_h}{\partial \theta}, \quad H_\phi = \frac{1}{rh_\phi^*} \frac{\partial^2 (r\psi_h)}{\partial r \partial \phi},$$

and the components of the TM-field are

$$E_r = \frac{-1}{rh_\theta^* h_\phi^*} \left\{ \frac{\partial}{\partial \theta} \left( \frac{h_\phi^*}{h_\theta^*} \frac{\partial \psi_e}{\partial \theta} \right) + \frac{\partial}{\partial \phi} \left( \frac{h_\theta^*}{h_\phi^*} \frac{\partial \psi_e}{\partial \phi} \right) \right\}, \quad H_r = 0,$$

$$E_{\theta} = \frac{1}{rh_{\theta}^*} \frac{\partial^2 (r\psi_e)}{\partial r \partial \theta}, \quad H_{\theta} = \frac{j\omega\epsilon_0}{h_{\phi}^*} \frac{\partial \psi_e}{\partial \phi}, \quad (3.10)$$

$$E_{\phi} = \frac{1}{rh_{\phi}^*} \frac{\partial^2 (r\psi_e)}{\partial r \partial \phi}, \quad H_{\phi} = \frac{-j\omega\epsilon_0}{h_{\theta}^*} \frac{\partial \psi_e}{\partial \theta}.$$

The expressions for the non-vanishing radial components are equal to  $-\nabla_t^2 \psi_{h,e}/r$  by equation (2.52c), hence, by using (2.66) and (2.69) we derive that these components equal  $\nu(\nu+1)\psi_{h,e}/r$ . We now use these results to determine the TE- and TM-fields inside the perfectly conducting cone described by  $\theta = \theta_0$ . At the cone surface the tangential electric field components must vanish, hence, from (3.9) and (3.10) we have the boundary conditions

$$\frac{\partial}{\partial \theta} (\psi_h) \Big|_{\theta_0} = 0, \quad (3.11)$$

$$\psi_e \Big|_{\theta_0} = 0, \quad (3.12)$$

for the TE- and TM-fields, respectively. Thus the potentials  $\psi_h$  and  $\psi_e$  must satisfy the Helmholtz equation (3.4a) and the homogeneous boundary condition (3.11) or (3.12). The latter problem has been extensively discussed in sections 2.4 and 2.5. By use of the method of separation of variables it has been found there that the problem has a denumerable set of eigensolutions or modes. The modes obtained are represented by products of spherical Bessel functions, nonperiodic  $\theta$  Lamé functions and simple-periodic  $\phi$  Lamé functions. We now choose the spherical Bessel function to be  $h_{\nu}^{(2)}(k^*r)$ , see (2.80), which means that the mode is propagating in the outward radial direction. Then the corresponding outward propagating TE- and TM-modes are derived from the potentials  $\psi_h$  and  $\psi_e$ , given by

$$h_{\nu}^{(2)}(k^*r) L_{cp\nu}^{(m)}(\theta) L_{c\nu}^{(m)}(\phi), \quad (3.13)$$

or

$$h_{\nu}^{(2)}(k^*r) L_{sp\nu}^{(m)}(\theta) L_{s\nu}^{(m)}(\phi), \quad (3.14)$$

in which the mode-number  $\nu$  is determined by either of the boundary conditions (3.11) or (3.12).

We list in full detail the expressions for the field components of the TE- and TM-modes inside the cone under consideration.

TE<sub>cmn</sub> mode:

$$E_r = 0,$$

$$E_\theta = \frac{-j\omega\mu_0}{h_\phi^*} h_{\nu_n}^{(2)}(k^*r) L_{cp\nu_n}^{(m)}(\theta) \frac{d}{d\phi} \{L_{c\nu_n}^{(m)}(\phi)\},$$

$$E_\phi = \frac{j\omega\mu_0}{h_\theta^*} h_{\nu_n}^{(2)}(k^*r) \frac{d}{d\theta} \{L_{cp\nu_n}^{(m)}(\theta)\} L_{c\nu_n}^{(m)}(\phi),$$

$$H_r = \frac{1}{r} \nu_n (\nu_n + 1) h_{\nu_n}^{(2)}(k^*r) L_{cp\nu_n}^{(m)}(\theta) L_{c\nu_n}^{(m)}(\phi), \quad (3.15)$$

$$H_\theta = \frac{1}{rh_\theta^*} \frac{d}{dr} \{rh_{\nu_n}^{(2)}(k^*r)\} \frac{d}{d\theta} \{L_{cp\nu_n}^{(m)}(\theta)\} L_{c\nu_n}^{(m)}(\phi),$$

$$H_\phi = \frac{1}{rh_\phi^*} \frac{d}{dr} \{rh_{\nu_n}^{(2)}(k^*r)\} L_{cp\nu_n}^{(m)}(\theta) \frac{d}{d\phi} \{L_{c\nu_n}^{(m)}(\phi)\},$$

where  $m = 0, 1, 2, \dots$ ,  $n = 1, 2, 3, \dots$ , and  $\nu_n$  is the  $n$ -th positive root of

$$\left. \frac{d}{d\theta} \{L_{cp\nu_n}^{(m)}(\theta)\} \right|_{\theta_0} = 0. \quad (3.16)$$

TE<sub>smn</sub> mode:

$$E_r = 0,$$

$$E_\theta = \frac{-j\omega\mu_0}{h_\phi^*} h_{\nu_n}^{(2)}(k^*r) L_{sp\nu_n}^{(m)}(\theta) \frac{d}{d\phi} \{L_{s\nu_n}^{(m)}(\phi)\},$$

$$E_\phi = \frac{j\omega\mu_0}{h_\theta^*} h_{\nu_n}^{(2)}(k^*r) \frac{d}{d\theta} \{L_{sp\nu_n}^{(m)}(\theta)\} L_{s\nu_n}^{(m)}(\phi), \quad (3.17)$$

$$H_r = \frac{1}{r} v_n (v_n + 1) h_{v_n}^{(2)}(k^*r) L_{spv_n}^{(m)}(\theta) L_{sv_n}^{(m)}(\phi),$$

$$H_\theta = \frac{1}{rh_\theta^*} \frac{d}{dr} \{rh_{v_n}^{(2)}(k^*r)\} \frac{d}{d\theta} \{L_{spv_n}^{(m)}(\theta)\} L_{sv_n}^{(m)}(\phi),$$

$$H_\phi = \frac{1}{rh_\phi^*} \frac{d}{dr} \{rh_{v_n}^{(2)}(k^*r)\} L_{spv_n}^{(m)}(\theta) \frac{d}{d\phi} \{L_{sv_n}^{(m)}(\phi)\},$$

where  $m = 1, 2, 3, \dots$ ,  $n = 1, 2, 3, \dots$ , and  $v_n$  is the  $n$ -th positive root of

$$\left. \frac{d}{d\theta} \{L_{spv_n}^{(m)}(\theta)\} \right|_{\theta_0} = 0. \quad (3.18)$$

TM<sub>cmn</sub> mode:

$$E_r = \frac{1}{r} v_n (v_n + 1) h_{v_n}^{(2)}(k^*r) L_{cpv_n}^{(m)}(\theta) L_{cv_n}^{(m)}(\phi),$$

$$E_\theta = \frac{1}{rh_\theta^*} \frac{d}{dr} \{rh_{v_n}^{(2)}(k^*r)\} \frac{d}{d\theta} \{L_{cpv_n}^{(m)}(\theta)\} L_{cv_n}^{(m)}(\phi),$$

$$E_\phi = \frac{1}{rh_\phi^*} \frac{d}{dr} \{rh_{v_n}^{(2)}(k^*r)\} L_{cpv_n}^{(m)}(\theta) \frac{d}{d\phi} \{L_{cv_n}^{(m)}(\phi)\},$$

(3.19)

$$H_r = 0,$$

$$H_\theta = \frac{j\omega\epsilon_0}{h_\theta^*} h_{v_n}^{(2)}(k^*r) L_{cpv_n}^{(m)}(\theta) \frac{d}{d\phi} \{L_{cv_n}^{(m)}(\phi)\},$$

$$H_\phi = \frac{-j\omega\epsilon_0}{h_\theta^*} h_{v_n}^{(2)}(k^*r) \frac{d}{d\theta} \{L_{cpv_n}^{(m)}(\theta)\} L_{cv_n}^{(m)}(\phi),$$

where  $m = 0, 1, 2, \dots$ ,  $n = 1, 2, 3, \dots$ , and  $v_n$  is the  $n$ -th positive root of

$$\left. L_{cpv_n}^{(m)}(\theta) \right|_{\theta_0} = 0. \quad (3.20)$$

TM<sub>snn</sub> mode:

$$E_r = \frac{1}{r} v_n (v_n + 1) h_{v_n}^{(2)}(k^*r) L_{spv_n}^{(m)}(\theta) L_{sv_n}^{(m)}(\phi),$$

$$E_\theta = \frac{1}{rh_\theta^*} \frac{d}{dr} \{rh_{v_n}^{(2)}(k^*r)\} \frac{d}{d\theta} \{L_{spv_n}^{(m)}(\theta)\} L_{sv_n}^{(m)}(\phi),$$

$$E_\phi = \frac{1}{rh_\phi^*} \frac{d}{dr} \{rh_{v_n}^{(2)}(k^*r)\} L_{spv_n}^{(m)}(\theta) \frac{d}{d\phi} \{L_{sv_n}^{(m)}(\phi)\},$$

(3.21)

$$H_r = 0,$$

$$H_\theta = \frac{j\omega\epsilon_0}{h_\phi^*} h_{v_n}^{(2)}(k^*r) L_{spv_n}^{(m)}(\theta) \frac{d}{d\phi} \{L_{sv_n}^{(m)}(\phi)\},$$

$$H_\phi = \frac{-j\omega\epsilon_0}{h_\theta^*} h_{v_n}^{(2)}(k^*r) \frac{d}{d\theta} \{L_{spv_n}^{(m)}(\theta)\} L_{sv_n}^{(m)}(\phi),$$

where  $m = 1, 2, 3, \dots$ ,  $n = 1, 2, 3, \dots$ , and  $v_n$  is the  $n$ -th positive root of

$$L_{spv_n}^{(m)}(\theta) \Big|_{\theta=0} = 0. \tag{3.22}$$

By use of the large-argument approximation (2.84) of  $h_{v_n}^{(2)}(k^*r)$ , it is found that for large  $k^*r$  the transverse field components of the modes decay according to  $r^{-1}$ , whereas the radial field components decay according to  $r^{-2}$ . Furthermore, the characteristic wave impedance in the radial direction, given by  $E_\theta/H_\phi$  or equivalently by  $-E_\phi/H_\theta$ , tends to the free-space wave impedance  $Z_0 = (\mu_0/\epsilon_0)^{1/2}$  for large values of  $k^*r$ .

We now investigate the symmetry properties of the fields and classify the modes accordingly into odd and even symmetric modes. A mode is called odd symmetric if the magnetic field is symmetric with respect to  $\phi = 0$ , that is with respect to the  $xz$ -plane in Figure 2.1a (the minor axis of the elliptical cone is in this plane). A mode is called even symmetric if the electric field is symmetric with respect to  $\phi = 0$ . Using the symmetry properties of the periodic Lamé functions, given by (2.95)-(2.98), we then derive that the TE<sub>cmn</sub> and TM<sub>snn</sub> modes are odd

symmetric because

$$H_{\theta}(\phi) = H_{\theta}(2\pi-\phi), \quad H_{\phi}(\phi) = -H_{\phi}(2\pi-\phi); \quad (3.23)$$

these modes will be denoted by  ${}_{\circ}TE_{mn}$  and  ${}_{\circ}TM_{mn}$ , respectively. Likewise, we derive that the  $TE_{smn}$  and  $TM_{cmn}$  modes are even symmetric because

$$E_{\theta}(\phi) = E_{\theta}(2\pi-\phi), \quad E_{\phi}(\phi) = -E_{\phi}(2\pi-\phi); \quad (3.24)$$

these modes will be denoted by  ${}_eTE_{mn}$  and  ${}_eTM_{mn}$ , respectively. We point out that this classification differs from those in [7] and [8], which are based on the symmetry properties of the potentials  $\psi_h$  and  $\psi_e$ .

As an example we present in Table 3.1 the numerical values of the mode-numbers  $\nu$  as a function of  $\theta_{\circ}$ , for the odd and even  $TE_{11}$  and  $TM_{11}$  modes in perfectly conducting elliptical cones with  $a_{r\theta} = \frac{1}{2}$ . In Table 3.2 we present the corresponding numerical results for a circular cone in which case  $a_{r\theta} = 1$ . Then the difference between odd and even symmetry disappears. The mode-numbers in Table 3.2 have also been calculated from equations (3.16), (3.18), (3.20) and (3.22). The results given in Tables 3.1 and 3.2 agree with those of [8] and [5], respectively. In the Figures 3.1a and 3.1b we have plotted examples of the normalized transverse electric field of the  ${}_{\circ}TE_{11}$  and  ${}_{\circ}TM_{11}$  modes. The examples pertain to an elliptical cone with the parameters  $\theta_{\circ} = 20^{\circ}$  and  $a_{r\theta} = \frac{1}{2}$ . The mode-numbers  $\nu$  are obtained from the Table 3.1. Note that the transverse fields in the  $yz$ -plane do not vanish at the boundary.

A comment on the convergence interval of the series representing the nonperiodic Lamé functions is now in order. According to [7, Theorem 3.3, p. 59] the series given by (2.115)-(2.118) converge uniformly on any closed subinterval of the interval  $0 \leq \theta < 2 \arctan\{(1+k)/(1-k)\}^{\frac{1}{2}} = \theta_c$ . Because  $0 \leq k \leq 1$  it is found that  $\theta_c \geq \pi/2$ . Cones described by  $\theta = \theta_{\circ} < \pi/2$  will be dealt with, so  $\theta_c > \theta_{\circ}$ , and the series represented by (2.115)-(2.118) suffice in the present study.

For an outward propagating TE mode the time-average power-flow in the radial direction through a spherical cap  $S$ , described by  $r = r_a$ ,  $0 \leq \theta \leq \theta_{\circ}$ ,  $0 \leq \phi < 2\pi$ , is given by [2]

$\theta_o$ (degr.)	$o^{TE}_{11}$	$e^{TE}_{11}$	$e^{TM}_{11}$	$o^{TM}_{11}$
5	19.7930	10.3396	38.7951	28.3210
6	16.4242	8.5711	32.2595	23.5592
7	14.0198	7.3135	27.5932	20.1642
8	12.2183	6.3752	24.0953	17.6233
9	10.8186	5.6497	21.3761	15.6516
10	9.7002	5.0729	19.2022	14.0784
11	8.7863	4.6043	17.4247	12.7948
12	8.0258	4.2167	15.9444	11.7283
13	7.3832	3.8913	14.6929	10.8287
14	6.8332	3.6148	13.6210	10.0602
15	6.3574	3.3772	12.6927	9.3964
16	5.9417	3.1712	11.8812	8.8177
17	5.5756	2.9911	11.1658	8.3089
18	5.2507	2.8325	10.5304	7.8583
19	4.9605	2.6921	9.9624	7.4566
20	4.6999	2.5669	9.4516	7.0965
21	4.4645	2.5549	8.9900	6.7719
22	4.2508	2.3540	8.5707	6.4780
23	4.0562	2.2629	8.1882	6.2106
24	3.8781	2.1802	7.8378	5.9665
25	3.7146	2.1050	7.5158	5.7427

Table 3.1. Numerical values of the mode-numbers  $\nu$  as a function of  $\theta_o$ , for the odd and even  $TE_{11}$  and  $TM_{11}$  modes in a perfectly conducting elliptical cone  $\theta = \theta_o$ , with  $a_{r\theta} = \frac{1}{2}$ .

$$P_r = \frac{1}{2} \operatorname{Re} \iint_S \bar{\mathbf{E}} \times \bar{\mathbf{H}}^* \cdot \hat{\mathbf{e}}_r \, dS = \frac{1}{2} \operatorname{Re} \iint_S \bar{\mathbf{E}}_t \times \bar{\mathbf{H}}_t^* \cdot \hat{\mathbf{e}}_r \, dS, \quad (3.25)$$

where  $dS = r_a^2 h_\theta^* h_\phi^* d\theta d\phi$ .  $P_r$  can be expressed as an integral of the square of  $v_h(\theta, \phi)$ , which represents the transverse dependence of the potential  $\psi_h$  of the TE mode, as will be shown now.

From equation (3.9) we find that the transverse fields, expressed in terms of the potential  $\psi_h$ , are given by

$$\bar{\mathbf{E}}_t = j\omega\mu_o \hat{\mathbf{e}}_r \times \nabla_t \psi_h, \quad (3.26)$$

$\theta_o$ (degr.)	TE <sub>11</sub>	TM <sub>11</sub>	$\theta_o$ (degr.)	TE <sub>11</sub>	TM <sub>11</sub>
5	20.6155	43.4110	16	6.1481	13.2304
6	17.1026	36.0935	17	5.7637	12.4239
7	14.5943	30.8669	18	5.4224	11.7070
8	12.7139	26.9471	19	5.1174	11.0657
9	11.2522	23.8985	20	4.8432	10.4885
10	10.0835	21.4598	21	4.5955	9.9664
11	9.1279	19.4645	22	4.3706	9.4918
12	8.3322	17.8019	23	4.1656	9.0585
13	7.6594	16.3952	24	3.9779	8.6613
14	7.0832	15.1895	25	3.8056	8.2960
15	6.5843	14.1446			

Table 3.2. Numerical values of the mode-numbers  $\nu$  as a function of  $\theta_o$ , for the TE<sub>11</sub> and TM<sub>11</sub> modes in a perfectly conducting circular cone  $\theta = \theta_o$ .

$$\bar{H}_t = \frac{1}{r} \frac{\partial}{\partial r} \nabla_t (r\psi_h). \quad (3.27)$$

Here  $\psi_h$  is given by either (3.13) or (3.14), which are shortly written as

$$\psi_h = h_\nu^{(2)}(k^*r) v_h(\theta, \phi), \quad (3.28)$$

where  $v_h(\theta, \phi)$  represents the transverse dependence. Then equations (3.26) and (3.27) reduce to

$$\bar{E}_t = j\omega\mu_o h_\nu^{(2)}(k^*r) \hat{a}_r \times \nabla_t v_h(\theta, \phi), \quad (3.29)$$

$$\bar{H}_t = \frac{1}{r} \frac{\partial}{\partial r} \{r h_\nu^{(2)}(k^*r)\} \nabla_t v_h(\theta, \phi). \quad (3.30)$$

Inserting (3.29) and (3.30) into (3.25) and using (2.75) and (2.85), we arrive at

$$P_r^{TE} = \frac{1}{2} \nu(\nu+1) Z_o \int_0^{\theta_o} \int_0^{2\pi} v_h^2(\theta, \phi) h_\theta^* h_\phi^* d\theta d\phi. \quad (3.31)$$

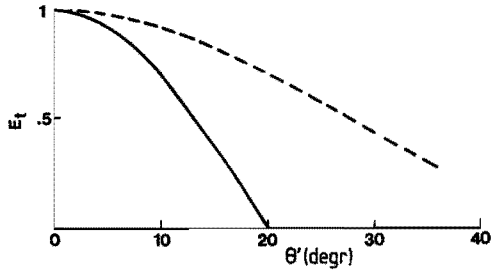


Fig. 3.1a. Normalized transverse electric field, in the xz-plane (—) and the yz-plane (---), of the  ${}^0\text{TE}_{11}$  mode in a perfectly conducting elliptical cone;  $\theta_0 = 20^\circ$ ,  $a_{r\theta} = \frac{1}{2}$ ,  $\theta'_0 = 36.05^\circ$ .

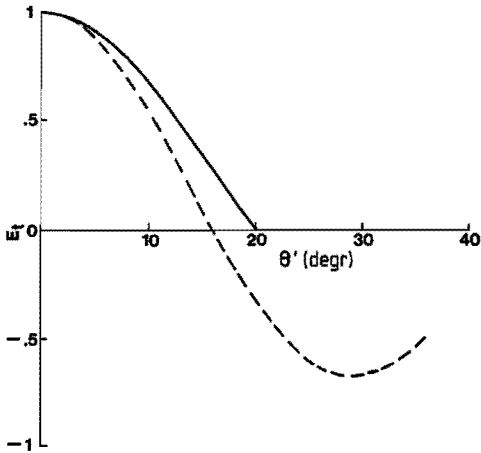


Fig. 3.1b. Normalized transverse electric field, in the xz-plane (—) and the yz-plane (---), of the  ${}^0\text{TM}_{11}$  mode in a perfectly conducting elliptical cone;  $\theta_0 = 20^\circ$ ,  $a_{r\theta} = \frac{1}{2}$ ,  $\theta'_0 = 36.05^\circ$ .

In the same manner we evaluate the radial power-flow of an outward propagating TM mode. The relationships between the transverse fields and the potential  $\psi_e$  are found from equation (3.10) to be

$$\bar{E}_t = \frac{1}{r} \frac{\partial}{\partial r} \nabla_t (r\psi_e), \quad (3.32)$$

$$\bar{H}_t = -j\omega\epsilon_0 \hat{e}_r \times \nabla_t \psi_e. \quad (3.33)$$

Here  $\psi_e$  is given by either (3.13) or (3.14), which are shortly written as

$$\psi_e = h_v^{(2)}(k^*r) v_e(\theta, \phi), \quad (3.34)$$

where  $v_e(\theta, \phi)$  represents the transverse dependence. Substituting this expression into (3.32) and (3.33) we find

$$\bar{E}_t = \frac{1}{r} \frac{\partial}{\partial r} \{rh_v^{(2)}(k^*r)\} \nabla_t v_e(\theta, \phi), \quad (3.35)$$

$$\bar{H}_t = -j\omega\epsilon_0 h_v^{(2)}(k^*r) \hat{e}_r \times \nabla_t v_e(\theta, \phi). \quad (3.36)$$

Inserting (3.35) and (3.36) into (3.25) and using again equations (2.75) and (2.85), we find

$$P_r^{TM} = \frac{1}{2} \nu(\nu+1) Z_0^{-1} \int_0^{\theta} \int_0^{2\pi} v_e^2(\theta, \phi) h_\theta^* h_\phi^* d\theta d\phi. \quad (3.37)$$

Note that  $P_r^{TE}$  and  $P_r^{TM}$  are independent of  $r$ . Hence, the mode power is preserved as it should.

Some brief remarks about the orthogonality (in integral sense) of the field components are in order. For any two different modes the radial field components are orthogonal by equation (2.73). The transverse electric fields of two different TE or TM modes are orthogonal by equation (2.74). The transverse electric fields of a TE and a TM mode are orthogonal, which can be proved by using equations (2.62) and (3.12). These statements also hold for the transverse magnetic fields.

Finally, we point out that the transverse fields inside a perfectly

conducting cone do not satisfy the relation  $\bar{E}_t = \pm j Z_0 \bar{H}_t$ . Hence, the fields at the aperture of a truncated cone do not satisfy this relation either, and as a consequence the radiated field in the far zone is not circularly polarized. To show this, we start from the expressions (3.15), (3.17), (3.19) and (3.21) for the field components of the TE and TM modes. For TE modes the transverse field components are related by

$$\frac{1}{r} \frac{\partial}{\partial r} (r \bar{E}_t) = j \omega \mu_0 \hat{e}_r \times \bar{H}_t, \quad (3.38)$$

whereas for TM modes one has

$$\frac{1}{r} \frac{\partial}{\partial r} (r \bar{H}_t) = -j \omega \epsilon_0 \hat{e}_r \times \bar{E}_t. \quad (3.39)$$

Clearly, neither of these relations is compatible with  $\bar{E}_t = \pm j Z_0 \bar{H}_t$ . Next we observe that for a combination of TE and TM modes the transverse field components are related by  $\bar{E}_t = \pm j Z_0 \bar{H}_t$ , if and only if  $\psi_e = \pm j Z_0 \psi_h$ . However, the cone under consideration imposes different boundary conditions on  $\psi_e$  and  $\psi_h$ ; see (3.11) and (3.12). Therefore, the relation  $\bar{E}_t = \pm j Z_0 \bar{H}_t$  is not satisfied by the transverse fields inside a perfectly conducting cone.

In the next section we consider the elliptical cone with an anisotropic boundary that imposes identical boundary conditions on  $\bar{E}_t$  and  $\bar{H}_t$ . Inside such a cone there do exist electromagnetic field solutions which satisfy the relation  $\bar{E}_t = \pm j Z_0 \bar{H}_t$ .

### 3.3. The elliptical cone with anisotropic boundary

Fields for which  $\bar{E}_t = \pm j Z_0 \bar{H}_t$  can be supported by devices with transversely corrugated boundaries as it is known, for instance, from the theory of circular conical horns [5] and of elliptical-cylindrical waveguides [6]. In the analysis of the latter devices the influence of the corrugations has been accounted for by impedance boundary conditions that involve constant radial (longitudinal in the waveguide case) and circumferential impedances. This model of the corrugated boundary is called the anisotropic surface-impedance model. For a circular conical horn with corrugations of proper depth and width, the boundary conditions are

$$E_r = Z_r H_\phi, \quad (3.40)$$

$$E_\phi = Z_\phi H_r, \quad (3.41)$$

where  $r$  and  $\phi$  are spherical coordinates. For an elliptical waveguide with proper corrugations, the boundary conditions read

$$E_z = Z_z H_\eta, \quad (3.42)$$

$$E_\eta = Z_\eta H_z, \quad (3.43)$$

where  $z$  and  $\eta$  are elliptical-cylindrical coordinates. The number of corrugations per wavelength must be sufficiently large. The corrugation depth must be approximately a quarter of a wavelength and the width of the dams must be small compared with the width of the corrugations. For a corrugated elliptical cone  $\theta = \theta_0$  we employ the same anisotropic surface-impedance model. Thus our starting point is that the influence of transverse corrugations of proper width and depth can be approximately described by the boundary conditions

$$E_r = Z_r H_\phi, \quad (3.44)$$

$$E_\phi = Z_\phi H_r, \quad (3.45)$$

at  $\theta = \theta_0$ ; here,  $r, \theta, \phi$  are sphero-conal coordinates. We restrict ourselves to the idealized case of impedances  $Z_\phi = 0$  and  $Z_r = \infty$ . As a result we then arrive at the boundary conditions

$$E_\phi = 0, \quad Z_0 H_\phi = 0, \quad (3.46)$$

$$E_r \neq 0, \quad Z_0 H_r \neq 0. \quad (3.47)$$

We now prove that these boundary conditions are only satisfied by specific hybrid fields, having both electric and magnetic field components in the radial direction. The proof is analogous to that given in the investigation of the anisotropic elliptical waveguide [6]. First we prove that neither a pure TE-field nor a pure TM-field satisfies the boundary conditions (3.46). From (3.15), together with (3.46), we find for a TE<sub>cm</sub>-field

$$\left. \frac{d}{d\theta} \{L_{cpv}^{(m)}(\theta)\} \right|_{\theta_0} = 0, \quad L_{cpv}^{(m)}(\theta_0) = 0. \quad (3.48)$$

These two conditions are not satisfied simultaneously. Likewise it can be shown that a  $TE_{sm}$ -,  $TM_{cm}$ - or  $TM_{sm}$ -field does not satisfy (3.46).

Next we consider a  $TE_c$ -field derived from the potential

$$\psi_h = h_v^{(2)}(k*r) \sum_{m=0}^{\infty} c_m L_{cpv}^{(m)}(\theta) L_{cv}^{(m)}(\phi). \quad (3.48a)$$

Then the boundary conditions (3.46) give rise to the set of equations

$$\sum_{m=0}^{\infty} c_m \frac{d}{d\theta} \{L_{cpv}^{(m)}(\theta_0)\} L_{cv}^{(m)}(\phi) = 0, \quad (3.49)$$

$$\sum_{m=0}^{\infty} c_m L_{cpv}^{(m)}(\theta_0) \frac{d}{d\phi} \{L_{cv}^{(m)}(\phi)\} = 0. \quad (3.50)$$

By use of the orthogonality relation (2.102) we derive from (3.49) the conditions

$$c_m \left. \frac{d}{d\theta} \{L_{cpv}^{(m)}(\theta)\} \right|_{\theta_0} = 0, \quad m = 0, 1, 2, \dots, \quad (3.51)$$

which obviously are not satisfied. Similarly it can be shown that a  $TE_s$ -,  $TM_c$ -, or  $TM_s$ -field does not satisfy (3.46). Even the sum of a  $TE_c$ - and a  $TE_s$ -field, derived from the potential

$$\psi_h = h_v^{(2)}(k*r) \left\{ \sum_{m=0}^{\infty} c_m L_{cpv}^{(m)}(\theta) L_{cv}^{(m)}(\phi) + \sum_{m=1}^{\infty} s_m L_{spv}^{(m)}(\theta) L_{sv}^{(m)}(\phi) \right\}, \quad (3.52)$$

does not satisfy (3.46). Now the boundary conditions (3.46) give rise to

$$\sum_{m=0}^{\infty} c_m \frac{d}{d\theta} \{L_{cpv}^{(m)}(\theta_0)\} L_{cv}^{(m)}(\phi) + \sum_{m=1}^{\infty} s_m \frac{d}{d\theta} \{L_{spv}^{(m)}(\theta_0)\} L_{sv}^{(m)}(\phi) = 0, \quad (3.53)$$

and

$$\sum_{m=0}^{\infty} c_m L_{cpv}^{(m)}(\theta_o) \frac{d}{d\phi} \{L_{cv}^{(m)}(\phi)\} + \sum_{m=1}^{\infty} s_m L_{spv}^{(m)}(\theta_o) \frac{d}{d\phi} \{L_{sv}^{(m)}(\phi)\} = 0. \quad (3.54)$$

From (3.53), together with (2.105), we find

$$c_m \frac{d}{d\theta} \{L_{cpv}^{(m)}(\theta)\} \Big|_{\theta_o} = 0, \quad m = 0, 1, 2, \dots, \quad (3.55)$$

$$s_m \frac{d}{d\theta} \{L_{spv}^{(m)}(\theta)\} \Big|_{\theta_o} = 0, \quad m = 1, 2, 3, \dots, \quad (3.56)$$

which clearly are not satisfied. Analogously it can be proved that the sum of a  $TM_c$ - and a  $TM_s$ -field will not satisfy (3.46).

From the analysis above we conclude that neither a TE-field nor a TM-field satisfies the boundary conditions (3.46).

We now consider the superposition of a TE-field and a TM-field. We start from a  $TE_c$ -field plus a  $TM_c$ -field, derived from the potentials

$$\psi_h = z_o^{-1} h_v^{(2)}(k^*r) \sum_{m=0}^{\infty} c_{1m} L_{cpv}^{(m)}(\theta) L_{cv}^{(m)}(\phi), \quad (3.57)$$

$$\psi_e = h_v^{(2)}(k^*r) \sum_{m=0}^{\infty} c_{2m} L_{cpv}^{(m)}(\theta) L_{cv}^{(m)}(\phi), \quad (3.58)$$

respectively. In this case the boundary conditions (3.46) give rise to

$$\frac{1}{h_\theta^*} \sum_{m=0}^{\infty} c_{1m} \frac{d}{d\theta} \{L_{cpv}^{(m)}(\theta_o)\} L_{cv}^{(m)}(\phi) - \frac{1}{h_\phi^*} \sum_{m=0}^{\infty} c_{2m} L_{cpv}^{(m)}(\theta_o) \frac{d}{d\phi} \{L_{cv}^{(m)}(\phi)\} = 0, \quad (3.59)$$

and

$$\frac{1}{h_\phi^*} \sum_{m=0}^{\infty} c_{1m} L_{cpv}^{(m)}(\theta_o) \frac{d}{d\phi} \{L_{cv}^{(m)}(\phi)\} + \frac{1}{h_\theta^*} \sum_{m=0}^{\infty} c_{2m} \frac{d}{d\theta} \{L_{cpv}^{(m)}(\theta_o)\} L_{cv}^{(m)}(\phi) = 0. \quad (3.60)$$

Here we have made use of

$$\frac{1}{r} \frac{d}{dr} \{rh_v^{(2)}(k^*r)\} \approx -jk^*h_v^{(2)}(k^*r), \quad (3.61)$$

which is valid for  $k^*r \gg 1$ , hence for points not too close to the apex

of the elliptical cone. From (3.59) and (3.60), together with (2.102) and

$$\int_0^{2\pi} \frac{d}{d\phi} \{L_{cv}^{(m)}(\phi)\} L_{cv}^{(n)}(\phi) d\phi = 0, \quad (3.62)$$

we find  $c_{1m} = c_{2m} = 0$  for every  $m$ . Hence, the superposition of a  $TE_c$ -field and a  $TM_c$ -field does not satisfy the boundary conditions (3.46). Similarly it can be shown that the sum of a  $TE_s$ -field and a  $TM_s$ -field will not satisfy (3.46).

Next we deal with the two remaining possibilities, viz. the superposition of a  $TE_c$ - and a  $TM_s$ -field, and the superposition of a  $TE_s$ - and a  $TM_c$ -field. We will show that in these two cases non-trivial solutions exist for the wave propagation problem in anisotropic cones. We start from a  $TE_c$ - plus a  $TM_s$ -field. The field components due to the  $TE_c$ -part are derived from the potential

$$\psi_h^I = Z_o^{-1} h_v^{(2)}(k^*r) \sum_{m=0}^{\infty} a_m L_{cpv}^{(m)}(\theta) L_{cv}^{(m)}(\phi), \quad (3.63)$$

and those due to the  $TM_s$ -part are derived from the potential

$$\psi_e^I = h_v^{(2)}(k^*r) \sum_{m=1}^{\infty} b_m L_{spv}^{(m)}(\theta) L_{sv}^{(m)}(\phi). \quad (3.64)$$

The following expressions for the field components apply, taken from (3.15) and (3.21):

$$E_r^I = \frac{1}{r} \nu(\nu+1) h_v^{(2)}(k^*r) \sum_{m=1}^{\infty} b_m L_{spv}^{(m)}(\theta) L_{sv}^{(m)}(\phi), \quad (3.65)$$

$$E_\theta^I = \frac{-jk^*}{h_\phi^*} h_v^{(2)}(k^*r) \sum_{m=0}^{\infty} a_m L_{cpv}^{(m)}(\theta) \frac{d}{d\phi} \{L_{cv}^{(m)}(\phi)\} +$$

$$+ \frac{1}{rh_\theta^*} \frac{d}{dr} \{rh_v^{(2)}(k^*r)\} \sum_{m=1}^{\infty} b_m \frac{d}{d\theta} \{L_{spv}^{(m)}(\theta)\} L_{sv}^{(m)}(\phi), \quad (3.66)$$

$$E_{\phi}^I = \frac{jk^*}{h_{\theta}^*} h_{\nu}^{(2)}(k^*r) \sum_{m=0}^{\infty} a_m \frac{d}{d\theta} \{L_{cpv}^{(m)}(\theta)\} L_{cv}^{(m)}(\phi) +$$

$$+ \frac{1}{rh_{\phi}^*} \frac{d}{dr} \{rh_{\nu}^{(2)}(k^*r)\} \sum_{m=1}^{\infty} b_m L_{spv}^{(m)}(\theta) \frac{d}{d\phi} \{L_{sv}^{(m)}(\phi)\}, \quad (3.67)$$

$$Z_o H_r^I = \frac{1}{r} \nu(\nu+1) h_{\nu}^{(2)}(k^*r) \sum_{m=0}^{\infty} a_m L_{cpv}^{(m)}(\theta) L_{cv}^{(m)}(\phi), \quad (3.68)$$

$$Z_o H_{\theta}^I = \frac{1}{rh_{\theta}^*} \frac{d}{dr} \{rh_{\nu}^{(2)}(k^*r)\} \sum_{m=0}^{\infty} a_m \frac{d}{d\theta} \{L_{cpv}^{(m)}(\theta)\} L_{cv}^{(m)}(\phi) +$$

$$+ \frac{jk^*}{h_{\phi}^*} h_{\nu}^{(2)}(k^*r) \sum_{m=1}^{\infty} b_m L_{spv}^{(m)}(\theta) \frac{d}{d\phi} \{L_{sv}^{(m)}(\phi)\}, \quad (3.69)$$

$$Z_o H_{\phi}^I = \frac{1}{rh_{\phi}^*} \frac{d}{dr} \{rh_{\nu}^{(2)}(k^*r)\} \sum_{m=0}^{\infty} a_m L_{cpv}^{(m)}(\theta) \frac{d}{d\phi} \{L_{cv}^{(m)}(\phi)\} -$$

$$- \frac{jk^*}{h_{\theta}^*} h_{\nu}^{(2)}(k^*r) \sum_{m=1}^{\infty} b_m \frac{d}{d\theta} \{L_{spv}^{(m)}(\theta)\} L_{sv}^{(m)}(\phi), \quad (3.70)$$

where it has been used that  $\omega\mu_o = k^*Z_o$  and  $\omega\epsilon_o Z_o = k^*$ . A field solution of the form (3.65)-(3.70) which satisfies the boundary conditions (3.46), is called a I-mode. Because of its composing parts,  $TE_c$ - and  $TM_s$ -fields, it is evident that it is an odd symmetric hybrid mode. We now remove the Hankel function derivatives by use of (3.61), which is valid for  $k^*r \gg 1$ . Then, by imposing the conditions (3.46) on the field components (3.67) and (3.70), we find

$$\frac{h_{\phi}^*}{h_{\theta}^*} \sum_{m=0}^{\infty} a_m \frac{d}{d\theta} \{L_{cpv}^{(m)}(\theta_o)\} L_{cv}^{(m)}(\phi) - \sum_{m=1}^{\infty} b_m L_{spv}^{(m)}(\theta_o) \frac{d}{d\phi} \{L_{sv}^{(m)}(\phi)\} = 0, \quad (3.71)$$

and

$$\sum_{m=0}^{\infty} a_m L_{cpv}^{(m)}(\theta_o) \frac{d}{d\phi} \{L_{cv}^{(m)}(\phi)\} + \frac{h_{\phi}^*}{h_{\theta}^*} \sum_{m=1}^{\infty} b_m \frac{d}{d\theta} \{L_{spv}^{(m)}(\theta_o)\} L_{sv}^{(m)}(\phi) = 0. \quad (3.72)$$

The derivatives of the periodic Lamé functions are expanded as

$$\frac{d}{d\phi}\{L_{sv}^{(m)}(\phi)\} = \sum_{n=0}^{\infty} r_{mn} (1-k'^2 \sin^2 \phi)^{-\frac{1}{2}} L_{cv}^{(n)}(\phi), \quad (3.73)$$

$$\frac{d}{d\phi}\{L_{cv}^{(m)}(\phi)\} = \sum_{n=1}^{\infty} q_{mn} (1-k'^2 \sin^2 \phi)^{-\frac{1}{2}} L_{sv}^{(n)}(\phi), \quad (3.74)$$

where, by use of the orthogonality properties (2.105),

$$r_{mn} = \frac{\int_0^{2\pi} \frac{d}{d\phi}\{L_{sv}^{(m)}(\phi)\} L_{cv}^{(n)}(\phi) d\phi}{\int_0^{2\pi} (1-k'^2 \sin^2 \phi)^{-\frac{1}{2}} \{L_{cv}^{(n)}(\phi)\}^2 d\phi}, \quad (3.75)$$

$$q_{mn} = \frac{\int_0^{2\pi} \frac{d}{d\phi}\{L_{cv}^{(m)}(\phi)\} L_{sv}^{(n)}(\phi) d\phi}{\int_0^{2\pi} (1-k'^2 \sin^2 \phi)^{-\frac{1}{2}} \{L_{sv}^{(n)}(\phi)\}^2 d\phi}. \quad (3.76)$$

We note that  $r_{mn} \neq r_{nm}$  and  $q_{mn} \neq q_{nm}$ . From (3.71) and (3.72), together with (3.75), (3.76), and the orthogonality properties (2.105), we find

$$a_i (1-k^2 \cos^2 \theta_o)^{\frac{1}{2}} \frac{d}{d\theta}\{L_{cpv}^{(i)}(\theta_o)\} = \sum_{m=1}^{\infty} b_m L_{spv}^{(m)}(\theta_o) r_{mi}, \quad i = 0, 1, 2, \dots, \quad (3.77)$$

$$b_i (1-k^2 \cos^2 \theta_o)^{\frac{1}{2}} \frac{d}{d\theta}\{L_{spv}^{(i)}(\theta_o)\} = -\sum_{m=0}^{\infty} a_m L_{cpv}^{(m)}(\theta_o) q_{mi}, \quad i = 1, 2, \dots \quad (3.78)$$

The unknowns in these equations are the coefficients  $a_i$ ,  $b_i$  and the mode-number  $v$ . We now introduce the vectors  $\bar{a} = [a_0, a_1, a_2, \dots]^T$ ,  $\bar{b} = [b_1, b_2, b_3, \dots]^T$ , and the diagonal matrices  $C, C', S, S'$  with diagonal elements

$$C_{ii} = L_{cpv}^{(i)}(\theta_o), \quad C'_{ii} = (1-k^2 \cos^2 \theta_o)^{\frac{1}{2}} \frac{d}{d\theta}\{L_{cpv}^{(i)}(\theta)\} \Big|_{\theta_o}, \quad (3.79)$$

$$S_{ii} = L_{spv}^{(i)}(\theta_o), \quad S'_{ii} = -(1-k^2 \cos^2 \theta_o)^{\frac{1}{2}} \frac{d}{d\theta}\{L_{spv}^{(i)}(\theta)\} \Big|_{\theta_o},$$

and the non-symmetric matrices  $R$  and  $Q$  defined by

$$R = \{r_{mi}\}, \quad Q = \{q_{mi}\}. \quad (3.80)$$

Then equations (3.77) and (3.78) can be shortly written as

$$C' \bar{a} = R^T S \bar{b}, \quad (3.81)$$

$$S' \bar{b} = Q^T C \bar{a}, \quad (3.82)$$

where T means transposed. Equations (3.81) and (3.82) clearly show that the TE- and TM-parts of the hybrid mode are coupled. With the abbreviations  $(C')^{-1} R^T S = A$  and  $(S')^{-1} Q^T C = B$  we find

$$BA\bar{b} = \bar{b}, \quad (3.83)$$

$$A\bar{b} = \bar{a}, \quad (3.84)$$

or equivalently

$$AB\bar{a} = \bar{a}, \quad (3.85)$$

$$B\bar{a} = \bar{b}. \quad (3.86)$$

Consequently, the problem of wave propagation in an elliptical cone with anisotropic boundary has been reduced to the problem of finding the numbers  $\nu$  for which an infinite non-symmetric matrix, namely, the matrix  $BA$ , has an eigenvalue equal to 1. The corresponding eigenvector then represents the vector  $\bar{b}$ , whereupon the vector  $\bar{a}$  is determined from (3.84). Some aspects of the numerical calculation of  $\nu$ ,  $\bar{a}$  and  $\bar{b}$ , will be discussed at the end of this section.

So far we have proved the existence of the odd symmetric hybrid mode, denoted by I-mode. We now show that a second type of solution, the so-called hybrid II-mode, is possible. The II-modes are obtained from the superposition of a  $TE_s$ - and a  $TM_c$ -field. These fields are even symmetric. Hence, a II-mode is even symmetric. The field components due to the  $TE_s$ -part are derived from the potential

$$\psi_h^{II} = Z_o^{-1} h_\nu^{(2)}(k^*r) \sum_{m=1}^{\infty} b_m L_{sp\nu}^{(m)}(\theta) L_{s\nu}^{(m)}(\phi), \quad (3.87)$$

and those due to the  $TM_c$ -part are derived from the potential

$$\psi_e^{II} = -h_\nu^{(2)}(k^*r) \sum_{m=0}^{\infty} a_m L_{cp\nu}^{(m)}(\theta) L_{c\nu}^{(m)}(\phi). \quad (3.88)$$

We note that

$$Z_o \psi_h^{II} = \psi_e^I, \quad (3.89)$$

$$\psi_e^{II} = -Z_o \psi_h^I. \quad (3.90)$$

The following expressions for the field components of a II-mode are obtained from (3.17) and (3.19):

$$E_r^{II} = -\frac{1}{r} v(v+1) h_v^{(2)}(k^*r) \sum_{m=0}^{\infty} a_m L_{cpv}^{(m)}(\theta) L_{cv}^{(m)}(\phi), \quad (3.91)$$

$$E_{\theta}^{II} = -\frac{jk^*}{h_{\phi}^*} h_v^{(2)}(k^*r) \sum_{m=1}^{\infty} b_m L_{spv}^{(m)}(\theta) \frac{d}{d\phi} \{L_{sv}^{(m)}(\phi)\} -$$

$$-\frac{1}{rh_{\theta}^*} \frac{d}{dr} \{rh_v^{(2)}(k^*r)\} \sum_{m=0}^{\infty} a_m \frac{d}{d\theta} \{L_{cpv}^{(m)}(\theta)\} L_{cv}^{(m)}(\phi), \quad (3.92)$$

$$E_{\phi}^{II} = \frac{jk^*}{h_{\theta}^*} h_v^{(2)}(k^*r) \sum_{m=1}^{\infty} b_m \frac{d}{d\theta} \{L_{spv}^{(m)}(\theta)\} L_{sv}^{(m)}(\phi) -$$

$$-\frac{1}{rh_{\phi}^*} \frac{d}{dr} \{rh_v^{(2)}(k^*r)\} \sum_{m=0}^{\infty} a_m L_{cpv}^{(m)}(\theta) \frac{d}{d\phi} \{L_{cv}^{(m)}(\phi)\}, \quad (3.93)$$

$$Z_o H_r^{II} = \frac{1}{r} v(v+1) h_v^{(2)}(k^*r) \sum_{m=1}^{\infty} b_m L_{spv}^{(m)}(\theta) L_{sv}^{(m)}(\phi), \quad (3.94)$$

$$Z_o H_{\theta}^{II} = \frac{1}{rh_{\theta}^*} \frac{d}{dr} \{rh_v^{(2)}(k^*r)\} \sum_{m=1}^{\infty} b_m \frac{d}{d\theta} \{L_{spv}^{(m)}(\theta)\} L_{sv}^{(m)}(\phi) -$$

$$-\frac{jk^*}{h_{\phi}^*} h_v^{(2)}(k^*r) \sum_{m=0}^{\infty} a_m L_{cpv}^{(m)}(\theta) \frac{d}{d\phi} \{L_{cv}^{(m)}(\phi)\}, \quad (3.95)$$

$$Z_o H_{\phi}^{II} = \frac{1}{rh_{\phi}^*} \frac{d}{dr} \{rh_v^{(2)}(k^*r)\} \sum_{m=1}^{\infty} b_m L_{spv}^{(m)}(\theta) \frac{d}{d\phi} \{L_{sv}^{(m)}(\phi)\} +$$

$$+\frac{jk^*}{h_{\theta}^*} h_v^{(2)}(k^*r) \sum_{m=0}^{\infty} a_m \frac{d}{d\theta} \{L_{cpv}^{(m)}(\theta)\} L_{cv}^{(m)}(\phi). \quad (3.96)$$

Note that the field components of I- and II-modes are related by

$$\bar{E}^I = Z_O \bar{H}^{II}, \quad (3.97)$$

$$\bar{E}^{II} = -Z_O \bar{H}^I. \quad (3.98)$$

The boundary conditions (3.46) yield for the II-mode

$$E_\phi^{II} = 0, \quad Z_O H_\phi^{II} = 0, \quad \text{at } \theta = \theta_O, \quad (3.99)$$

from which the unknowns  $\nu$ ,  $\bar{a}$  and  $\bar{b}$  must be determined. Using (3.97) and (3.98), the conditions (3.99) are found to be equivalent to the boundary conditions for the I-mode, viz.

$$Z_O H_\phi^I = 0, \quad E_\phi^I = 0, \quad \text{at } \theta = \theta_O. \quad (3.100)$$

Consequently, it has been found that the wave propagation problem in an anisotropic elliptical cone admits two types of solutions, viz. odd and even symmetric hybrid modes, that have pairwise identical mode-numbers  $\nu$ , identical vectors  $\bar{a}$  and identical vectors  $\bar{b}$ . At this point it is stressed that the hybrid modes have been found subject to (3.61), which is valid for  $k*r \gg 1$ .

Some remarks are now in order; throughout it is understood that  $k*r \gg 1$ , such that the approximations (3.61) and (2.84) apply.

1. The transverse electric and magnetic fields are perpendicular,

$$\bar{E}_t^I \perp \bar{H}_t^I, \quad \bar{E}_t^{II} \perp \bar{H}_t^{II}. \quad (3.101)$$

2. The transverse electric and magnetic field components are related by

$$E_\theta^I = Z_O H_\phi^I, \quad E_\phi^I = -Z_O H_\theta^I, \quad (3.102)$$

$$E_\theta^{II} = Z_O H_\phi^{II}, \quad E_\phi^{II} = -Z_O H_\theta^{II}, \quad (3.103)$$

or equivalently,

$$Z_0 \bar{H}_t^{-I} = \hat{e}_r \times \bar{E}_t^{-I}, \quad Z_0 \bar{H}_t^{-II} = \hat{e}_r \times \bar{E}_t^{-II}. \quad (3.104)$$

3. From (3.102) and (3.103), together with the anisotropic boundary conditions (3.46), we deduce that all transverse field components vanish at  $\theta = \theta_0$ .

4. The time-average power-flow in the radial direction, through a spherical cap  $S$  in the cone  $\theta = \theta_0$ , is derived from (3.25). The derivation in the case of a hybrid mode runs along the same lines as that of  $P_r^{TE}$  and  $P_r^{TM}$  in (3.31) and (3.37), respectively. As an example we now determine the power-flow  $P_r^I$  of a I-mode. Let

$$v_h^I = \psi_h^I/h_v^{(2)}(k^*r), \quad v_e^I = \psi_e^I/h_v^{(2)}(k^*r), \quad (3.105)$$

in which  $\psi_h^I$  and  $\psi_e^I$  are given by (3.63) and (3.64), respectively. From (3.29), (3.30), (3.35) and (3.36), together with (2.84), we then find that the transverse fields expressed in terms of  $v_h^I$  and  $v_e^I$ , are given by

$$\bar{E}_t^{-I} = j r^{-1} (Z_0 \hat{e}_r \times \nabla_t v_h^I - \nabla_t v_e^I) \exp\{-j(k^*r - \frac{v+1}{2}\pi)\}, \quad (3.106)$$

$$\bar{H}_t^{-I} = -j r^{-1} (\nabla_t v_h^I + Z_0^{-1} \hat{e}_r \times \nabla_t v_e^I) \exp\{-j(k^*r - \frac{v+1}{2}\pi)\}. \quad (3.107)$$

By substitution of (3.106) and (3.107) into (3.25) and by use of (2.62), one is led to

$$P_r^I = \frac{1}{2} Z_0 \int_0^{\theta_0} \int_0^{2\pi} |\nabla_t v_h^I|^2 h_\theta^* h_\phi^* d\theta d\phi + \frac{1}{2} Z_0^{-1} \int_0^{\theta_0} \int_0^{2\pi} |\nabla_t v_e^I|^2 h_\theta^* h_\phi^* d\theta d\phi + \int_0^{2\pi} \left\{ v_e^I \frac{d}{d\phi} (v_h^I) \right\} \Big|_{\theta_0} d\phi. \quad (3.108)$$

From (3.25), together with (3.97) and (3.98), we find that the power-flow  $P_r^{II}$  of a II-mode is equal to the power-flow  $P_r^I$  of a I-mode.

5. If a I- and a II-mode, differing in phase by  $90^\circ$ , are combined as  $(\bar{E}^I, \bar{H}^I) + j(\bar{E}^{II}, \bar{H}^{II}) = (\bar{E}, \bar{H})$ , we find that the total field satisfies  $\bar{E} = -jZ_0 \bar{H}$ . This is exactly the kind of field we need for circular polarization applications.

6. Thus far we have dealt with outward propagating I- and II-modes. The analysis for inward propagating modes runs along the same lines. Expressions for the inward propagating modes are obtained when replacing  $h_V^{(2)}(k^*r)$  by  $h_V^{(1)}(k^*r)$  in (3.65)-(3.70) and (3.91)-(3.96). Provided  $k^*r \gg 1$ , the boundary conditions (3.46) then lead to the set of equations

$$BA\bar{b}' = \bar{b}', \quad (3.109)$$

$$A\bar{b}' = -\bar{a}', \quad (3.110)$$

or equivalently

$$AB\bar{a}' = \bar{a}', \quad (3.111)$$

$$B\bar{a}' = -\bar{b}'. \quad (3.112)$$

The primes on the vectors  $\bar{a}'$ ;  $\bar{b}'$  have been introduced to distinguish them from the vectors  $\bar{a}$ ,  $\bar{b}$ , pertaining to outward propagating modes. We note that (3.109)-(3.112) involve the same matrices A and B as (3.83)-(3.86). Hence, an inward propagating mode and its outward propagating counterpart have identical mode-numbers  $\nu$ . From (3.83)-(3.84) and (3.109)-(3.110) we find that either the vector  $\bar{a}$  or the vector  $\bar{b}$  changes sign if the propagation direction of a mode is reversed. The transverse field components of the inward propagating modes are related by

$$Z_0 \bar{H}_t = -\bar{a}_r \times \bar{E}_t. \quad (3.113)$$

We now investigate (3.83) and (3.84) in more detail. On closer examination of the expansion coefficients  $r_{mn}$ ,  $q_{mn}$ , given by (3.75), (3.76), we find that

$$r_{mn} = q_{mn} = 0, \quad \text{if } m+n \text{ is odd,} \quad (3.114)$$

which is due to the symmetry properties of the simple-periodic Lamé functions; see Appendix 3.4. Consequently, the matrices R and Q, as well as the matrices A, B, AB and BA, are so-called chessboard matrices. This implies that (3.83) can be split into two sets of equations, one for the eigenvector  $[b_2, b_4, b_6, \dots]^T$  and one for the eigenvector  $[b_1, b_3, b_5, \dots]^T$ . Hence, the problem of determining the hybrid I- and II-modes separates into independent problems for the modes of period  $\pi$  in  $\phi$  and for the modes of period  $2\pi$  in  $\phi$ . This can be seen as follows. The number  $m+n$  is even if both  $m$  and  $n$  are even or if both  $m$  and  $n$  are odd. In the first case the modal solution involves the simple-periodic Lamé functions of the classes I and III having period  $\pi$ . In the second case the modal solution involves the simple-periodic Lamé functions of the classes II and IV having period  $2\pi$ .

It can be shown that the modal fields of period  $\pi$ , when used as the fields at the aperture of a truncated cone, give rise to radiation patterns with a dip in the forward direction. Applications that utilize this property will not be dealt with in the present study. Henceforth, we restrict the investigation to the modes of period  $2\pi$  in  $\phi$ . In accordance with [1] the I- and II-modes of period  $\pi$  in  $\phi$  are labeled  ${}^o\text{EH}$  and  ${}^e\text{EH}$  modes, respectively, and those of period  $2\pi$  in  $\phi$  are labeled  ${}^o\text{HE}$  and  ${}^e\text{HE}$  modes, respectively; here the subscripts  $o$  and  $e$  refer to odd and even symmetric, respectively, as defined in (3.23) and (3.24).

For the HE modes we have numerically solved (3.83) and (3.84). The matrix BA and the vectors  $\bar{a}$  and  $\bar{b}$  are truncated to a finite size N, where the choice of N depends on the mode and on the aspect ratio  $a_{r\theta}$  of the cone under consideration. The lower the aspect ratio the higher the size N must be. In the most important range of the aspect ratio,  $\frac{1}{4}$  to  $\frac{1}{2}$ , we have used a size N ranging between 6 and 9. The elements of the matrices contain nonperiodic Lamé functions, their derivatives, and integrals of the simple-periodic Lamé functions. Numerical procedures developed by Jansen [7] have been used for the computation of the Lamé functions and their derivatives. The series, representing the Lamé functions, have been truncated. Approximately 25 terms suffice for the computations if the aspect ratio is in the range mentioned above. Standard numerical procedures have been used for determining the eigenvalues of the matrix BA as a function of the parameter  $v$ . In this manner we have ascertained intervals for  $v$ , in which BA

has an eigenvalue  $\lambda$  equal to 1. Then, using a rootfinding procedure we have determined, with a high degree of accuracy, the value of  $\nu$  such that  $\lambda - 1 = 0$ . Furthermore, the corresponding eigenvector has been computed. Having obtained  $\nu$  and  $\bar{b}$ , we can determine  $\bar{a}$  and all the field components of the mode under consideration.

As an example we present in Table 3.3 the numerical values of  $\nu$  as a function of  $\theta_0$  and  $a_{r\theta}$ , for the odd or even symmetric  $HE_{11}$  mode in anisotropic elliptical cones. The results for the circular cone ( $a_{r\theta} = 1$ ), computed by means of the theory for the elliptical cone in the manner mentioned above, agree with those in [5], [1], which have been obtained from a simpler theory. In the Figures 3.2a-b we have plotted the normalized transverse electric field of the  $HE_{11}$  mode for some anisotropic elliptical cones, whereas in the Figure 3.2c the same has been done for the  $HE_{31}$  mode. The corresponding numerical values of the elements of the truncated vectors  $\bar{a}$  and  $\bar{b}$  have been listed below these figures.

In conclusion we summarize the main results of this section. The problem of wave propagation in a corrugated elliptical cone has been solved by use of the idealized anisotropic surface-impedance model. It has been proved that only specific fields satisfy the anisotropic boundary conditions. These field solutions are valid at points not too close to the apex of the cone. They have both electric and magnetic field components in the radial direction, and they are called hybrid modes. Odd and even symmetric hybrid modes have been found and it has been shown that these modes can be combined to yield an electromagnetic field ( $\bar{E}$ ,  $\bar{H}$ ) that satisfies the relation  $\bar{E} = \pm jZ_0 \bar{H}$ .

The problem of determining the hybrid modes has been formulated in matrix notation. The unknowns of the latter problem are the mode-number  $\nu$ , and the vectors  $\bar{a}$  and  $\bar{b}$ . It has been found that the odd and even symmetric hybrid modes have pairwise identical mode-numbers  $\nu$ , identical vectors  $\bar{a}$  and identical vectors  $\bar{b}$ . The unknowns  $\nu$ ,  $\bar{a}$  and  $\bar{b}$  have been numerically determined and the results have been presented in tables and figures. For given  $\nu$ ,  $\bar{a}$  and  $\bar{b}$ , the electromagnetic fields inside a cone can be determined. In the calculation of the radiation of a truncated cone we will assume that the electromagnetic fields at the aperture of the cone are the same as would exist there if the cone extended to infinity. Radiation computations will be dealt with in the next chapter.

$\theta_0 \backslash a_{r\theta}$	1	1/2	1/3	1/4	0.1	0.05
5	27.0739	21.2033	19.7893	19.1911	18.3070	18.1079
6	22.4844	17.6086	16.4392	15.9479	15.2397	15.0901
7	19.2071	15.0443	14.0507	13.6367	13.0544	12.9381
8	16.7499	13.1240	12.2632	11.9076	11.4195	11.3265
9	14.8395	11.6331	10.8763	10.5664	10.1508	10.0749
10	13.3119	10.4426	9.7691	9.4966	9.1383	9.0750
11	12.0626	9.4706	8.8665	8.6238	8.3117	8.2582
12	11.0221	8.6623	8.1162	7.8988	7.6243	7.5785
13	10.1422	7.9523	7.4832	7.2872	7.0440	7.0042
14	9.3885	7.3968	6.9423	6.7646	6.5476	6.5128
15	8.7357	6.8926	6.4750	6.3132	6.1183	6.0875
16	8.1649	6.4527	6.0675	5.9195	5.7435	5.7161
17	7.6617	6.0657	5.7092	5.5733	5.4135	5.3889
18	7.2148	5.7227	5.3917	5.2665	5.1208	5.0986
19	6.8152	5.4167	5.1087	4.9929	4.8595	4.8394
20	6.4560	5.1422	4.8548	4.7475	4.6248	4.6065
21	6.1313	4.8947	4.6259	4.5262	4.4130	4.3962
22	5.8364	4.6704	4.4186	4.3256	4.2209	4.2054
23	5.5674	4.4663	4.2299	4.1431	4.0458	4.0315
24	5.3212	4.2799	4.0576	3.9764	3.8858	3.8725
25	5.0949	4.1099	3.8997	3.8235	3.7389	3.7266

Table 3.3. Numerical values of the mode-numbers  $\nu$  as a function of  $\theta_0$  (degr.) and  $a_{r\theta}$ , for the  $HE_{11}$  mode in anisotropic elliptical cones.

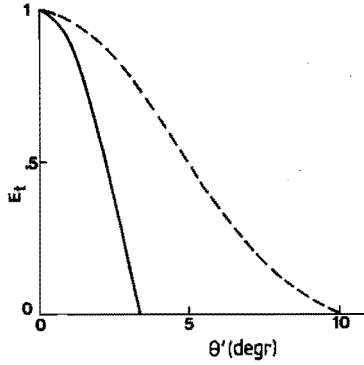


Fig. 3.2a. Normalized transverse electric field, in the xz-plane (—) and the yz-plane (---), of the  $HE_{11}$  mode in an anisotropic elliptical cone;  $a_{r\theta} = 1/3$ ,  $\theta'_0 = 3.37^\circ$ ,  $\theta''_0 = 10^\circ$ ,  $\nu = 29.5328$ .

The numerical values of the elements of the truncated vectors  $\bar{a}$  and  $\bar{b}$  are

$$\begin{aligned}
 a_1 &= -6.6380 \cdot 10^{+1}, & b_1 &= 9.9283 \cdot 10^{-1}, \\
 a_3 &= 3.2634, & b_3 &= -1.1947 \cdot 10^{-1}, \\
 a_5 &= -5.2264 \cdot 10^{-2}, & b_5 &= 2.4594 \cdot 10^{-3}, \\
 a_7 &= 3.0084 \cdot 10^{-4}, & b_7 &= -4.1047 \cdot 10^{-6}, \\
 a_9 &= -8.1008 \cdot 10^{-6}, & b_9 &= -2.1196 \cdot 10^{-7}, \\
 a_{11} &= 3.4782 \cdot 10^{-6}, & b_{11} &= 5.4525 \cdot 10^{-8}, \\
 a_{13} &= -1.1035 \cdot 10^{-6}, & b_{13} &= -1.4557 \cdot 10^{-8}, \\
 a_{15} &= 3.2784 \cdot 10^{-7}, & b_{15} &= 3.7113 \cdot 10^{-9}, \\
 a_{17} &= -7.8957 \cdot 10^{-8}, & b_{17} &= -7.8371 \cdot 10^{-10}.
 \end{aligned}$$

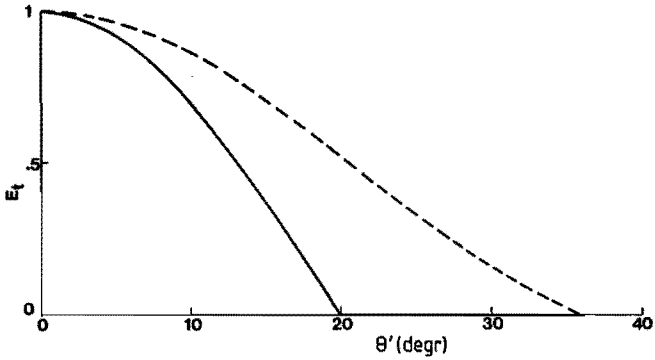


Fig. 3.2b. Normalized transverse electric field, in the xz-plane (—) and the yz-plane (---), of the  $HE_{11}^o$  mode in an anisotropic elliptical cone;  $a_{r\theta} = 1/2$ ,  $\theta_o = 20^\circ$ ,  $\theta'_o = 36.05^\circ$ ,  $\nu = 5.1422$ .

The numerical values of the elements of the truncated vectors  $\bar{a}$  and  $\bar{b}$  are

$$\begin{array}{ll}
 a_1 = 7.2311 & , \quad b_1 = -9.9900 \cdot 10^{-1} \\
 a_3 = 2.4916 \cdot 10^{-1} & , \quad b_3 = 4.4756 \cdot 10^{-2} \\
 a_5 = -1.4311 \cdot 10^{-3} & , \quad b_5 = 6.9231 \cdot 10^{-5} \\
 a_7 = -2.2483 \cdot 10^{-5} & , \quad b_7 = 9.7053 \cdot 10^{-7} \\
 a_9 = -1.2682 \cdot 10^{-7} & , \quad b_9 = 1.8333 \cdot 10^{-8} \\
 a_{11} = -1.7738 \cdot 10^{-8} & , \quad b_{11} = -6.7075 \cdot 10^{-10} \\
 a_{13} = 1.7721 \cdot 10^{-9} & , \quad b_{13} = 7.7768 \cdot 10^{-11} \\
 a_{15} = -2.0433 \cdot 10^{-10} & , \quad b_{15} = -7.5356 \cdot 10^{-12} \\
 a_{17} = 2.0559 \cdot 10^{-11} & , \quad b_{17} = 6.6897 \cdot 10^{-13}
 \end{array}$$

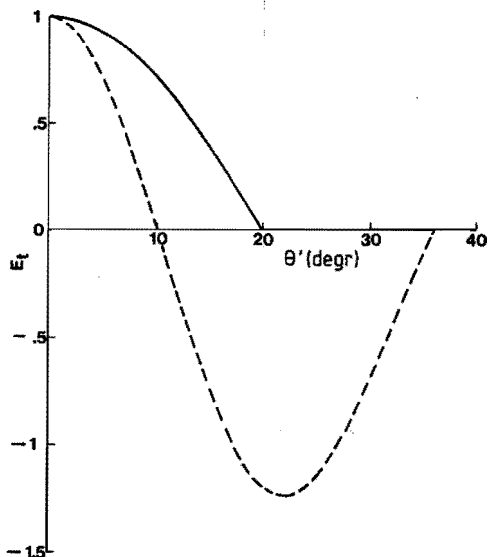


Fig. 3.2c. Normalized transverse electric field, in the  $xz$ -plane (—) and the  $yz$ -plane (---), of the  ${}_{\circ}HE_{31}$  mode in an anisotropic elliptical cone;  $a_{r\theta} = 1/2$ ,  $\theta_{\circ} = 20^{\circ}$ ,  $\theta'_{\circ} = 36.05^{\circ}$ ,  $\nu = 9.3115$ .

The numerical values of the elements of the truncated vectors  $\bar{a}$  and  $\bar{b}$  are

$$\begin{array}{ll}
 a_1 = -7.4668 \cdot 10^{-1} , & b_1 = -5.3613 \cdot 10^{-1} , \\
 a_3 = 3.4378 & , & b_3 = -8.4394 \cdot 10^{-1} , \\
 a_5 = -1.3546 \cdot 10^{-1} , & b_5 = 1.8273 \cdot 10^{-2} , \\
 a_7 = -4.7788 \cdot 10^{-4} , & b_7 = 8.4286 \cdot 10^{-6} , \\
 a_9 = -1.1697 \cdot 10^{-5} , & b_9 = 3.8788 \cdot 10^{-7} , \\
 a_{11} = -1.6194 \cdot 10^{-7} , & b_{11} = 5.9187 \cdot 10^{-9} , \\
 a_{13} = -3.6537 \cdot 10^{-9} , & b_{13} = 9.1656 \cdot 10^{-12} , \\
 a_{15} = 1.0602 \cdot 10^{-10} , & b_{15} = 5.8942 \cdot 10^{-12} , \\
 a_{17} = -1.3422 \cdot 10^{-11} , & b_{17} = -4.2397 \cdot 10^{-13} .
 \end{array}$$

### 3.4. Appendix

Through integration by parts and by use of the periodicity properties of the periodic Lamé functions, it is easily seen that the numerator of (3.75), and that of (3.76) with  $m$  and  $n$  interchanged, are opposite. Hence, to prove (3.114) it is sufficient to verify that  $r_{mn} = 0$  if  $m + n$  is odd. The numerator of expression (3.75) for  $r_{mn}$  can be written as

$$\int_0^{2\pi} L_{cv}^{(n)}(\phi) \frac{d}{d\phi} \{L_{sv}^{(m)}(\phi)\} d\phi = \int_0^{\pi} L_{cv}^{(n)}(\phi) \frac{d}{d\phi} \{L_{sv}^{(m)}(\phi)\} d\phi +$$

$$+ \int_0^{\pi} L_{cv}^{(n)}(\phi+\pi) \frac{d}{d\phi} \{L_{sv}^{(m)}(\phi+\pi)\} d\phi. \quad (3.115)$$

For even superscripts we have (see equations (2.95)-(2.98)),

$$L_{cv}^{(n)}(\phi) = L_{cv}^{(n)}(\phi+\pi), \quad (3.116)$$

$$L_{sv}^{(m)}(\phi) = L_{sv}^{(m)}(\phi+\pi), \quad (3.117)$$

and for odd superscripts one has

$$L_{cv}^{(n)}(\phi) = -L_{cv}^{(n)}(\phi+\pi), \quad (3.118)$$

$$L_{sv}^{(m)}(\phi) = -L_{sv}^{(m)}(\phi+\pi). \quad (3.119)$$

Consequently, the two integrals in the right-hand side of (3.115) cancel if  $m+n$  is odd, which proves (3.114).

### 3.5. References

- [1] Clarricoats, P.J.B., and P.K. Saha, Propagation and radiation behaviour of corrugated feeds. Part 2. Corrugated-conical-horn feed. Proc. IEE 118 (1971), 1177-1186.
- [2] Collin, R.E., Field Theory of Guided Waves. McGraw-Hill, New York, 1960, p. 10.
- [3] Fasold, D., L. Heichele, M. Lieke, H. Pecher, and A. Ruthlein, Der Entwicklungsstand der Sendeantenne des Fernsehrundfunksatelliten TV-SAT. Nachrichtentechnische Gesellschaft-Fachberichte, Band 78, Antennen '82, 115-119.
- [4] Final Acts of the World Administrative Radio Conference for the Planning of the Broadcasting-Satellite Service in Frequency Bands 11.7-12.2 GHz (in Regions 2 and 3) and 11.7-12.5 GHz (in Region 1). International Telecommunication Union, Geneva, 1977.
- [5] Jansen, J.K.M., M.E.J. Jeuken, and C.W. Lambrechtse, The scalar feed. Archiv für Elektronik und Übertragungstechnik 26 (1972), 22-30.
- [6] Jansen, J.K.M., and M.E.J. Jeuken, Propagation and Radiation Properties of Elliptical Waveguide with Anisotropic Boundary. Eindhoven University of Technology, ESTEC-contract no. 1657/72 HP, Eindhoven, 1973.
- [7] Jansen, J.K.M., Simple-periodic and Non-periodic Lamé Functions. Mathematical Centre Tracts 72, Math. Centrum, Amsterdam, 1977.
- [8] Kong, A.C., The Propagation and Radiation Properties of Waveguides and Horns of Elliptical Cross-section. Ph.D. Thesis, University of Surrey, Guildford, 1971.
- [9] Vokurka, V.J., Elliptical corrugated horn for broadcasting-satellite antennas. Electronics Letters 15 (1979), 652-654.
- [10] Vokurka, V.J., Elliptical corrugated horns for frequency-reuse applications. IEEE AP-S International Symposium Digest, 221-223, Québec, Canada, 1980.

#### 4. RADIATION CHARACTERISTICS OF ELLIPTICAL HORNS WITH ANISOTROPIC BOUNDARY

##### 4.1. Introduction

The radiation behaviour of truncated elliptical cones will be discussed in this chapter. A theory is developed starting from the Kirchhoff-Huygens approximation to the radiation problem and computed results will be compared with experimental results.

In general, knowledge of the tangential fields on a closed surface surrounding the sources of radiation is necessary and sufficient to determine the radiation field outside the surface. In the Kirchhoff-Huygens approximation it is assumed that the radiation field is completely determined by the field distribution at the antenna aperture surface only. The aperture field is thereby taken to be identical to some given modal field of the infinite cone. This simplification of the radiation problem is permissible provided the following assumptions are valid [2]:

1. the outside surface of the horn does not contribute to the radiation;
2. unwanted modes, possibly generated at the throat and at the mouth of the horn, can be neglected.

To meet these assumptions it is required that

- a. the horn antenna has been constructed from electrically good conducting material;
- b. the horn flare angle is not too large, say less than 45 degrees;
- c. the horn length is large in terms of wavelength.

Regarding the application of such horns in communication links it is required that two orthogonal modes of one type of polarization (linear or circular), give rise to identical radiation patterns. It will be found that the elliptical horns with anisotropic boundary meet this requirement.

On the basis of the Kirchhoff-Huygens approximation the radiation field of the horn is given by an integral representation in terms of the aperture field. From this integral representation general radiation properties of horn aperture fields are derived, dependent on the properties of the exciting modal field.

Two methods are employed for the computation of the radiation pattern of the horn. One method, the aperture-field integration method, is suitable

to evaluate the radiating near-field and far-field patterns. In this method the Kirchhoff-Huygens integral representation for the radiation field is converted into a sampling-like representation by a series of products of Fresnel integrals and Fourier coefficients of the aperture field.

In the second method, the wave-expansion method, the fields outside the horn are expanded in terms of sphero-conal TE and TM modes. If the aperture fields are known, the expansion coefficients can be determined by matching the fields at the aperture and by using the orthogonality properties of the TE and TM modes of free space. In principle this method can be used to evaluate the radiation field at any observation point outside the horn. On the other hand, from the computational point of view the expansion method is more involved than the integration method, in particular for long horns.

The well-known wave-expansion method for the analysis of circular horns [5] is a special case of the expansion method mentioned above. In the far-field region of circular horns the aperture-field integration method and the wave-expansion method are mathematically equivalent [9].

In section 4.5 numerical results obtained by the integration and expansion methods will be compared with each other and with experimental results.

#### 4.2. General properties of radiation fields from elliptical horns with anisotropic boundary

This section deals with general radiation properties of horn aperture fields caused by the hybrid modes discussed in section 3.3. These properties are best derived from the integral representations for the fields outside the horn and the properties of the modes mentioned.

Consider an elliptical horn with an aperture  $S_a$  (see Figure 4.1). The aperture fields denoted by  $\bar{E}(\bar{r}_a)$  and  $\bar{H}(\bar{r}_a)$ , are the only sources of the electromagnetic fields outside the horn. Then the fields outside the horn are given by [11, p. 19]

$$\bar{E}(\bar{r}_p) = \nabla_p \times \iint_{S_a} \{\hat{n} \times \bar{E}(\bar{r}_a)\} G(\bar{r}_p, \bar{r}_a) dS + (j\omega\epsilon_0)^{-1} \nabla_p \times \nabla_p \times \iint_{S_a} \{\hat{n} \times \bar{H}(\bar{r}_a)\} G(\bar{r}_p, \bar{r}_a) dS, \quad (4.1)$$

and

$$\begin{aligned} \bar{H}(\bar{r}_p) &= \nabla_p \times \iint_{S_a} \{\hat{n} \times \bar{H}(\bar{r}_a)\} G(\bar{r}_p, \bar{r}_a) dS - \\ &-(j\omega\mu_0)^{-1} \nabla_p \times \nabla_p \times \iint_{S_a} \{\hat{n} \times \bar{E}(\bar{r}_a)\} G(\bar{r}_p, \bar{r}_a) dS, \end{aligned} \quad (4.2)$$

with

$$G(\bar{r}_p, \bar{r}_a) = \frac{\exp(-jk^*|\bar{r}_p - \bar{r}_a|)}{4\pi|\bar{r}_p - \bar{r}_a|},$$

in which (see Figure 4.1):

$\bar{r}_a$  is the position vector of the aperture point Q,

$\bar{r}_p$  is the position vector of the observation point P,

$\hat{n}$  is the unit vector normal to  $S_a$  at Q,

$\nabla_p$  is the curl operator with respect to the coordinates of P.

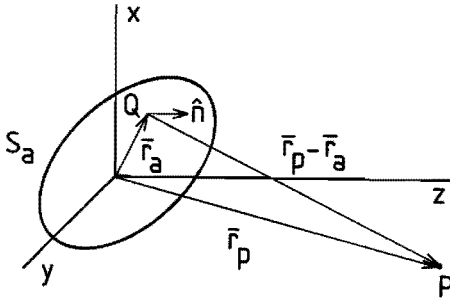


Fig. 4.1. Horn aperture  $S_a$  and the observation point P.

If the horn aperture fields are related by  $\bar{E}(\bar{r}_a) = \pm jZ_0 \bar{H}(\bar{r}_a)$ , then it is found from (4.1) and (4.2) that the fields at an arbitrary observation point P satisfy the relation  $\bar{E}(\bar{r}_p) = \pm jZ_0 \bar{H}(\bar{r}_p)$ .

Equations (4.1) and (4.2) express that the fields at P are obtainable from the tangential fields on  $S_a$ . As the fields in the immediate vicinity of the aperture  $S_a$  are not of interest in the present study, it is assumed that  $k^*|\bar{r}_p - \bar{r}_a| \gg 1$ , where  $k^* = 2\pi/\lambda_0$  and  $\lambda_0$  is the free-space wavelength. This assumption restricts the investigation to the radiating near-field and far-field regions of the horn antenna. The

first region extends from a few wavelengths away from the antenna to  $2D^2/\lambda_0$ , where  $D$  is the diameter of the antenna aperture. The second region is commonly taken to exist beyond a distance  $2D^2/\lambda_0$  from the antenna [8].

Carrying out the vector operations  $\nabla_{\mathbf{p}} \times$  in (4.1) and (4.2), and assuming that  $k^* |\bar{\mathbf{r}}_{\mathbf{p}} - \bar{\mathbf{r}}_{\mathbf{a}}| \gg 1$ , it is found that these representations simplify to [11, p. 20]

$$\bar{\mathbf{E}}(\bar{\mathbf{r}}_{\mathbf{p}}) = \frac{-jk^*}{4\pi} \iint_{S_a} [\hat{\mathbf{f}}_1 \times \{\hat{\mathbf{n}} \times \bar{\mathbf{E}}(\bar{\mathbf{r}}_{\mathbf{a}})\} - Z_0 \hat{\mathbf{f}}_1 \times \{\hat{\mathbf{f}}_1 \times \{\hat{\mathbf{n}} \times \bar{\mathbf{H}}(\bar{\mathbf{r}}_{\mathbf{a}})\}\}] \frac{1}{r_1} \exp(-jk^* r_1) dS, \quad (4.3)$$

and

$$Z_0 \bar{\mathbf{H}}(\bar{\mathbf{r}}_{\mathbf{p}}) = \frac{-jk^*}{4\pi} \iint_{S_a} [Z_0 \hat{\mathbf{f}}_1 \times \{\hat{\mathbf{n}} \times \bar{\mathbf{H}}(\bar{\mathbf{r}}_{\mathbf{a}})\} + \hat{\mathbf{f}}_1 \times \{\hat{\mathbf{f}}_1 \times \{\hat{\mathbf{n}} \times \bar{\mathbf{E}}(\bar{\mathbf{r}}_{\mathbf{a}})\}\}] \frac{1}{r_1} \exp(-jk^* r_1) dS, \quad (4.4)$$

in which  $\bar{\mathbf{r}}_1 = \bar{\mathbf{r}}_{\mathbf{p}} - \bar{\mathbf{r}}_{\mathbf{a}}$ ,  $r_1 = |\bar{\mathbf{r}}_1|$ , and  $\hat{\mathbf{r}}_1 = \bar{\mathbf{r}}_1 / r_1$ .

In the radiating near-field and far-field regions further approximations can be made [11, p. 20-25]. The unit vector  $\hat{\mathbf{r}}_1$  is replaced by the unit vector  $\hat{\mathbf{f}}_{\mathbf{p}}$  along  $\bar{\mathbf{r}}_{\mathbf{p}}$ , and  $r_1$  in the denominator is replaced by  $r_{\mathbf{p}}$ . In the exponential function a more accurate approximation of the distance  $r_1$ , denoted by  $\tilde{r}_1$ , must be used [7], [11, p. 22-23]. Explicit expressions for  $\tilde{r}_1$  are given in subsequent sections. Inserting the approximations into (4.3) and (4.4) one finds

$$\bar{\mathbf{E}}(\bar{\mathbf{r}}_{\mathbf{p}}) = \frac{-jk^*}{4\pi r_{\mathbf{p}}} \hat{\mathbf{f}}_{\mathbf{p}} \times \iint_{S_a} [\hat{\mathbf{n}} \times \bar{\mathbf{E}}(\bar{\mathbf{r}}_{\mathbf{a}}) - Z_0 \hat{\mathbf{f}}_{\mathbf{p}} \times \{\hat{\mathbf{n}} \times \bar{\mathbf{H}}(\bar{\mathbf{r}}_{\mathbf{a}})\}] \exp(-jk^* \tilde{r}_1) dS, \quad (4.5)$$

and

$$Z_0 \bar{\mathbf{H}}(\bar{\mathbf{r}}_{\mathbf{p}}) = \frac{-jk^*}{4\pi r_{\mathbf{p}}} \hat{\mathbf{f}}_{\mathbf{p}} \times \iint_{S_a} [Z_0 \hat{\mathbf{n}} \times \bar{\mathbf{H}}(\bar{\mathbf{r}}_{\mathbf{a}}) + \hat{\mathbf{f}}_{\mathbf{p}} \times \{\hat{\mathbf{n}} \times \bar{\mathbf{E}}(\bar{\mathbf{r}}_{\mathbf{a}})\}] \exp(-jk^* \tilde{r}_1) dS. \quad (4.6)$$

From these equations it is readily seen that

$$Z_0 \bar{\mathbf{H}}(\bar{\mathbf{r}}_{\mathbf{p}}) = \hat{\mathbf{f}}_{\mathbf{p}} \times \bar{\mathbf{E}}(\bar{\mathbf{r}}_{\mathbf{p}}). \quad (4.7)$$

It is recalled that if the aperture fields are related by  $\bar{\mathbf{E}}(\bar{\mathbf{r}}_{\mathbf{a}}) = +jZ_0 \bar{\mathbf{H}}(\bar{\mathbf{r}}_{\mathbf{a}})$ , then the fields at a point  $P$  satisfy  $\bar{\mathbf{E}}(\bar{\mathbf{r}}_{\mathbf{p}}) = +jZ_0 \bar{\mathbf{H}}(\bar{\mathbf{r}}_{\mathbf{p}})$ . From the latter relation and (4.7) it follows that  $\bar{\mathbf{E}}(\bar{\mathbf{r}}_{\mathbf{p}}) \cdot \bar{\mathbf{E}}(\bar{\mathbf{r}}_{\mathbf{p}}) = 0$ ,

hence, subject to the approximations mentioned above, the field at P is circularly polarized. If in the double-signed expressions the upper(lower) sign applies, then the circular polarization is counter-clockwise(clockwise) with respect to the direction of propagation. Thus, aperture fields that satisfy  $\vec{E}(\vec{r}_a) = \pm jZ_0 \vec{H}(\vec{r}_a)$  generate purely circularly polarized fields. Such aperture fields are obtained by a suitable combination of I- and II-modes, as has been shown in section 3.3; in fact, this is a consequence of (3.97) and (3.98). If these modes are utilized separately, then the electric fields denoted by  $\vec{E}^I(\vec{r}_p)$  and  $\vec{E}^{II}(\vec{r}_p)$ , respectively, are geometrically orthogonal. The orthogonality is proved as follows. From (3.97), (3.98), it is found that  $\vec{E}^I(\vec{r}_a) = Z_0 \vec{H}^{II}(\vec{r}_a)$  and  $\vec{E}^{II}(\vec{r}_a) = -Z_0 \vec{H}^I(\vec{r}_a)$ . From these relations and (4.5)-(4.7) we then derive

$$\vec{E}^I(\vec{r}_p) = \hat{f}_p \times \vec{E}^{II}(\vec{r}_p), \quad (4.8)$$

which implies the orthogonality

$$\vec{E}^I(\vec{r}_p) \cdot \vec{E}^{II}(\vec{r}_p) = 0. \quad (4.9)$$

The properties of some power radiation patterns are now investigated by considering Poynting's vector

$$\vec{P}(\vec{r}_p) = \frac{1}{2} \text{Re}\{\vec{E}(\vec{r}_p) \times \vec{H}^*(\vec{r}_p)\}. \quad (4.10)$$

From (4.10) and (4.7) one has

$$\vec{P}(\vec{r}_p) = \frac{1}{2Z_0} |\vec{E}(\vec{r}_p)|^2 \hat{f}_p. \quad (4.11)$$

Let  $\vec{E}_\alpha(\vec{r}_a) = \vec{E}^I(\vec{r}_a) - j\vec{E}^{II}(\vec{r}_a)$  and  $\vec{H}_\alpha(\vec{r}_a) = \vec{H}^I(\vec{r}_a) - j\vec{H}^{II}(\vec{r}_a)$  be the aperture fields of an  $\alpha$ -mode. By use of the relations (3.97), (3.98), it is found that these fields satisfy  $\vec{E}_\alpha(\vec{r}_a) = jZ_0 \vec{H}_\alpha(\vec{r}_a)$ . The fields  $\vec{E}_\alpha(\vec{r}_p)$  and  $\vec{H}_\alpha(\vec{r}_p)$ , determined from (4.5) and (4.6), then give rise to the Poynting vector

$$\begin{aligned} \vec{P}(\vec{r}_p) &= \frac{1}{2Z_0} \{ |\vec{E}^I(\vec{r}_p)|^2 + |\vec{E}^{II}(\vec{r}_p)|^2 \} \hat{f}_p \\ &= \frac{1}{Z_0} |\vec{E}^I(\vec{r}_p)|^2 \hat{f}_p, \end{aligned} \quad (4.12)$$

where use has been made of (4.8). Note that the  $\alpha$ -mode generates radiation fields that are counter-clockwise circularly polarized.

Let  $\vec{E}_\beta(\vec{r}_a) = \vec{E}^I(\vec{r}_a) + j\vec{E}^{II}(\vec{r}_a)$  and  $\vec{H}_\beta(\vec{r}_a) = \vec{H}^I(\vec{r}_a) + j\vec{H}^{II}(\vec{r}_a)$  be the aperture fields of a  $\beta$ -mode. Using (3.97) and (3.98), it is found that these fields satisfy  $\vec{E}_\beta(\vec{r}_a) = -jZ_0 \vec{H}_\beta(\vec{r}_a)$ . The equality of the Poynting vectors for the  $\alpha$ - and the  $\beta$ -modes can be easily shown. Hence, these two modes give rise to the same power radiation patterns, while from the analysis of the polarization properties it is known that the associated radiation fields are oppositely circularly polarized.

From (4.11) and (4.8) it readily follows that the power radiation patterns of a I- and a II-mode are equal. The associated radiation fields, however, are perpendicular to each other.

The analysis given above has revealed a number of interesting properties of the radiation fields of the elliptical horn with anisotropic boundary. These properties are of great importance in telecommunications applications.

#### 4.3. Sphero-conal wave-expansion method for radiation computation

In recent years, corrugated elliptical horns have received a lot of attention in view of their application as a primary radiator in satellite antennas for the direct TV broadcasting service [16], [17]. The use of such a horn for the illumination of a single offset parabolic reflector has been described in [6]. The major axis of the horn aperture is  $6\lambda_0$  at the frequency 12 GHz, whereas the focal length of the reflector is 1.5 m. The reflector is in the radiating near-field region of the horn. This region extends to approximately 1.8 m from the horn aperture.

One approach to the calculation of the radiation fields from elliptical horns employs a wave-expansion method. Consider an elliptical horn with a radial length  $r_a$ , an opening angle  $\theta_0$ , and an aspect ratio  $a_{r\theta}$ ; see Figure 4.2. The observation point and the aperture point are described by sphero-conal coordinates  $(r_p, \theta_p, \phi_p)$  and  $(r_a, \theta, \phi)$ , respectively.

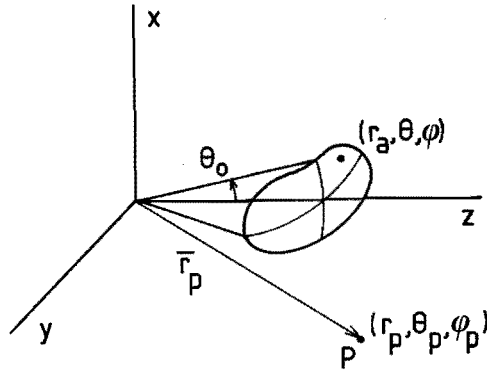


Fig. 4.2. Coordinates for the wave-expansion computations.

In the free-space region outside the sphere of radius  $r_a$ , any electromagnetic field can be decomposed into TE and TM modes. Since the region is simply connected, such a decomposition exists by [10, Theorem 5.3, p. 86].

The expansion coefficients are determined by matching to the given tangential fields on the sphere of radius  $r = r_a$ , and by invoking the orthogonality properties of the TE and TM modes of free space. Knowing the coefficients, the electromagnetic fields outside the sphere of radius  $r_a$  can be calculated. It is thereby assumed that on the sphere  $r = r_a$ , the fields are non-zero only at the cap  $0 \leq \theta \leq \theta_0$ , in accordance with the adopted Kirchoff-Huygens approximation; see section 4.1.

The equations needed for handling the computation problem stated above, are now given. The assumed time dependence  $\exp(j\omega t)$  will be suppressed throughout. With reference to (3.3) and (3.4), the decomposition for odd symmetric fields, valid for  $r_p \geq r_a$ , reads

$$\vec{E}_o(\vec{r}_p) = \sum_{\nu=1}^{\infty} \sum_{n=0}^{\nu} [-a_{\nu}^{(n)} \nabla_{\mathbf{x}} \{r_p \psi_{\nu}^{(n)}(\vec{r}_p) \hat{r}_p\} + b_{\nu}^{(n)} \frac{1}{k^*} \nabla_{\mathbf{x}} \nabla_{\mathbf{x}} \{r_p \psi_{\nu}^{(n)}(\vec{r}_p) \hat{r}_p\}], \tag{4.13}$$

$$jZ_0 \bar{H}_o(\bar{r}_p) = \sum_{v=1}^{\infty} \sum_{n=0}^v [a_{cv}^{(n)} \frac{1}{k^*} \nabla_x \nabla_x \{r_p \psi_{p,cv}^{(n)}(\bar{r}_p) \hat{r}_p\} - b_{sv}^{(n)} \nabla_x \{r_p \psi_{p,sv}^{(n)}(\bar{r}_p) \hat{r}_p\}], \quad (4.14)$$

where  $a_{cv}^{(n)}$  and  $b_{sv}^{(n)}$  are the coefficients of the odd symmetric  $TE_c$  and  $TM_s$  free-space modes, respectively. These modes are derived from the potentials  $\psi_{cv}^{(n)}$  and  $\psi_{sv}^{(n)}$ , which are solutions of the scalar Helmholtz equation (3.4a) that are regular in the region  $r_p \geq r_a$ ,  $0 \leq \theta_p \leq \pi$ ,  $0 \leq \phi_p \leq 2\pi$ . Such solutions have been determined in section 2.5.2, viz.

$$\psi_{cv}^{(n)}(\bar{r}_p) = h_v^{(2)}(k^* r_p) v_{cv}^{(n)}(\theta_p, \phi_p), \quad \psi_{sv}^{(n)}(\bar{r}_p) = h_v^{(2)}(k^* r_p) v_{sv}^{(n)}(\theta_p, \phi_p), \quad (4.15)$$

where  $v_{cv}^{(n)}$ ,  $v_{sv}^{(n)}$  are given by (2.158a-d).

Likewise, the decomposition for even symmetric fields reads

$$\bar{E}_e(\bar{r}_p) = \sum_{v=1}^{\infty} \sum_{n=0}^v [-a_{sv}^{(n)} \nabla_x \{r_p \psi_{p,sv}^{(n)}(\bar{r}_p) \hat{r}_p\} + b_{cv}^{(n)} \frac{1}{k^*} \nabla_x \nabla_x \{r_p \psi_{p,cv}^{(n)}(\bar{r}_p) \hat{r}_p\}], \quad (4.16)$$

$$jZ_0 \bar{H}_e(\bar{r}_p) = \sum_{v=1}^{\infty} \sum_{n=0}^v [a_{sv}^{(n)} \frac{1}{k^*} \nabla_x \nabla_x \{r_p \psi_{p,sv}^{(n)}(\bar{r}_p) \hat{r}_p\} - b_{cv}^{(n)} \nabla_x \{r_p \psi_{p,cv}^{(n)}(\bar{r}_p) \hat{r}_p\}], \quad (4.17)$$

where  $a_{sv}^{(n)}$  and  $b_{cv}^{(n)}$  are the coefficients of the even symmetric  $TE_s$  and  $TM_c$  free-space modes, respectively. The definitions of odd and even symmetric fields are in accordance with (3.23) and (3.24), respectively.

Introduce the vectors

$$\bar{M}_{cv}^{(n)}(\bar{r}_p) = -\nabla_x \{r_p \psi_{p,cv}^{(n)}(\bar{r}_p) \hat{r}_p\}, \quad \bar{M}_{sv}^{(n)}(\bar{r}_p) = -\nabla_x \{r_p \psi_{p,sv}^{(n)}(\bar{r}_p) \hat{r}_p\}, \quad (4.18)$$

$$\bar{N}_{cv}^{(n)}(\bar{r}_p) = \frac{1}{k^*} \nabla_x \nabla_x \{r_p \psi_{p,cv}^{(n)}(\bar{r}_p) \hat{r}_p\}, \quad \bar{N}_{sv}^{(n)}(\bar{r}_p) = \frac{1}{k^*} \nabla_x \nabla_x \{r_p \psi_{p,sv}^{(n)}(\bar{r}_p) \hat{r}_p\}, \quad (4.19)$$

then the expansions (4.13) and (4.14) can be shortly written as

$$\bar{E}_o(\bar{r}_p) = \sum_{v=1}^{\infty} \sum_{n=0}^v \{a_{cv}^{(n)} \bar{M}_{cv}^{-(n)}(\bar{r}_p) + b_{sv}^{(n)} \bar{N}_{sv}^{-(n)}(\bar{r}_p)\}, \quad (4.20)$$

$$jZ_o \bar{H}_o(\bar{r}_p) = \sum_{v=1}^{\infty} \sum_{n=0}^v \{a_{cv}^{(n)} \bar{N}_{cv}^{-(n)}(\bar{r}_p) + b_{sv}^{(n)} \bar{M}_{sv}^{-(n)}(\bar{r}_p)\}, \quad (4.21)$$

whereas (4.16) and (4.17) become

$$\bar{E}_e(\bar{r}_p) = \sum_{v=1}^{\infty} \sum_{n=0}^v \{a_{sv}^{(n)} \bar{M}_{sv}^{-(n)}(\bar{r}_p) + b_{cv}^{(n)} \bar{N}_{cv}^{-(n)}(\bar{r}_p)\}, \quad (4.22)$$

$$jZ_o \bar{H}_e(\bar{r}_p) = \sum_{v=1}^{\infty} \sum_{n=0}^v \{a_{sv}^{(n)} \bar{N}_{sv}^{-(n)}(\bar{r}_p) + b_{cv}^{(n)} \bar{M}_{cv}^{-(n)}(\bar{r}_p)\}. \quad (4.23)$$

It can easily be shown that  $\bar{M}$  and  $\bar{N}$  are related by

$$\nabla_{xM_{cv}} \bar{M}_{cv}^{-(n)} = -k^* \bar{N}_{cv}^{-(n)}, \quad \nabla_{xM_{sv}} \bar{M}_{sv}^{-(n)} = -k^* \bar{N}_{sv}^{-(n)}, \quad (4.24)$$

$$\nabla_{xN_{cv}} \bar{N}_{cv}^{-(n)} = -k^* \bar{M}_{cv}^{-(n)}, \quad \nabla_{xN_{sv}} \bar{N}_{sv}^{-(n)} = -k^* \bar{M}_{sv}^{-(n)}. \quad (4.25)$$

Using these equations it is readily verified that the fields represented by (4.20), (4.21), satisfy

$$\nabla_x \bar{E}_o(\bar{r}_p) = -j\omega \mu_o \bar{H}_o(\bar{r}_p), \quad \nabla_x \bar{H}_o(\bar{r}_p) = j\omega \epsilon_o \bar{E}_o(\bar{r}_p), \quad (4.26)$$

and those represented by (4.22), (4.23), satisfy

$$\nabla_x \bar{E}_e(\bar{r}_p) = -j\omega \mu_o \bar{H}_e(\bar{r}_p), \quad \nabla_x \bar{H}_e(\bar{r}_p) = j\omega \epsilon_o \bar{E}_e(\bar{r}_p), \quad (4.27)$$

which are Maxwell's equations.

By use of (4.15) the vectors  $\bar{M}$  and  $\bar{N}$  can be expressed in terms of the spherical Hankel function  $h_v^{(2)}(k^* r_p)$  and the functions  $v_{cv}^{(n)}$ ,  $v_{sv}^{(n)}$ , viz.

$$\bar{M}_{cv}^{-(n)}(\bar{r}_p) = h_v^{(2)}(k^* r_p) \hat{r}_p \times \nabla_t v_{cv}^{(n)}(\theta_p, \phi_p), \quad (4.28)$$

$$\begin{aligned} \bar{N}_{cv}^{-(n)}(\bar{r}_p) &= (k^* r_p)^{-1} [v(v+1) h_v^{(2)}(k^* r_p) v_{cv}^{(n)}(\theta_p, \phi_p) \hat{r}_p + \\ &+ \frac{d}{dr_p} \{r_p h_v^{(2)}(k^* r_p)\} \nabla_t v_{cv}^{(n)}(\theta_p, \phi_p)], \end{aligned} \quad (4.29)$$

$$\bar{M}_{sv}^{(n)}(\bar{r}_p) = h_v^{(2)}(k^*r_p) \hat{r}_p \times \nabla_t v_{sv}^{(n)}(\theta_p, \phi_p), \quad (4.30)$$

$$\begin{aligned} \bar{N}_{sv}^{(n)}(\bar{r}_p) &= (k^*r_p)^{-1} [v(v+1)h_v^{(2)}(k^*r_p) v_{sv}^{(n)}(\theta_p, \phi_p) \hat{r}_p + \\ &+ \frac{d}{dr_p} \{r_p h_v^{(2)}(k^*r_p)\} \nabla_t v_{sv}^{(n)}(\theta_p, \phi_p)], \end{aligned} \quad (4.31)$$

in which the vector operation  $\nabla_p \times$  has been partly carried out. According to (2.158a-d) the functions  $v_{cv}^{(n)}$ ,  $v_{sv}^{(n)}$  are products of Lamé functions,

$$v_{cv}^{(n)}(\theta_p, \phi_p) = L_{cpv}^{(n)}(\theta_p) L_{cv}^{(n)}(\phi_p), \quad v_{sv}^{(n)}(\theta_p, \phi_p) = L_{spv}^{(n)}(\theta_p) L_{sv}^{(n)}(\phi_p). \quad (4.32)$$

The vector operation  $\nabla_t$  in (4.28) and (4.29) can be carried out by means of (2.49c), thus leading to the following expressions for the vectors  $\bar{M}_{cv}^{(n)}$  and  $\bar{N}_{cv}^{(n)}$ :

$$\begin{aligned} \bar{M}_{cv}^{(n)}(\bar{r}_p) &= -\frac{1}{h_\phi^*} h_v^{(2)}(k^*r_p) L_{cpv}^{(n)}(\theta_p) \frac{d}{d\phi_p} \{L_{cv}^{(n)}(\phi_p)\} \hat{e}_\theta + \\ &+ \frac{1}{h_\theta^*} h_v^{(2)}(k^*r_p) \frac{d}{d\theta_p} \{L_{cpv}^{(n)}(\theta_p)\} L_{cv}^{(n)}(\phi_p) \hat{e}_\phi, \end{aligned} \quad (4.33)$$

$$\begin{aligned} \bar{N}_{cv}^{(n)}(\bar{r}_p) &= \frac{v(v+1)}{k^*r_p} h_v^{(2)}(k^*r_p) L_{cpv}^{(n)}(\theta_p) L_{cv}^{(n)}(\phi_p) \hat{r}_p + \\ &+ \frac{1}{k^*r_p h_\theta^*} \frac{d}{dr_p} \{r_p h_v^{(2)}(k^*r_p)\} \frac{d}{d\theta_p} \{L_{cpv}^{(n)}(\theta_p)\} L_{cv}^{(n)}(\phi_p) \hat{e}_\theta + \\ &+ \frac{1}{k^*r_p h_\phi^*} \frac{d}{dr_p} \{r_p h_v^{(2)}(k^*r_p)\} L_{cpv}^{(n)}(\theta_p) \frac{d}{d\phi_p} \{L_{cv}^{(n)}(\phi_p)\} \hat{e}_\phi. \end{aligned} \quad (4.34)$$

Here,  $\hat{r}_p, \hat{e}_\theta, \hat{e}_\phi$  are the sphero-conal unit vectors at the observation point P; furthermore,  $h_\theta^* = h_\theta/r, h_\phi^* = h_\phi/r$ , where the scale factors  $h_\theta, h_\phi$ , are given by (2.9), (2.10), with  $\theta = \theta_p, \phi = \phi_p$ . Expressions for the vectors  $\bar{M}_{sv}^{(n)}$  and  $\bar{N}_{sv}^{(n)}$  are found from (4.33) and (4.34) when replacing the subscript c by s.

To determine the expansion coefficients we make use of the vectors  $\bar{M}$  and  $\bar{N}$  being orthogonal in integral sense. To show this, let  $v_1, v_2$ , be any pair of functions from the complete set  $v_{cv}^{(n)}, v_{sv}^{(n)}, v = 0, 1, 2, \dots, n = 0, 1, \dots, \nu$ , as given by (4.32). Furthermore, let  $\Omega$  denote the unit sphere described by  $r_p = 1, 0 \leq \theta_p \leq \pi, 0 \leq \phi_p \leq 2\pi$ . Then, in view of (2.163), (2.174a-c) and (2.176a-c), we have the orthogonality relations

$$\iint_{\Omega} (\hat{r}_p \times \nabla_t v_1) \cdot (\hat{r}_p \times \nabla_t v_2) d\Omega = \iint_{\Omega} \nabla_t v_1 \cdot \nabla_t v_2 d\Omega = 0 \quad \text{if } v_1 \neq v_2, \quad (4.35)$$

$$\iint_{\Omega} \hat{r}_p \times \nabla_t v_1 \cdot \nabla_t v_2 d\Omega = \iint_{\Omega} \nabla_t v_1 \times \nabla_t v_2 \cdot \hat{r}_p d\Omega = 0, \quad (4.36)$$

$$\iint_{\Omega} v_1 v_2 d\Omega = 0 \quad \text{if } v_1 \neq v_2. \quad (4.37)$$

Together with (4.28) - (4.31) these relations imply that the vector functions  $\bar{M}_{cv}^{(n)}, \bar{M}_{sv}^{(n)}, \bar{N}_{cv}^{(n)}, \bar{N}_{sv}^{(n)}$  form an orthogonal system on the unit sphere. It is easily verified that also the vectors  $\bar{M}$  and  $\bar{N}_t$  are orthogonal in integral sense; here  $\bar{N}_t$  denotes the transverse part of  $\bar{N}$ .

As an example we now deal in detail with the expansion of the odd symmetric fields of the elliptical horn with anisotropic boundary, in the region  $r_p \geq r_a, 0 \leq \theta_p \leq \pi, 0 \leq \phi_p < 2\pi$ . The electric field  $\bar{E}_a(\bar{r}_a)$  tangential to the sphere  $r = r_a$  is taken to be zero outside the aperture of the horn. At the aperture,  $\bar{E}_a(\bar{r}_a)$  is taken to be equal to the tangential field of the odd symmetric I-mode of the infinite cone. This tangential field has components given by (3.66) and (3.67), in which the notation  $\nu$  for the mode-number is changed into  $\nu'$ , to avoid confusion. The modal field is assumed to have period  $2\pi$  in  $\phi$  (HE mode), hence the coefficients  $a_{2m}$  and  $b_{2m}$  (with even subscripts) in (3.66) and (3.67) vanish. It is understood that the mode-number  $\nu'$  and the sequences  $\{a_{2m+1}\}, \{b_{2m+1}\}$ , have been determined in the manner described below (3.86).

The expansion of  $\bar{E}_a(\bar{r}_a)$  according to (4.20) now reads

$$\bar{E}_a(\bar{r}_a) = \sum_{\nu=1}^{\infty} \left[ \sum_{n=0}^{(\nu-1)/2} \{ a_{cv}^{(2n+1)} \bar{M}_{cv}^{(2n+1)}(\bar{r}_a) + b_{sv}^{(2n+1)} \bar{N}_{tsv}^{(2n+1)}(\bar{r}_a) \} \right], \quad (4.38)$$

in which  $\bar{N}_{tsv}^{(2n+1)}$  denotes the transverse part of  $\bar{N}_{sv}^{(2n+1)}$ ; see (4.31). To determine a specific expansion coefficient, multiply (4.38) by the appropriate  $\bar{M}$  or  $\bar{N}_t$  and integrate the result over the sphere  $r = r_a$ . By use of the orthogonality properties of  $\bar{M}$  and  $\bar{N}$ , it is then found that

$$a_{cv}^{(2n+1)} = \int_0^{\theta_0} \int_0^{2\pi} \bar{E}_a(\bar{r}_a) \cdot \bar{M}_{cv}^{(2n+1)}(\bar{r}_a) h_{\theta}^* h_{\phi}^* d\theta d\phi / \int_0^{\pi} \int_0^{2\pi} |\bar{M}_{cv}^{(2n+1)}(\bar{r}_a)|^2 h_{\theta}^* h_{\phi}^* d\theta d\phi, \quad (4.39)$$

and

$$b_{sv}^{(2n+1)} = \int_0^{\theta_0} \int_0^{2\pi} \bar{E}_a(\bar{r}_a) \cdot \bar{N}_{tsv}^{(2n+1)}(\bar{r}_a) h_{\theta}^* h_{\phi}^* d\theta d\phi / \int_0^{\pi} \int_0^{2\pi} |\bar{N}_{tsv}^{(2n+1)}(\bar{r}_a)|^2 h_{\theta}^* h_{\phi}^* d\theta d\phi. \quad (4.40)$$

The integral in the denominator of (4.39) can be reduced to an integral of the square of  $v_{cv}^{(2n+1)}$ . Indeed, by use of (4.28) and (2.166) we derive

$$\int_0^{\pi} \int_0^{2\pi} |\bar{M}_{cv}^{(2n+1)}(\bar{r}_a)|^2 h_{\theta}^* h_{\phi}^* d\theta d\phi = \{ h_{\nu}^{(2)}(k^* r_a) \}^2 I_{cv}^{(2n+1)}, \quad (4.41)$$

in which

$$I_{cv}^{(2n+1)} = \nu(\nu+1) \int_0^{\pi} \int_0^{2\pi} \{ v_{cv}^{(2n+1)}(\theta, \phi) \}^2 h_{\theta}^* h_{\phi}^* d\theta d\phi. \quad (4.42)$$

The integral in the denominator of (4.40) is likewise reducible to an integral of the square of  $v_{sv}^{(2n+1)}$ . By use of the transverse part of (4.31), together with (2.166), we now find

$$\int_0^{\pi} \int_0^{2\pi} |\bar{N}_{tsv}^{(2n+1)}(\bar{r}_a)|^2 h_{\theta}^* h_{\phi}^* d\theta d\phi = (k^* r_a)^{-2} \left[ \frac{d}{dr} \{ r h_v^{(2)}(k^* r) \} \right]^2 \Big|_{r_a} I_{sv}^{(2n+1)}, \quad (4.43)$$

where

$$I_{sv}^{(2n+1)} = v(v+1) \int_0^{\pi} \int_0^{2\pi} \{ \bar{N}_{sv}^{(2n+1)}(\theta, \phi) \}^2 h_{\theta}^* h_{\phi}^* d\theta d\phi. \quad (4.44)$$

To evaluate the numerators of (4.39) and (4.40), we insert the expansions (3.66) and (3.67) for the components of the aperture field  $\bar{E}_a(\bar{r}_a)$ . The resulting double integrals can be further reduced by means of the integral relations for simple-periodic and nonperiodic Lamé functions. Explicit expressions for these numerators are given in Appendix 4.6.1. Note that if  $a_{r\theta} = 1$ , corresponding to the case of a circular cone, all integrals can be evaluated, thus leading to closed-form expressions for the expansion coefficients [12].

After having evaluated  $a_{cv}^{(2n+1)}$ ,  $b_{sv}^{(2n+1)}$ , the fields at an arbitrary observation point P outside the sphere  $r = r_a$  are determined from (4.20), (4.21). In numerical computations the summations over  $v$  are truncated at some integer  $v_{\max}$ , which is related to the electrical length  $k^* r_a$  of the horn. An acceptable truncation value is  $v_{\max} = [k^* r_a]$ , in which  $[k^* r_a]$  denotes the largest integer  $\leq k^* r_a$ . Free-space modes with  $v > v_{\max}$  do not contribute significantly, as is confirmed by the comparison of the modal power-flow  $P_a$  through the aperture, and the running total of the radiation power of the expansion modes as a function of  $v$ . The total radiation power  $P_{\text{tot}}$  of the expansion modes equals  $P_a$ . The power flow  $P_a$  is determined from (3.108). The power flow  $P_{\text{tot}}$  through the sphere of radius  $r_p$  is found by integration of the radial component of the time-average Poynting vector  $\bar{P}(\bar{r}_p)$  given by

$$\bar{P}(\bar{r}_p) = \frac{1}{2} \text{Re} \{ \bar{E}_o(\bar{r}_p) \times \bar{H}_o^*(\bar{r}_p) \}. \quad (4.45)$$

By substitution of (4.20) and (4.21) into (4.45), and by integration over the sphere of radius  $r_p$ , using the orthogonality properties of  $\bar{M}$  and  $\bar{N}$ , and the property (2.85) of the spherical Bessel functions, it is found that  $P_{\text{tot}}$ , due to the odd symmetric HE mode, equals

$$P_{\text{tot}} = (2Z_0 k^2)^{-1} \sum_{\nu=1}^{\infty} \left[ \frac{(\nu-1)/2}{\sum_{n=0}^{\nu-1} (|a_{c\nu}^{(2n+1)}|^2 I_{c\nu}^{(2n+1)} + |b_{s\nu}^{(2n+1)}|^2 I_{s\nu}^{(2n+1)})} \right]. \quad (4.46)$$

Features characterizing the radiation behaviour of a horn are the power radiation pattern, the gain function, the phase pattern and the phase centre.

The power radiation pattern  $F(\bar{r}_p)$  and the gain function  $g(\bar{r}_p)$  of the horn are defined by

$$F(\bar{r}_p) = P_r(\bar{r}_p) / P_r(r_p, 0, 0), \quad (4.47)$$

and

$$g(\bar{r}_p) = 4\pi P_r(\bar{r}_p) / P_a, \quad (4.48)$$

in which  $P_r(\bar{r}_p)$ , the power radiated per unit solid angle, is defined by

$$P_r(\bar{r}_p) = r_p^2 |\bar{P}(\bar{r}_p) \cdot \hat{r}_p|. \quad (4.49)$$

The phase pattern is equal to the difference between the phases of the electric field at the observation point and at a reference point. From the phase pattern one may determine the surfaces of constant phase or equiphase surfaces. Consider next the equiphase lines which arise as the intersection of the equiphase surfaces with a plane  $V$  through the axis of the horn ( $z$ -axis). In the far-field region these equiphase lines are approximately circles and their centre of curvature is called the phase centre in the plane  $V$ . To determine the location of the phase centre, we refer to the planar cross-section through the  $z$ -axis shown in Figure 4.3. Here, the point  $O$  is the apex of the horn;  $P_c$  is the phase centre;  $P$  is the observation point;  $P_o$  is the reference point;  $P$  and  $P_o$  are described by sphero-conal coordinates  $(r_p, \theta_p, \phi_p)$  and  $(r_p, 0, 0)$ , respectively. It is assumed that the equiphase line through  $P_o$  is a circle with centre  $P_c$ . Let the electric fields at  $P$  and at  $P_o$  differ in phase by  $\delta$ . Then the displacement  $\Delta$  of  $P_c$  relative to the

apex O is given by

$$\Delta = \delta / [k^* \{ 1 - (1 - k'^2 \sin^2 \phi_p)^{1/2} \cos \theta_p \}], \quad (\theta_p, \phi_p) \neq (0, 0). \quad (4.50)$$

This result can be derived in the same manner as in [11, p. 63], [15]. It should be noted that (4.50) is valid only in the far-field region. Moreover, it has been assumed that the equiphase lines are circles, at least to a good approximation, with their centre on the z-axis. If these conditions are not met, general formulae for the centre of curvature of an equiphase line must be used [13], [14].

In general  $\Delta \neq 0$ , hence the origin of the sphero-conal coordinate system used in the wave-expansion method does not coincide with the phase centre; the latter point is commonly taken as the point relative to which measurements are carried out. Furthermore, measured results are recorded as a function of spherical coordinates, whereas computed results are determined as a function of sphero-conal coordinates. The spherical coordinates of an observation point on a sphere centred at  $P_c$  can always be transformed into the sphero-conal coordinates of that point, now on a sphere centred at the apex of the horn. So extra transformations and computations will be needed in order to compare the computed and measured results. The details of these calculations, however, will be omitted.

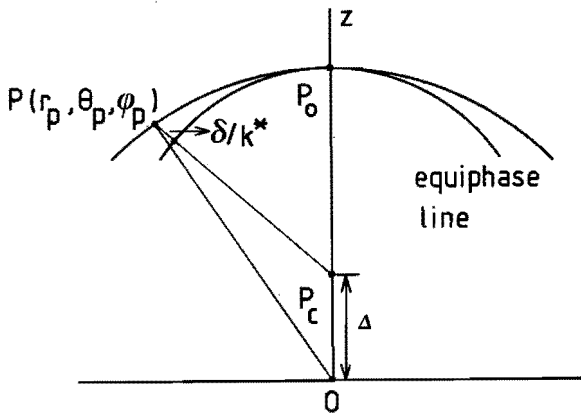


Fig. 4.3. Geometry for the phase centre computation.

Some remarks about the wave-expansion method are now in order. For each occurring pair of integers  $v, n$ , the coefficients  $a_{cv}^{(2n+1)}$ ,  $b_{sv}^{(2n+1)}$ , of the free-space modes, and the Fourier coefficients  $A_{2r+1}^{(2n+1)}$ ,  $B_{2r+1}^{(2n+1)}$ , of the Lamé functions have to be computed. For each observation point arrays of sines, cosines and associated Legendre functions must be calculated to determine the Lamé functions and their derivatives. Next, the summations according to (4.20) and (4.21) must be carried out. Therefore, both core memory usage and computer processing time rapidly become excessive if  $v_{\max}$  is large. Consequently, from the numerical point of view the proposed wave-expansion method is not very suitable for the calculation of the radiation properties of elliptical horns that are long in terms of wavelength. The next section deals with a method which for long horns is more favourable from the computational point of view.

Numerical results based on the wave-expansion method and experimental results for elliptical horns with anisotropic boundary are given in section 4.5.

#### 4.4. Aperture-field integration method for radiation computation

An alternative approach to the calculation of the radiation fields of horn antennas employs an aperture-field integration method. The basic equations have already been presented in section 4.2 where the fields  $\vec{E}(\vec{r}_p)$ ,  $\vec{H}(\vec{r}_p)$ , at an observation point P have been expressed in terms of integrals of the aperture-field vectors  $\vec{E}(\vec{r}_a)$ ,  $\vec{H}(\vec{r}_a)$ , over the aperture surface  $S_a$ . For convenience equations (4.3) and (4.4) are recalled:

$$\vec{E}(\vec{r}_p) = \frac{-jk^*}{4\pi} \iint_{S_a} [\hat{r}_1 x \{\hat{n} x \vec{E}(\vec{r}_a)\} - Z_0 \hat{r}_1 x \{\hat{r}_1 x \{\hat{n} x \vec{H}(\vec{r}_a)\}\}] \frac{1}{r_1} \exp(-jk^* r_1) dS, \quad (4.51)$$

$$Z_0 \vec{H}(\vec{r}_p) = \frac{-jk^*}{4\pi} \iint_{S_a} [Z_0 \hat{r}_1 x \{\hat{n} x \vec{H}(\vec{r}_a)\} + \hat{r}_1 x \{\hat{r}_1 x \{\hat{n} x \vec{E}(\vec{r}_a)\}\}] \frac{1}{r_1} \exp(-jk^* r_1) dS, \quad (4.52)$$

in which  $\vec{r}_1 = \vec{r}_p - \vec{r}_a$ ,  $r_1 = |\vec{r}_1|$ , and  $\hat{r}_1 = \vec{r}_1 / r_1$ .

These expressions will now be simplified to a form convenient for the numerical evaluation of the radiating near-field and the far field of horn antennas. In sections 4.4.1 and 4.4.2 the analysis is carried out for the aperture surface coinciding with a spherical cap and for a planar aperture, respectively. In both cases sampling-like representations for the fields at P will result; compare with [4].

4.4.1. The spherical cap aperture

Consider an elliptical horn of length  $r_a$ , with an opening angle  $\theta_o$  and an aspect ratio  $a_{r\theta}$ ; see Figure 4.4. The geometry of such a horn has been described in section 2.2. The apex of the horn is at the origin of the coordinate system. The aperture surface  $S_a$  is a spherical cap of radius  $r_a$ . The aperture point  $Q$  is described by the position vector  $\vec{r}_a = (x, y, z)$ , where  $(x, y, z)$  are Cartesian coordinates. The  $z$ -coordinate of the point  $Q$  is related to  $r_a, x, y$ , by

$$z = (r_a^2 - x^2 - y^2)^{1/2}. \tag{4.52a}$$

The surface area element  $dS$  of the spherical cap is given by

$$dS = \left\{ 1 + \left( \frac{\partial z}{\partial x} \right)^2 + \left( \frac{\partial z}{\partial y} \right)^2 \right\}^{1/2} dx dy = (r_a/z) dx dy. \tag{4.52b}$$

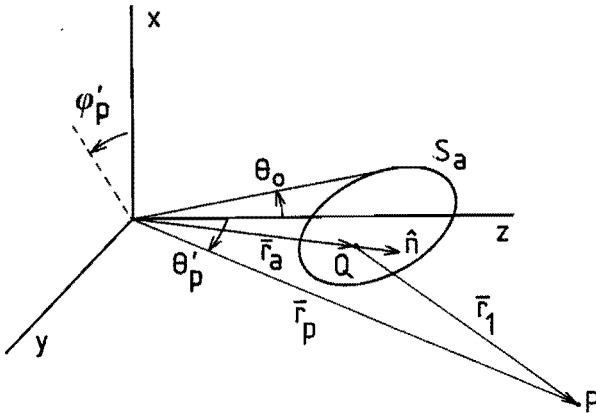


Fig. 4.4. Coordinates for the radiation computation;  $S_a$  is a spherical cap aperture.

The observation point  $P$  has spherical coordinates  $(r_p, \theta'_p, \phi'_p)$  and Cartesian coordinates  $(x_p, y_p, z_p)$ . The unit vector  $\hat{r}_1$  is given by

$$\begin{aligned} \hat{r}_1 &= \bar{r}_1/r_1 = (\bar{r}_p - \bar{r}_a) / |\bar{r}_p - \bar{r}_a| = \\ &= \{(x_p - x)\hat{e}_x + (y_p - y)\hat{e}_y + (z_p - z)\hat{e}_z\} / r_1. \end{aligned} \quad (4.53)$$

The unit vector  $\hat{n}$  at Q, normal to the aperture, equals the unit vector  $\hat{r}_a$ , viz.

$$\hat{n} = \hat{r}_a = (x\hat{e}_x + y\hat{e}_y + z\hat{e}_z) / r_a. \quad (4.54)$$

In the integrands of (4.51) and (4.52) the distance  $r_1$  occurs in the denominator of an amplitude-type expression and in the exponential expression  $\exp(-jk^*r_1)$ . In the denominator,  $r_1$  is approximated by

$$r_{10} = (r_p^2 + r_a^2 - 2r_a z_p)^{1/2}, \quad (4.55)$$

that is the distance from P to the centre of the aperture on the z-axis. In the exponential expression an approximation of  $r_1$  is used that is correct up to quadratic terms in x and y. Such an approximation is obtained by retaining the relevant terms in the expansion of the distance  $r_1 = QP$  in powers of x, y. This distance is

$$r_1 = |\bar{r}_p - \bar{r}_a| = (\bar{r}_p - \bar{r}_a, \bar{r}_p - \bar{r}_a)^{1/2} = \{r_p^2 + r_a^2 - 2(\bar{r}_a, \bar{r}_p)\}^{1/2}. \quad (4.56)$$

On the spherical cap one has, up to quadratic terms in x, y,

$$z \approx r_a - \frac{x^2 + y^2}{2r_a}, \quad \text{if } x^2 + y^2 \ll r_a^2. \quad (4.57)$$

By substitution of (4.57) into (4.56) and by use of (4.55) it is found that

$$r_1 \approx \{r_{10}^2 - 2(xx_p + yy_p - \frac{x^2 + y^2}{2r_a} z_p)\}^{1/2}. \quad (4.58)$$

The latter expression is expanded in powers of x, y, up to second order. Thus we find for  $r_1$  the approximation

$$\tilde{r}_1 = r_{10} - \frac{xx_p + yy_p}{r_{10}} - \frac{xyx_p y_p}{r_{10}^3} + (\frac{z_p}{r_a} - \frac{x^2}{r_{10}^2}) \frac{x^2}{2r_{10}} + (\frac{z_p}{r_a} - \frac{y^2}{r_{10}^2}) \frac{y^2}{2r_{10}}. \quad (4.59)$$

In Table 4.1 some values of the phase error, due to the replacement of  $r_1$  by  $\tilde{r}_1$  in the exponential expression  $\exp(-jk*r_1)$ , are given.

$\theta'_p$	(a)		(b)	
	$\phi'_p = 90^\circ$	$\phi'_p = 270^\circ$	$\phi'_p = 90^\circ$	$\phi'_p = 270^\circ$
$10^\circ$	$0.54^\circ$	$-0.55^\circ$	$-0.96^\circ$	$-2.05^\circ$
$20^\circ$	$0.73^\circ$	$-0.68^\circ$	$-3.92^\circ$	$-5.33^\circ$
$30^\circ$	$0.59^\circ$	$-0.52^\circ$	$-6.74^\circ$	$-7.85^\circ$

Table 4.1. Phase errors (degr.) due to the replacement of  $r_1$  in  $\exp(-jk*r_1)$  by

(a)  $\tilde{r}_1$ , given by (4.59);

(b) the Fresnel small-angle approximation of  $\tilde{r}_1$ , which is obtained by discarding terms with  $x_p y_p$ ,  $x_p^2$  and  $y_p^2$  in (4.59);

$r_p = 0.9m$ ,  $r_a = 0.44m$ ,  $x = 0m$ ,  $y = 0.03m$ , frequency 12 GHz.

Because of the approximation (4.57), the present analysis is restricted to long horn antennas with small flare angle. The aperture fields of such horns satisfy the relation  $Z_o \bar{H}(\bar{r}_a) = \hat{r}_a \times \bar{E}(\bar{r}_a)$ ; see (3.104). Hence, the electric field  $\bar{E}(\bar{r}_p)$  is found by the integration of, for instance,  $\bar{H}(\bar{r}_a)$  over the aperture of the horn according to (4.51). The expressions for the Cartesian components of the electric field at P are derived from (4.51) by carrying out the vector products and by inserting the approximate expressions for  $r_1$ . Thus we find

$$E_x(\bar{r}_p) = \frac{jk*Z_o}{4\pi r_{10}} [r_{10} r_a (I_9 - y_p I_5 + z_p I_4 - I_2) + x_p y_p (I_1 - I_7) + x_p z_p (I_6 - I_8) + x_p (I_{16} - I_{18}) + y_p (I_{11} - I_{17} + 2I_{13} - 2I_{21}) + z_p (2I_{22} - 2I_{24} - I_{10} + I_{14}) + (r_a^2 + y_p^2 + z_p^2) (I_2 - I_9)],$$

(4.60)

$$E_Y(\vec{r}_p) = \frac{jk^*z_o}{4\pi r_{10}^3} [r_{10} r_a (I_1 - z_p I_3 + x_p I_5 - I_7) + y_p z_p (I_6 - I_8) + x_p y_p (I_9 - I_2) + y_p (I_{20} - I_{16}) + z_p (I_{12} - I_{15} + 2I_{23} - 2I_{19}) + x_p (2I_{17} - 2I_{11} - I_{13} + I_{21}) + (r_a^2 + x_p^2 + z_p^2) (I_7 - I_1)], \quad (4.61)$$

$$E_Z(\vec{r}_p) = \frac{jk^*z_o}{4\pi r_{10}^3} [r_{10} r_a (I_6 - x_p I_4 + y_p I_3 - I_8) + x_p z_p (I_9 - I_2) + y_p z_p (I_1 - I_7) + z_p (I_{18} - I_{20}) + x_p (I_{24} - I_{22} + 2I_{10} - 2I_{14}) + y_p (2I_{15} - 2I_{12} - I_{23} + I_{19}) + (r_a^2 + x_p^2 + y_p^2) (I_8 - I_6)]. \quad (4.62)$$

Here,

$$I_i = \iint_{S_{xy}} h_i(x,y) \exp(-jk^* \tilde{r}_i) dx dy, \quad i = 1, 2, \dots, 24, \quad (4.63)$$

in which the integration domain  $S_{xy}$  is described by

$$\frac{x^2}{r_a^2 \sin^2 \theta_o} + \frac{y^2}{r_a^2 (1 - k^2 \cos^2 \theta_o)} \leq 1, \quad (4.64)$$

as follows from (2.24a) with  $r_o$  replaced by  $r_a$ . The parameter  $k$  is found from (2.24). The semi-axes of the elliptical domain  $S_{xy}$  are  $b_\theta^* = r_a \sin \theta_o$  and  $a_\theta = r_a (1 - k^2 \cos^2 \theta_o)^{1/2}$ .

The expressions for  $h_i(x,y)$  in terms of the coordinates  $x, y, z$ , and the Cartesian components of  $\vec{H}(\vec{r}_a)$  are listed in Appendix 4.6.2. Note that  $z$  is determined by (4.52a).

The evaluation of the integrals (4.63) is now discussed. The integration variables  $\xi = x/b_\theta^*$  and  $\eta = y/a_\theta$  are introduced. Furthermore, it is assumed that the Fresnel small-angle (FSA) approximation can be applied [7]. This means that in (4.59) terms with  $x_p y_p$ ,  $x_p^2$  and  $y_p^2$  are neglected. Common to these terms is that they are proportional to  $\sin^2 \theta_p$ .

In Table 4.1 some values of the phase error, due to the replacement of  $r_1$  in  $\exp(-jk^* r_1)$  by the FSA approximation of  $\tilde{r}_1$ , are given.

Now  $I_i$  can be recast in the form

$$I_i = c_o \int_{-1}^1 \int_{-1}^1 h_i(b_\theta^* \xi, a_\theta \eta) \exp\{j(\alpha_1 \xi + \alpha_2 \eta - \beta_1 \frac{\xi^2}{2} - \beta_2 \frac{\eta^2}{2})\} d\xi d\eta, \quad i = 1, 2, \dots, 24, \quad (4.65)$$

where

$$c_o = b_\theta^* a_\theta \exp(-jk^* r_{10}), \quad (4.66)$$

$$\alpha_1 = k^* b_\theta^* x_p / r_{10}, \quad \alpha_2 = k^* a_\theta y_p / r_{10}, \quad (4.67)$$

$$\beta_1 = k^* b_\theta^{*2} z_p / (r_a r_{10}), \quad \beta_2 = k^* a_\theta^2 z_p / (r_a r_{10}), \quad (4.68)$$

if  $\xi^2 + \eta^2 > 1$  then  $h_i(b_\theta^* \xi, a_\theta \eta) \equiv 0$ , else as defined in Appendix 4.6.2. (4.69)

Introduce the inner product

$$\langle f, g \rangle = \int_{-1}^1 \int_{-1}^1 F^* g \, d\xi d\eta, \quad (4.70)$$

where the asterisk means complex conjugation, then (4.65) can be expressed as

$$I_i = c_o \langle h_i^*, \exp\{j(\alpha_1 \xi + \alpha_2 \eta - \beta_1 \frac{\xi^2}{2} - \beta_2 \frac{\eta^2}{2})\} \rangle, \quad i = 1, 2, \dots, 24. \quad (4.71)$$

Furthermore, the basis functions

$$f_{mn}(\xi, \eta) = \frac{1}{2} \exp\{j(m\pi\xi + n\pi\eta)\}, \quad m, n = 0, \pm 1, \pm 2, \dots, \quad (4.72)$$

are introduced, which are orthonormal on the square  $-1 \leq \xi \leq 1$ ,  $-1 \leq \eta \leq 1$ . By expansion of  $h_i$  in terms of  $f_{mn}$  it is found that  $I_i$  can be written as

$$I_i = c_o \sum_{m=-\infty}^{\infty} \sum_{n=-\infty}^{\infty} H_i(m\pi, n\pi) \psi_{mn}(\alpha_1, \beta_1, \alpha_2, \beta_2), \quad i = 1, 2, \dots, 24, \quad (4.73)$$

in which

$$\begin{aligned}
 H_i(m\pi, n\pi) &= 2 \langle h_i^*, f_{mn} \rangle = \\
 &= \int_{-1}^1 \int_{-1}^1 h_i(b_\theta^* \xi, a_\theta \eta) \exp\{j(m\pi\xi + n\pi\eta)\} d\xi d\eta, \quad (4.74)
 \end{aligned}$$

and

$$\begin{aligned}
 \psi_{mn}(\alpha_1, \beta_1, \alpha_2, \beta_2) &= \frac{1}{2} \langle f_{mn}, \exp\{j(\alpha_1 \xi + \alpha_2 \eta - \beta_1 \frac{\xi^2}{2} - \beta_2 \frac{\eta^2}{2})\} \rangle = \\
 &= \left[ \frac{1}{2} \int_{-1}^1 \exp\{j(\alpha_1' \xi - \beta_1 \frac{\xi^2}{2})\} d\xi \right] \left[ \frac{1}{2} \int_{-1}^1 \exp\{j(\alpha_2' \eta - \beta_2 \frac{\eta^2}{2})\} d\eta \right] = \\
 &= \left[ \frac{1}{2} \Phi(\alpha_1', \beta_1) \right] \left[ \frac{1}{2} \Phi(\alpha_2', \beta_2) \right], \quad (4.75)
 \end{aligned}$$

with

$$\alpha_1' = \alpha_1 - m\pi, \quad \alpha_2' = \alpha_2 - n\pi, \quad (4.76)$$

$$\Phi(\alpha, \beta) = \int_{-1}^1 \exp\{j(\alpha\xi - \beta \frac{\xi^2}{2})\} d\xi. \quad (4.77)$$

The coefficients  $H_i(m\pi, n\pi)$  are the two-dimensional Fourier coefficients of the functions  $h_i(b_\theta^* \xi, a_\theta \eta)$ . These coefficients are calculated from samples of  $h_i$  by use of the Fast Fourier Transform (FFT) technique [3a]. The coefficients  $H_i(m\pi, n\pi)$  only depend on the aperture field and the geometry of the elliptical horn; they are independent of the coordinates of the observation point P. The functions  $\psi_{mn}$ , however, are independent of the aperture field; they only depend on the coordinates of P and the geometry of the horn antenna.

Some properties of  $\Phi(\alpha, \beta)$  and its representation in terms of Fresnel integrals are given in Appendix 4.6.3. The numerical computation of the Fresnel integrals has been based on the algorithm given in [3].

The foregoing analysis leads to the following procedure for the determination of the radiation field of a long horn antenna with small flare angle:

1. Specify the horn parameters  $r_a$ ,  $\theta_0$ ,  $a_{r\theta}$ , and compute  $k$ ,  $b_\theta^*$ ,  $a_\theta$ ; see (2.24), (2.25).

2. Specify the hybrid mode. The corresponding modal field can be computed by means of the method described in section 3.3.
3. Choose discrete sample points  $(\xi, \eta)$  and determine the Cartesian, spherical and sphero-conal coordinates of these points; see the end of section 2.2. Next determine the samples of  $h_i$  from the modal field.
4. Compute the Fourier coefficients  $H_i(m\pi, n\pi)$  of  $h_i$  by use of FFT.
5. Specify the observation point P, and calculate  $\psi_{mn}$  and  $I_i$ .
6. Determine the electric field components at P.
7. Repeat steps 5 and 6 for other observation points and determine the radiation properties of the horn antenna.

In order to compare the computed and the measured results, extra transformations of the computed electric field components are necessary if the coordinate systems for the computations and for the measurements do not coincide. The observation angles and distances, especially in the radiating near-field region of the horn, are sensitive to a displacement of the origin, as can be seen in Figure 4.4a. These transformations are however simple and will not be presented in detail.

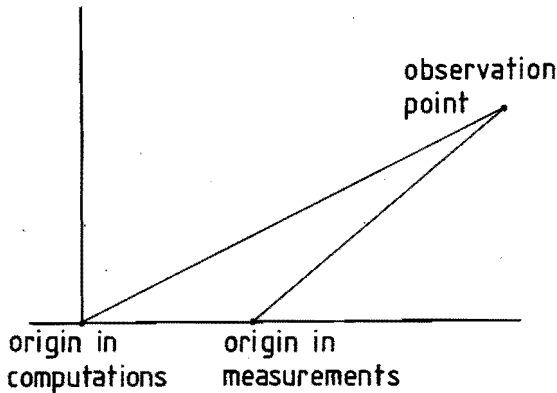


Fig. 4.4a. Displacement of the origin for the coordinate systems used in the computations and in the measurements.

The computation of a large number of integrals is necessary if the method described above is employed. Each of these integrals, however, can easily be evaluated. Fewer integrals have to be calculated if the aperture of the horn is a planar surface, as will be shown in the next section.

#### 4.4.2. The planar aperture

Consider again the elliptical horn with an opening angle  $\theta_0$  and an aspect ratio  $a/r_0$ . The aperture surface  $S_a$  of the horn is now a planar surface perpendicular to the z-axis at  $z = z_a$ ; see Figure 4.5.

To simplify (4.51) and (4.52) to a form convenient for numerical evaluation, we proceed along the same lines as in the previous section.

The aperture point Q is given by the position vector  $\vec{r}_a = (x, y, z_a)$ . The vector  $\hat{n}$ , normal to  $S_a$ , equals the unit vector in the z-direction. The surface area element of  $S_a$  is given by  $dS = dx dy$ . The observation point P has spherical coordinates  $(r_p, \theta'_p, \phi'_p)$  and Cartesian coordinates  $(x_p, y_p, z_p)$ .

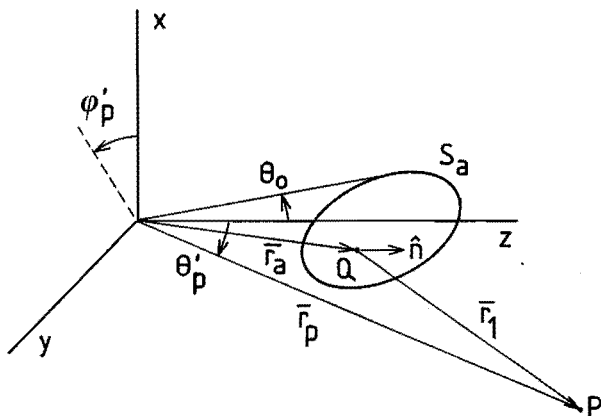


Fig. 4.5. Coordinates for the radiation computation;  $S_a$  is a planar aperture.

The unit vector  $\hat{r}_1$  is given by

$$\begin{aligned} \hat{r}_1 &= \vec{r}_1/r_1 = (\vec{r}_p - \vec{r}_a)/|\vec{r}_p - \vec{r}_a| = \\ &= \{(x_p - x)\hat{e}_x + (y_p - y)\hat{e}_y + (z_p - z_a)\hat{e}_z\}/r_1. \end{aligned} \quad (4.78)$$

In the denominator of amplitude-type expressions, as occurring in the integrands of (4.51) and (4.52),  $r_1$  is approximated by

$$r_{10} = (r_p^2 + z_a^2 - 2z_p z_a)^{1/2}, \quad (4.79)$$

that is the distance from P to the centre of the aperture on the z-axis. In the exponential expression  $\exp(-jk^*r_1)$  an approximation of  $r_1$  is used that is correct up to quadratic terms in x and y. This approximation is obtained by retaining the relevant terms in the expansion of  $r_1$  in powers of x,y. By use of (4.79) it is found that

$$\begin{aligned}
 r_1 &= |\bar{r}_p - \bar{r}_a| = (\bar{r}_p - \bar{r}_a, \bar{r}_p - \bar{r}_a)^{\frac{1}{2}} = \\
 &= \{r_p^2 + z_a^2 - 2z_p z_a - 2(xx_p + yy_p) + x^2 + y^2\}^{\frac{1}{2}} = \\
 &= \{r_{10}^2 - 2(xx_p + yy_p) + x^2 + y^2\}^{\frac{1}{2}}. \tag{4.80}
 \end{aligned}$$

By expansion of (4.80) in powers of x,y, up to second order, we find for  $r_1$  the approximation

$$\tilde{r}_1 = r_{10} - \frac{xx_p + yy_p}{r_{10}} - \frac{xyx_p y_p}{r_{10}^3} + \left(1 - \frac{x_p^2}{r_{10}^2}\right) \frac{x^2}{2r_{10}} + \left(1 - \frac{y_p^2}{r_{10}^2}\right) \frac{y^2}{2r_{10}}. \tag{4.81}$$

Note that  $\tilde{r}_1$  has been derived without the assumption  $x^2 + y^2 \ll r_a^2$  as in (4.57). Hence, the present analysis is not restricted to long horn antennas with small flare angle, in contrast with the analysis in section 4.4.1.

In Table 4.2 some values of the phase error, due to the replacement of  $r_1$  by  $\tilde{r}_1$  in the exponential expression  $\exp(-jk^*r_1)$ , are given.

$\theta'_p$	(a)		(b)	
	$\phi'_p = 90^\circ$	$\phi'_p = 270^\circ$	$\phi'_p = 90^\circ$	$\phi'_p = 270^\circ$
$10^\circ$	$0.25^\circ$	$-0.26^\circ$	$-1.25^\circ$	$-1.76^\circ$
$20^\circ$	$0.29^\circ$	$-0.28^\circ$	$-4.36^\circ$	$-4.93^\circ$
$30^\circ$	$0.18^\circ$	$-0.17^\circ$	$-7.14^\circ$	$-7.50^\circ$

Table 4.2. Phase errors(degr.) due to the replacement of  $r_1$  in  $\exp(-jk^*r_1)$  by

(a)  $\tilde{r}_1$ , given by (4.81);

(b) the Fresnel small-angle approximation of  $\tilde{r}_1$ , which is obtained by discarding terms with  $x_p y_p$ ,  $x_p^2$  and  $y_p^2$  in (4.81);

$r_p = 0.9m$ ,  $z_a = 0.44m$ ,  $x = 0m$ ,  $y = 0.03m$ , frequency 12 GHz.

The Cartesian components of  $\bar{E}(\bar{r}_p)$  are again derived from (4.51) by carrying out the vector products and by inserting the approximate expressions for  $r_1$ . We now arrive at

$$E_x(\bar{r}_p) = \frac{jk^*}{4\pi r_{10}^3} [r_{10}(z_p - z_a)K_1 - x_p K_8 - y_p(K_7 + 2K_{10}) + x_p y_p K_5 + \\ + \{y_p^2 + (z_p - z_a)^2\}K_6 + K_{12} + K_{13}] , \quad (4.82)$$

$$E_y(\bar{r}_p) = \frac{jk^*}{4\pi r_{10}^3} [r_{10}(z_p - z_a)K_2 + x_p(2K_7 + K_{10}) + y_p K_9 - x_p y_p K_6 - \\ - \{x_p^2 + (z_p - z_a)^2\}K_5 - K_{11} - K_{14}] , \quad (4.83)$$

$$E_z(\bar{r}_p) = \frac{jk^*}{4\pi r_{10}^3} [r_{10}(K_3 + K_4 - x_p K_1 - y_p K_2) + (z_p - z_a)(-x_p K_6 + y_p K_5 - K_8 + K_9)] , \quad (4.84)$$

where

$$K_i = \iint_{S_{xy}} g_i(x, y) \exp(-jk^* \tilde{r}_1) dx dy, \quad i = 1, 2, \dots, 14. \quad (4.85)$$

The expressions for  $g_i(x, y)$  in terms of the coordinates  $x, y$ , and the Cartesian components of the aperture fields, are listed in Appendix 4.6.4.

The integration domain  $S_{xy}$  is described by

$$\frac{x^2}{z_a^2 \tan^2 \theta_0} + \frac{y^2}{z_a^2 (k^{-2} \sec^2 \theta_0 - 1)} \leq 1, \quad (4.86)$$

found from (2.19a) with  $z_1$  replaced by  $z_a$ . The semi-axes of this elliptical domain are  $b_\theta = |z_a \tan \theta_0|$  and  $a_\theta = |z_a (1 - k^2 \cos^2 \theta_0)^{1/2} / (k \cos \theta_0)|$ .

The evaluation of  $K_i$  is analogous to that of  $I_i$ , discussed in the previous section. The integration variables  $\xi = x/b_\theta$  and  $\eta = y/a_\theta$  are introduced. For convenience it is again assumed that the Fresnel small-angle (FSA) approximation can be applied. This means that in (4.81) terms with  $x_p y_p$ ,  $x_p^2$  and

$y_p^2$  are neglected. In Table 4.2 some values of the phase error, due to the replacement of  $r_1$  in  $\exp(-jk^*r_1)$  by the FSA approximation of  $\tilde{r}_1$ , are given.

The integral  $K_i$  can be converted into the series representation

$$K_i = c_1 \sum_{m=-\infty}^{\infty} \sum_{n=-\infty}^{\infty} G_i(m\pi, n\pi) \psi_{mn}(\alpha_3, \beta_3, \alpha_4, \beta_4), \quad i = 1, 2, \dots, 14, \quad (4.87)$$

where

$$G_i(m\pi, n\pi) = \int_{-1}^1 \int_{-1}^1 g_i(b_\theta \xi, a_\theta \eta) \exp\{j(m\pi\xi + n\pi\eta)\} d\xi d\eta, \quad (4.88)$$

$$\psi_{mn}(\alpha_3, \beta_3, \alpha_4, \beta_4) = \frac{1}{4} \phi(\alpha_3 - m\pi, \beta_3) \phi(\alpha_4 - n\pi, \beta_4), \text{ with } \phi \text{ given by (4.77), (4.88a)}$$

$$c_1 = b_\theta a_\theta \exp(-jk^*r_{10}), \quad (4.89)$$

$$\alpha_3 = k^* b_\theta x_p / r_{10}, \quad \alpha_4 = k^* a_\theta y_p / r_{10}, \quad (4.90)$$

$$\beta_3 = k^* b_\theta^2 / r_{10}, \quad \beta_4 = k^* a_\theta^2 / r_{10}, \quad (4.91)$$

if  $\xi^2 + \eta^2 > 1$  then  $g_i(b_\theta \xi, a_\theta \eta) \equiv 0$ , else as defined in Appendix 4.6.4. (4.92)

The coefficients  $G_i(m\pi, n\pi)$  are the two-dimensional Fourier coefficients of the functions  $g_i(b_\theta \xi, a_\theta \eta)$ . These coefficients are calculated from samples of  $g_i$  by use of the FFT technique.

It is pointed out that the coefficients  $G_i(m\pi, n\pi)$  are only dependent on the aperture fields and the geometry of the horn antenna, whereas the functions  $\psi_{mn}$  are only dependent on the coordinates of the observation point and on the horn geometry.

The stepwise procedure presented in the previous section for finding the radiation field of an elliptical horn antenna here also applies.

Extra transformations and computations may again be necessary in order to compare the computed and the measured results, as has been outlined at the end of section 4.4.1.

Comparing the methods developed in sections 4.4.1 and 4.4.2, we conclude that in the case of the planar aperture less integrals have to be computed and that the phase errors introduced are about the same.

#### 4.5. Numerical and experimental results

The numerical evaluation of the radiation fields of some elliptical horn antennas has been carried out by means of a digital computer. Results based on the sphero-conal wave-expansion method of section 4.3 and the aperture-field integration method of section 4.4.2 will be discussed.

Three different horn antennas are dealt with. For future reference they are labeled A,B,C. The main parameters of these antennas are summarized in Table 4.3.

Antenna	Length (m)	$\theta_o$ (degr.)	$a_{r\theta}$
A	0.05	$30^\circ$	1/3
B	0.33	$3.37^\circ$	1/3
C	0.44	$3.37^\circ$	1/3

Table 4.3. Main parameters of the elliptical horn antennas A,B,C.

Antenna A is considered first. It is assumed that the odd symmetric  $HE_{11}$  mode, denoted by  $HE_{o11}$ , is incident. The mode-number  $\nu'$  is determined by use of the method described in section 3.3. It is found that  $\nu' = 3.2743$ . The radiation properties are determined by use of the wave-expansion method described in section 4.3. The frequency is taken to be 12 GHz. The expansion coefficients  $a_{cv}^{(2n+1)}$  and  $b_{sv}^{(2n+1)}$ , where  $\nu = 1, 2, \dots, 13 = \nu_{max}$ ,  $n = 0, 1, 2, \dots, [(\nu-1)/2]$ , are calculated by means of (4.39) and (4.40), respectively. Next the radiation properties are determined from the electric field as given by (4.20). The computed results are shown in the Figures 4.6.1-4.6.7. The values of  $r_p$  (the distance from the observation point to the apex of the horn) are 0.15m, 0.3m, 0.6m, 1.2m, and the associated curves are labeled a,b,c,d, respectively. The spherical angle with the positive z-axis (the forward direction of the antenna) is displayed along the horizontal axis of the plots.

The radiation patterns in the  $xz$ -plane (Figure 4.6.1) broaden gradually for increasing  $r_p$ . The phase diagrams in the  $xz$ -plane (Figure 4.6.3) show that the phase decreases for increasing angle with the horn axis, indicating that the phase centres in the  $xz$ -plane (Figure 4.6.5) are not located at the apex of the horn.

The radiation patterns in the  $yz$ -plane (Figure 4.6.2) are nearly independent of  $r_p$  over a large angular range. The phase diagrams in the  $yz$ -plane (Figure 4.6.4) show that the phase is almost constant over a large angular range which means that the phase centres in the  $yz$ -plane (Figure 4.6.6) are located in the immediate vicinity of the apex of the horn. Note that the phase centres in the  $xz$ - and the  $yz$ -planes do not coincide. The ratio of the -3 dB beamwidths in the  $xz$ - and the  $yz$ -planes increases for increasing  $r_p$ . Numerical values are 1:1.59, 1:1.35, 1:1.24, 1:1.19, for the cases a,b,c,d, respectively. The beamwidths of the patterns in the  $xz$ -plane (the minor axis of the horn is in this plane) are smaller than those in the  $yz$ -plane.

The relative power contributions (percentage of the power  $P_a$ ) of the free-space modes to the total radiated power are plotted as a function of the mode-number  $v$  in Figure 4.6.7. For given integer  $v$  the contributions of the free-space modes with  $n = 0, 1, 2, \dots, [(v-1)/2]$ , to the total radiated power are taken together. From this plot it is readily seen that the free-space modes with  $v \gtrsim v_{\max} = 13$  hardly contribute.

The computed values of the on-axis gain are 14.67 dB, 14.19 dB, 13.92 dB, 13.79 dB, for the cases a,b,c,d, respectively.

Some computed results for antenna B are now discussed. As in the case of antenna A the  $HE_{11}$  mode is assumed to be incident and the frequency is taken to be 12 GHz. The mode-number is  $v' = 29.5328$ . The numerical results obtained by the sphero-conal wave-expansion method are shown in Figures 4.7.1 - 4.7.3. The values of  $r_p$  are 0.625m, 0.74m, 1.25m, 2.5m, and the associated curves are labeled a,b,c,d, respectively.

The radiation patterns in the  $xz$ -plane (Figure 4.7.1) and in the  $yz$ -plane (Figure 4.7.2) broaden for increasing  $r_p$ . The ratios of the -3 dB beamwidths in the  $xz$ - and the  $yz$ -planes are 1.98:1, 2.06:1, 2.15:1, 2.21:1, for the cases a,b,c,d, respectively. The ratio of the beamwidths increases for increasing  $r_p$ . Note that now the broadest patterns are found in the plane of the minor axis of the horn antenna ( $xz$ -plane).

From the far-field phase pattern at  $r_p = 2.5\text{m}$  (which has not been plotted), it is found that the corresponding phase centre in the  $xz$ -plane is located inside the horn slightly behind the aperture of the antenna. The phase centre in the  $yz$ -plane is located inside the horn, approximately  $0.8 \lambda_0$  behind the aperture.

The relative power contributions of the free-space modes to the total radiated power of antenna B are plotted as a function of  $\nu$  in Figure 4.7.3. For given integer  $\nu$  the contributions of the free-space modes with  $n = 0, 1, 2, \dots, [(\nu-1)/2]$  are again taken together. In this example  $\nu_{\max} = 84$ , and from Figure 4.7.3 it is concluded that the summation over  $\nu$  can indeed be truncated at this value of  $\nu_{\max}$ . The computed values of the on-axis gain are 22.53 dB, 21.34 dB, 19.09 dB, 17.75 dB, for the case a,b,c,d, respectively.

Finally, numerical and experimental results for antenna C are presented. For the computations it is assumed that the  ${}_{\circ}HE_{11}$  mode is incident. The mode-number  $\nu'$  is again determined by use of the method of section 3.3 which utilizes the anisotropic surface-impedance model for the corrugated boundary. As in the case of the  ${}_{\circ}HE_{11}$  mode in antenna B the mode-number is  $\nu' = 29.5328$ .

The aperture surface of antenna C is a planar surface. The computed radiation fields of antenna C are obtained by use of the aperture-field integration method of section 4.4.2 and by use of the wave-expansion method of section 4.3. The wave-expansion method is used despite the fact that the horn has a planar aperture. Because of the large horn length and the small flare angle the deviation of the spherical cap aperture from the planar aperture is small. The measured radiation patterns of the antenna excited by the odd symmetric  ${}_{\circ}HE_{11}$  and the even symmetric  ${}_{\circ}e_{11}^{HE}$  modes have been recorded in an indoor test facility. In far-field measurements a standard gain horn is used as the transmitting antenna, whereas the horn under test is used as the receiving antenna. In near-field measurements a dielectric loaded P-band receiving probe is applied and the horn is used as the transmitting antenna. By rotating the horn, radiation patterns are recorded as a function of the spherical angle with the horn axis. The centre of rotation coincides with either the apex of the horn or the phase centre in the plane of measurement. Some results are shown in Figures 4.8.1 - 4.8.6. Experimental results for antenna C have been published before by Vokurka [17].

In Figures 4.8.1 - 4.8.3 experimental and computed results for the radiating near-field region are plotted. The distance between the observation points and the apex of the horn is constant, viz.  $r_p = 0.94\text{m}$ . The computed value of the on-axis gain at 12 GHz is 23.7 dB.

In Figures 4.8.4 - 4.8.6 the results of far-field measurements and computations are shown. Now the distance between the observation points and the appropriate phase centres on the z-axis is constant, namely 2.5m. The computed value of the on-axis gain at 12 GHz is now 20.4 dB.

The locations of the phase centres differ for the radiating near-field and far-field situations. In the former case the positions are 0.19m and 0.01m from the aperture centre (inside the horn), in the yz-plane and the xz-plane, respectively; for the odd (even) symmetric mode the yz-plane coincides with the  $E^o(H^e)$  plane, and the xz-plane coincides with the  $H^o(E^e)$  plane. In the far-field situation the respective positions of the phase centres are 0.056m and 0.012m from the aperture centre (inside the horn). The positions mentioned follow from experiments at 12 GHz.

From Figures 4.8.1 - 4.8.6 the following conclusions are drawn.

1. The computed results, obtained from the wave-expansion method and the aperture-field integration method, and the measured results agree to a large extent in the radiating near-field region as well as in the far-field region. Hence, both numerical methods are suitable for the calculation of the near-field and far-field radiation patterns of the antenna under consideration.
2. The measured radiation patterns of the odd and even hybrid modes are almost equal in a large angular region at all frequencies considered. These results, valid in both the near-field and the far-field regions, are in agreement with the theoretical results of section 4.2, which have been derived by use of the properties of the hybrid modes given in section 3.3.
3. The concept of phase centre is feasible only for small angular regions around the beam axis as can be seen from the phase diagrams. However, the locations of the phase centres differ if the planes of measurement are different. Consequently, phase errors will be inevitable if this type of horn is used for the illumination of a parabolic reflector antenna.

At the end of section 4.3 it has been indicated that for long horns the wave-expansion method is not very suitable from the computational point of view. Comparison of core memory usage and computer processing times for the two numerical methods employed, shows indeed that the wave-expansion method is at a disadvantage by approximately a factor 5.

Finally, our overall conclusion is that the results obtained so far, inspire confidence in the method for the investigation of the wave propagation in corrugated elliptical cones (section 3.3), in the methods for the computation of the radiation fields of corrugated elliptical horns (chapter 4), and in the assumptions which underlie these methods.

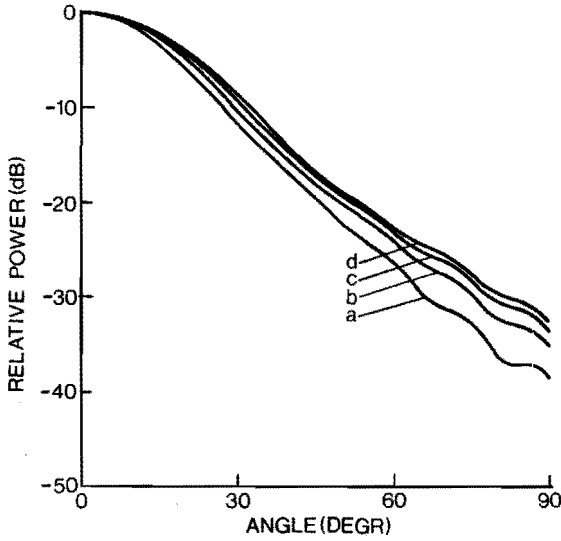


Fig. 4.6.1. Computed radiation patterns in the xz-plane for antenna A excited by the  ${}_{\circ}HE_{11}$  mode; frequency 12 GHz; (a)  $r_p = 0.15$  m; (b)  $r_p = 0.3$  m; (c)  $r_p = 0.6$  m; (d)  $r_p = 1.2$  m; (wave-expansion method).

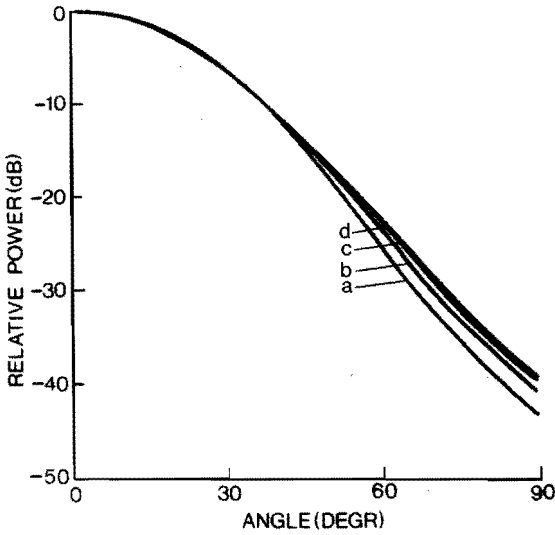


Fig. 4.6.2. Computed radiation patterns in the yz-plane for antenna A excited by the  ${}_{\circ}HE_{11}$  mode; frequency 12 GHz; (a)  $r_p = 0.15$  m; (b)  $r_p = 0.3$  m; (c)  $r_p = 0.6$  m; (d)  $r_p = 1.2$  m; (wave-expansion method).

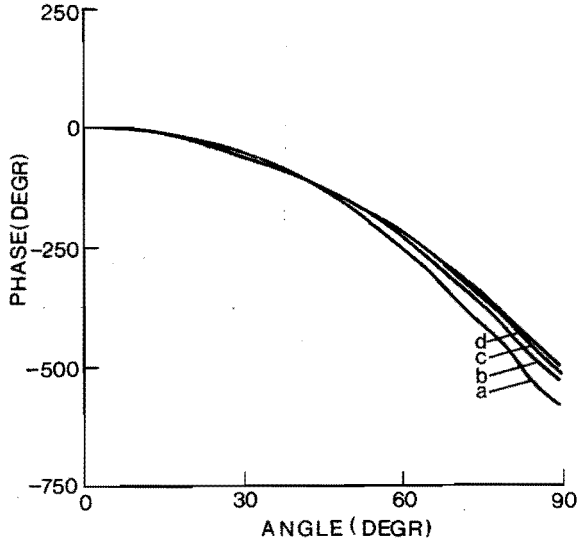


Fig. 4.6.3. Computed phase patterns in the xz-plane for antenna A excited by the  ${}_{\circ}HE_{11}$  mode; frequency 12 GHz; (a)  $r_p = 0.15$  m; (b)  $r_p = 0.3$  m; (c)  $r_p = 0.6$  m; (d)  $r_p = 1.2$  m; (wave-expansion method).

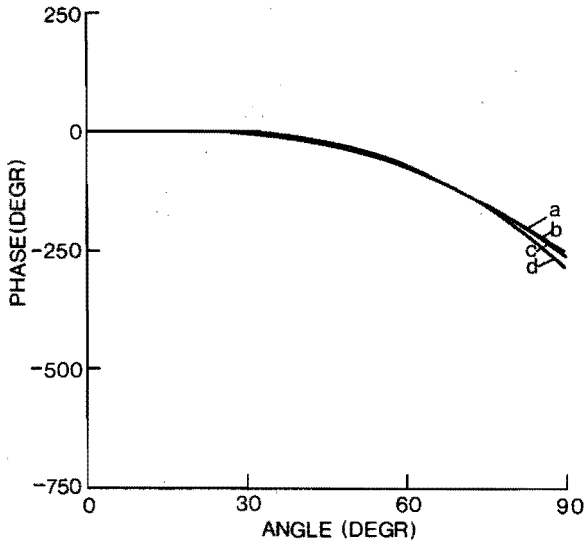


Fig. 4.6.4. Computed phase patterns in the yz-plane for antenna A excited by the  ${}_{\circ}HE_{11}$  mode; frequency 12 GHz; (a)  $r_p = 0.15$  m; (b)  $r_p = 0.3$  m; (c)  $r_p = 0.6$  m; (d)  $r_p = 1.2$  m; (wave-expansion method).

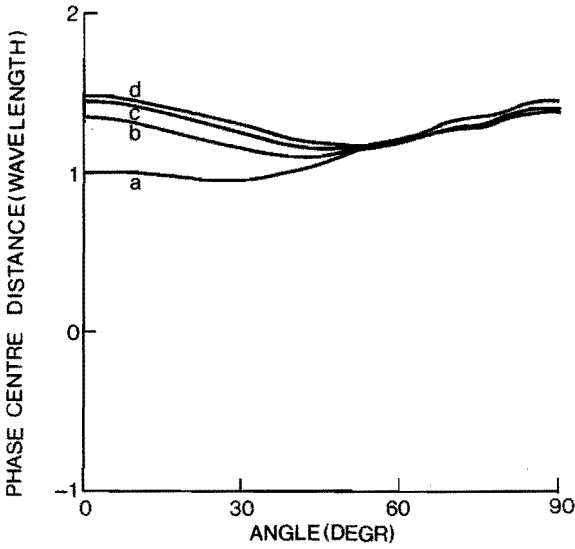


Fig. 4.6.5. Distance to the apex, of the phase centre in the xz-plane for Antenna A excited by the  ${}_{\circ}HE_{11}$  mode; frequency 12 GHz; (a)  $r_p = 0.15$  m; (b)  $r_p = 0.3$  m; (c)  $r_p = 0.6$  m; (d)  $r_p = 1.2$  m; (wave-expansion method).

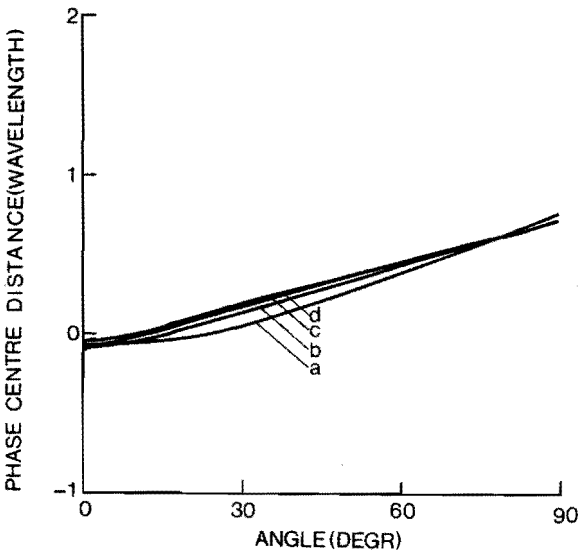


Fig. 4.6.6. Distance to the apex, of the phase centre in the yz-plane for Antenna A excited by the  ${}_{\circ}HE_{11}$  mode; frequency 12 GHz; (a)  $r_p = 0.15$  m; (b)  $r_p = 0.3$  m; (c)  $r_p = 0.6$  m; (d)  $r_p = 1.2$  m; (wave-expansion method).

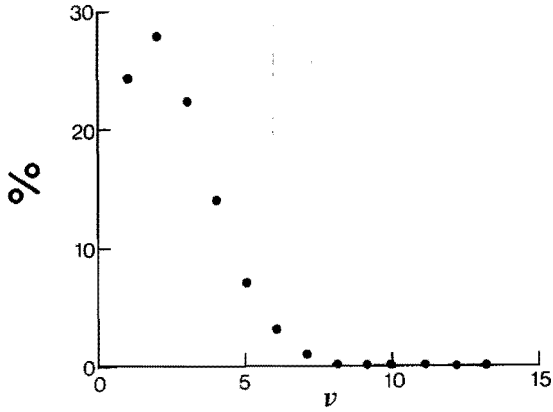


Fig. 4.6.7. Relative power contribution of the expansion modes to the total radiated power of antenna A excited by the  ${}_{0}^{HE}_{11}$  mode; frequency 12 GHz;  $1 \leq \nu \leq \nu_{\max} = 13$ . For given  $\nu$  the contributions of the expansion modes with  $n = 0, 1, 2, \dots, [(\nu-1)/2]$ , are taken together.

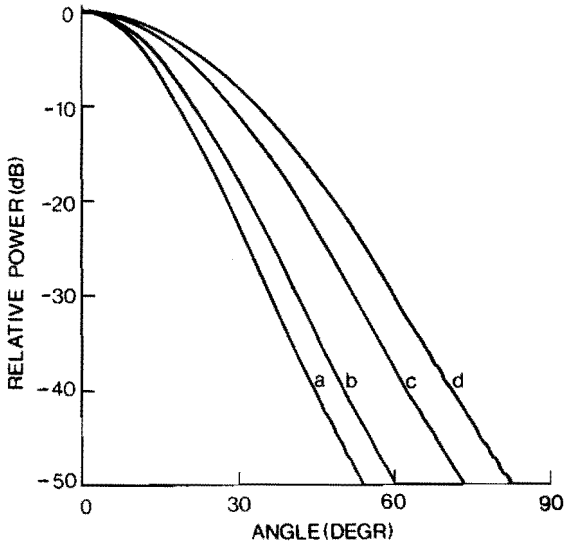


Fig. 4.7.1. Computed radiation patterns in the xz-plane for antenna B excited by the  ${}_{\circ}HE_{11}$  mode; frequency 12 GHz; (a)  $r_p = 0.625$  m; (b)  $r_p = 0.74$  m; (c)  $r_p = 1.25$  m; (d)  $r_p = 2.5$  m; (wave-expansion method).

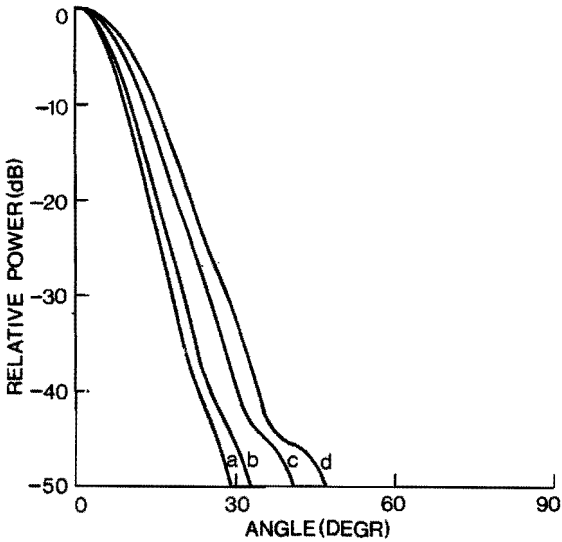


Fig. 4.7.2. Computed radiation patterns in the yz-plane for antenna B excited by the  ${}_{\circ}HE_{11}$  mode; frequency 12 GHz; (a)  $r_p = 0.625$  m; (b)  $r_p = 0.74$  m; (c)  $r_p = 1.25$  m; (d)  $r_p = 2.5$  m; (wave-expansion method).

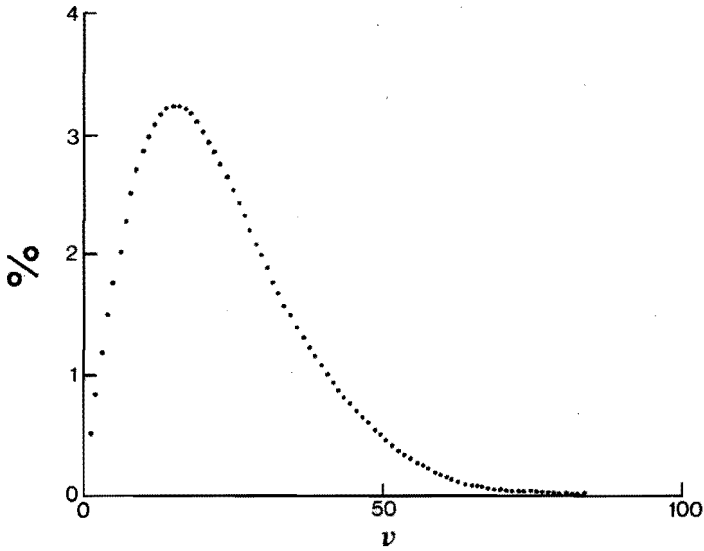


Fig. 4.7.3. Relative power contribution of the expansion modes to the total radiated power of antenna B excited by the  ${}_{\circ}HE_{11}$  mode; frequency 12 GHz;  $1 \leq \nu \leq \nu_{\max} = 84$ . For given  $\nu$  the contributions of the expansion modes with  $n = 0, 1, 2, \dots, [(\nu-1)/2]$ , are taken together.

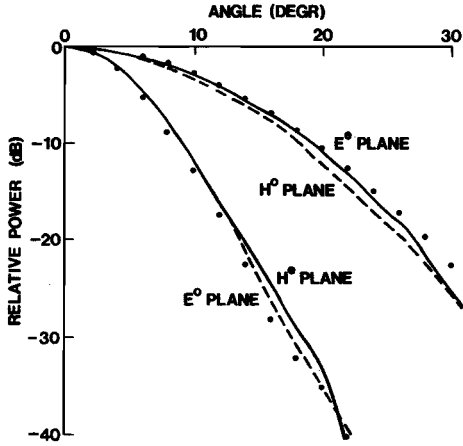


Fig. 4.8.1. Radiating near-field patterns for antenna C;

frequency 10.25 GHz;  $r_p = 0.94$  m;

- .... computed,  ${}_{\circ}HE_{11}$  mode, aperture-field integration method;
- measured,  ${}_{\circ}HE_{11}$  mode;
- measured,  ${}_{e}HE_{11}$  mode.

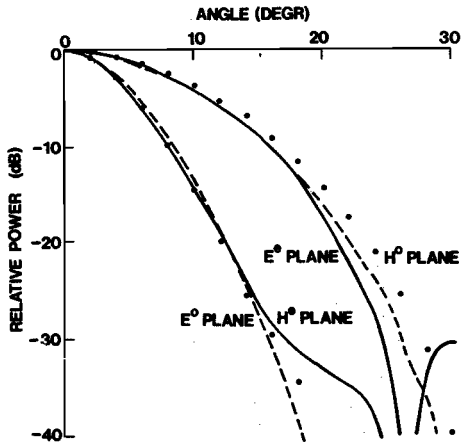


Fig. 4.8.2. Radiating near-field patterns for antenna C;

frequency 11.75 GHz;  $r_p = 0.94$  m;

- .... computed,  ${}_{\circ}HE_{11}$  mode, aperture-field integration method;
- measured,  ${}_{\circ}HE_{11}$  mode;
- measured,  ${}_{e}HE_{11}$  mode.

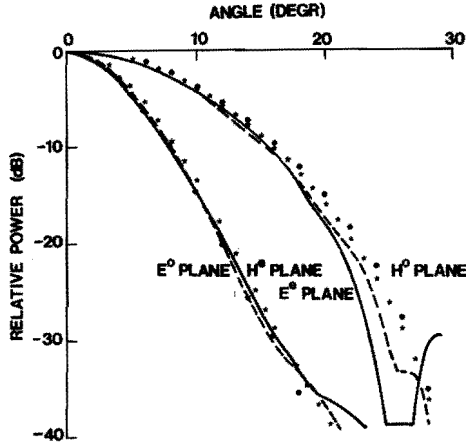


Fig. 4.8.3. Radiating near-field patterns for antenna C;  
 frequency 12 GHz;  $r_p = 0.94$  m;  
 .... computed,  ${}_{\circ}HE_{11}$  mode, aperture-field integration method;  
 \*\*\*\* computed,  ${}_{\circ}HE_{11}$  mode, wave-expansion method;  
 ---- measured,  ${}_{\circ}HE_{11}$  mode;  
 — measured,  ${}_eHE_{11}$  mode.

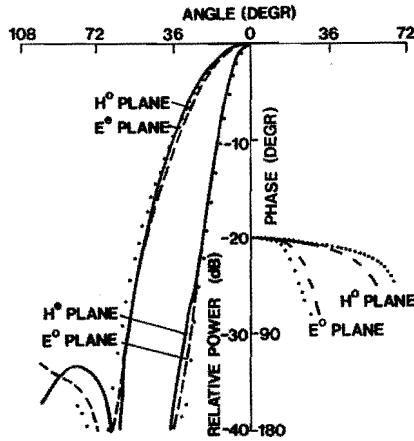


Fig. 4.8.4. Far-field patterns for antenna C; frequency 10.25 GHz;  
 .... computed,  ${}_{\circ}HE_{11}$  mode, aperture-field integration method;  
 ---- measured,  ${}_{\circ}HE_{11}$  mode;  
 — measured,  ${}_eHE_{11}$  mode;  
 the distance between the observation point and the phase  
 centre is 2.5 m.

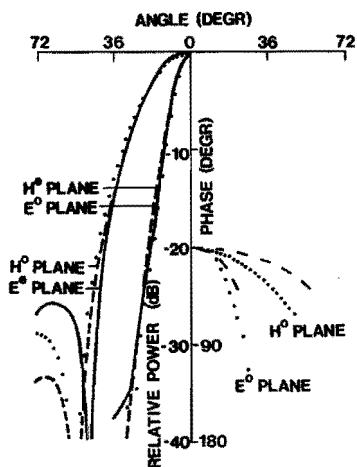


Fig. 4.8.5. Far-field patterns for antenna C; frequency 11.75 GHz;  
 .... computed,  ${}_{o}HE_{11}$  mode, aperture-field integration method;  
 ---- measured,  ${}_{o}HE_{11}$  mode;  
 — measured,  ${}_{e}HE_{11}$  mode;  
 the distance between the observation point and the phase  
 centre is 2.5 m.

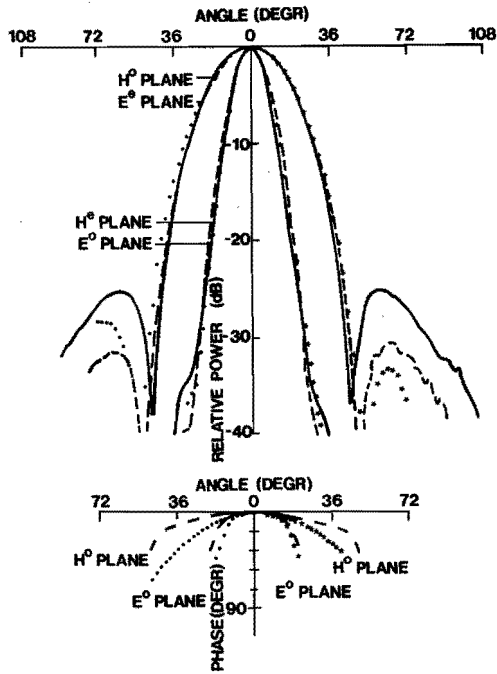


Fig. 4.8.6. Far-field patterns for antenna C; frequency 12 GHz;

.... computed,  $HE_{11}$  mode, aperture-field integration method;

\*\*\*\* computed,  $HE_{11}$  mode, wave-expansion method;

---- measured,  $HE_{11}$  mode;

— measured,  $e_{11}$  mode;

the distance between the observation point and the phase centre is 2.5 m.

4.6. Appendices

4.6.1. Evaluation of the numerators of (4.39) and (4.40)

The aperture field  $\bar{E}_a(\bar{r}_a)$  is equal to the tangential field of the odd symmetric HE mode of the infinite cone. This tangential field has components given by (3.66) and (3.67), in which  $a_{2m} = b_{2m} = 0$  and  $v$  should be replaced by  $v'$ . Insert the expansions (3.66) and (3.67) into the numerator of (4.39). Then the resulting double integrals can be reduced by use of the integral relations (2.101) and (2.122) for simple-periodic and nonperiodic Lamé functions. As a result it is found that the numerator of (4.39) can be expressed as

$$\begin{aligned}
 & jk^* h_{v'}^{(2)}(k^* r_a) h_v^{(2)}(k^* r_a) \frac{(1-k^2 \cos^2 \theta_o)^{\frac{1}{2}}}{\mu^{*'} - \mu^*} \sum_{m=0}^{\infty} a_{2m+1} [\mu^{*'} L_{cpv'}^{(2m+1)}(\theta_o) \frac{d}{d\theta} \{L_{cpv}^{(2n+1)}(\theta_o)\} - \\
 & - \mu^* L_{cpv}^{(2n+1)}(\theta_o) \frac{d}{d\theta} \{L_{cpv'}^{(2m+1)}(\theta_o)\}] \int_0^{2\pi} (1-k'^2 \sin^2 \phi)^{-\frac{1}{2}} L_{cv'}^{(2m+1)}(\phi) L_{cv}^{(2n+1)}(\phi) d\phi + \\
 & + \frac{1}{r_a} \frac{d}{dr} \{r h_{v'}^{(2)}(k^* r)\} \Big|_{r_a} h_v^{(2)}(k^* r_a). \\
 & \sum_{m=0}^{\infty} b_{2m+1} L_{cpv}^{(2n+1)}(\theta_o) L_{spv'}^{(2m+1)}(\theta_o) \int_0^{2\pi} L_{cv}^{(2n+1)}(\phi) \frac{d}{d\phi} \{L_{sv'}^{(2m+1)}(\phi)\} d\phi, \quad (4.93)
 \end{aligned}$$

where  $\mu^{*'} = v'(v'+1)$ ,  $\mu^* = v(v+1)$ .

By use of the Fourier-series representations (2.96) and (2.98) for simple-periodic Lamé functions, the final integral in (4.93) can be evaluated as

$$\int_0^{2\pi} L_{cv}^{(2n+1)}(\phi) \frac{d}{d\phi} \{L_{sv'}^{(2m+1)}(\phi)\} d\phi = \pi \sum_{t=0}^{\infty} (2t+1) A_{2t+1}^{(2n+1)} B_{2t+1}^{(2m+1)}. \quad (4.93a)$$

Here it should be kept in mind that the coefficients  $A_{2t+1}^{(2n+1)}$ ,  $B_{2t+1}^{(2m+1)}$ , also depend on  $v$ ,  $v'$ , respectively; this dependence has been suppressed in the notation.

In the same manner it is found that the numerator of (4.40) can be expressed as

$$\begin{aligned} & \frac{1}{k^* r_a^2} \frac{d}{dr} [rh_v^{(2)}(k^* r)] \frac{d}{dr} [rh_v^{(2)}(k^* r)] \Big|_{r_a} \frac{(1-k^2 \cos^2 \theta_0)^{\frac{1}{2}}}{\mu^* - \mu^*} . \\ & \cdot \sum_{m=0}^{\infty} b_{2m+1} [\mu^* L_{spv}^{(2m+1)}(\theta_0) \frac{d}{d\theta} \{L_{spv}^{(2n+1)}(\theta_0)\} - \mu^* L_{spv}^{(2n+1)}(\theta_0) \frac{d}{d\theta} \{L_{spv}^{(2m+1)}(\theta_0)\}] . \\ & \cdot \int_0^{2\pi} (1-k^2 \sin^2 \phi)^{-\frac{1}{2}} L_{sv}^{(2m+1)}(\phi) L_{sv}^{(2n+1)}(\phi) d\phi + \frac{j}{r_a} h_v^{(2)}(k^* r_a) \frac{d}{dr} [rh_v^{(2)}(k^* r)] \Big|_{r_a} . \\ & \cdot \sum_{m=0}^{\infty} a_{2m+1} L_{cpv}^{(2m+1)}(\theta_0) L_{spv}^{(2n+1)}(\theta_0) \int_0^{2\pi} L_{cv}^{(2m+1)}(\phi) \frac{d}{d\phi} \{L_{sv}^{(2n+1)}(\phi)\} d\phi . \quad (4.94) \end{aligned}$$

The final integral in (4.94) can be evaluated as

$$\int_0^{2\pi} L_{cv}^{(2m+1)}(\phi) \frac{d}{d\phi} \{L_{sv}^{(2n+1)}(\phi)\} d\phi = \pi \sum_{t=0}^{\infty} (2t+1) A_{2t+1}^{(2m+1)} B_{2t+1}^{(2n+1)} . \quad (4.94a)$$

#### 4.6.2. Expressions for $h_i(x, y)$ , $i = 1, 2, \dots, 24$

The expressions for  $h_i = h_i(x, y)$  are given by

$$\begin{aligned} h_1 &= H_x , & h_7 &= xH_z/z , & h_{13} &= y^2 H_z/z , & h_{19} &= xH_z , \\ h_2 &= H_y , & h_8 &= yH_x/z , & h_{14} &= xyH_x/z , & h_{20} &= yH_x , \\ h_3 &= H_x/z , & h_9 &= yH_z/z , & h_{15} &= xyH_y/z , & h_{21} &= yH_y , \\ h_4 &= H_y/z , & h_{10} &= x^2 H_y/z , & h_{16} &= xyH_z/z , & h_{22} &= yH_z , \\ h_5 &= H_z/z , & h_{11} &= x^2 H_z/z , & h_{17} &= xH_x , & h_{23} &= zH_x , \\ h_6 &= xH_y/z , & h_{12} &= y^2 H_x/z , & h_{18} &= xH_y , & h_{24} &= zH_y . \end{aligned}$$

4.6.3. Properties of  $\Phi(\alpha, \beta)$

The function  $\Phi(\alpha, \beta)$  is defined by

$$\Phi(\alpha, \beta) = \int_{-1}^1 \exp\{j(\alpha\xi - \beta \frac{\xi^2}{2})\} d\xi, \quad (4.95)$$

where  $\alpha, \beta$ , are assumed to be real; furthermore,  $\beta \geq 0$ .

The following properties of  $\Phi(\alpha, \beta)$  can easily be proved:

$$\Phi(0, 0) = 2, \quad \Phi(\alpha, 0) = 2\sin(\alpha)/\alpha; \quad (4.96)$$

$$\Phi(\alpha, \beta) = \Phi(-\alpha, \beta), \quad \Phi(\alpha, -\beta) = \Phi^*(\alpha, \beta); \quad (4.97)$$

$$\begin{aligned} \Phi(\alpha, \beta) &= \left(\frac{\pi}{\beta}\right)^{\frac{1}{2}} \exp(j\frac{\alpha^2}{2\beta}) \left\{ C\left(\frac{\alpha+\beta}{(\pi\beta)^{\frac{1}{2}}}\right) - jS\left(\frac{\alpha+\beta}{(\pi\beta)^{\frac{1}{2}}}\right) - C\left(\frac{\alpha-\beta}{(\pi\beta)^{\frac{1}{2}}}\right) + jS\left(\frac{\alpha-\beta}{(\pi\beta)^{\frac{1}{2}}}\right) \right\} = \\ &= \left(\frac{\pi}{\beta}\right)^{\frac{1}{2}} \exp(j\frac{\alpha^2}{2\beta}) \left[ \left\{ C_2\left(\frac{(\alpha+\beta)^2}{2\beta}\right) - jS_2\left(\frac{(\alpha+\beta)^2}{2\beta}\right) \right\} \operatorname{sgn}(\alpha+\beta) - \right. \\ &\quad \left. - \left\{ C_2\left(\frac{(\alpha-\beta)^2}{2\beta}\right) - jS_2\left(\frac{(\alpha-\beta)^2}{2\beta}\right) \right\} \operatorname{sgn}(\alpha-\beta) \right] = \\ &= \left(\frac{\pi}{\beta}\right)^{\frac{1}{2}} \exp(j\frac{\alpha^2}{2\beta}) \left\{ F\left(\frac{(\alpha+\beta)^2}{2\beta}\right) \operatorname{sgn}(\alpha+\beta) - F\left(\frac{(\alpha-\beta)^2}{2\beta}\right) \operatorname{sgn}(\alpha-\beta) \right\}, \quad (4.98) \end{aligned}$$

if  $\beta > 0$ .

The Fresnel-type integrals occurring in (4.98) are defined by

$$C(x) = \int_0^x \cos\left(\frac{\pi}{2}t^2\right) dt, \quad S(x) = \int_0^x \sin\left(\frac{\pi}{2}t^2\right) dt, \quad [1, \text{p. 300}], \quad (4.99)$$

$$C_2(x) = (2\pi)^{-\frac{1}{2}} \int_0^x t^{-\frac{1}{2}} \cos t \, dt, \quad S_2(x) = (2\pi)^{-\frac{1}{2}} \int_0^x t^{-\frac{1}{2}} \sin t \, dt, \quad x \geq 0, \\ [1, \text{p. 300}], \quad (4.100)$$

$$C(x) = C_2\left(\frac{\pi}{2}x^2\right) \operatorname{sgn}(x), \quad S(x) = S_2\left(\frac{\pi}{2}x^2\right) \operatorname{sgn}(x), \quad (4.101)$$

$$F(x) = C_2(x) - jS_2(x), \quad x \geq 0, \quad [3]. \quad (4.102)$$

4.6.4. Expressions for  $g_i(x,y)$ ,  $i = 1,2,\dots,14$

The expressions for  $g_i = g_i(x,y)$  are given by

$$g_1 = E_x, \quad g_5 = Z_{O_x} H_x, \quad g_9 = xZ_{O_y} H_y, \quad g_{13} = xyZ_{O_x} H_x,$$

$$g_2 = E_y, \quad g_6 = Z_{O_y} H_y, \quad g_{10} = yZ_{O_y} H_y, \quad g_{14} = xyZ_{O_y} H_y.$$

$$g_3 = xE_x, \quad g_7 = xZ_{O_x} H_x, \quad g_{11} = x^2 Z_{O_x} H_x,$$

$$g_4 = yE_y, \quad g_8 = yZ_{O_x} H_x, \quad g_{12} = y^2 Z_{O_y} H_y,$$

#### 4.7. References

- [1] Abramowitz, M., and I.A. Stegun (Editors), Handbook of Mathematical Functions, with Formulas, Graphs and Mathematical Tables. National Bureau of Standards, Washington, 1964. (Applied Mathematics Series, no. 55).
- [2] Barrow, W.L., and L.J. Chu, Theory of the electromagnetic horn. Proc. IRE 27 (1939), 51-64.
- [3] Boersma, J., Computation of Fresnel integrals. Mathematics of Computation 14 (1960), 380.
- [3a] Brigham, E.O., and R.E. Morrow, The fast Fourier transform. IEEE Spectrum 4 (1967), No. 12, 63-70.
- [4] Bucci, O.M., G. Francheschetti, and R. Pierri, Reflector antenna fields. An exact aperture-like approach. IEEE Trans. Antennas and Propagat. AP-29 (1981), 580-586.
- [5] Clarricoats, P.J.B., and P.K. Saha, Propagation and radiation behaviour of corrugated feeds. Part 2. Corrugated-conical-horn feed. Proc. IEE 118 (1971), 1177-1186.
- [6] Fasold, D., L. Heichele, M. Lieke, H. Pecher, and A. Ruthlein, Der Entwicklungsstand der Sendeantenne des Fernseh Rundfunksatelliten TV-SAT. Nachrichtentechnische Gesellschaft-Fachberichte, Band 78, Antennen '82, 115-119.
- [7] Galindo-Israel, V., and Y.Rahmat-Samii, A new look at Fresnel field computation using the Jacobi-Bessel series. IEEE Trans. Antennas and Propagat. AP-29 (1981), 885-898.
- [8] Hansen, R.C., Microwave Scanning Antennas, Vol. I: Apertures. Academic Press, New York, 1964, Chapter 1.
- [9] James, J.R., and L.W. Longdon, Calculation of radiation patterns. Electronics Letters 5 (1969), 567-569.
- [10] Jansen, J.K.M., Simple-periodic and Non-periodic Lamé Functions. Mathematical Centre Tracts 72, Math. Centrum, Amsterdam, 1977.
- [11] Jeuken, M.E.J., Frequency-independence and Symmetry Properties of Corrugated Conical Horn Antennas with Small Flare Angles. Ph.D. Thesis, Eindhoven University of Technology, Eindhoven, 1970.
- [12] Mahmoud, S.F., and P.J.B. Clarricoats, Radiation from wide flare-angle corrugated conical horns. IEE Proc. H 129 (1982), 221-228.

- [13] Muehldorf, E.I., The phase centre of horn antennas. IEEE Trans. Antennas and Propagat. AP-18 (1970), 753-760.
- [14] Nagelberg, E.R., Fresnel-region phase centre of circular aperture antennas. IEEE Trans. Antennas and Propagat. AP-13 (1965), 479-480.
- [15] Teichman, M., Determination of horn antenna phase centres by edge diffraction theory. IEEE Trans. Aerospace and Electronic Systems AES-9 (1973), 875-882.
- [16] Vokurka, V.J., Elliptical corrugated horn for broadcasting-satellite antennas. Electronics Letters 15 (1979), 652-654.
- [17] Vokurka, V.J., Elliptical corrugated horns for frequency-reuse applications. IEEE AP-S International Symposium Digest, 221-223, Québec, Canada, 1980.

5. ELECTRICAL PERFORMANCE OF AN OFFSET REFLECTOR ANTENNA SYSTEM FED BY A CORRUGATED ELLIPTICAL HORN RADIATOR

5.1. Introduction

In section 1.3 we have briefly reviewed some designs for high-performance broadcasting-satellite transmitting antennas. Particular attention was paid to the antenna system that consists of a single offset parabolic reflector and a corrugated elliptical horn as the primary radiator. This antenna system has favourable properties with respect to its electrical performance: from experiments it was found that the secondary radiation pattern is characterized by a main lobe with an elliptical cross-section, by low copolarized sidelobe radiation (level below -30 dB), and by low cross-polarized radiation of circular polarization (level below -33 dB). In the present chapter the radiation field of the antenna system is evaluated by analytical and numerical methods. We will calculate the main lobe of the secondary radiation pattern, the copolarized sidelobe radiation, and the cross-polarized radiation in the angular region around boresight. The numerical results obtained are compared with the results of measurements on the antenna system.

The radiation field of the antenna system is determined from the well-known integral representation for the electromagnetic field in terms of the surface current  $\bar{J}_s$  induced in the parabolic reflector surface. The surface current is induced by the primary radiation from the corrugated elliptical horn, which acts as an incident electromagnetic wave on the reflector surface. The exact value of the current  $\bar{J}_s$  cannot be determined analytically. Therefore, the standard physical-optics approximation is employed, whereby the surface current is approximated by  $\bar{J}_s = 2\hat{n} \times \bar{H}^i$ . Here,  $\bar{H}^i$  is the magnetic field of the incident primary radiation at the reflector surface, and  $\hat{n}$  is the unit vector normal to the reflector surface at the point of incidence pointing towards the illuminated side of the parabolic reflector. The magnetic field  $\bar{H}^i$  is determined from an integral representation for the primary radiation field in terms of the field distribution in the horn aperture, based on the Kirchhoff-Huygens approximation; see chapter 4. Thereby the field in the aperture of the corrugated elliptical horn is taken to be equal to the modal field of an infinitely long corrugated elliptical cone. In this manner the radiation field is completely determined analytically. Starting from this analytical formulation we next develop a numerical procedure for the computation of the secondary radiation

pattern of the antenna system.

The results of measurements on the antenna system under consideration were placed at our disposal by Messerschmitt-Bölkow-Blohm GmbH, Munich, Germany. Since these measurements refer to linearly polarized radiation from the antenna system, our numerical results are restricted to this case only. In the case of circularly polarized radiation from the antenna system, the radiation field may be calculated in the same manner; however, we have not carried out the actual calculation.

### 5.2. Evaluation of the radiation field of the antenna system

This section deals with the analytical and numerical evaluation of the secondary radiation field of a single offset parabolic reflector illuminated by a corrugated elliptical horn radiator. First we introduce suitable coordinates to describe the geometry of the antenna system. We shall employ Cartesian coordinates  $x, y, z$  and spherical coordinates  $r, \theta, \phi$ , which are related as in (2.34) - (2.36). Notice the slight difference in notation: the present spherical coordinates should not be confused with the sphero-conal coordinates of chapter 2. The unit vectors of the coordinate systems are denoted by  $\hat{x}, \hat{y}, \hat{z}$ , and  $\hat{r}, \hat{\theta}, \hat{\phi}$ , respectively.

The reflector surface  $S$ , of which the cross-section with the  $yz$ -plane is shown in Figure 5.1a, is part of a paraboloid of revolution. The paraboloid has a focal length  $f$ , its focal point  $F$  is at the origin of the coordinate systems, and its axis of revolution coincides with the  $z$ -axis.

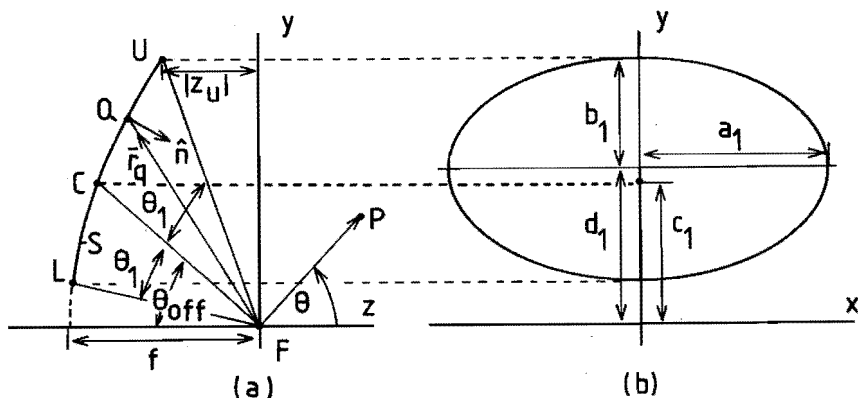


Fig. 5.1. Geometry of the offset parabolic reflector.

The equation of the paraboloid is

$$z = -f + \frac{x^2 + y^2}{4f}, \quad (5.1)$$

$$r = \frac{2f}{1 - \cos\theta}, \quad (5.2)$$

in Cartesian and spherical coordinates, respectively. The surface area element  $dS$  of the paraboloid is

$$dS = \left\{ 1 + \left(\frac{\partial z}{\partial x}\right)^2 + \left(\frac{\partial z}{\partial y}\right)^2 \right\}^{\frac{1}{2}} dx dy = \left( 1 + \frac{x^2 + y^2}{4f^2} \right)^{\frac{1}{2}} dx dy. \quad (5.3)$$

Let  $Q$  be an arbitrary point on  $S$ , with position vector  $\vec{r}_Q$  and spherical coordinates  $(r_Q, \theta_Q, \phi_Q)$ . Then the unit vector  $\hat{n}$  at  $Q$ , normal to  $S$  and with a positive  $z$ -component, is given by

$$\hat{n} = -\cos \frac{\theta_Q}{2} \cos \phi_Q \hat{x} - \cos \frac{\theta_Q}{2} \sin \phi_Q \hat{y} + \sin \frac{\theta_Q}{2} \hat{z}, \quad (5.4)$$

or

$$\hat{n} = -\sin \frac{\theta_Q}{2} \hat{r} - \cos \frac{\theta_Q}{2} \hat{\theta}. \quad (5.5)$$

The offset reflector is cut out from the paraboloid surface by an elliptical cylinder given by the equation

$$\left(\frac{x}{a_1}\right)^2 + \left(\frac{y-d_1}{b_1}\right)^2 = 1. \quad (5.6)$$

Obviously, the projection of the rim of the offset reflector onto a plane  $z = \text{constant}$  is an ellipse with semi-major axis  $a_1$  along the  $x$ -axis and semi-minor axis  $b_1$  along the  $y$ -axis. In particular, the ellipse in the plane  $z = z_u$  through the point  $U$  encloses the projected aperture of the reflector; see Figure 5.1b. We note that this aperture and the one shown in Figure 1.6 have slightly different shapes.

In Figure 5.1a the angle between the lines  $FL$  and  $FU$  is denoted by  $2\theta_1$ . This angle is bisected by the line  $FC$ . The angle between the line  $FC$  and the negative  $z$ -axis is denoted by  $\theta_{\text{off}}$ , the so-called offset angle of the reflector. The offset plane, that is the symmetry plane of the reflector, coincides with the  $yz$ -plane. The  $y$ -coordinate of the point  $C$  is denoted by  $c_1$ . The following relations for the geometrical parameters of the reflector can easily be derived, viz.

$$b_1 = \frac{2f \sin \theta_1}{\cos \theta_{\text{off}} + \cos \theta_1}, \quad c_1 = \frac{2f \sin \theta_{\text{off}}}{1 + \cos \theta_{\text{off}}}, \quad d_1 = \frac{2f \sin \theta_{\text{off}}}{\cos \theta_{\text{off}} + \cos \theta_1}. \quad (5.7)$$

Note that  $d_1 > c_1$ , hence, the point C is not on the axis of the elliptical cylinder.

Next we describe the geometry of the feed system that consists of a corrugated elliptical horn with an opening angle  $\theta_o$  and an aspect ratio  $a_{r\theta}$ . The apex of the horn is at the point O, and the horn axis lies in the yz-plane and passes through the focal point F; see Figure 5.2. The horn has a planar elliptical aperture at the distance  $z_a$  from the apex. The major axis of the elliptical aperture is in the yz-plane, and the minor axis is in the plane through OF perpendicular to the yz-plane. The angle subtended by the minor axis at the apex O is equal to  $2\theta_o$ .

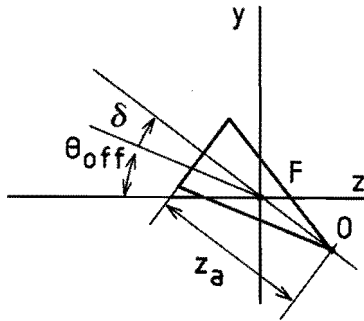


Fig. 5.2. Geometry of the elliptical horn radiator.

To fix the position of the horn it remains to specify the distance OF between the apex O of the horn and the focal point F of the reflector, and the angle  $\theta_{\text{off}} + \delta$  between the horn axis and the negative z-axis; see Figure 5.2. The distance OF also determines the distances between the focus of the reflector and the phase centres of the radiation field of the horn. The angle  $\delta$  measures the deflection of the horn axis from the bisector FC; for most practical offset reflectors one has  $0 < \delta \leq 4^\circ$ , [4], [5]. The geometrical parameters OF and  $\delta$  serve as input parameters in the computational procedure for the determination of the radiation field of the antenna system. By varying these input parameters one may search for the best horn position so as to realize an optimal illumination of the offset parabolic reflector. In this manner the distance OF

and the angle  $\delta$  are ascertained on the basis of computations.

We now turn to the evaluation of the radiation field of the antenna system. The secondary radiation field is viewed as arising from the surface current  $\bar{J}_s(\bar{r}_q)$  induced in the parabolic reflector surface; here  $\bar{r}_q$  is the position vector of the point Q on the reflector (see Figure 5.1a). Let P be an observation point, with position vector  $\bar{r}$  and spherical coordinates  $(r, \theta, \phi)$ , in the far-zone region of the reflector. Then the radiation field  $\bar{E}(\bar{r})$ ,  $\bar{H}(\bar{r})$  at P is given by the following integral representation in terms of the surface current  $\bar{J}_s(\bar{r}_q)$ :

$$\bar{E}(\bar{r}) = c \iint_S [\bar{J}_s(\bar{r}_q) - \{\bar{J}_s(\bar{r}_q) \cdot \hat{r}\} \hat{r}] \exp(jk^* \bar{r}_q \cdot \hat{r}) dS, \quad (5.8)$$

$$\bar{H}(\bar{r}) = \hat{z}_o^{-1} \hat{r} \times \bar{E}(\bar{r}), \quad (5.9)$$

where

$$c = -\frac{j\omega\mu_o}{4\pi r} \exp(-jk^* r), \quad (5.10)$$

$$\hat{r} = \sin\theta\cos\phi\hat{x} + \sin\theta\sin\phi\hat{y} + \cos\theta\hat{z}; \quad (5.11)$$

see [3, Sections 2.5 and 3.6]. The surface current is induced by the primary radiation from the corrugated elliptical horn, which acts as an incident wave on the reflector surface. The exact value of the current  $\bar{J}_s$  cannot be determined analytically. Therefore we employ the standard physical-optics approximation in which the surface current is approximated by

$$\bar{J}_s = 2\hat{n} \times \bar{H}^i; \quad (5.12)$$

see [3, Section 3.6.]. Here,  $\bar{H}^i$  is the magnetic field of the incident primary radiation at the reflector surface, and  $\hat{n}$  is the unit normal vector introduced in (5.4) and (5.5). The vector  $\bar{J}_s$  is expressed as

$$\bar{J}_s = J_x \hat{x} + J_y \hat{y} + J_z \hat{z}. \quad (5.13)$$

From (5.8), (5.11) and (5.13) the Cartesian components  $E_x$ ,  $E_y$ ,  $E_z$  of the electric field at P are found to be given by

$$E_x = I_x (1 - \sin^2 \theta \cos^2 \phi) - I_y \sin^2 \theta \cos \phi \sin \phi - I_z \cos \theta \sin \theta \cos \phi, \quad (5.14)$$

$$E_y = -I_x \sin^2 \theta \cos \phi \sin \phi + I_y (1 - \sin^2 \theta \sin^2 \phi) - I_z \cos \theta \sin \theta \sin \phi, \quad (5.15)$$

$$E_z = -I_x \cos \theta \sin \theta \cos \phi - I_y \cos \theta \sin \theta \sin \phi + I_z \sin^2 \theta, \quad (5.16)$$

where

$$I_i = C \iint_S J_i \exp(jk \vec{r}_q \cdot \vec{r}) dS, \quad i = x, y, z. \quad (5.17)$$

The spherical components  $E_\theta$ ,  $E_\phi$  of the electric field at P are given by

$$E_\theta = I_x \cos \theta \cos \phi + I_y \cos \theta \sin \phi - I_z \sin \theta, \quad (5.18)$$

$$E_\phi = -I_x \sin \phi + I_y \cos \phi, \quad (5.19)$$

while the radial component  $E_r$  vanishes. The electric field at P depends on the surface current component  $J_z$  through the integral  $I_z$ . From (5.18) and (5.19) it is seen that  $J_z$  makes no contribution to the field component  $E_\phi$ , whereas its contribution to the component  $E_\theta$  is small for angles  $\theta$  close to zero. Hence, in the angular region around the positive z-axis ( $\theta = 0$ ) the contribution of the surface current  $J_z$  to the radiation field is a second-order effect [7, Section 12.4].

To enable a comparison with measured data, the radiation field of the antenna system is decomposed into copolarized and cross-polarized radiation fields. The directions of these fields are described by the orthogonal unit vectors  $\hat{e}_{co}$  and  $\hat{e}_{cr}$ , respectively. These vectors are now specified in concurrence with standard measurement practice [6].

Consider first the case of a radiation field that is due to excitation of the horn by an odd symmetric mode. Then at  $\theta = 0$  the radiation field is polarized in the  $\hat{y}$ -direction. In this case the unit vectors  $\hat{e}_{co}$  and  $\hat{e}_{cr}$  are specified by [6, eq. (8a,b)]

$$\begin{aligned} \hat{e}_{co} &= \sin \phi \hat{\theta} + \cos \phi \hat{\phi} \\ &= -(1 - \cos \theta) \cos \phi \sin \phi \hat{x} + \{1 - (1 - \cos \theta) \sin^2 \phi\} \hat{y} + \sin \theta \sin \phi \hat{z}, \end{aligned} \quad (5.20)$$

$$\begin{aligned} \hat{e}_{cr} &= \cos \phi \hat{\theta} - \sin \phi \hat{\phi} \\ &= \{1 - (1 - \cos \theta) \cos^2 \phi\} \hat{x} - (1 - \cos \theta) \cos \phi \sin \phi \hat{y} - \sin \theta \cos \phi \hat{z}. \end{aligned} \quad (5.21)$$

Likewise, in the case of excitation by an even symmetric mode, the radiation field at  $\theta=0$  is polarized in the  $\hat{x}$ -direction. Then the vectors  $\hat{e}_{co}$  and  $\hat{e}_{cr}$  are given by (5.20) and (5.21) with  $\phi$  replaced by  $\phi + \pi/2$ , corresponding to an interchange of roles of the vectors. The copolarized radiation field  $\bar{E}_{co}(\vec{r})$  and the cross-polarized radiation field  $\bar{E}_{cr}(\vec{r})$  at P are now determined from

$$\bar{E}_{co}(\vec{r}) = \{\bar{E}(\vec{r}) \cdot \hat{e}_{co}\} \hat{e}_{co}, \quad \bar{E}_{cr}(\vec{r}) = \{\bar{E}(\vec{r}) \cdot \hat{e}_{cr}\} \hat{e}_{cr}. \quad (5.22)$$

The copolarized radiation pattern  $F_{co}(\vec{r})$  and the cross-polarized radiation pattern  $F_{cr}(\vec{r})$  are defined by

$$F_{co}(\vec{r}) = P_{co}(\vec{r})/P_{co}(r,0,0), \quad F_{cr}(\vec{r}) = P_{cr}(\vec{r})/P_{cr}(r,0,0), \quad (5.23)$$

in which

$$P_{co}(\vec{r}) = (2Z_0)^{-1} r^2 |\bar{E}_{co}(\vec{r})|^2, \quad P_{cr}(\vec{r}) = (2Z_0)^{-1} r^2 |\bar{E}_{cr}(\vec{r})|^2. \quad (5.24)$$

To numerically evaluate the copolarized and cross-polarized radiation patterns, it is necessary to compute the two-dimensional integrals (5.17). By use of (5.1), (5.3) and (5.11), we rewrite (5.17) as

$$I_i = C \iint_{S_{xy}} J_i \exp[jk^* \{ \sin\theta(x\cos\phi + y\sin\phi) + \cos\theta(\frac{x^2+y^2}{4f} - f) \}] (1 + \frac{x^2+y^2}{4f^2})^{1/2} dx dy, \quad (5.25)$$

$i = x, y, z,$

where the elliptical integration domain  $S_{xy}$  is described by

$$(\frac{x}{a_1})^2 + (\frac{y-d_1}{b_1})^2 \leq 1. \quad (5.26)$$

The normalized integration variables  $\xi = x/a_1$  and  $\eta = (y-d_1)/b_1$  are introduced. Then  $I_i$  can be recast in the form

$$I_i = C_a \int_{-1}^1 \int_{-1}^1 k_1(\xi, \eta) \exp\{j(\alpha_1 \xi + \alpha_2 \eta - \beta_1 \frac{\xi^2}{2} - \beta_2 \frac{\eta^2}{2})\} d\xi d\eta, \quad (5.27)$$

where

$$C_a = C a_1 b_1 \exp[jk^* \{ (\frac{d_1}{4f} - f) \cos\theta + \alpha_1 \sin\theta \sin\phi \}], \quad (5.28)$$

$$\alpha_1 = k^* a_1 \sin\theta \cos\phi, \quad \alpha_2 = k^* b_1 \sin\theta \sin\phi + \frac{k^* b_1 d_1}{2f} (\cos\theta - 1), \quad (5.29)$$

$$\beta_1 = \frac{k^* a_1^2}{2f} (1 - \cos\theta), \quad \beta_2 = \frac{k^* b_1^2}{2f} (1 - \cos\theta), \quad (5.30)$$

$$k_i(\xi, \eta) = J_i \left\{ 1 + \frac{a_1^2 \xi^2 + (b_1 \eta + d_1)^2}{4f^2} \right\}^{\frac{1}{2}} \exp\left[ \frac{jk^*}{4f} (a_1^2 \xi^2 + b_1^2 \eta^2 + 2b_1 d_1 \eta) \right] \\ \text{if } \xi^2 + \eta^2 \leq 1, \quad (5.31)$$

$$k_i(\xi, \eta) \equiv 0 \quad \text{if } \xi^2 + \eta^2 > 1. \quad (5.32)$$

The integral (5.27) is evaluated by the same numerical procedure as has been used in the calculation of the horn radiation, based on the aperture-field integration method; see sections 4.4.1 and 4.4.2. Thus by expansion of  $k_i(\xi, \eta)$  in terms of the basis functions  $f_{mn}(\xi, \eta)$  introduced in (4.72), the integral  $I_i$  is reduced to the sampling-like representation

$$I_i = C_a \sum_{m=-\infty}^{\infty} \sum_{n=-\infty}^{\infty} K_i(m\pi, n\pi) \psi_{mn}(\alpha_1, \beta_1, \alpha_2, \beta_2), \quad (5.33)$$

in which

$$K_i(m\pi, n\pi) = \int_{-1}^1 \int_{-1}^1 k_i(\xi, \eta) \exp\{j(m\pi\xi + n\pi\eta)\} d\xi d\eta, \quad (5.34)$$

and

$$\psi_{mn}(\alpha_1, \beta_1, \alpha_2, \beta_2) = \frac{1}{4} \Phi(\alpha_1 - m\pi, \beta_1) \Phi(\alpha_2 - n\pi, \beta_2), \quad (5.35)$$

with  $\Phi$  given by (4.77). The coefficients  $K_i(m\pi, n\pi)$  are the two-dimensional Fourier coefficients of the functions  $k_i(\xi, \eta)$ . These coefficients are calculated from samples of  $k_i$  by use of the Fast Fourier Transform (FFT) technique [2]. The coefficients  $K_i(m\pi, n\pi)$  depend only on the geometry of the reflector and on the induced current in the reflector surface; they are independent of the coordinates of the observation point P. The functions  $\psi_{mn}$ , however, are independent of the induced current; they only depend on the coordinates of P and on the geometry of the reflector.

The mathematical procedure developed here, leads to the following scheme to numerically evaluate the radiation patterns of the antenna system:

1. Specify the horn and reflector parameters, the position of the horn relative to the focal point  $F$ , and the direction of the horn axis.
2. Choose discrete sample points  $(\xi, \eta)$ , and calculate the coordinates of the associated points on the reflector.
3. Compute the samples  $k_i(\xi, \eta)$ . The components  $J_i$  of the surface current are found from  $\vec{J}_s = 2\hat{n} \times \vec{H}^i$ . The incident magnetic field  $\vec{H}^i$  at the reflector surface due to the primary radiation from the horn, is calculated by means of the aperture-field integration method of section 4.4.2.
4. Compute the Fourier coefficients  $K_i(m\pi, n\pi)$  of  $k_i$  by use of FFT.
5. Specify the coordinates of the observation point  $P$ , and calculate  $\psi_{mn}$  and  $I_i$ .
6. Compute the copolarized radiation field  $\vec{E}_{co}$  and the cross-polarized radiation field  $\vec{E}_{cr}$  at  $P$ .
7. Repeat steps 5 and 6 for other observation points and determine the radiation patterns of the antenna system.

### 5.3. Numerical and experimental results

In this section we present numerical and experimental results for the radiation field of the antenna system that consists of a single offset parabolic reflector and a corrugated elliptical horn as the primary radiator. The geometry of the antenna system has been described in the previous section. The geometrical parameters of the horn and of the reflector will be specified below. The measured results have been recorded for the antenna system in the two cases of  ${}_{o}HE_{11}$ -mode excitation and  ${}_{e}HE_{11}$ -mode excitation of the horn. A theoretical analysis of the radiation fields in these two cases is presented in Appendix 5.4. There it is shown that the radiation fields due to excitations by odd and even modes are orthogonal, and the corresponding copolarized radiation patterns are equal, both up to a good approximation. The errors involved in these approximate results are small if the angle  $\theta$  is close to zero, i.e. in the angular region around the positive  $z$ -axis. Because of the (approximate) equality of radiation patterns, the numerical computation of the radiation field of the antenna system is

restricted to the case of  ${}^{\circ}\text{HE}_{11}$ -mode excitation of the horn. Throughout the frequency is set at 12 GHz.

The geometrical parameters of the offset parabolic reflector considered are given by (cf. Figure 5.1)

$$f = 1.50 \text{ m} ; \quad \theta_{\text{off}} = 34.8^{\circ} ; \quad \theta_1 = 27.15^{\circ} ;$$
$$a_1 = 1.30 \text{ m} ; \quad b_1 = 0.80 \text{ m} ; \quad c_1 = 0.94 \text{ m} ; \quad d_1 = 1.00 \text{ m}.$$

The semi-opening angle in the plane perpendicular to the offset plane, subtended at the focus, is  $42.5^{\circ}$ .

The primary radiator considered is the corrugated elliptical horn with the parameters (cf. Figure 5.2)

$$z_a = 0.324 \text{ m} ; \quad \theta_o = 5.04^{\circ} ; \quad a_{r\theta} = 0.5.$$

The position of the horn is specified by (cf. Figure 5.2)

$$\text{OF} = 0.31 \text{ m} ; \quad \delta = 2^{\circ}.$$

The computed phase centres in the  $\text{H}^{\circ}$  and  $\text{E}^{\circ}$  planes (principal planes of the horn) are located at the centre of the horn aperture, and inside the horn on the horn axis at 0.034 m from the aperture, respectively. Hence, the focal point of the reflector lies between the two phase centres, at 0.014 m from the phase centre in the  $\text{H}^{\circ}$  plane and at 0.02 m from the phase centre in the  $\text{E}^{\circ}$  plane. In Figures 5.3 and 5.4 computed and measured results for the radiation patterns of the antenna system are plotted as a function of the spherical angle  $\theta$ . The computer processing time for the field evaluation following the stepwise procedure given in section 5.2, is approximately 4 seconds per observation point.

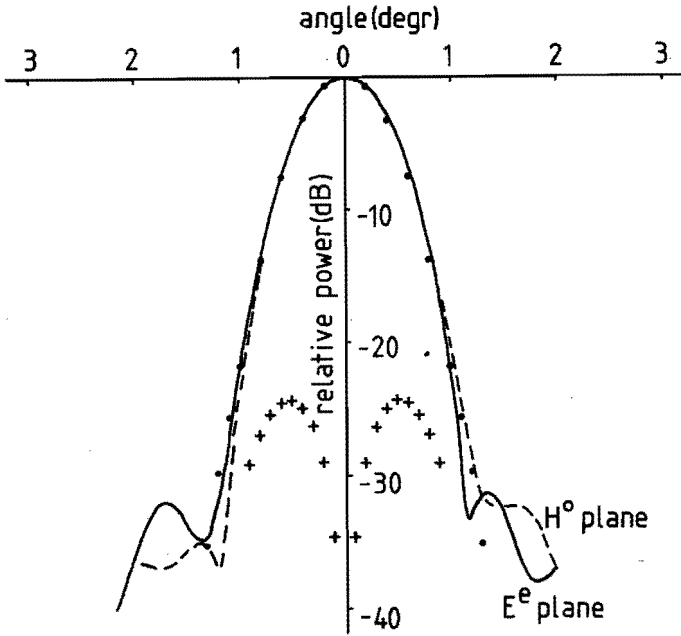


Fig. 5.3. Far-field patterns in the  $H^\circ$ ,  $E^\circ$  plane ( $xz$ -plane) for the single offset parabolic reflector fed by a corrugated elliptical horn; frequency 12 GHz;

- .... computed copolarized radiation,  ${}_{\circ}HE_{11}$ -mode excitation;
- ++++ computed cross-polarized radiation,  ${}_{\circ}HE_{11}$ -mode excitation;
- measured copolarized radiation,  ${}_{\circ}HE_{11}$ -mode excitation;
- measured copolarized radiation,  ${}_{e}HE_{11}$ -mode excitation;

(measurements, courtesy of MBB, Munich).

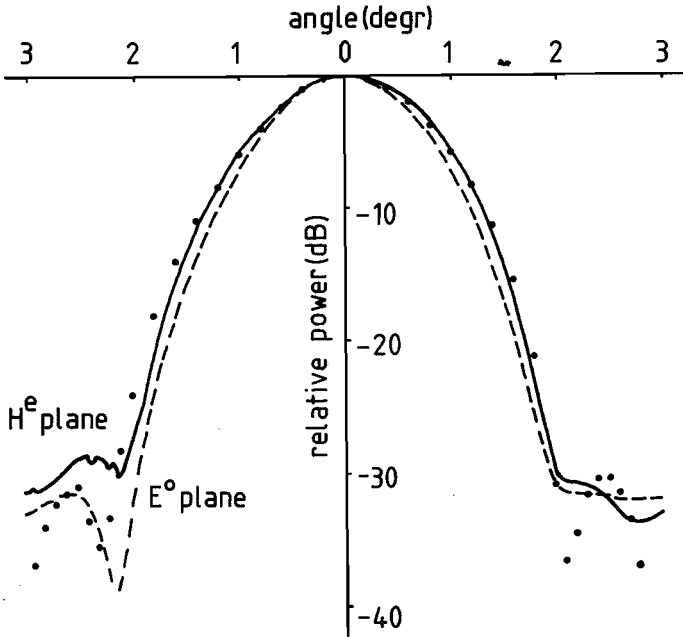


Fig. 5.4. Far-field patterns in the  $E^o$ ,  $H^e$  plane ( $yz$ -plane) for the single offset parabolic reflector fed by a corrugated elliptical horn; frequency 12 GHz;  
.... computed copolarized radiation,  ${}_{o}HE_{11}$ -mode excitation;  
---- measured copolarized radiation,  ${}_{o}HE_{11}$ -mode excitation;  
— measured copolarized radiation,  ${}_{e}HE_{11}$ -mode excitation;  
(measurements, courtesy of MBB, Munich).

From the computed and measured results for the radiation in the xz-plane ( $H^o$ ,  $E^e$  plane of the antenna system), as shown in Figure 5.3, the following conclusions are drawn:

1. Excellent agreement between the computed and measured results in the region of the main lobe is observed.
2. The radiation patterns of the antenna system in the two cases of  ${}^oHE_{11}$ - and  ${}^eHE_{11}$ -mode excitation of the horn are virtually identical.
3. The patterns are symmetric with respect to the direction  $\theta = 0$ .
4. The measured sidelobe levels are below -31 dB, whereas the computed sidelobe levels are below -40 dB.
5. The computed maximum level of the cross-polarized radiation (in the case of linear polarization) is -24.3 dB.
6. The angle of -3 dB beamwidth is  $0.77^\circ$ .

From the computed and measured results for the radiation in the yz-plane ( $E^o$ ,  $H^e$  plane of the antenna system), as shown in Figure 5.4, the following conclusions are drawn:

1. Very good agreement between the computed and measured results is established.
2. The radiation pattern of the antenna system in the case of  ${}^oHE_{11}$ -mode excitation of the horn is somewhat narrower than the one corresponding to  ${}^eHE_{11}$ -mode excitation of the horn. This is attributed to a slightly broader primary radiation pattern in the yz-plane in the case of  ${}^oHE_{11}$ -mode excitation.
3. The computed and measured radiation patterns show a small asymmetry with respect to the direction  $\theta = 0$ . In general, the radiation level at the angle  $\theta$  is higher in the half-plane  $\phi = \pi/2$  (left part of Figure 5.4) than it is in the half-plane  $\phi = 3\pi/2$  (right part of Figure 5.4). Computed results show that the asymmetry increases for decreasing  $\delta$ . The asymmetry of the patterns is attributed to the asymmetric reflector geometry, which results in the upper part of the reflector being under-illuminated relative to the lower part of the reflector.
4. The computed sidelobes are well defined. The level of sidelobe radiation is below -30 dB.
5. Cross-polarized radiation in the yz-plane (the offset plane of the reflector) is absent.
6. The angle of -3 dB beamwidth is  $1.41^\circ$ .

Computed results for the copolarized radiation in the  $E^{\circ}$  plane of the antenna system in the case of  $HE_{11}^{\circ}$ -mode excitation, show a very small pattern shift away from the direction  $\theta = 0$ . The maximum of the copolarized radiation occurs in the direction  $\theta = 0.02^{\circ}$  in the half-plane  $\phi = 3\pi/2$  (cf. Figure 5.4). This shift of the radiation pattern in the offset plane of the antenna system is known as the beam squint for linearly polarized radiation [1]. From the computed results it is furthermore observed that the copolarized radiation in the xz-plane is below the reference curve A, given in Figure 1.4. The main lobe of the copolarized radiation in the yz-plane, however, is not everywhere below the reference curve A.

Our final conclusions are the following:

1. The single offset parabolic reflector fed by a corrugated elliptical horn, can indeed provide a secondary radiation pattern that has a rapidly decaying main lobe with an elliptical cross-section, and that has low sidelobes. Furthermore, the secondary radiation patterns of the antenna system in the cases of  $HE_{11}^{\circ}$ - and  $HE_{11}^e$ -mode excitation of the horn are virtually the same.
2. The horn and reflector geometries are input parameters of the computational procedure to numerically determine the radiation field of the antenna system. By varying these input parameters one may search for an antenna design that is optimal with regard to electrical performance. In this manner the computational procedure provides a design through computation versus the alternative of a design based on experimentation.
3. The analytical and numerical approach to the evaluation of the electrical performance of the antenna system, as developed in this section, is rapid (with respect to computer processing time), successful and reliable.

5.4. Appendix

As a supplement to section 5.2, this appendix deals with the radiation fields of the antenna system in the two cases of excitation of the horn by an odd symmetric mode (I-mode) and by the associated even symmetric mode (II-mode). The resulting electromagnetic fields are distinguished by the superscripts I and II, respectively. It has been shown in section 4.2 that in the radiating near-field and far-field regions of the horn the primary radiation fields ( $\vec{E}^I, \vec{H}^I$ ) and ( $\vec{E}^{II}, \vec{H}^{II}$ ) are related by (see (4.7) and (4.8))

$$Z_{\circ} \vec{H}^I = \hat{r} \times \vec{E}^I, \quad Z_{\circ} \vec{H}^{II} = \hat{r} \times \vec{E}^{II}, \quad \vec{E}^I = \hat{r} \times \vec{E}^{II}, \quad (5.36)$$

where the unit vector  $\hat{r}$  at the observation point points in the outward radial direction. These primary radiation fields act as incident fields on the parabolic reflector of the antenna system. Then we have from (5.36) that the spherical components of the incident fields at the reflector surface satisfy

$$E_{\theta}^I = Z_{\circ} H_{\phi}^I = -E_{\phi}^{II} = Z_{\circ} H_{\theta}^{II}, \quad (5.37)$$

$$E_{\phi}^I = -Z_{\circ} H_{\theta}^I = E_{\theta}^{II} = Z_{\circ} H_{\phi}^{II}. \quad (5.38)$$

The surface currents  $\vec{J}_s^I, \vec{J}_s^{II}$  induced in the reflector are determined from the physical-optics approximation (5.12), which is now further evaluated by use of (5.5). At the point  $(r_q, \theta_q, \phi_q)$  of the reflector surface the Cartesian components  $J_x, J_y, J_z$  of the surface current are found to be given by

$$J_x = 2(H_{\theta} \sin \phi_q - H_{\phi} \cos \phi_q) \sin \frac{\theta_q}{2}, \quad (5.39)$$

$$J_y = -2(H_{\theta} \cos \phi_q + H_{\phi} \sin \phi_q) \sin \frac{\theta_q}{2}, \quad (5.40)$$

$$J_z = -2H_{\phi} \cos \frac{\theta_q}{2}, \quad (5.41)$$

where the superscripts I and II have been suppressed for simplicity. By means of (5.37) and (5.38) it easily follows that the current components are related by

$$J_x^I = J_y^{II}, \quad J_y^I = -J_x^{II}. \quad (5.42)$$

Consequently, the radiation integrals  $I_i$  introduced in (5.17) are related by

$$I_x^I = I_y^{II}, \quad I_y^I = -I_x^{II}. \quad (5.43)$$

The secondary radiation fields ( $\vec{E}^I, \vec{H}^I$ ) and ( $\vec{E}^{II}, \vec{H}^{II}$ ) of the antenna system are considered to be due to the surface currents  $\vec{J}_s^I$  and  $\vec{J}_s^{II}$ , respectively. The spherical components of the electric fields  $\vec{E}^I$  and  $\vec{E}^{II}$  at the observation point  $(r, \theta, \phi)$  are given by (5.18) - (5.19), expressed in terms of the corresponding integrals  $I_x, I_y$  and  $I_z$ . We now assume that the spherical angle  $\theta$  is close to zero such that  $\cos\theta \approx 1$  and the term  $I_z \sin\theta$  may be neglected in (5.18). Then the spherical components of the electric fields are approximately given by

$$E_\theta^I = I_x^I \cos\phi + I_y^I \sin\phi, \quad E_\phi^I = -I_x^I \sin\phi + I_y^I \cos\phi, \quad (5.44)$$

$$E_\theta^{II} = I_x^{II} \cos\phi + I_y^{II} \sin\phi, \quad E_\phi^{II} = -I_x^{II} \sin\phi + I_y^{II} \cos\phi. \quad (5.45)$$

By use of (5.43) we immediately find that  $E_\theta^I = E_\phi^{II}, E_\phi^I = -E_\theta^{II}$ , which means that the electric fields  $\vec{E}^I$  and  $\vec{E}^{II}$  are orthogonal and have equal strength.

The copolarized radiation fields of the antenna system due to excitation by the I- and II- modes are denoted by  $\vec{E}_{CO}^I$  and  $\vec{E}_{CO}^{II}$ , respectively. The directions of these fields are described by the unit vectors  $\hat{e}_{CO}^I$  and  $\hat{e}_{CO}^{II}$ , given by (cf. (5.20))

$$\hat{e}_{CO}^I = \sin\phi \hat{\theta} + \cos\phi \hat{\phi}, \quad \hat{e}_{CO}^{II} = \cos\phi \hat{\theta} - \sin\phi \hat{\phi}. \quad (5.46)$$

From (5.22) and (5.44) - (5.45) it is easily found that

$$|\vec{E}_{CO}^I| = |I_y^I|, \quad |\vec{E}_{CO}^{II}| = |I_x^{II}|. \quad (5.47)$$

Hence, because of (5.43), the field vectors  $\vec{E}_{CO}^I$  and  $\vec{E}_{CO}^{II}$  have equal strength and the corresponding radiation patterns are identical.

Summarizing, we have shown that the secondary radiation fields due to excitations by odd and even symmetric modes are orthogonal, and the corresponding copolarized radiation patterns are equal. From the derivation it is clear that these results are valid up to a good approximation if the angle  $\theta$  is close to zero, i.e. in the angular region around the positive z-axis.

## 5.5. References

- [1] Boswell, A.G.P., and R.W. Ashton, Beam squint in a linearly polarized offset reflector antenna. *Electronics Letters* 12 (1976), 596-597.
- [2] Brigham, E.O., and R.E. Morrow, The fast Fourier transform. *IEEE Spectrum* 4 (1967), No. 12, 63-70.
- [3] Collin, R.E., and F.J. Zucker, *Antenna Theory, Part 1*. McGraw-Hill, New York, 1969.
- [4] Huang, J., and Y. Rahmat-Samii, A GTD study of pyramidal horns for offset reflector antenna applications. *IEEE Trans. Antennas and Propagat.* AP-31 (1983), 305-309.
- [5] Jamnejad-Dailami, V., and Y. Rahmat-Samii, Some important geometrical features of conic-section-generated offset reflector antennas. *IEEE Trans. Antennas and Propagat.* AP-28 (1980), 952-957.
- [6] Ludwig, A.C., The definition of cross polarization. *IEEE Trans. Antennas and Propagat.* AP-21 (1973), 116-119.
- [7] Silver, S., *Microwave Antenna Theory and Design*. McGraw-Hill, New York, 1949.



## 6. SUMMARY AND CONCLUSIONS

In chapter 1 the design requirements for the transmitting antenna of a broadcasting satellite have been reviewed. Such an antenna should radiate a circularly polarized field and the radiation pattern must have a main lobe with a prescribed cross-section, low sidelobes and a low level of cross polarization. As a most likely candidate to fulfil these requirements we have considered the antenna system that consists of a single offset parabolic reflector fed by a corrugated elliptical horn radiator. The approach to evaluate the electrical performance of this antenna system has been outlined.

Chapter 2 deals with a number of mathematical preliminaries. The geometry of the elliptical conical horn has been described in terms of sphero-conal coordinates. In this orthogonal coordinate system the scalar Helmholtz equation can be solved by separation of variables. The special mathematical functions involved, viz. the simple-periodic and nonperiodic Lamé functions, have been treated in detail.

In chapter 3 the wave propagation in elliptical cones has been studied. Our investigation started with the introduction of transverse electric (TE) and transverse magnetic (TM) field solutions to Maxwell's equations in the sphero-conal coordinate system. These solutions constitute a complete set of modes, in terms of which an arbitrary field can be expanded. The problem of wave propagation in a corrugated elliptical cone has been solved on the basis of the idealized anisotropic surface-impedance model for the corrugated boundary of the cone. It has been shown that only specific fields satisfy the associated anisotropic boundary conditions. These field solutions which are valid at points not too close to the apex of the cone, comprise both electric and magnetic field components in the radial direction, and they are called hybrid modes. Odd and even symmetric hybrid modes have been found and it has been shown that these modes can be combined to yield an electromagnetic field  $(\vec{E}, \vec{H})$  that satisfies the relation  $\vec{E} = +jZ_0 \vec{H}$ . The field components of the hybrid modes are represented by series of products of simple-periodic and non-periodic Lamé functions, multiplied by a spherical Hankel function of order  $\nu + \frac{1}{2}$ . The series-representations involve two sets of expansion coefficients which have been shortly denoted by the (infinite-dimensional) coefficient vectors  $\vec{a}$  and  $\vec{b}$ . Then the problem of determining the

hybrid modes has been reduced to a problem in linear algebra, in which the unknowns are the mode-number  $\nu$ , and the vectors  $\bar{a}$  and  $\bar{b}$ . It has been found that the odd and even symmetric hybrid modes have pairwise identical mode-numbers  $\nu$ , and are pairwise described by the same coefficient vectors  $\bar{a}$  and  $\bar{b}$ . For a number of corrugated elliptical cones the quantities  $\nu$ ,  $\bar{a}$  and  $\bar{b}$  have been numerically determined, whereupon the modal fields inside the cone can be evaluated. The results have been presented in tables and figures.

Chapter 4 deals with the radiation characteristics of elliptical horns with an anisotropic boundary. Our analysis of the radiation problem is based on the Kirchhoff-Huygens approximation, in which it is assumed that the radiation field is completely determined by the field distribution at the horn aperture only. The latter aperture field is then taken to be identical to some given modal field of the infinite corrugated cone, as determined in section 3.3. In this manner the radiation field of the horn is found to be given by an integral representation in terms of the aperture field. From this integral representation general radiation properties of horn aperture fields have been derived, dependent on the properties of the exciting modal field. Thus it has been shown that the radiation fields due to an odd symmetric hybrid mode and to the associated even symmetric hybrid mode, are orthogonal, while the corresponding power radiation patterns are identical. Furthermore, it has been shown that if the horn aperture fields are related by  $\bar{E} = \pm jZ_0 \bar{H}$ , then the same relation holds for the electromagnetic field  $(\bar{E}, \bar{H})$  at an arbitrary observation point in the radiating near-field or far-field regions, thus leading to a circularly polarized radiation field in these regions.

Two methods have been employed for the calculation of the radiation pattern of the horn. One method, the aperture-field integration method, is suitable to determine the radiating near-field and far-field patterns. In this method the Kirchhoff-Huygens integral representation for the radiation field is converted into a sampling-like representation by a series of products of Fresnel integrals and Fourier coefficients of the aperture field. These Fourier coefficients have been numerically evaluated by means of the Fast Fourier Transform technique.

In the second method, called the wave-expansion method, the electromagnetic field outside the horn is expanded in terms of sphero-conal TE

and TM modes. For a given horn aperture field the expansion coefficients can be determined by matching the fields at the aperture and by using the orthogonality properties of the TE and TM modes of free space. Then the radiation field can be numerically evaluated at any observation point outside the horn. It has been pointed out that the wave-expansion method is not very suitable in the case of a long horn, because of the slow convergence of the modal expansion for the radiation field.

Numerical results obtained by both methods and experimental results have been presented. The computed results and the measured results agree to a large extent both in the radiating near-field region and in the far-field region. Radiation patterns with an elliptical cross-section have been found. The measured radiation patterns due to an odd symmetric hybrid mode and to the associated even symmetric hybrid mode, are almost equal in a large angular region at all frequencies considered. This equality of measured radiation patterns is in agreement with the theoretical result. As a consequence, if a corrugated elliptical horn is excited by the combination of an odd symmetric hybrid mode and the associated even symmetric hybrid mode with a phase difference  $\pi/2$ , the resulting radiation field will indeed be circularly polarized and the radiation pattern has an elliptical cross-section. Furthermore, it has been found that the concept of phase centre of the radiated far field is feasible only in a small angular range around the beam axis. However, the location of the phase centre differs if the planes of measurement (or of computation) are different. Consequently, phase errors will be inevitable if this type of horn is used for the illumination of a parabolic reflector antenna. Also, the positioning of the horn relative to the focal point of the reflector requires careful consideration.

In chapter 5 we have investigated the radiation characteristics of the single offset parabolic reflector fed by a corrugated elliptical horn radiator. The secondary radiation field, that is the field radiated by the reflector, has been determined from the well-known integral representation for the field in terms of the induced surface current  $\bar{J}_s$  in the reflector. In the physical-optics approximation the current  $\bar{J}_s$  is simply related to the tangential components of the incident magnetic field  $\bar{H}^i$  at the reflector surface. This incident field which is due to the primary radiation by the corrugated elliptical horn, can be

determined by the methods of chapter 4. Here it is understood that the primary radiation is excited by some given modal field of the infinite corrugated cone. To numerically evaluate the secondary radiation field, the integral representation for the field has again been converted into a sampling-like representation by a series of products of Fresnel integrals and Fourier coefficients of the reflector current. These Fourier coefficients have been determined by means of the Fast Fourier Transform technique.

From a theoretical analysis it has been found that the radiation fields of the antenna system due to excitations of the horn by odd and even symmetric modes are orthogonal, and the corresponding copolarized radiation patterns are equal, both up to a good approximation. These results are confirmed by experiments: the measured radiation patterns of the antenna system in the two cases of  ${}_{\circ}HE_{11}$ - and  ${}_eHE_{11}$ -mode excitation of the horn are virtually identical. Very good agreement has been established between the computed results and measured data for the secondary radiation of the antenna system. The single offset parabolic reflector fed by a corrugated elliptical horn radiator does provide a secondary radiation pattern that has a rapidly decaying main lobe with an elliptical cross-section, and that has low sidelobes.

The geometrical parameters of the horn and of the parabolic reflector are input parameters of the computational procedure to numerically determine the radiation field of the antenna system. By varying these input parameters one may search for an antenna design that is optimal with respect to electrical performance. In this manner the computational procedure provides a design through computation versus the alternative of a design based on experimentation. The analytical and numerical approach to the evaluation of the electrical performance of the antenna system is rapid (with respect to computer processing time), successful and reliable.

ACKNOWLEDGEMENTS

The author wishes to thank:

Mr. A.P.M. Baayens of the Numerical Mathematics and Service Group of the Department of Mathematics, Eindhoven University of Technology, for writing the computer programs used in the computation of the modes in the elliptical cone (chapter 3);

Mr. M.H.M. Knoben of the Group Electromagnetism and Circuit Theory of the Department of Electrical Engineering, Eindhoven University of Technology, for carrying out the measurements on the corrugated elliptical horn (chapter 4), and for preparing a number of drawings;

Dr. D. Fasold, Head of the Antenna Department, Messerschmitt-Bölkow-Blohm GmbH (Munich, Germany), for making available the measurements on the antenna system (chapter 5);

Miss T.J.F.M. Pellegrino and Miss M.P. Verhoeven for devotedly typing this thesis.



## SAMENVATTING

Dit proefschrift gaat over de bepaling van het stralingsdiagram van het antennesysteem dat bestaat uit een parabolische reflektor gevoed door een gegroefde elliptische hoornstraler. Een dergelijk antennesysteem kan zodanig ontworpen worden dat het stralingsdiagram gekenmerkt wordt door een hoofdlus met een elliptische doorsnede, door lage zijlussen, en door een laag niveau van kruispolarisatie in het geval van circulair gepolariseerde straling. Vanwege deze eigenschappen kan het antennesysteem gebruikt worden als zendantenne van een omroep-satelliet.

In het onderzoek van de stralingseigenschappen van het antennesysteem kunnen twee deelbijdragen worden onderscheiden. De eerste bijdrage die in dit proefschrift wordt beschreven, betreft de ontwikkeling van een theorie voor de verklaring van golfvoortplanting in en straling van een gegroefde elliptische hoorn met willekeurige geometrische parameters. Het deelprobleem van de golfvoortplanting wordt opgelost op basis van het anisotrope oppervlakte-impedantiemodel voor de gegroefde wand van de hoorn. De straling van de hoorn wordt geanalyseerd uitgaande van de Kirchhoff-Huygens benadering van het stralingsprobleem. In deze benadering wordt aangenomen dat het stralingsveld volledig bepaald wordt door de veldverdeling in de apertuur van de hoorn. Twee methoden worden toegepast voor de berekening van de straling van de hoorn, namelijk de methode waarbij het stralingsveld voorgesteld wordt door integralen in termen van het apertuurveld, en de methode waarbij het stralingsveld ontwikkeld wordt naar modi. Numerieke resultaten bepaald met beide methoden, en experimentele resultaten worden gegeven.

De tweede bijdrage van het onderzoek bestaat uit de ontwikkeling van een rekenprocedure voor de numerieke bepaling van de straling van het antennesysteem. Het (secundaire) stralingsveld wordt veroorzaakt door de elektrische stromen die in de parabolische reflektor worden geïnduceerd door het (primaire) stralingsveld van de hoorn. De rekenprocedure heeft als invoergegevens de geometrische parameters van de hoorn en de reflektor. Door stralingsberekeningen uit te voeren voor verschillende waarden van de invoergegevens kan men vaststellen bij welke parameterwaarden het stralingsveld van het antennesysteem aan de vereiste specificaties voldoet. Op deze wijze is het mogelijk om een antennesysteem te ontwerpen op basis van berekeningen in plaats van op basis van experimenten. Numerieke en experimentele resultaten voor de straling van het antennesysteem worden gegeven.



CURRICULUM VITAE

De auteur van dit proefschrift werd op 13 juli 1949 geboren te Bladel. Van 1961 tot 1966 volgde hij de opleiding HBS-B aan het Rythovius College te Eersel. Van 1966 tot 1970 doorliep hij de HTS, afdeling Elektrotechniek, aan het Instituut voor Hoger Beroepsonderwijs te Eindhoven. Van 1972 tot 1978 volgde hij de studie voor elektrotechnisch ingenieur aan de Technische Hogeschool Eindhoven. Van 1978 tot 1984 werkte hij als wetenschappelijk assistent in de vakgroep Theoretische Elektrotechniek, afdeling Elektrotechniek, Technische Hogeschool Eindhoven. Het in dit proefschrift beschreven onderzoek werd in deze periode uitgevoerd.











Stellingen

behorend bij het proefschrift van

S.C.J. Worm

Eindhoven, 14 mei 1985

1. De sterkte van een ontvangen stoorsignaal is lager naarmate de ontvangantenne een lagere gevoeligheid heeft in de richting van het stoorsignaal. De door Ishimaru en Held ontwikkelde methode voor de synthese van een stralingsdiagram met een aantal zijlusen van hetzelfde niveau, is in aangepaste vorm bruikbaar voor de synthese van een stralingsdiagram met een zijlus van een verlaagd niveau in de richting van het stoorsignaal.

*Ishimaru, A., and G.Held, Analysis and synthesis of radiation patterns from circular apertures.*

*Can. J. Phys. 38 (1960), 78-99.*

*Worm, S.C.J., Radiation patterns of circular apertures with prescribed sidelobe levels. TH-Report 79-E-97, Eindhoven University of Technology, Eindhoven, 1979.*

2. Laat het elektromagnetisch veld in een circulaire apertuur  $0 \leq r \leq 1$ ,  $0 \leq \phi < 2\pi$ , beschreven worden door een rotatiesymmetrische apertuurverdeling  $f(r)$  met randwaarde  $f(1) = 0$ ; hierbij zijn  $r, \phi$  poolcoördinaten. Dan is de verhouding van het apertuurrendement en de ruimtelijke spreiding van het uitgestraalde vermogen maximaal indien  $f(r) = 1 - r^2$ .

*Worm, S.C.J., Optimization of some aperture antenna performance indices with and without pattern constraints.*

*TH-Report 80-E-112, Eindhoven University of Technology, Eindhoven, 1980.*

3. De lengte van een 'dual-hybrid-mode' belichter voor efficiënte belichting van een radiotelescoop zoals die gegeven wordt door Vu, kan aanzienlijk gereduceerd worden.

*Vu, T.B., Low-noise dual-hybrid-mode horn - an experimental model. Int. J. Electron. 34 (1973), 391-400.*

*Worm, S.C.J., Compact dual-hybrid-mode feeds with low crosspolar radiation. Electronics Letters 15 (1979), 740-741.*

4. Het verdient de voorkeur om voor TE- en TM-modi in elliptische cilindfers en in elliptische kegels, de classificatie naar modi met even en oneven symmetrie te baseren op de symmetrie-eigenschappen van de elektrische veldlijnen.
  
5. De door Thurlings gebruikte methode ter bepaling van de groefdiepte nodig voor de realisatie van een anisotrope impedantiewand met impedanties  $Z_{\eta} = 0$  en  $Z_z = \infty$  in een gegroefde elliptische golfpijp, is onjuist.

*Thurlings, L.F.G., Some properties of the corrugated elliptical waveguide. Report ET-5-1975, Eindhoven University of Technology, Eindhoven, 1975.*

6. Chaviello beweert dat voor signaalontvangst van geostationaire satellieten met geringe tussenruimte, gebruik moet worden gemaakt van een ontvangantenne met elliptische apertuur waarvan de lange as loodrecht op het vlak van de geostationaire baan staat. Deze bewering is onjuist.

*Chaviello, A., 2<sup>o</sup> Satellite spacing: an FCC challenge to microwave engineers. Microwave Journal 26 (1983), No. 9, 36-44.*

7. Volgens Dragone worden in de apertuur van een gegroefde rechthoekige hoorn, bij excitatie door een oneven symmetrische hybride mode en bij excitatie door de overeenkomstige even symmetrische hybride mode, identieke amplitude-verdelingen gerealiseerd. Deze bewering wordt niet gestaafd door experimentele resultaten.

*Dragone, C., A rectangular horn of four corrugated plates. IEEE Trans. Antennas and Propagat. AP-33 (1985), 160-164.*

8. Het stralingsdiagram van een gegroefde elliptische hoornantenne is rotatiesymmetrisch bij een bepaalde keuze van de hoornafmetingen.
9. De depotvondst van IJzertijdkeramiek op de Werft te Bladel doet vermoeden dat archeologisch onderzoek aldaar, naar een nederzetting uit de IJzertijd, met succes kan worden uitgevoerd.

*Brabantse Oudheden, Bijdragen tot de studie van het  
Brabants Heem, Deel XVI, Eindhoven, 1977.*